Surface Coatings of Nickel-Rich NCM Based Cathode Active Materials for Improved Electrochemical Performance of Lithium-Ion Batteries

Dem Fachbereich Biologie und Chemie
der Justus-Liebig-Universität Gießen

vorgelegte Dissertation
zur Erlangung des akademischen Grades

Doktor der Naturwissenschaften
-Dr. rer. nat. –

von

Rajendra Singh Negi

Gießen, September 2021

Dekan / Dean	Prof. Dr. Thomas Wilke
1. Gutachter / 1st Reviewer	Dr. Matthias T. Elm (Justus-Liebig-Universität Gießen)
2. Gutachter / 2nd Reviewer	Prof. Dr. Jürgen Janek (Justus-Liebig-Universität Gießen)

The present work was carried out in the period from March 1st, 2018 to August 30th, 2021 at the Center for Materials Research (LaMa) of Justus-Liebig-Universität Gießen under the supervision of Dr. Matthias T. Elm.

I declare that I have completed this dissertation single-handedly without the unauthorized help of a second party and only with the assistance acknowledged therein. I have appropriately acknowledged and cited all text passages that are derived verbatim from or are based on the content of published work of others, and all information relating to verbal communications. I consent to the use of an anti-plagiarism software to check my thesis. I have abided by the principles of good scientific conduct laid down in the charter of the Justus Liebig University Giessen „Satzung der Justus-Liebig-Universität Gießen zur Sicherung gutter wissenschaftlicher Praxis“ in carrying out the investigations described in the dissertation.

Giessen, September 2021

_____

Rajendra Singh Negi

Acknowledgments

First of all, I would like to thank Dr. Matthias T. Elm for providing me the opportunity to work in such an excellent group towards my Ph.D. (Dr. rer. nat.) thesis. It was my great honor to work with him on this challenging field of coatings for Li-ion batteries. His excellent guidance, discussions, and encouragements have not only made me gain scientific knowledge, but also made me think like a scientist. All of the acquired knowledge and experiences will play a very crucial role in my future work and support me for the rest of my life.

I would like to thank Prof. J. Janek for his interest in being the co-supervisor of this thesis. The extremely professional working environment of his group along with his guidance contributed significantly to the success of this thesis. Without his support and possibility to conduct various experiments in his lab, this thesis would not have been possible. I also want to thank him for the readings and comments in various scientific publications.

I want to sincerely thank Franz Schmidt and Ryo Takata from Evonik GmbH, to provide me the opportunity to do an industrial internship at Evonik GmbH. Especially for providing the coating material, along with discussions on how to improve the coating properties itself. The improvement in the electrochemical performance would not have been possible, without the permanent optimization of the coating materials done by them.

I would also like to thank our cooperation partners, Dr. Torsten Brenzensinski, Andrey Mazilkin from Karlsruhe Institute of Technology (KIT), Prof. Kerstin Volz, Shamail Ahmed from Philipps University Marburg, and Prof Jürgen Senker, Robert Staglich from University of Bayreuth, Germany, for their high-quality support in all matters relating to TEM and NMR analysis, which have contributed significantly in the success of my scientific publications.

Many thanks to Dr. Sean culver for sharing his knowledge and providing his immense support during the preparation of various manuscripts. Many thanks to Dr. Ruijun Pan for help me to understand various aspects of the coating along with designing the test set-up and writing various manuscripts together. Thanks to Dr. Jan Binder for teaching me cell preparation and cell testing. Thanks also to Erdogan Celik for the beneficial discussions about my experimental results and all other members of the AG Elm and AG Janek.

I am very grateful to the German Federal Ministry of Education and Research (BMBF) for the funding of this thesis via the NanoMatFutur project NiKo (03XP0093).

At last, I would like to express gratitude to my mother, sister, brother, family, and friends for their continuous support during my Ph.D. time and for always being there for me during my good and bad times.

Abstract

Ni-rich NCM based cathodes are considered the most promising cathode candidates for next-generation high-performance Lithium-ion batteries (LIBs). Despite very good electrochemical performance, Ni-rich NCM based cathodes still suffer practical cycling problems, which need to be addressed before their successful commercialization. Surface modification by coating has become one of the feasible approaches to tackle these issues and in turn improve the electrochemical performance. However, the most common coating methods are rather complex, time-consuming and expensive. Thus, a practical coating technique for the commercialization of these cathodes is highly needed.

The main objective of this thesis is the development of such an efficient coating process that not only improves the electrochemical performance of Ni-rich NCM based cathodes but also brings them one step closer to their successful commercialization. For this purpose, several simple, low-temperature, cost-effective coating processes have been developed. The developed coating processes resulted in very homogenous and conformal coatings, which in turn led to an improvement in the C-rate performance, long-term cycling stability, and particle cracking of Ni-rich NCM based cathodes in LIBs.

Several coating materials have been tested and reported for NCM based cathode. However, due to their different properties, one standardized coating material has not been agreed upon. Nevertheless, Al_2O_3 based coating materials are considered as most promising coating material. Thus the major part of this thesis focuses upon Al_2O_3 and its analogous as coating material. In addition, a $Li_4Ti_5O_{12}$ based coating has also been tested due to its increasing popularity among coating materials. It has been found that the physical properties of a coating such as coating homogeneity, conformity and thickness, as well the coating's chemical composition can have a significant effect on the electrochemical performance of NCM based cathodes. Furthermore, it is demonstrated that a post-annealing step after coating can play a crucial role in improving the electrochemical performance of NCM based cathodes, as it helps in improving the ionic conductivity of the coating layer due to the insertion of Li^+-ion inside the coating layer. In addition, in-depth investigations have been performed to understand the beneficial effect of the coatings on the electrochemical performance of NCM based cathodes, which allowed better insights into the ongoing degradation mechanism of NCM based cathodes during cycling. The knowledge gained in this thesis is considered to be imperative for further developments of surface coating strategies.

To conclude, this thesis offers various practical surface coating strategies for Ni-rich NCM based cathodes. The developed coating strategies are very simple, easy, cost-effective, environment friendly, and significantly improve the electrochemical performance of NCM based LIBs. These improvements combined with the potential of these coating strategies for scalability make them suitable for large-scale industrial application and in turn for the commercialization of Ni-rich NCM cathodes for next-generation LIBS. Last but not the least, the in-depth knowledge regarding the impact of coatings during electrochemical cycling on Ni-rich NCM provides a strong fundamental for further future research.

Table of Content

1. Introduction

Motivation and Outline

The abusive utilization of fossil fuels over the last century has led to the release of greenhouse gases (such as carbon dioxide and methane) into the atmosphere resulting in heat trapping and ultimately causing global warming (making it the most concerning issue of the 21st century), global warming is a serious threat to the health of current world population and also to the environment. In addition, the resources for fossil fuels are finite and have an uneven global distributon[1]. At present, conventional fossil fuels (such as coal, gas and oil) are still the primary source of energy production around the world as shown in Figure 1[2,3]. Concerning these impacts and issues related to fossil fuels, the development of sustainable energy technologies has become exceptionally urgent.

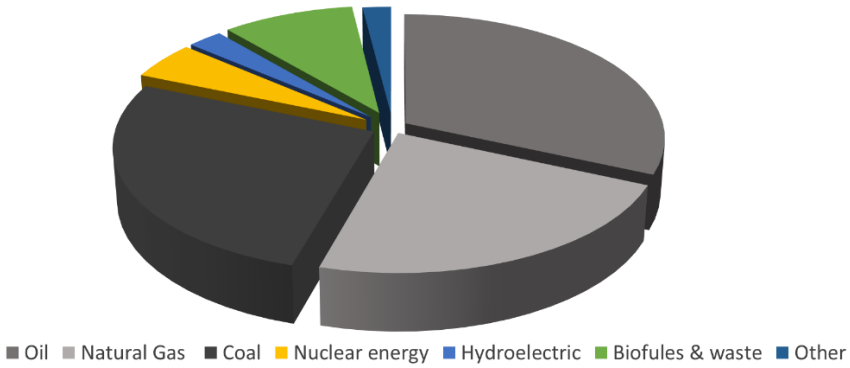

Figure 1: Distribution of world energy supply in 2018[2,3]

Production and utilization of renewable energy is the most promising approach for sustainable development. Future nuclear energy sources seem attractive, but they suffer from potentially high radiation threats along with low efficiency and very high operation and maintenance costs. However, considering nuclear energy as an alternative for fossil fuels is still under debate due to the production of high amount of toxic nuclear waste. Hydropower has been successfully used to produce electricity in combination with tidal or wave energy around the globe. Over the last few decades, extensive research and financial support have been made to the development of different renewable energy technologies, such as wind power, solar power and geothermal energy. However, even the rapid development of these alternative renewable energy technologies will not have a predictable impact unless there is an efficient way to use and store the energy produced by them. Therefore, the development of high-performance energy-storage systems and devices with high power and energy density is needed at the moment[4].

Among all, two different electrochemical devices, rechargeable Li-ion battery, and electrochemical super-capacitor are considered as the most promising candidates for energy storage and supply[5]. The energy-storage technology in combination with renewable energy resources can secure a sustainable energy supply for most of the world population and thus reduce the dependency on fossil fuel-based energy resulting in a clean-energy supply. In comparison to super-capacitors, Li-ion battery (LIBs) technology are been preferred due to its high energy-density[6-9]. LIBs also promise superior performance due to their effective power density, safety, cost, efficiency and longevity. The LIBs based energy storage systems have been widely regarded as the most promising

storage technology for renewable energy resources which are the immediate alternative for ever-declining fossil-fuel energy resources in the current society, due to their vast application in almost every sector of human progression[8,9].

Awarding the Nobel Prize 2019 in chemistry to John B. Goodenough, M. Stanley Whittingham, and Akira Yoshino for developing Li-ion batteries further demonstrate the significance of energy storage technology. The electrochemical performance of Li-ion batteries predominantly depends on the properties of their electrodes: cathode and anode. Enormous research has been done in developing safe and environment-friendly electrode materials with high energy density, improved rate-capability, and cycling stability, along with high operating voltage[9]. For the anode, lithium alloy-based anode materials (such as lithium-silicon (Li-Si) and lithium-tin (Li-Sn)), have been shown to provide improved cycling stability, better rate capabilities, along with higher specific capacity as compared to conventional carbon-based anodes[7-9]. On the other hand, conventional cathode materials have much lower theoretical capacity as compared to anodes and they also suffer from structural instability when cycled to higher voltages or at elevated temperatures[10]. For instance, conventional Li-stoichiometric cathode materials, such as layered $LiCoO_2$, olivine $LiFePO_4$, and spinel $LiMn_2O_4$, have a low specific capacity ($\approx$ 170 mAh/g) and compromised cycling stability at elevated temperatures[11-16].

Among all, $LiCoO_2$ has been the most widely used cathode material due to its high theoretical capacity and reasonable cycling stability. However, its low achievable practical capacity along with high toxicity and synthesis cost hinders its ability to serve as next-generation cathode material[17,18]. Thus for the development of next-generation high-performance Li-ion battery, a significant improvement of the electrochemical properties of cathode materials is required.

An established approach to developing next-generation cathode materials with higher achievable capacity, better cycling stability, lower toxicity, lower cost, and higher thermal stability is to integrate the advantages of three materials $LiNiO_2$, $LiCoO_2$ and $LiMn_2O_4$. At the same time the combination of these three materials limits their individual disadvantages. These types of cathode materials are known as NCM ($LiNi_xMn_yCo_{1-x-y}O_2$) cathodes and are among the most promising candidates for next-generation cathodes[19,20]. Since the development of $Li[Ni_{1/3}Co_{1/3}Mn_{1/3}]O_2$ (NCM111) by Ohzuku et. al., several studies have been performed on the further development of NCM based cathodes. In contrast to LCO, NCM based cathodes show a flexible stoichiometry, allowing researcher to adjust the electrochemical properties[19,21].

The most researched NCM composition (NCM111) was considered as one of the most promising cathode materials in this category. However, Ni-rich NCM based cathodes (NCM622, NCM811, etc.) have been developed in past few years and have shown promising results in higher achievable capacity (>200mAh/g)[21]. However, these Ni-rich NCM cathodes suffer from major drawbacks regrading commercialization, such as poor rate capability, faster capacity fade, gas evolution, thermal instability, Li/Ni cation mixing, and so on. In literature different mechanisms are discussed to be responsible for these problems such as (1) Dissolution of transition metals corroded by HF present in the electrolyte; (2) Undesired side reactions occurring between the cathode and the electrolyte catalyzed by delithiated NCM with simultaneous oxygen release; (3) layered

to spinel phase transition at the cathode surface; (4) crack formation inside the NCM particle due to volume changes during cycling. These parasitic issues (such as side reactions and particle cracking) related to Ni-rich NCM cathodes result in a faster capacity decay[22-27].

To address the above-mentioned obstacles related to NCM based cathodes several efforts have been made. Among all, surface modifications via surface coating have been emerged as the most promising method to improve the performance of NCM based cathodes[28,29]. Surface coating with metal oxides is considered as most effective method to improve the structural and thermal stability of the cathode material. The coating not only enhances the surface stability of the NCM particles but also provides new chemical, physical and mechanical properties to the particle[30-34]. However, the existing problems in the commercialization of coating material can be mainly divided into two categories: 1) Developing a simple, cost-effective coating strategy for modifying the cathode surface to improve the electrochemical performance of the cathode and 2) understanding the properties of the coating itself along with how it benefits the cycling performance.

Thus, this thesis mainly focuses on the development of various efficient coating approaches, to improve the electrochemical performance of Ni-rich NCM based cathodes and in turn, meet the requirement for the commercialization of Ni-rich NCM based LIBs. Therefore, four different easy, fast and facile coating processes have been successfully designed, to achieve a thin and conformal coating layer on NCM powder and ready-to-use cathodes. The coatings have led to an excellent electrochemical property of the Ni-rich NCM in terms of C-rate performance and long-term cycling. Additional drying and sintering steps required in other commonly used coating processes are not necessary to achieve the final coating in our study to achieve a better long-term cycling performance. Therefore, the coating processes developed in this study are facile, cost-effective, energy-efficient, easy to scale up, and can be applied to every type of cathode, making these coating methods highly suitable for large-scale industrial application and commercialization of Ni-rich NCM based cathodes. A fundamental understanding of the working principle of the coating during electrochemical cycling is essential to further optimize the efficiency of the coating layer as up to now, a majority of factors related to the coating are still unclear. Therefore, in-depth structural investigations of the properties of coating have been performed to elucidate the cause of the improved electrochemical performance of the coated cathodes. The results all together are expected to help the scientific community to better understand the effect of coatings on NCM based cathodes and the underlying cause for the improved electrochemical performance, and thus expected to create a strong foundation for further research.

Before focusing on the main outcome of this thesis, a brief introduction related to the state-of-art LIBs is provided. First, the working principle of a typical LIB is discussed in detail. Then, a detailed overview of the most commonly used cathodes along with their features is presented. Ni-rich NCM based cathodes have been highlighted as one of the most promising cathodes for next-generation LIBs. Next, surface behavior (such as side reaction, phase transition and particle cracking) of the cathode during cycling is discussed in detail, which usually results in poor cycling performance of these cathodes. Subsequently, surface modification of the cathodes is discussed, i.e. its role, characteristics, and kinds of coatings. Thereafter, surface modification via coating has

been discussed in depth with respect to coating methods and coating materials, along with their properties.

In the result section, three different coating approaches are presented for $LiNi_{0.7}Mn_{0.15}Co_{0.15}O_2$ using different kinds of coating material (i.e. Al_2O_3, $LiAlO_2$, and LTO). Subsequently, the structural characterization of the coating layer is described in detail. Showing thin, conformal and homogenous coating on the surface of NCM resulting in much improved electrochemical performance. Thereafter, detailed electrochemical characterization showed much improved C-rate performance, capacity retention and long-term cycling stability, along with signification reduction in solid electrolyte interface (SEI) and charge transfer (CT) impedance after the coating. Furthermore, post mortem analysis of the cycled cathodes displays that particle disintegration is effectively prevented by the coating, which is found to be stable during electrochemical cycling.

The first publication *"Optimized atomic layer deposition of homogeneous, conductive Al_2O_3 coatings for high-nickel NCM containing ready-to-use electrodes"*, focuses on an ALD-based Al_2O_3 coating for Ni-rich NCM based ready-to-use cathode materials for improved electrochemical performance.

In the second publication *"Enhancing the Electrochemical Performance of $LiNi_{0.7}Mn_{0.15}Co_{0.15}O_2$ Cathodes Using a Practical Solution-Based Al_2O_3 Coating"*, a low-temperature, wet-chemical-based Al_2O_3 coating process to coat Ni-rich NCM cathode is developed. The achieved thin, homogenous coating not only consumes the unfavorable surface residuals on the NCM surface preventing side reactions at the interface but also prevents particle cracking during cycling.

The third publication *"Insights into the Positive Effect of Post-Annealing on the Electrochemical Performance of Al_2O_3-Coated Ni-Rich NCM Cathodes for Lithium-Ion Batteries",* focuses on the effect of high-temperature annealing on the structural properties of Al_2O_3 coating used in the second publication and how it affects the electrochemical performance of Ni-rich NCM based cathodes. It is observed that annealing Al_2O_3 coated cathode at 600 ^oC, resulted in the formation of an $Al_2O_3/LiAlO_2$ coating layer and improved the electrochemical performance.

Afterward, the knowledge gained regarding the coatings from the previous work has been transferred to All-solid-state batteries. A new non-destructive dry-processed lithium titanite (LTO) coating method for NCM based cathode in thiophosphate-based All-solid-state batteries have been developed. My work demonstrates that the improvement in the electrochemical performance arises from a reduced interfacial resistance between the cathode and solid electrolyte during cycling. These results are discussed in our fourth publication, entitled "*Stabilizing the cathode/electrolyte interface with dry-processed lithium titanate coating for all-solid-state-batteries"*

In the fifth publication entitled *"A dry-processed $Al_2O_3/LiAlO_2$ coating for stabilizing the cathode/electrolyte interface in High-Ni NCM-based All-solid-state-batteries"*, the benefit of post-annealing treatment is further demonstrated in dry-coated Al_2O_3 coated NCM cathodes for all-solid-state batteries. It is demonstrated that annealing improves various expects of the coating layer (such as homogeneity, better interface, coating thickness), which in combination improved the electrochemical performance of ASSBs.

Finally, in the last section, the presented results of this thesis have been summarized and evaluated with regard to scientific literature. In addition, a brief outlook on the potential of the above-developed coating approaches for next-generation LIBs and ASSBs are provided considering future research goals. At last, a comprehensive opinion of the author regarding the development of next-generation LIBs is provided.

2. Fundamentals

2.1 The Principle of a Li-ion Battery (LIB)

The Li-ion battery is one of the most promising energy storage systems due to its various advantages in terms of specific capacity, operating voltage, rate capability, long-term cycling performance, and safety in comparison to traditional nickel-cadmium batteries, lead-acid batteries, or nickel-metal hydride battery[10,35]. For instance, the optimal operating voltage for commercial $LiCoO_2$-based LIBs is 3.7 V, which is nearly 3 times of the commercial lead-acid battery. Since the release of first commercial rechargeable LIBs by SONY in 1991, the LIB has rapidly owned the commercial market as a major power source for portable electronic devices. Recently it has also been advanced as a power source for electric and hybrid electric vehicles, with potential as power sources for future air transportation[36-37].

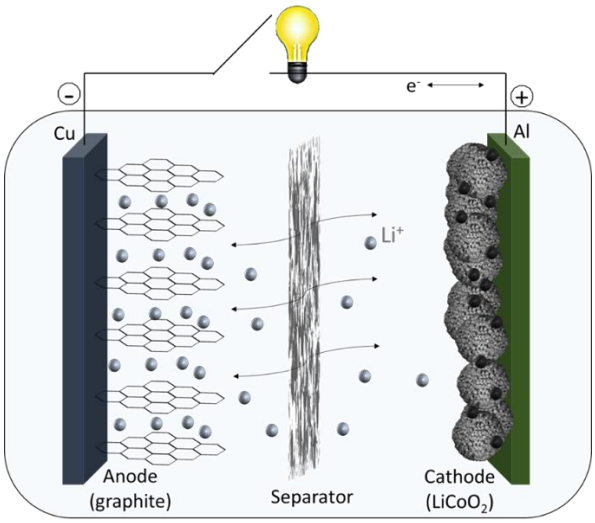

Figure 2: Schematic illustration of a lithium-ion battery based on $LiCoO_2/Li^+$ -based electrolyte/graphite.

As shown in Fig. 2, a LIB has mainly three primary functional components: Cathode, anode, and electrolyte [38,39]. The cathode and anode are separated by the so-called separator layer, immersed in electrolyte. The different current collector is used for cathode and anode, Al for cathode and Cu for anode. The common cathode materials used are $LiCoO_2$, $LiMn_2O_4$, $LiFePO_4$, or $LiMn_{1/3}Co_{1/3}Ni_{1/3}O$. Common anode materials used are graphite, silicon-based materials, graphene, or $Li_4Ti_5O_{12}$[40-43]. The commonly used electrolyte consists of lithium salt, such as $LiPF_6$ dissolved in organic solvents (ethylene carbonate (EC), dimethyl carbonate (DMC), and diethyl carbonate (DEC), etc)[44,45]. The energy storage and conversion in LIBs are based on the migration of Li-ions between cathode and anode through Li^+ migration, along with simultaneous charge transfer via external circuit[39,46-48]. The corresponding reaction taking place in LIBs during charge/discharge is given by:

Cathode:

$$LiCoO_2 \rightleftharpoons Li_{1-x}CoO_2 + xLi^+ + xe^-$$

Anode:

$$6C + xLi^+ + xe^- \rightleftharpoons Li_xC_6$$

Total reaction:

$$LiCoO_2 + 6C \rightleftharpoons Li_{1-x}CoO_2 + LixC_6$$

During the charging step, Li ions are extracted from the LCO cathode. At the same time, Li-ions are inserted inside the graphite anode. During the subsequent discharge step, transfer of Li-ions from anode to cathode takes place. Altogether, the specific capacity and energy conversion efficiency of LIBs mainly depends on the combination of electrochemical properties of cathode and anode[49,50]. Among all the components of LIBs, the cathode material is considered very crucial for the advancement of LIBs.

2.2 Cathode Materials for LIBs

During the last decade, the increasing demand for electric vehicles has stimulated the development of high-performance next-generation LIBs across the globe. The bottleneck for the advancement of next-generation LIBs is the development of novel electrode materials with superior performance. At the anode side, lithium-silicon (Li-Si) and lithium-tin (Li-Sn) have shown excellent cycling stability and higher rate capability, along with much higher specific capacity (4000 and 990 mAh g^{-1}, respectively)[51]. However, state-of-the-art cathode materials are not able to meet the high-energy and power density required for the rapid development of EVs and HEVs, as cathode materials have generally a much lower theoretical capacity as compared to that of the anode[52]. Next-generation cathodes are subject to meet the following criteria for the development of next-generation LIBs[48,53]:

I. **Chemical and Physical Properties:** The Li-containing cathode must reversibly oxidize and reduce during charge/discharge cycles. In addition, the cathode materials should exhibit a high Li-ion diffusion coefficient along with high electronic conductivity. Furthermore, the cathode materials need to show excellent mechanical stability in order to keep the host structure intact during charging/discharging.

II. **Wide Operating Voltage Window:** The cathode materials need to have high chemical potential (vs. Li-metal), to achieve a wide operating voltage window of LIBs.

III. **High Energy and Power Density:** The cathode materials should provide high energy and power density, to enable the intercalation and deintercalation of a large amount of li-ion. This in turn provides a higher practical achievable specific capacity and better C-rate performance compared to standard cathode materials.

IV. **Outstanding Long-term Cycling Performance:** Improved battery engineering (morphology and size of cathode materials, along with battery design) enables the

extraction of higher capacity from the traditional cathode materials during the initial charge/discharge cycles. However, these improvements result in a faster capacity fading during long-term cycling. Hence, the new cathode materials should also provide better long-term cycling stability along with higher energy and power density.

V. **Wide Working Temperature Range:** Due to the extension of LIBs applications from portable electronic devices to almost every energy-related sector. Thus, State of the art LIBs are mostly optimized for a temperature range (0 ^{o}C to 40 ^{o}C), are exposed to much harsher temperature ranges. Thus, the new cathode materials should be able to show optimal performance in a wider temperature range.

VI. **Low Manufacturing Cost:** The manufacturing cost needs to be low, which in turn relies on the availability of the raw materials required.

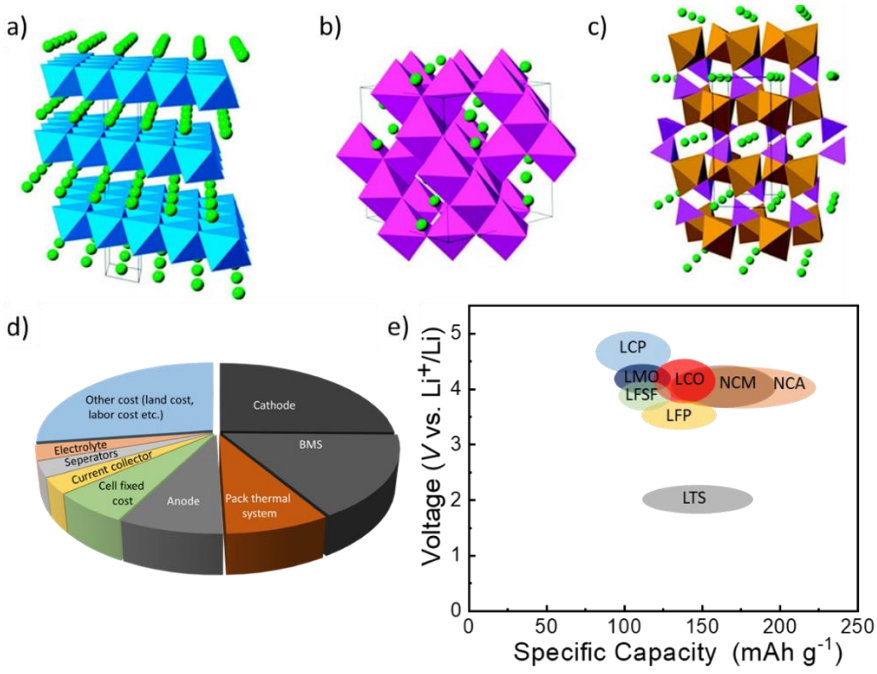

Figure 3: Crystal structure of a) Layered $LiMO_2$, b) Spinel-structured LiM_2O_4, and c) Olivine-structured $LiMPO_4$ (M = Co, Ni, Mn, etc.) (Redesigned with permission from Ref. [51] Copyright 2012 Elsevier B.V.). d) The cost components of a representative LIB. (e) Voltage vs capacity chart of main cathode materials.

The main division of current cathode materials includes layered $LiCoO_2$, poly-anion $LiFePO_4$, spinel $LiMn_2O_4$, and their derivatives[54,55]. The crystal structures of different cathode materials are shown in Fig. 3a, b, c[56]. Fig. 3d illustrated the cost components of a representative LIB. Within all the major parts of a battery, the cathodes are the most expensive part. This arises due to the low abundance and rather complicated extraction process of nickel, cobalt, and manganese[57]. Six different kinds of cathode materials are shown in Fig. 3e according to their theoretical specific capacity vs. voltage. To achieve higher energy density, scientists are looking for those cathode materials that either

provide higher energy density or higher discharge capacity. Fig. 3c also shows that NCM based cathode materials have great potential as next-generation cathode materials for LIBs, as they provide higher practical capacity and a wider voltage window as compared to state-of-art LCO based cathodes.

During the last decade, scientists have been dedicated to exploring advanced cathode materials to maximize the efficiency of cathode materials, either by developing new cathode materials or by modifying the existing cathode materials [36,53,58-60]. While all these efforts have given successful outcomes, still most of the outcomes end up with a crucial concern- the cathode's surface. The cathode surface is the region where the transfer of Li-ions takes place between the cathode and the electrolyte. Thus, most of the parasitic side reactions take place at the surface of the cathode due to non-equilibrium diffusion[61,62]. In the past decades, several attempts have been made to modify the surface of cathode in order to adjust the physical and chemical properties of the material, but the underlying problems have not been successfully solved yet. Thus, in the following section, the surface properties of cathode materials will be briefly discussed.

2.3 Degradation Behaviour of Cathode Material

Aging of cathode active material (i.e. NCM) during cycling still remains a major problem resulting in loss of performance during long-term cycling, and thus hinders the development of next-generation LIBs[63-72]. Although not all causes for cathode aging are fully understood yet, there are well-known issues that are discussed in detail in the following section.

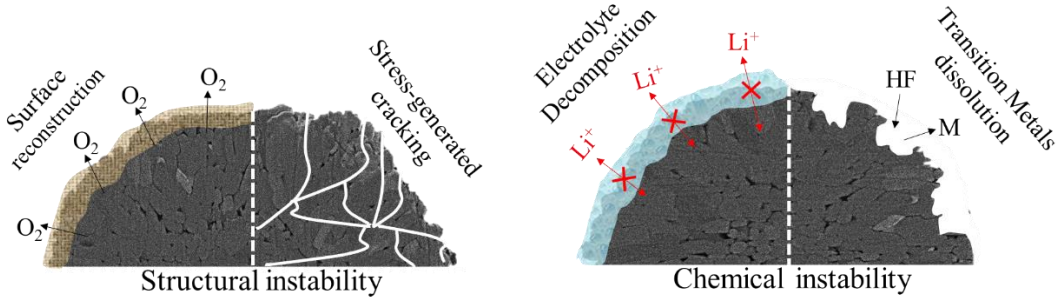

Figure 4: Schematic overview of the degradation mechanisms of cathode particles.

As schematically depicted in Fig. 4, aging of the cathode material during cycling arises at the atomic and micrometer scale, because of structural instabilities (surface reconstruction, stress-generated cracking) and chemical instability (electrolyte decomposition and transition metal dissolution). All these factors result in a poor C-rate and long-term cycling performance[73-78].

2.3.1 Surface Reconstruction

a) Layered $LiMeO_2$ (Me = Ni, Mn, Co)

As discussed before, $LiCoO_2$ (LCO) has been considered one of the most successful cathode materials for conventional LIBs. LCO has a layered structure and belongs to the rhombohedral space group $R\bar{3}m$ with edge-sharing CoO_6 octahedral, resulting in CoO_2 sheets.[79] The Li-ion sits in between the CoO_2 sheets. The electrochemical deintercalation

forms Li_xCO_2[80]. The theoretical capacity of LCO is 272 $mAhg^{-1}$ resulted from the complete removal of Li from LCO. However, in practical use only half of the theoretical capacity can be extracted, resulted in $Li_{0.5}CoO_2$ phase within a cut-off voltage of 4.5 V[80]. This is because LCO undergoes a phase transition (from layered to quasi-spinel structure) when more than half of the Li is extracted. This transition happens due to the migration of Co ion into the Li planes[81]. Dahn et. al. initially reported the low temperature (400 ^oC) synthesis of $Li_{1+y}Co_2O_4$ (also called QS-$LiCoO_2$) in $Fd\bar{3}m$ space group. The thermodynamic stability of this material is lower than for LCO[82]. In-depth studies of the two different LCO phases reveal that the QS-LCO phase has a much lower capacity and a much higher polarization as compared to layered LCO, thus making it an inferior cathode candidate[81]. X-ray absorption near-edge spectra (XANES) also confirm the existence of different intermediate phases between the layered and spinel structure because of higher oxidation states of spinel $LiCoO_2$.[83] Thackeray et. al. identifies this phase to be $Li_xCo_{1-x}[Co_2]O_4$[85]. The transformation of layered LCO into the spinel phase originates from the surface and extends to the complete bulk structure upon rigorous cycling when extending the voltage window or operating under high temperatures. Transmission electron microscopy (TEM) studies on the cycled LCO cathodes reveal internal strain and dislocations in the LCO lattice even at low long-term cycles, suggested that the accumulation of these defects is responsible for faster capacity fade[85,86]. A recent study on the post-heat treated LCO has shown that a thin spinel $Li_xCo_2O_4$ layer forms on the surface of LCO and improves the cycling performance significantly because of a higher conductivity of the spinel phase[87].

The attempt of doping the fundamental layered oxide has introduced various derivatives, which have been considered of remarkable value at present. Among them, $LiNi_xMnyCo_{1-x-y}O_2$ (NMC) and $LiNi_xCo_yAl_{1-x-y}O_2$ (NCA) are the most widely used and studied cathode materials for EVs and HEVs application. Higher achievable practical capacity along with a high operating voltage has made these cathode materials surpass many other cathode candidates[88-92].

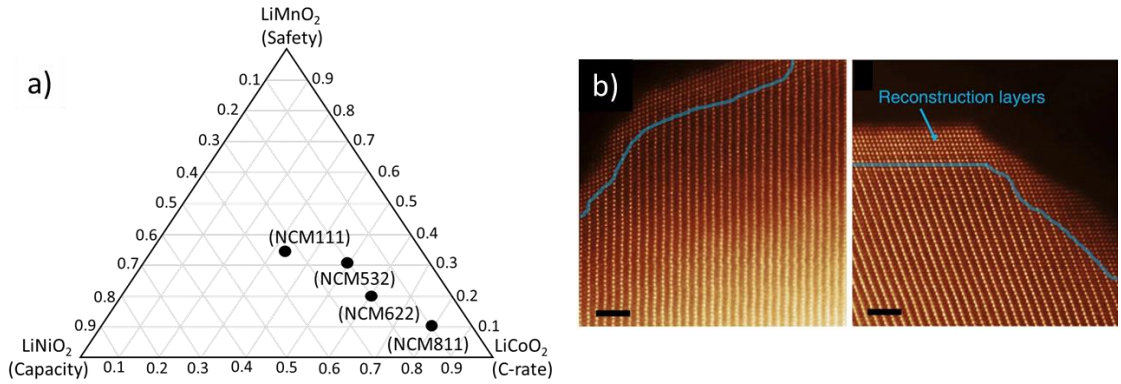

Figure 5: (a) Compositional phase diagram of $LiCoO_2$-$LiMnO_2$-$LiNiO_2$; (b) Reconstructed surface layer after 1st cycle of NCM (Reproduced from Ref. [89] with permission, copyright 2014 Nature Publishers).

Within the NCM layered cathodes, various NCM based cathodes (Fig. 5a) have been tested and proven to be beneficial for achieving higher capacity and longer cycle life. As it combines the rate capability performance of $LiCoO_2$, the capacity performance of $LiNiO_2$, and the safety performance of $LiMnO_2$. However, surface reconstruction upon

exposure to electrolyte has also been reported in these materials, as shown in Fig. 5b[89]. In order to produce high energy density cathode materials for EVs and HEVs, Ni-rich NCM based cathode with high achievable capacity has become a major focus in recent years. However, increasing the Ni-content in the material results in preparation difficulties and safety issues[67]. Due to similar ionic radii and charge states of Li^+ and Ni^{2+}, these cathodes are found to have a very high degree of interlayer cation mixing between Ni^{2+} and Li^+, resulting in strong phase transformation and capacity decay[93]. Various studies have shown that stabilizing the cathode surface of NCM is the prime key to improve the long-term electrochemical performance of NCM based cathodes[94,95].

b) Li-rich Layered $LiMeO_2$ (Me = Co, Mn, Ni)

Li-rich layered oxides are controversially discussed as either solid solution or nano-domains of $LiMeO_2$ (Me= Ni, Mn, Co, rhombohedral, $R\bar{3}m$) and Li_2MnO_3 (monoclinic, C2/m)[96]. The typical crystal structure of Li-rich layered NCM based materials is shown in Fig. 6a, Li^+ occupies part of the sites of the transition metals and results in an off-stoichiometric Li-content compared to conventional NCM based cathode materials. These kinds of materials have drawn much attention due to their very high achievable capacity (250 $mAhg^{-1}$) and wide voltage window[97]. Unlike other layered NCM based cathode materials, these types of materials show a rather abnormal voltage plateau around 4.5 V during the initial charging step, which is considered to be the limit of the final oxidation state of most other transition metals. Initially, the abnormal charge plateau has been considered arise due to the simultaneous removal of oxygen and lithium for the NCM lattice. However, Bruce et. al. proved by differential electrochemical mass spectrometry (DEMS) that there is indeed an O_2 release when this material is initially charged above 4.2 V. The Li^+ intercalation/deintercalation at different cut-off voltages for Li-rich NCM cathodes is shown in Fig. 6a[98]. As shown, when the cut-off voltage is kept 4.2 V, Li-rich NCM cathode just behaves like a conventional NCM, in which Li^+ is removed only from the Li layers. However, if the cut-off voltage is above 4.2 V (4.8 V), the Li^+ residing in the transition metal layer gets extracted facilitating the loss of O^{2-}. The O^{2-} is eventually oxidized to O_2 and is responsible for the 'abnormal voltage plateau'. The generated oxygen vacancies de-stabilize the transition metal ions (mostly Ni), resulting in inter-diffusion of the metal ions into the Li layer and the formation of a Li^+ blocking spinel phase takes place[99]. Yabuuchi et. al. investigated the surface behavior of these Li-rich layered NCM materials using X-ray absorption spectroscopy (XAS), X-ray photoelectron spectroscopy (XPS), X-ray diffraction (SXRD), and time-of-flight secondary ion mass spectroscopy (TOF-SIMS). They suggested that the release of O_2 facilitates the decomposition of the electrolyte at the surface at high operating voltage, resulting in the formation of an undesirable solid electrolyte interphase (SEI), a lower columbic efficiency and a higher impedance growth[100]. Furthermore, the O_2 release also increases the possibility of thermal runaway, leading to safety concerns regarding the battery.

Apart from the O_2 release, a severe voltage drop has also been reported in these kinds of cathode materials as shown in Fig. 6b[102]. The voltage drop is assumed to be the major factor hindering the commercialization of Li-rich NCM materials, as it results in a drop in the cell energy density. Gu et. al. investigated the phase distribution in $Li_{1.2}Ni0.2Mn_{0.6}O_2$ as shown in Fig. 6c[102,103]. They suggested that the distribution of Ni is rather inhomogeneous, which in turn indicates that there is phase segregation happening

during cycling. This results in poor C-rate performance and low capacity retention. The phase segregation at the surface of Li-rich NCM results in sluggish Li-ion diffusion, which in turn is responsible for the voltage decay during cycling. Therefore, several studies aiming to improve the voltage decay during cycling are mostly focussing on the suppression of the phase transformation on the surface of Li-rich NCM

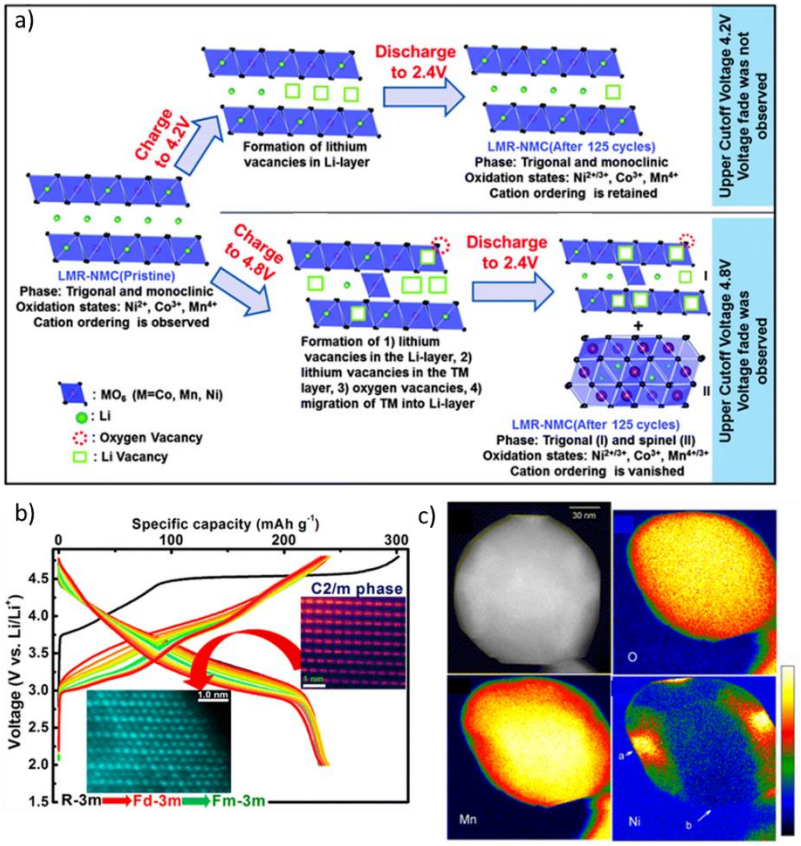

Figure 6: (a) Schematic illustration of phase changes occurring in NCM cathodes under different cut-off voltages (Reproduced from Ref. [98] with permission, copyright 2013 Royal Society of Chemistry). (b) Typical charge/discharge curves of NCM representing voltage decay (Reproduce from Ref. [101] with permission, copyright 201511 American Chemical Society). (c) XEDS maps showing the non-uniform distribution of elements after cycling in NCM particle (Reproduced from Ref. [102] with permission, copyright 2013 American Chemical Society).

c) Spinel $LiMn_2O_4$

The spinel-type $LiMn_2O_4$ cathode materials belong to the space group of $Fd\bar{3}m$, where Mn has an average valence of 3.5, indicating the coexisting Mn^{3+} and Mn^{4+}.[104] However, the $Mn^{3+/4+}$ equilibrium is easily broken by Li^+ intercalation/deintercalation or by changing the temperature, which causes a Jahn-Teller distortion of Mn^{3+} at octahedral sites. The Jahn-Teller distortion starts at 4.0 V, which is regarded as the main cause for the capacity loss[105]. Structural characterization of $LiMn_2O_4$ suggests that the net valence differs between surface and bulk, which arises due to the presence of high Mn^{3+} amount at the surface caused by a non-equipoised dynamic of Li^+ insertion/extraction at the surface. This valence difference results in the formation of $Li_2Mn_2O_4$, which is suggested to be less electrochemically reactive[106,107]. However, the phase transition from cubic to

tetragonal is postulated to create a phase boundary towards the particle surface and prevents Li^+ diffusion. Various doping strategies have been applied to the spinel $LiMn_2O_4$ cathode material in order to suppress the Jahn-Teller distortion[108]. Among all, doping $LiMn_2O_4$ with Ni in order to form $LiNi_{0.5}Mn_{1.5}O_4$ has been the most successful approach, due to the disappearance of Mn^{3+} and electrochemical reactivity of Ni^{2+}. In addition, the incorporation of Ni provides two voltage plateaus (Ni^{2+}/Ni^{3+}, $Ni^{3+/}Ni^{4+}$) at around 4.7V, making it one of the most promising high voltage cathode materials[109].

2.3.2 Stress-generated Cracking

Cathode materials also suffer from crack formation during cycling at high C-rates, where the Li^+ does not have enough time to diffuse homogeneously. This leads to additional stress in the particles[110,111]. The internal stress of the cathode material during synthesis and also due to phase transformation (such as Jahn-Teller distortion, O_2 release) can lead to the formation of cracks[112]. Additionally, it can result in contact loss from the binder or conductive carbon. This results in the formation of gaps in the electrode. Moreover, the formation of cracks in cathode materials can deteriorate the contact between the parts of cathode and the electrolyte, which can lead to an increase in cell impedance and ultimately to battery failure. As shown in Fig 7, Miller et. al. has demonstrated the crack formation and separation of the cathode particle from the electrolyte after cycling. In addition, they have shown that the crack formation takes place even during the first cycle, indicating that the prevention of crack formation is of high importance for the commercialization of next-generation cathode materials[113].

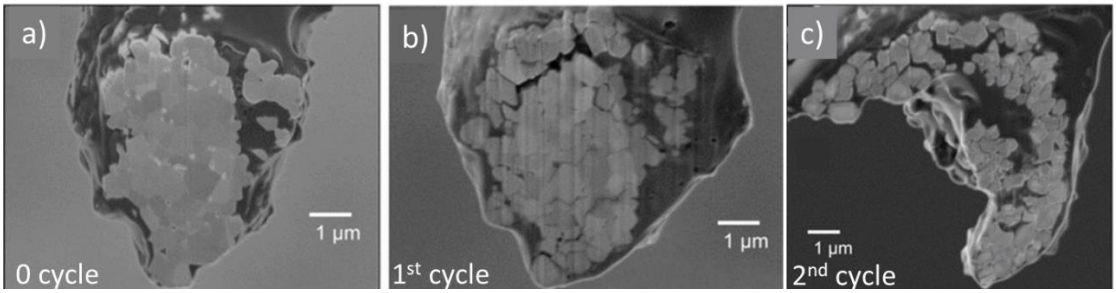

Figure 7: SEM micrographs showing particle cracking in NCA cathode particles after (a) 0, (b) 1st, (c) 2nd cycles (Reproduced from Ref. [113] with permission, copyright WILEY-VCH 2013).

2.3.3 Electrolyte Decomposition and Transition Metal Dissolution

a) Electrolyte Decomposition

Electrolytes for next-generation LIBs are generally liquids or solids with high ionic conductivity (10^{-4} S/cm) and low electronic conductivity (10^{-10} S/cm)[8]. Organic esters, including ethylene carbonate (EC), diethylene carbonate (DEC), propylene carbonate (PC), ethylmethyl carbonate (EMC), and dimethylene carbonate (DMC) are most widely used as solvents to dissolve the most common Li-salt $LiPF_6$ currently used in commercial liquid electrolytes[114,115]. The electrochemical operating voltage window of these electrolytes mostly lies between 1 - 4.7 V vs Li/Li^+. Therefore, any cathode material, which has cut-off voltage over 4.7 V unavoidably involves the oxidative decomposition of these electrolytes[116,117]. Due to the decomposition of the electrolytes the formation of

a passivating SEI layer (containing inorganic salts such as Li_2CO_3, LiF, and organic species like poly(ethylene carbonate)) at the surface of the cathode materials takes place. In addition, due to the oxidative nature of the cathode material itself, the decomposition of the electrolyte also results in gas evolution (such as CO_2, O_2)[50,118-122]. The formed SEI layer at the surface of the cathode is a poor Li^+ conductor causing irreversible capacity loss during cycling and poor cycling performance of the LIB.

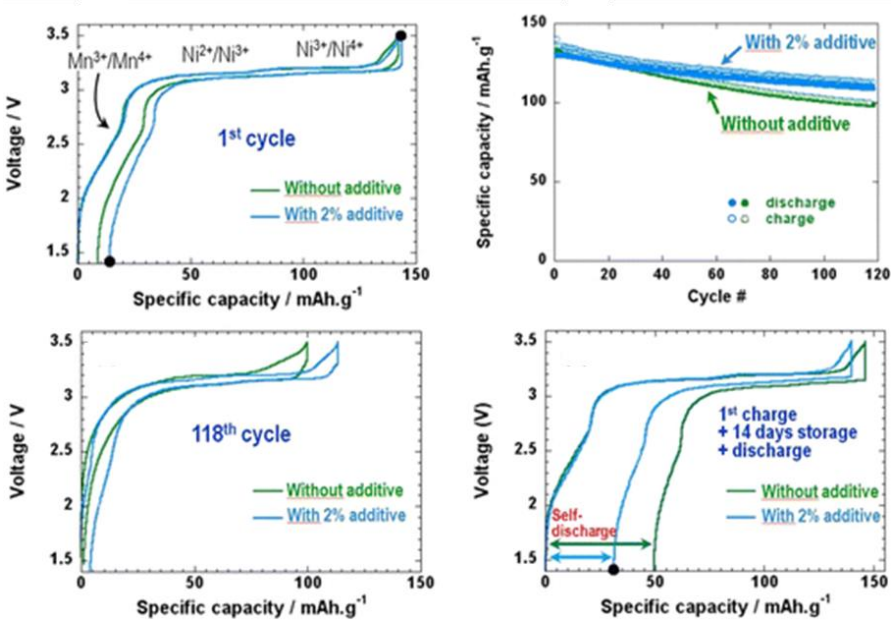

Figure 8: Comparison of the electrochemical behavior of LNM/LTO cells cycled with and without electrolyte additives (Reproduced from Ref. [124] with permission, copyright WILEY-VCH 2013).

The capacity consumption during the electrolyte decomposition for the formation of SEI is unfavorable for the battery performance, and the oxidation of the electrolyte at the cathode surface requires continuous electron transfer[8,123]. However, the SEI layer being electronically insulating commonly prevents further decomposition of the electrolyte. Thus, an SEI layer with a certain thickness and stability is considered to be necessary for an optimal battery performance[114]. Initially, sacrificial electrolyte additives have been added. These additives act as moderator of the electrolyte decomposition and in turn stabilizes the SEI as shown in Fig. 8[124]. Many suitable electrolyte additives have been reported, such as lithium bos(oxalato) borate (LiBOB), glutaric anhydride, 2,5-dihydrofuran, γ- butyrolactone, 2-(Pentafluorophenyl)-tetrafluoro-1,3,2-benzodioxaborole, 1,1-Difluoro-1- alkenes etc. They have found to improve the stability of the SEI layer[124-128]. The problems associated with the SEI formation and the positive effect of electrolyte additives on the electrochemical performance have motivated scientists to develop an artificial SEI on the surface of cathode employing surface coatings.

b) Transition Metal Dissolution

The electrolyte decomposition at the cathode surface not only affects the electrolyte but also the cathode itself. Practically, there is always moisture present either on the surface of the cathode or in the electrolyte. During the electrolyte decomposition on the cathode

surface LiF and PF_5 are formed, which is mostly followed by the hydrolysis of PF_5: $PF_5 + H_2O \rightarrow POF_3 + 2HF$, as suggested by Aurbach and Heiders's theory[129]. Thus, HF is produced from hydrolysis and is inherently present in the electrolyte. It triggers additional unwanted side reactions at the cathode surface[114,130]. Taking the example of $LiMn_2O_4$, it has been demonstrated that cathode materials with higher Mn content suffer from a high degree of manganese dissolution from the cathode into the electrolyte[131,132]. Mn^{3+} undergoes a disproportionation reaction, $2Mn^{3+} \rightarrow Mn^{2+} + Mn^{4+}$ at the cathode surface. Among the products, Mn^{4+} remains in the cathode material while Mn^{2+} dissolves in the electrolyte. Aoshima et. al. found that the dissolved Mn^{2+} tends to form a layer of MnF_2 and ramsdellite-$Li_{0.5}MnO_2$ on the cathode surface. Metallic Mn is found on the anode surface. They concluded that this synergetic degradation of the cathode and anode is responsible for a faster capacity fading[133]. Later Kanno et.al. found that the Mn dissolution also depends on the crystal plane of the cathode exposed to the electrolyte, i.e. (110) plane are less stable as compared to (111) plane. The negative effect of the Mn dissolution not only affects the performance of the cathode but also involves the degradation of the anode material[130]. Zahn et. al. showed an improvement in cycling performance for surface-modified $LiMn_2O_4$ cathode as compared to bare-$LiMn_2O_4$ (Fig. 9), which is attributed to a reduction of metal dissolution. They also proposed an 'ion-exchange model' in order to explain the reaction of dissolved Mn taking place at the anode surface as shown in Fig. 9. It has been proposed that Mn reacts with the formed SEI layer and changes its composition by exchanging the Li^+ in the SEI layer. As the SEI layer becomes rich in the Mn, it blocks the Li^+ diffusion pathways, which results in an impedance growth[134]. Thus, strategies to prevent transition metal dissolution via surface modifications are very crucial for developing next-generation cathode materials.

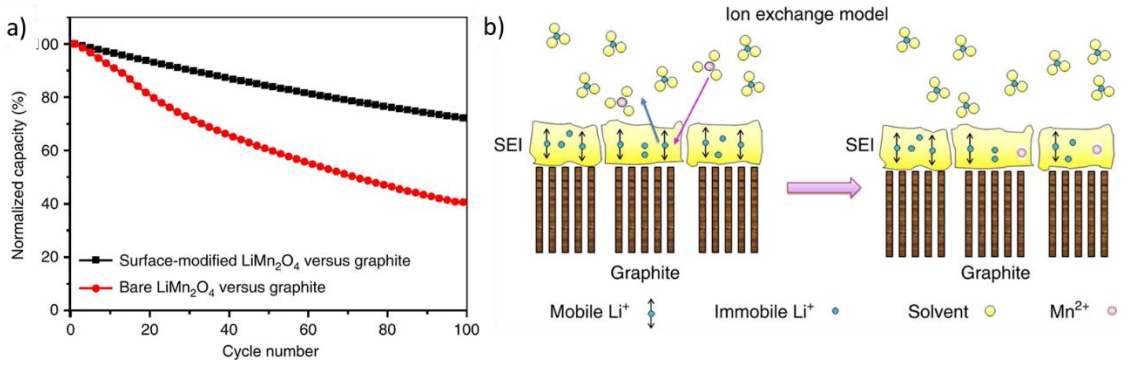

Figure 9: (a) Comparison of the electrochemical behavior of LMO with and without surface modification. (b) Schematic illustration of the Mn-Li exchange model mechanism for the deposition of Mn on graphite in a graphite/LMO cell (Reproduced from Ref. [134] with permission, Copyright 2013 Nature Publishers).

2.4 Surface Modification — Role and Characteristics

2.4.1 Preventing Phase Transitions

Surface modification of NCM based cathodes is performed mostly either by surface doping or surface coating. Both of these modification methods have their own advantages and disadvantages. Over the past decades, surface doping of the cathode particle has been extensively studied in order to control the phase transition at the cathode surface during cycling or to increase the Li^+ diffusivity within the cathode particle. For bulk doping,

mostly elements like Al, Zr, or Ti have been used, which are normally electrochemically inactive. In order to minimize the loss in capacity, doping with these elements has been restricted to the surface only. Several studies have been done to investigate the impact of doping of LCO based cathode materials with Al, Zr and Sn. In the early studies, Cho et. al. suggested that doping the LCO surface with Al results in only small change in the LCO structure during first cycle as compared pristine LCO thus resulted in better cycling performance. A similar observation was found for Zr doped LCO[135-137]. However, later Dahn et. al. found no structural difference in Zr doped LCO as compared to pristine LCO after cycling, contradicting the observation by Cho et. al.[138,139]. Therefore, many rigorous studies on how doping of the cathode materials helps to prevent the phase transition are still needed. In a recent study, Cho et. al. was able to force Ni^{2+} to reside in the Li slabs at the surface of $LiNi_{0.62}Co_{0.14}Mn_{0.24}O_2$. The material was found to show exceptional structural stability especially at elevated temperatures[140]. Similarly, Cabana et. al. doped $LiMn_2O_4$ with Al_2O_3 at the surface and found that on the surface of $LiMn_2O_4$ an epitaxially grown Mn^{3+}-depleted phase was formed, where Mn^{3+} has been replaced by non-soluble Al^{3+} as shown in Fig. 10a, b[141]. The incorporation of Al^{3+} on the surface of $LiMn_2O_4$ was found to significantly reduce the risk of surface reconstruction during cycling, which in turn results in much better cycling performance. This observation was later supported by Amine et. al[142].

When a phase transition is caused by Jahn-teller distortion, surface doping strategies mostly seem to be promising in improving the performance of the cathode material. Taking the example of $LiMn_2O_4$, the Jahn-Teller distortion is found to be most intense near the surface where the Li^+ diffusion always disrupts charge equilibrium. Taking this effect into consideration, many scientists suggested that modifying the surface of $LiMn_2O_4$ to replace some part of Jahn-Teller active ions might help to improve the performance at the expense of minimal capacity loss[143]. Xiong et. al. first coated $LiMn_2O_4$ with Al_2O_3 and subjected the coated particle to annealing. They found that some part of Al has been incorporated into the $LiMn_2O_4$ which helped in the suppression of Jahn-Teller distortion at the surface. In addition, the coating helps to prevent the electrolyte to react with the surface and in turn, prevents Mn dissolution[144].

Surface doping of the cathode material has also proven to be beneficial for the suppression of O_2 evolution in Li-rich cathodes. It is well known that the release of O_2 from the Li-rich cathodes results in simultaneous leaching of Li_2O. Park et. al. showed that the incorporation of heteroatoms (such as Al) into the surface layer is responsible for extra stress at the Li-rich cathode surface and in turn, affects the cycling behavior as shown in Fig. 10c[145]. They deposited a layer of Al_2O_3 or $AlPO_4$ on the surface of Li-rich $Li[Li_{0.167}Ni_{0.233}Co_{0.100}Mn_{0.467}Mo_{0.0333}]O_2$, followed by heat treatment of the cathode material resulting in the diffusion of Al into the surface lattice. During the electrochemical measurement, they measured the pressure change during cycling. They found that the pressure inside the cell dropped noticeably for the doped cathode due to the suppression of O_2 release. They suggest that the diffused Al bonds strongly with the O present close to the surface and that smaller domains of $LiMn_2O_3$ have been created simultaneously.

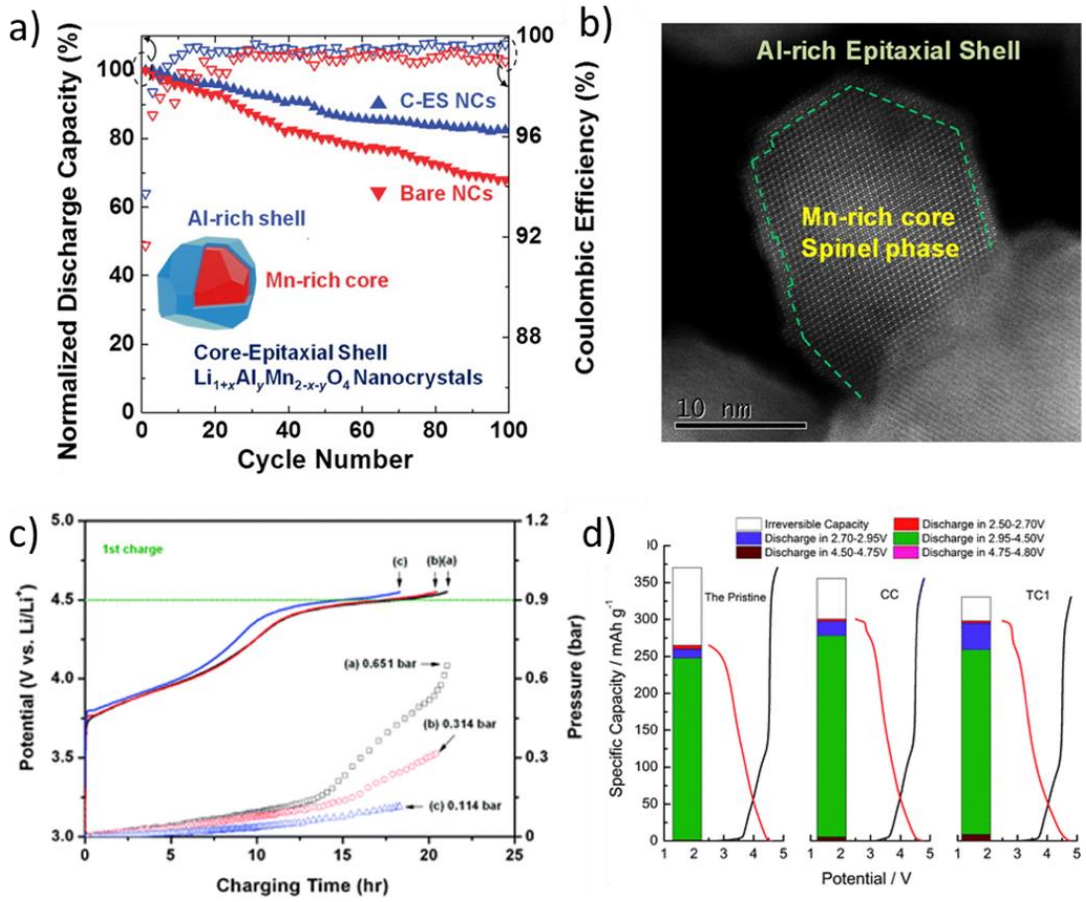

Figure 10: (a) Stability test of bare $LiMn_2O_4$ and Al-modified $LiMn_2O_4$ under 55 ^oC. (b) High-resolution HAADF image indicating an Al-rich surface on the $LiMn_2O_4$ nanoparticle (Reproduced from Ref. [141] with permission, copyright 2014 American Chemical Society). (c) In situ pressure profiles for pristine and modified $Li[Li_{0.167}Ni_{0.233}Co_{0.100}Mn_{0.467}Mo_{0.033}]O_2$ during the first charge (CC mode) (Reproduced from Ref. [145] with permission, copyright 2014 American Chemical Society). (d) Initial charge/discharge performance of the pristine and modified samples (Reproduced from Ref. [146] with permission, copyright 2014 American Chemical Society).

Previous doping strategies have mostly focussed on the diffusion of metal ions into the bulk or the surface of the cathode material. Another possible consequence of annealing is the diffusion of surface Li or transition metals inside the coating layer to form a second phase inside the coating layer. This possibility has been initially reported by Wu. et. al. (Fig. 10d)[146]. They report an improvement in the electrochemical performance of MnO_x coated $Li[Ni_{0.2}Li_{0.2}Mn_{0.6}]O_2$ after post heat treatment. The improvement in the performance is associated with the generation of Li vacancies on the surface of the cathode due to Li diffusion into the coating layer. The lithium-depleted surface results in oxygen depletion and in turn decrease the chance of O_2 evolution. Furthermore, the doped coating layer is expected to facilitate a better Li-ion diffusion. Similar results have been reported by Hahn et. al. They studied the effect of temperature on Al_2O_3 coated Ni-rich NCM based cathodes and concluded that high-temperature annealing results in the migration of Li inside the Al_2O_3 layer, which leads to the formation of an $Al_2O_3/LiAlO_2$ coating layer[147].

Unlike surface doping, the effect of surface coatings on the phase transition of cathode materials is still under debate. In general, the phase transformation at the surface caused by cation disorder is an intrinsic property of the cathode. Therefore large parts of the scientific community consider that coating of the cathode surface is not effective to suppress phase transitions during electrochemical cycling[148]. However, an AlF_3 coating is among the few materials, which is reported to be effectively preventing the phase transition in Li-rich cathode as it improves the structural stability[149]. Although Al_2O_3 based coatings are one of the most applied and studied coating materials for cathodes, their effectiveness towards the suppression of phase transitions during cycling is still debatable[150-153].

Recently, Wang et. al. used STEM-EELS measurements to visualize the suppression of a phase transition in Al_2O_3 coated $Li_{1.2}Ni_{0.2}Mn_{0.6}O_2$ during cycling as shown in Fig. 11a[154]. It can be seen; the uncoated cathode particle shows a drop of the Mn valence at the surface only after 40 charge/discharge cycles. In contrast, the coated particle shows a rather stable composition after the same number of cycles. In addition, severe surface reconstruction is found for the uncoated particles after cycling, which is not observed for the coated particles. This results in an improved electrochemical performance as shown in Fig.11b. the results further reveal that the effect of surface coating on the suppression of surface phase transition is rather complex and thus more research regarding this topic is required.

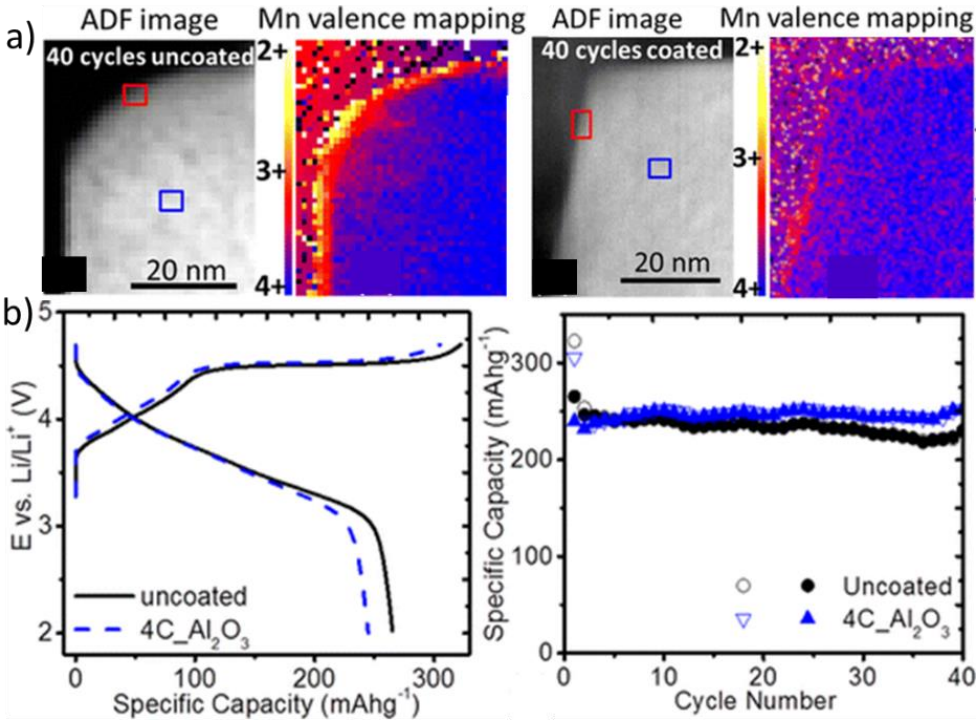

Figure 11: (a) STEM-EELS study of pristine and Al_2O_3 coated LNMO and corresponding lattice images after cycling. (b) Charge/discharge and long-term cycling performance of pristine and Al_2O_3 coated LNMO (Reproduced from Ref. [154] with permission, copyright 2016 American Chemical Society).

2.4.2 Preventing Crack Formation

There are several reports focussing on the suppression of the crack formation in the anode but less work has been done regarding the cathode materials. Surface modifications to

prevent crack formation should be able to accommodate the particle strain generated during electrochemical cycling. Some specific oxide coatings (Al_2O_3 and AlF_3) have been investigated regarding this aspect and have been found to be effective to some extent[155-157]. However, as these coating materials are brittle in nature, particle cracking might also result in the peeling of coating during cycling, which leads to worse cycling performance. Taking these issues into consideration, polymer-based coating materials have been proposed. However, these polymer-based coatings have a low operating voltage window, which needs to be addressed for the successful implication of these coatings on cathode materials[158,159]. Moreover, the phase transition is also the main cause of particle cracking. Thus, the strategies discussed in the previous section might also be helpful in suppressing crack formation.

2.4.3 Surface Modification Acting as HF Scavenger

Using a surface modification of cathode materials for HF scavenging is a very common approach, as HF formation always happens on the NCM surface or inside the electrolyte. Mostly, metal oxide-based coatings are applied on the cathode surface in order to neutralize the generated HF inside the electrolyte according to the following reactions[160-164]:

$$Al_2O_3 + 6HF \rightarrow 2AlF_3 + 3H_2O$$

$$TiO_2 + 4HF \rightarrow TiF_4 + 4H_2O$$

$$ZrO_2 + 4HF \rightarrow ZrF_4 + 4H_2O$$

$$ZnO + 2HF \rightarrow ZnF_2 + H_2O$$

$$MgO + 2HF \rightarrow MgO + H_2O$$

The metal fluorides formed during these reactions are more stable in non-aqueous electrolytes, which in turn prevents the cathode surface from further degradation if the metal oxide layer is completely consumed during extensive cycling. Therefore, direct use of these metal fluorides as a coating layer has also been reported. In addition, HF generation is also found to be the cause of metal dissolutions. As discussed before, transition metal reduction (in particular Mn) is the main cause of metal dissolution[165-168]. Several studies have shown that surface coatings of different metal oxides ($LiTaO_3$, Al_2O_3) apparently suppress the dissolution of transition metals during extensive cycling. Wu et. al. has reported that a pre-lithiation method enables manual reduction of the electrolyte during charging results in the generation of a more stable solid electrolyte interface (SEI) layer resulting in better electrochemical performance. Therefore, surface modifications are effective against HF scavenging and ultimately reduces metal ion dissolution[169].

2.4.4 Acting as Metal-Oxygen Bond Stabilizer

The transition metal dissolution mainly originates from the breaking of metal-oxygen bonds close to the cathode surface. Thus, stabilizing and strengthening the metal-oxygen bonds can be helpful in improving the cycling performance. Surface modifications using coatings prevent the direct physical contact between cathode and electrolyte and in turn are helpful in preventing metal-ion dissolution. The main concern with surface coatings

is the restriction of electronic and ionic charge diffusion during the cycling. This can be improved by lithiation of the coating layer, which commonly enhances the ion diffusion inside the coating layer. Successful efforts have been made towards modifying the cathode surface via doping, which can deal with the above-mentioned problems. However, doping of the cathode material also raises concerns regarding the loss of active components in the cathode material, which in turn compromises the practical achievable capacity. Surface doping of cathode materials is beneficial in two aspects regarding the suppression of metal dissolution. Firstly, stabilizes the metal-oxygen bond and secondly, minimizes the amount of susceptible metal ions close to the surface without affecting the cathode's structural integrity. Cabana et. al. has systematically studied the role of Mg doping on $LiNi_{0.5}Mn_{1.5}O_4$ based cathode materials[170]. They found that charging the cell to very high voltage (5 V) results in intensive chemical changes of the pristine cathode because the Ni-O bonds in the cathode materials are highly oxidized. They become unstable making them very susceptible to electrolyte-based reduction. However, Mg-doped cathode results in much robust Ni-O bonds at the surface, which in turn prevents severe electrolyte-assisted reduction of the cathode during intensive cycling. As stated above, surface doping also causes a replacement of soluble metal ions from the surface of the cathode. Daheron et. al. doped LCO based cathode materials with Al in order to form a $LiCo_{1-x}Al_xO_2$ solid solution on the surface of LCO. They tracked the surface acid-base properties of $LiCo_{1-x}Al_xO_2$ while changing the value of *x* using XPS[171]. They found that the surface basicity drops significantly when Al is doped inside LCO and suggests that less basicity makes the doped LCO less susceptible to HF, in turn improves the electrochemical performance.

2.4.5 Acting as Electronic/Ionic Conductivity Enhancer

Surface coatings usually do not change the inherent electronic/ionic conductivity of the cathode material itself. However, it can provide a conductive network among the individual cathode particles in order to maximize the utilization of cathode material. The function of coatings as an electronic/ionic enhancer totally depends on the properties of the coating material along with the way they are deposited.

a) In-situ Deposition of Electronic/Ionic Conductivity Enhancing Coating

This paragraph discusses the coating materials having intrinsic electronic/ionic conductivity. Metals like Al, Ag, and Cu have been extensively studied as coating materials. However, due to their high costs along with non-homogenous coverage and acidic nature of the electrolyte (which can dissolve the metal), they are not considered to be effective coating material[172,173]. Similarly, metal compounds such as TiN, RuO_2 and TiO_2 have also been considered as coating materials due to their considerable electronic conductivity[174,175]. Wang et. al. reported the deposition of rutile TiO_2 on the cathode surface, which enhances the electronic conductivity and in turn improves the electrochemical performance[176].

On the other hand, growing the conductive polymer coatings on the surface of cathode material have been widely studied and reported. These kinds of polymers include polypropylene (PPy), polyaniline (PANi), polythiophene (PT) and poly(3,4-ethylenedioxythiophene) (PEDOT). The beneficial effect of in-situ grown polymer-based coatings is that the monomer units can easily be nucleated on the cathode surface. The

polymerization is achieved with the help of catalyst resulting in a very uniform coating[177, 178-180].

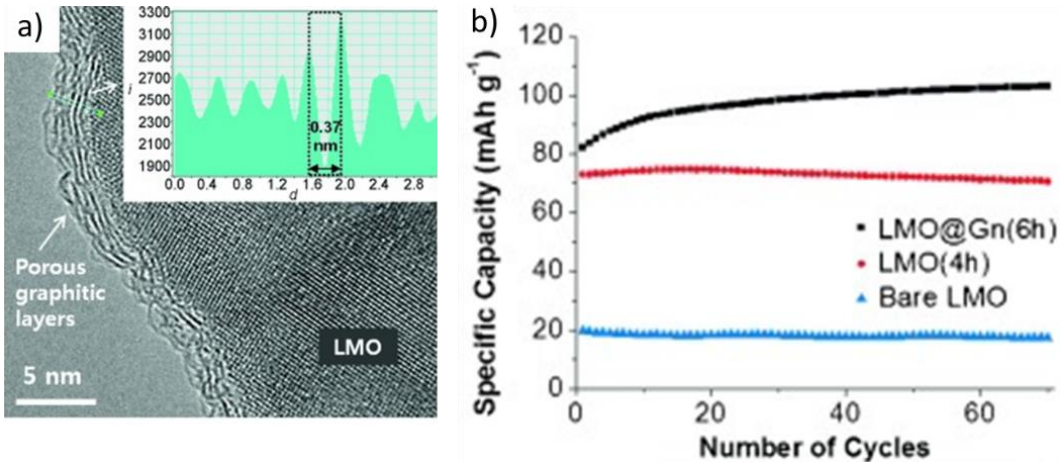

Figure 12: (a) TEM micrograph of porous graphite coating of LMO. (b) Comparison of the long-term cycling performance of pristine and coated LMO (Reproduced from Ref. [182], copyright 2014 Wiley-VCH).

Alternatively, carbon-based materials (such as graphite, graphene, carbon nanotubes (CNTs) and amorphous carbon) have been used to form composite [181-184]. These carbon-based materials specifically help to build a three-dimensional electronically conductive network around the cathode active material. Taking this idea, Song et. al. has coated very thin layers of porous graphite on the surface of $LiMn_2O_4$ via high-speed ball milling method. They found an improvement in the achievable capacity accompanied by better performance, as shown in Fig. 12. Furthermore, researchers have also developed hybrid coatings (composite coatings containing both electronic and ionic conductors)[185]. In addition, the use of Li^+ conducting coatings has also been reported, as they facilitate Li-ion transport across the cathode surface.

b) Depositing Electronic/Ionic Conductor via Post-treatment

The pyrolysis of carbon-based materials via solid-state methods or chemical vapor deposition on the cathode surface has proven to be beneficial for improving the electrochemical performance of cathode materials. This holds in particular for those, which have low intrinsic electronic conductivity, such as $LiMnPO_4$ and $LiFePO_4$, as they are resistant to reduction during pyrolysis[186]. However, carbon coatings for $LiMO_x$ (M= Ni, Mn, Co, etc.) are rather hard to achieve as they easily oxidize under high-temperature treatment, which might deteriorate the electrochemical performance. Nevertheless, many researchers are testing carbon coatings on these materials deposited at low temperatures (350 ^oC) in air. The suitability of this approach is still debatable[185,187-189]. There are extensive reports on doping the surface coating in order to enhance the surface conductivity. Manthiram et. al. reported for NCM based cathodes that Al_2O_3 coating followed by thermal treatment results in interaction between NCM and Al_2O_3 forming $LiAlO_2$ on the surface. As $LiAlO_2$ is a good Li^+ conductor, the thermal treatment, in turn, improves the long-term cycling performance[191].

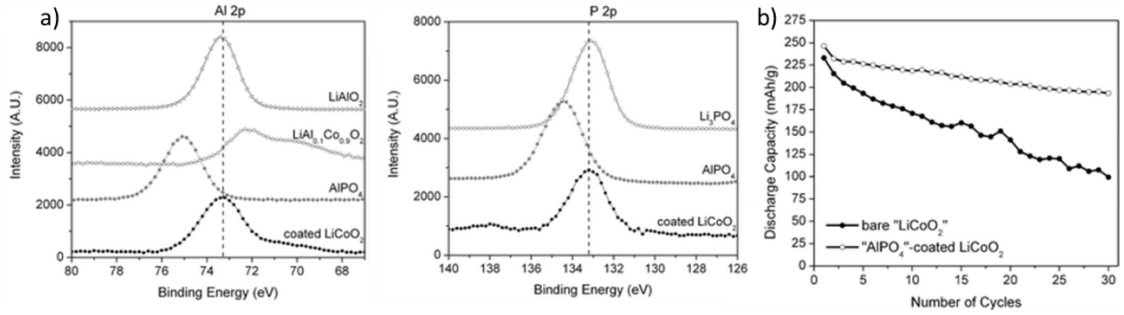

Figure 13: (a) Comparison of XPS spectra of the Al 2p and P 2p peak of $AlPO_4$ coated LCO. (b) Comparison of the long-term cycling performance of pristine and coated LCO (Reproduced from Ref. [190] Copyright 2007 American Chemical Society).

Similarly, Zhang et. al. reported the formation of Li_2ZrO_3 after annealing ZrO_2 coated NCM cathodes, which shows an improved electrochemical performance[192]. In a more complicated study, Yang et. al. coated $AlPO_4$ on LCO followed by heat treatment. They found that the Li_2CO_3 present on the surface of LCO reacts with $AlPO_4$ forming $LiCo_{1-y}Al_yO_2$ in the cathode and Li_3PO_4 in the coating layer. This conversion between the LCO surface and the coating layer results in an improved electrochemical performance as shown in Fig. 13[190].

c) Formation of Electronic/Ionic Conducting Coatings via Lithiation/delithiation

Surface coating materials have been found to turn into good Li^+ conductors during cycling due to the accommodation of Li^+ in the coating layer during reversible lithiation/delithiataion. For instance, Ta_2O_5 undergoes the following structural changes during cycling:

$$Ta_2O_5 + 10Li^+ + 10e^- \rightarrow 2Ta^{5+} + 5Li_2O$$

$$Li_2O + Ta_2O_5 \rightarrow 2LiTaO_3$$

The formation of $LiTaO_3$ during cycling improves the cycling performance of the cathode material. Wagemaker et. al. has theoretically calculated the formation of $LiTiO_2$ from TiO_2 during cycling. They predict better conductivity of $LiTiO_2$ as compared to TiO_2 and suggests this to be helpful in improving the electrochemical performance[193].

In order to theoretically predict the criteria for coating materials, Wolverton et. al. has calculated the thermodynamics of the reactions of the most common coating materials, such as metal oxides and fluorides[194]. By assuming the following conversion reactions:

$$M_xO_{1/2} + Li \rightarrow xM + 1/2Li_2O$$

$$M_xF + Li \rightarrow xM + LiF$$

They calculated the density function theory (DFT) voltages of oxide/fluorides with the experimental voltages, as shown in Fig. 14.

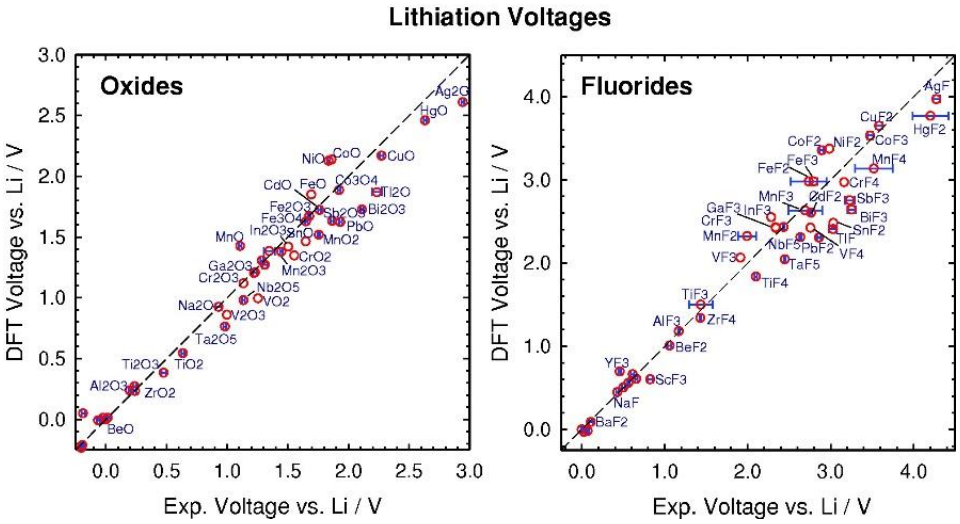

Figure 14: Calculated average voltages for oxides and fluorides versus voltages estimated from experimental formation enthalpies (Reproduced from Ref. [194] with permission, copyright 2014 Wiley-VCH).

They suggested that the higher the lithiation voltage, the more likely the lithiation of the coating takes place during electrochemical cycling. They report that fluorides-based coating materials generally have higher lithiation voltage as compared to oxides, because of their higher electronegativity. The chart presented in Fig. 14 is considered as an important support for selecting coating materials in terms of in-situ lithiation during electrochemical cycling.

2.5 Methods of Surface Modification

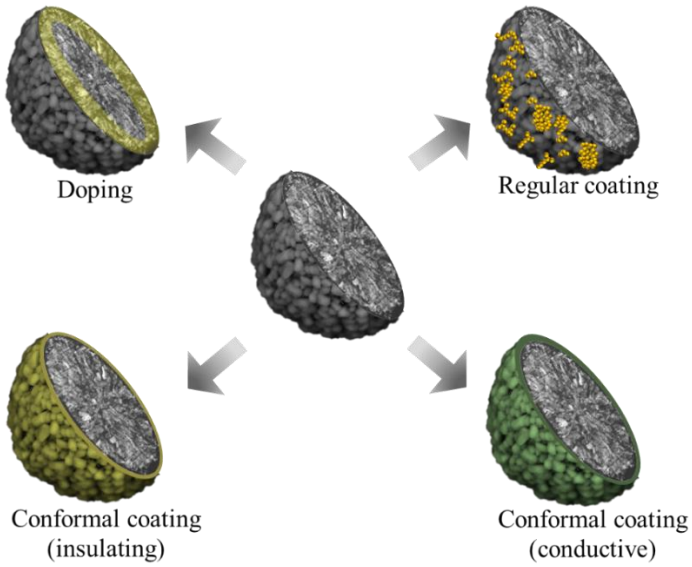

Figure 15: Schematic representation of possible ways of surface modification.

Different methods of surface modification approaches are summarized in Fig 15. The surface modification methods have been extensively studied in the literature. Defining an ideal modification method is difficult as the appropriate modification method significantly depends on the issues that need to be addressed. Surface doping of the

cathode can suppress the phase transition and can decrease metal-ion dissolution, but it is more restricted to a selection of the doping element as well as the extent of doping. Regular surface coating is effective against the suppression of metal-ion dissolution, decomposition of the electrolyte and acts as an HF scavenger. But the coating methods often produce an inhomogeneous coating on the surface of the cathode. Which is not highly effective in preventing the HF attack and the phase transition. Thus, conformal coatings are necessary to protect the cathode surface in a controlled manner from mostly all above-mentioned issues. However, the hermetic nature of insulating coating layers can prohibit electron and ion diffusion, resulting in a worse cathode performance. These issues of conformal coatings can be solved by either converting the insulating coating into conductive coating or by applying a conductive conformal coating in the first place.

2.5.1 Doping

Doping of cathodes is considered one of the most effective methods to improve the electrochemical performance of the LIB, depending on the properties of the doping elements[192-202]. Mostly, metal cations or non-metal anions have been doped into the bulk phase of cathodes with a very low percentage (usually < 5 wt.%). Generally, doping improves the following properties of the cathodes: (1) Doping significantly improves the electronic conductivity and enhances the Li^+ conductivity within the cathodes, resulting in improved C-rate performance. (2) Doping reduces the Li/Ni disorder in Ni-rich cathodes, resulting in the stabilization of the crystal structure during prolonged cycling. (3) Doping minimizes the volume change within the cathode during charge/discharge cycles. (4) Phase transformation of the cathode at higher voltages due to oxygen loss can be prevented by the incorporation of doping elements[21,200-209].

Cation dopants such as Al, Mg, Nb, Si, Zr, Ti, and Ca, are the most common doping elements for Ni-rich cathodes[210-219.] Since Ni/Li cation mixing is more common in Ni-rich cathodes, Ni is mostly substituted by cation dopants. However, as these doping elements are electrochemically inactive, the doping results in a lower achievable capacity with increasing doping amount. Therefore, introduction of doping elements in cathode results in a trade-off between capacity and stability[196,211,213,219].

Anion doping of cathodes is less common and only a few anion dopants have been tested. The most common anion dopants, such as fluorine, chlorine, and sulfur, results in improved electrochemical performance of Ni-rich cathodes, because of the similar atomic radii with oxygen[220-224]. However, the impact of anion doping on the improvement of the electrochemical performance of the cathodes is still controversially discussed[225.]

2.5.2 Surface Coating

Surface coating of the cathodes is found to be a very effective approach to improve the electrochemical performance of LIBs. Several factors such as C-rate capability, long-term stability, material conductivity, or structural stability can be significantly improved via surface coatings[16,226-228]. Surface coatings play various roles on the surface of the cathode in order to improve performance. (1) The surface coating layer acts as a direct physical barrier between the cathode and the electrolyte, preventing parasitic side reactions between cathode and electrolyte. (2) The surface coating layer can effectively prevent the cathode from HF attack, resulting in prevention of transition metal ions dissolution. (3)

The coating can reduce crack formation by accommodating the volume expansion during cycling. (4) Conductive coating layers can improve the ionic and electronic transports properties of the cathode, resulting in reduced cell polarization. Surface modification of the cathode via coating has been widely accepted and employed in next-generation Ni-rich cathodes in order to meet the demand of next-generation LIBs[194,229-231]. However, there is still a need to find a simple, easy, cost-effective coating method in order to fully commercialize Ni-rich NCM based cathodes for next-generation applications.

2.6 Methods of Coating

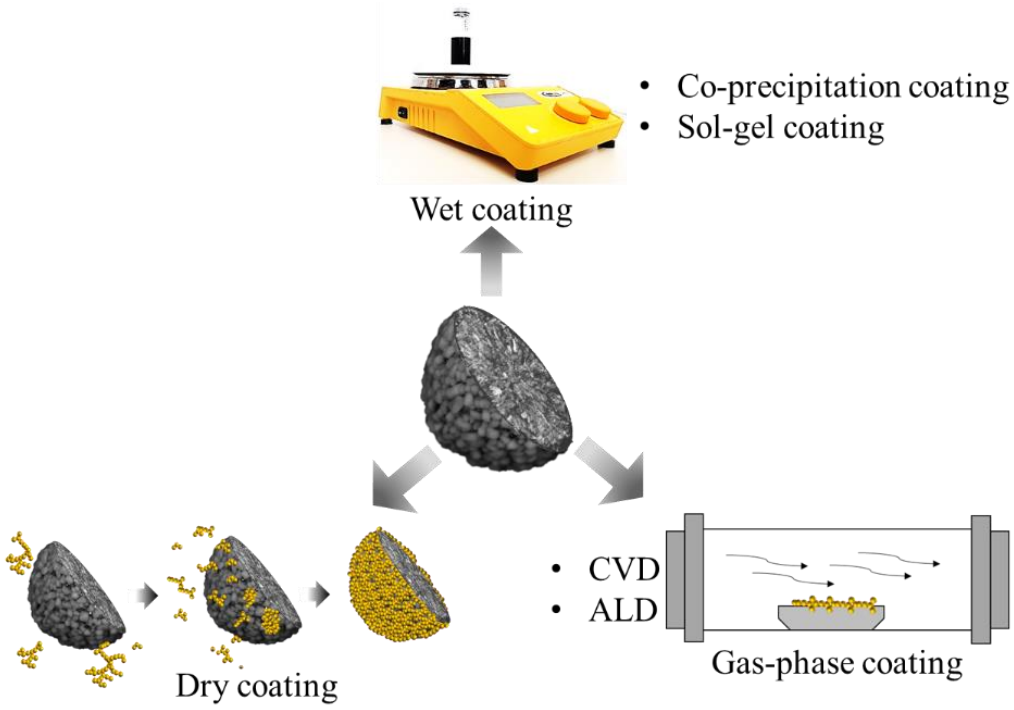

Figure 16: Overview of surface coating methods for cathode particles.

The electrochemical performance of the cathode material can vary significantly depending on the coating method, suggesting that the coating method itself has a significant influence on the cathode properties[16,226,229]. The influence of the coating method on the cathode performance can be due to the following reasons:

I. For the same coating material, different coating methods can result in a different coating microstructure on the cathode surface, which can lead to differences in Li^+ transport properties through the coating layer.
II. The coating method can have a negative impact on the surface structure of the cathode itself. For instance, the surface of Ni-rich layered cathodes is very sensitive to water. If the coating method is water-assisted then it can negatively affect the electrochemical performance of the cathode.

Thus, the coating methods should be chosen very carefully considering the properties of the cathode materials. Fig. 16 shows the schematics of commonly used coating methods.

2.6.1 Co-precipitation Coating Methods

Co-precipitation coating methods are a very common coating strategy by which a mono-/multi-layer of coating material is deposited on the surface of cathode particles via a precipitation reaction of inorganic compounds[232-234]. For instance, Aboulaich et. al. successfully coated LCO with MF_3 (M = Al or Ce) using $M(NO_3)_3.xH_2O$ (M = Al or Ce) and NH_4F as coating precursor (Fig. 17a). The MF_3 coating is found to improve the electrochemical performance of LCO based cathodes by suppressing surface reactions and scavenging the HF attack[232]. Co-precipitation coating methods have been widely used because of their simple and practicable nature along with their low cost. However, as can be seen in Fig. 17b, various parameters such as pH value, temperature, the solution used, and the reagent dropping speed can greatly influence the coating properties and in turn can influence the electrochemical performance of the cathode.

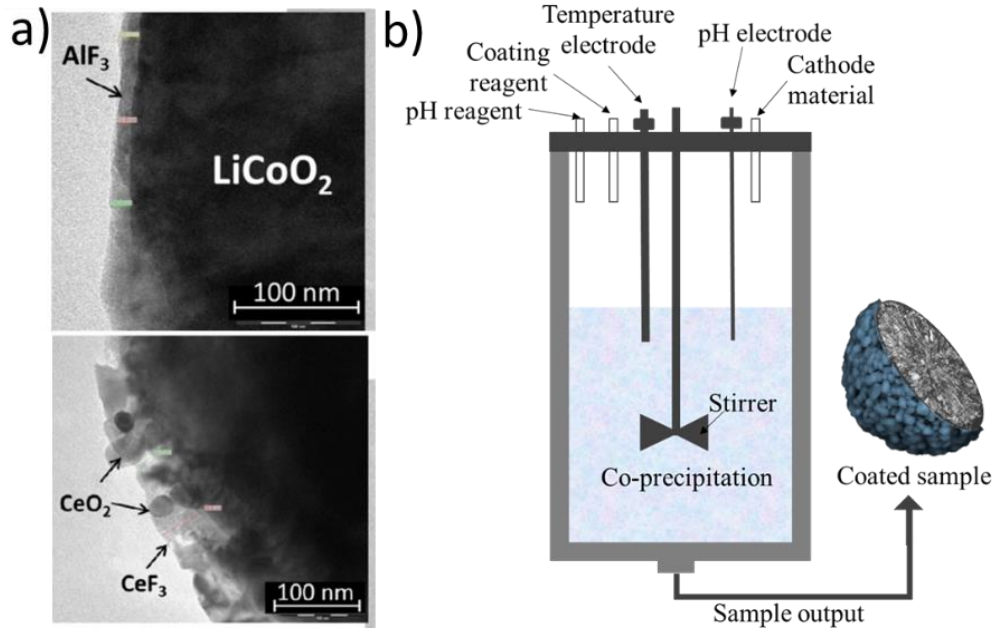

Figure 17: (a) TEM micrograph showing the successful AlF_3 and CeO_2 coating via a co-precipitation method (Reproduced from Ref. [232] with permission, copyright 2014 Wiley-VCH). (b) The schematic diagram for the co-precipitation coating method.

2.6.2 Sol-gel Coating Methods

As shown in Fig. 18, in sol-gel methods the cathode particles are dispersed in a prepared solution. The gel is formed by applying specific reaction conditions, which in turn results in the coating of the cathode particles[235,236]. For example, Shi et. al. reported the successful $La_{0.7}Sr_{0.3}Mn_{0.7}Co_{0.3}O_3$ coating of $LiMn_2O_4$ via sol-gel process. Which resulted in much better C-rate and cycling performance[237]. The sol-gel coating method provides chemical uniformity of multi-component systems, along with easily controllable coating process as compared to other coating methods[238,239]. However, the time required to complete the coating process is rather long. In addition, most of the raw materials used in the process are organic compounds resulting in an increase in costs. Furthermore, the microstructure and chemical properties of the coating layer can be greatly influenced by certain factors (pH value, concentration, temperature etc.), which can significantly affect the electrochemical performance of the cathode[239].

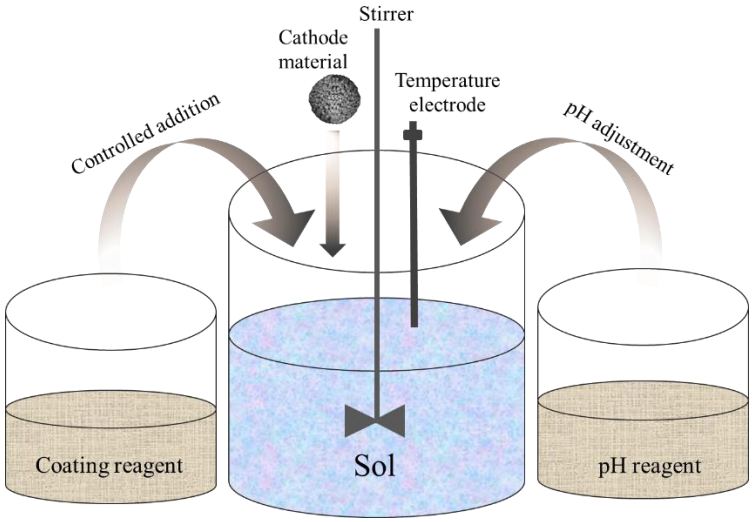

Figure 18: Schematic illustration of the sol-gel coating process.

2.6.3 Dry Coating Methods

In dry coating methods, the particles with a larger size (cathode material) are coated with nanoparticles (coating material) by mechanical mixing in a mixer as shown schematically in Fig. 19. Dry coating methods are considered very cost-effective and have insignificant environmental impact. Thus, they have attracted more attention in recent years[240,241]. For instance, Herzog et. al. successfully coated NCM particles with Al_2O_3 nanoparticles using a dry coating method. The coating was rather uniform resulting in a much-improved electrochemical performance of the cathode as shown in Fig. 19[242]. Other studies have also shown that using appropriate conditions, dry coating methods lead to a highly uniform coating layer on the cathode particle. Moreover, dry coating methods are simpler and cheaper than solution-based coating methods. However, in order to obtain a uniform coating around the cathode particles, the particle size of the cathode and the coating material should be carefully examined before coating[243,244].

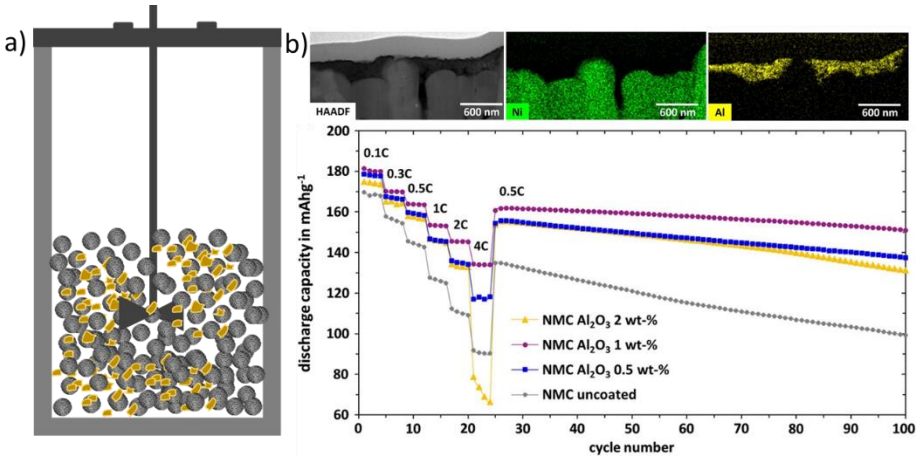

Figure 19: (a) Schematic diagram of the dry coating process. (b) Comparison of the electrochemical performance of pristine and dry-coated Al_2O_3 sample (Reproduced from Ref. [242] with permission, copyright 2014 Wiley-VCH).

2.6.4 Chemical vapor deposition (CVD) Coating Methods

In CVD, the cathode particles come in contact with the flowing gaseous precursor and react with the cathode particle, similar to the liquid state and results in coating[245,246]. For instance, Tian et. al. prepared and compared carbon-coated $LiFePO_4$ particles via two different approaches (Hydrothermal and CVD), using solid glucose as carbon source. They reported that the CVD-based coating is much more uniform as compared to hydrothermal-based one, resulting in a much better C-rate performance[247]. However, there are lots of problems associated with CVD-based coatings. Firstly, the coating particles are usually present in the form of aggregates, thus the formation mechanism becomes vital in order to control uniformity of the coating layer. Secondly, during the coating process the nucleation and coating formation takes place simultaneously, which ultimately can affect the coating uniformity. In conclusion, the CVD-based coating process can provide a more uniform coating but the coating process is rather complicated and costly compared to other methods.

2.6.5 Atomic Layer Deposition (ALD) Based Coating Methods

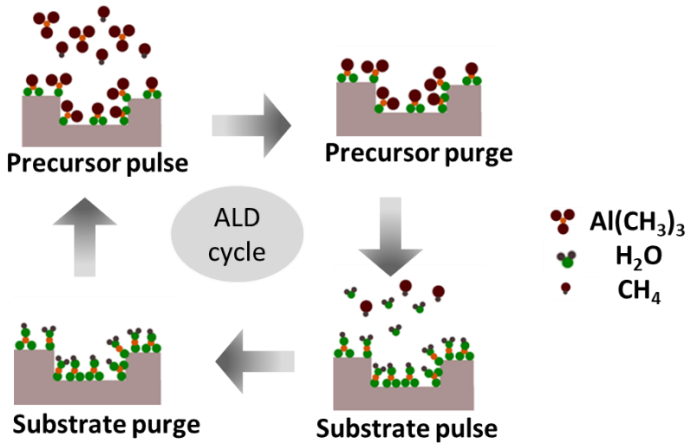

Figure 20: Schematic diagram of the different steps of an ALD coating process.

In comparison to other coating methods, ALD is very unique as it can provide ultrathin coating layers along with high conformity and a precise thickness control on the atomic level[248]. As illustrated in Fig,20, ALD allows the deposition of a very thin coating on the surface of the substrate (cathode particle) through a sequence of chemisorption and self-terminating surface reactions. During a typical ALD process, the substrate surface is initially functionalized using an oxidative precursor, such as H_2O or ozone, yielding a conformal and complete coverage of the substrate surface with hydroxyl groups. This step is followed by purging the by-products and the residual H_2O or ozone with an inert gas flux. Afterward, an organometallic precursor of the desired metal is introduced in order to react with the active hydroxyl group, forming a monolayer of desire metal oxide on the surface of the substrate bridged by oxygen bond. The second purging step is introduced to remove the unreacted precursor and the by-products. These self-limiting pulsing and purging steps are repeated during the ALD process, resulting in a precise atomic level-controlled growth of the coating layer[249-251]. Hence, coatings grown via ALD are typically dense, homogenous, uniform and conformal. It is worth noting that ALD-based coatings are chemically bonded to the substrate in contrast to other coating methods which are

only physically attached[252,253]. Another discrete advantage of ALD is that it can be used to directly coat ready-to-use cathode sheets with a high aspect ratio. During the ALD-based coating of ready-to-use cathodes. The gas-phase precursor can directly penetrate inside the pores present in the composite cathode consisting of cathode active material, conductive carbon and polymer binder, forming a conformal coating on the surface of ready-to-use cathodes. Thus, ALD provides the flexibility of coating either individual cathode particles or complete ready-to-use cathodes[252-254].

2.6.6 Other Coating Methods

In addition to the above-mentioned coating methods, there are few alternative coating methods such as electroless plating[255] and organics pyrolysis method[256].

In the case of the electroless plating method, metals are deposited by chemical method without current[257]. For example, Jiang et. al. coated nano-sized Ag on $LiMn_2O_4$ via electroless plating method, which resulted in an improvement in the electronic conductivity and thus in an improvement of the cycling performance[258]. However, the cost of this method is very high.

In the case of the organic pyrolysis coating method, a carbon coating is the main outcome, which is typically completed by the carbonization of organic compounds[259]. This coating method has been considered very suitable for industrial applications. However, the coating produced in this method is relatively rough, which affects the integrity and uniformity of the coating.

2.7 Types of Surface Coating and Their Properties

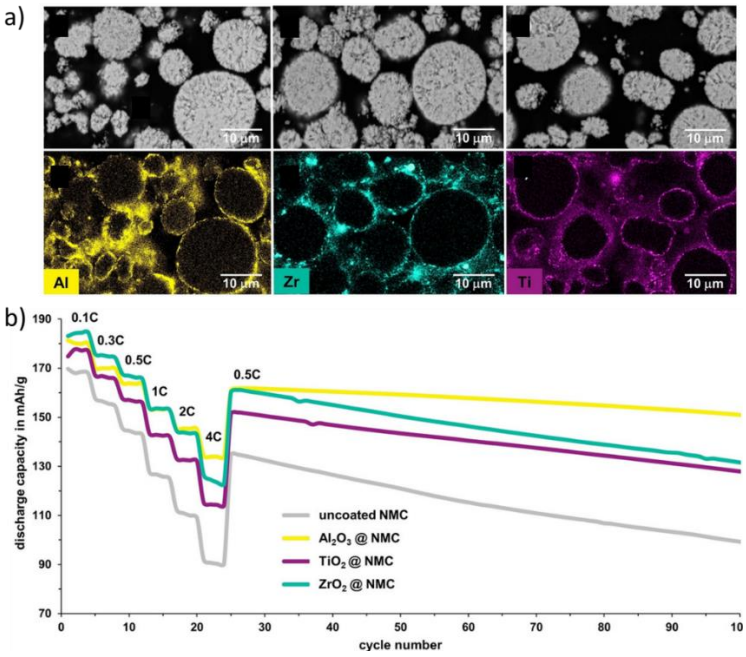

Figure 21: (a) SEM-EDX micrograph of Al_2O_3 coated NCM powder. (b) Comparison of the electrochemical performance of pristine and dry-coated Al_2O_3 samples (Reproduced from Ref. [260] with permission, copyright 2014 Wiley-VCH).

Coating layers that act as a physical barrier between cathode and the electrolyte should possess the following properties:

I. The coating layer should be chemically stable in order to prevent side reactions from taking place between the coating layer and the cathode or the electrolyte.

II. The coating layer should have a very high redox potential, which can prevent the oxidation of the coating layer during high-voltage operations.

According to the above-mentioned requirements, a wide range of chemical compounds can be chosen as coating candidates. However, the physicochemical properties of these compounds can significantly influence the electrochemical performance of the cathode. For instance, as recently reported by Herzog et. al. coating of the same cathode with different coating materials leads to differences in the electrochemical performance cycling as shown in Fig. 21[260]. Thus, concluding from literature, currently used coating materials can be divided into the following categories: oxides, active electrode materials, phosphates and carbon materials.

2.7.1 Oxide-Based Coatings

The most commonly used oxide coatings are Al_2O_3, ZrO_2, TiO_2, ZnO_2, and SiO_2. Different oxide-based coatings have different chemical and electrochemical properties, which can significantly influence the electrochemical performance of the coated cathode material[92,261-265]. As shown in Fig. 22, Herzog et. al. coated NCM based cathode materials with different oxides, which showed an improved cycling performance[260].

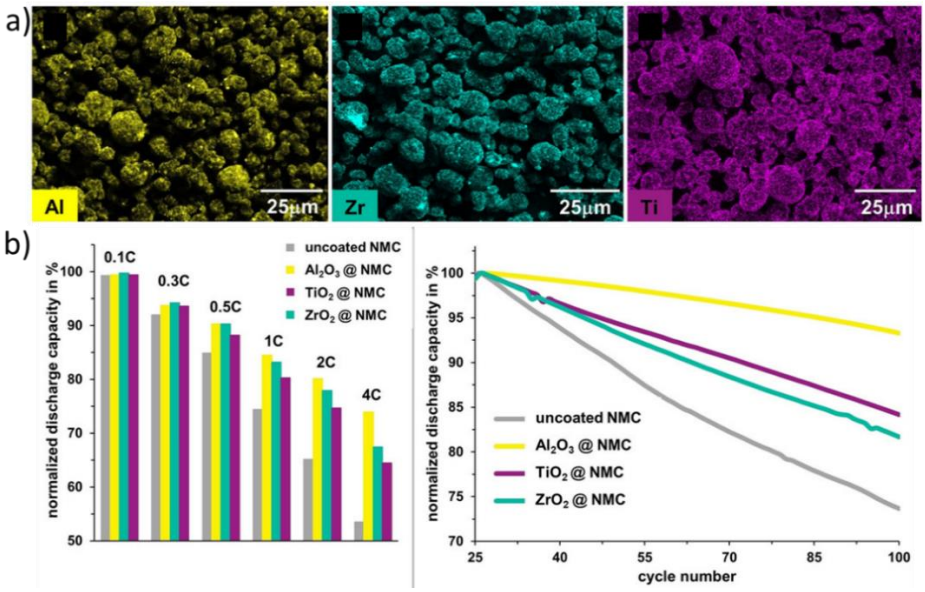

Figure 22: (a) EDX micrograph of Al_2O_3, ZrO_2 and TiO_2 coated NCM powder. (b) Comparison of the electrochemical performance of pristine and dry-coated samples (Reproduced from Ref. [260] with permission, copyright 2014 Wiley-VCH).

However, differences in the electrochemical behavior are found for the different coating materials. The influence of the coating material is typically depending on the unique physical and chemical properties of the oxide itself. For instance, Al_2O_3 is used commercially as coating material because of its high melting point and stability against the acidic or alkali environment. In addition, it is also corrosion resistant and can form layered $LiAlO_2$ via high-temperature annealing, being beneficial for Li^+ diffusion through the coating layer[266]. In comparison to Al_2O_3, semiconducting oxides such as ZrO_2 or TiO_2,

have a higher conductivity and can facilitate Li^+ diffusion through the coating layer during cycling[260]. Takamatsu et. al. reported the formation of Zr salt from ZrO_2 on the surface of cathode particles during cycling, which improved the Li^+ diffusion through the coating layer and thus improved the electrochemical performance[267]. In contrast to the majority of oxide materials, SiO_2 based coatings, which exhibit a lower conductivity, reduces the electrochemical performance when a thick coating layer is used[268]. Thus, in case of oxide coatings with low conductivity, a thinner coating layer is favored for a better electrochemical performance[269].

2.7.2 Phosphate-Based Coatings

The most commonly used phosphate-based coating materials are $AlPO_4$, $Co_3(PO_4)_2$, $FePO_4$, etc.[270,271]Among all, $AlPO_4$-based coatings are most widely used, due to strong covalent bonding between Al^{3+} and PO_4 polyanion along with strong P=O bonds. In $AlPO_4$-coated cathodes, the coating can effectively prevent the interaction between the cathode and the electrolyte, which in turn prevents the metal dissolution[272,273]. Cho et.al. compared Al_2O_3 and $AlPO_4$ as coating material on the electrochemical performance of LCO. They reported no significant differences between both the coatings. when the cells were charged up to 4.6 V. However, the capacity retention was much better for $AlPO_4$ coated sample as compared to Al_2O_3, when the cells were charged up to 4.8 V accompanied with a higher thermal stability[274]. $Co_3(PO_4)_2$ is also a commonly used phosphate-based coating material. It has been found that $Co_3(PO_4)_2$ reacted with cathode impurities (Li_2CO_3 and LiOH) during heat-treatment to form olivine Li_xCoPO_4 phase at the surface of NCM, resulting in the suppression of side reaction and metal-ion dissolution, which improves the electrochemical performance[275,276]. $FePO_4$ based materials have proven to be a promising 3V cathode candidate for LIBs due it's low cost and high thermal stability. Considering its advantages, Xiao et. al. reported that ALD-based coatings of $FePO_4$ on $LiNi_{0.5}Mn_{1.5}O_4$ results in a much higher capacity during cycling[277,278].

2.7.3 Active Electrode Material-Based Coatings

Using active electrode materials as a coating layer is a fairly new concept for NCM based cathodes. It has been suggested that coating the cathode with active electrode material might be beneficial, as the coating layer exhibits better ionic conductivity as compared to oxides or phosphate-based coating materials. It also prevents side reactions between electrode and electrolyte. The most commonly used active electrode material for the coating of NCM based cathodes include $Li_4Ti_5O_{12}$, $LiNiPO_4$, and $LiFePO_4$ etc[200,279-282]. Among all $Li_4Ti_5O_{12}$ has been most widely employed as a coating material due to its high stability, smooth discharge plateau and reluctance against overcharge and discharge[283]. Furthermore, $Li_4Ti_5O_{12}$ has a very unique structural feature of 'zero strain', which can avoid structural damages arising due to volumetric changes and maintain structural stability even at high operating voltage. For $Li_4Ti_5O_{12}$ coated Li-rich cathode material, it is reported that the coating layer effectively stabilizes the main cathode structure and also prevents the reaction between cathode and electrolyte, resulting in much better electrochemical performance[284,285]. $LiFePO_4$ also shows improved structural stability, voltage plateau and excellent safety, making it another promising coating material. In addition, it has higher thermal stability and superior high-temperature performance

compared to most of the cathode materials, resulting in a much better electrochemical performance for $LiFePO_4$ coated cathodes[286,287]. Kim et. al. coated $LiFePO_4$ on $Li[Ni_{0.5}Co_{0.2}Mn_{0.3}]O_2$ using a co-precipitation method and compared its electrochemical performance with inactive oxide coatings (Al_2O_3, ZnO and MgO), reporting far superior capacity retention at 50 ^oC[282].

2.7.4 Carbon-Based Coatings

Carbon-based coatings exhibit good electronic conductivity and Li^+ diffusivity. They are used for the cathodes with poor electronic conductivity, such as $LiFePO_4$, Li_2MnSiO_4 and $Li_2V_2(PO_4)_3$ etc[287-289]. Generally, carbon-based coating layer deposited on the cathode surfaces have the following effects:

1. The coating layer increases the conductivity between the cathode particles.
2. The coating layer inhibits the grain growth during post-synthesis heat treatment.
3. The coating layer acts as a reducing agent in order to prevent metal-ion oxidation.

For in-situ carbon coating, the reaction atmosphere must be inert as carbon acts as a reducing agent for the high valence metal ions in the cathode[290]. Thus, in-situ high-temperature carbon coating is not suitable for layered and spinel cathode materials. Liu et. al. coated $Li[Li_{0.2}Mn_{0.54}Ni_{0.13}Co_{0.13}]O_2$ with carbon and found that the surface conductivity has been enhanced by 40% without degrading the cathode structure, resulting in a much better C-rate and electrochemical performance[291]. Jin et. al. coated $LiNi_{0.4}Ti_{0.1}Mn_{1.5}O_4$ with carbon via solid-state reaction and found an improved columbic efficiency along with higher capacity retention. This improvement was correlated to the suppression of SEI formation and faster kinetics of Li^+ in the coated sample[292].

2.7.5 Other Coating Materials

In addition to the above-mentioned coating materials, there are materials worth mentioning, such as fluoride, polymers, silicates, metals, etc[173,232,293,294]. As already discussed, the generation of HF is unavoidable inside the battery, which results in corrosion of the cathode, which deteriorates the battery performance. In contrast, fluoride-based coating layers don't react with HF and in turn resist HF erosion of the cathode, thus resulting in much better electrochemical performance and thermal stability[165]. Similarly, polymer-based coatings are also very common to modify the cathode surface. For example, coating the cathode with conductive polymer polypyrrole (PPy) results in an improvement of the cathode conductivity and in turn in a higher capacity and improved electrochemical performance[295]. Furthermore, silicate-based coating materials effectively block chemical erosion of the cathode surface due to the presence of strong Si-O bonds and thus results in much better cycling performance of the coated cathode[296]. In addition, metallic coatings can improve the electronic conductivity on the cathode surface and can increase the electrical contact in the cathode composite, which can further increase the electrochemical performance of the cathode[297]. However, metals with a high conductivity might not be suitable as a coating material due to negative oxidation effect, so there is a need for studying the modification mechanism of metal-based coatings.

3. Results and Discussion

NCM based cathodes are widely used and studied in LIBs due to their higher achievable capacity (200 mAh g^{-1}) in the same operating voltage window as compared to LCO. In particular Ni-rich NCM based cathodes are projected to launch for the next-generation LIBs for EV application and thus $LiNi_{0.7}Mn_{0.15}Co_{0.15}O_2$ has been selected for most of the studies. However, using Ni-rich NCM is often accompanied by detrimental side reactions at the interface between the cathode and the electrolyte, which in turn limits the battery performance. The surface coating has been shown to effectively mitigate these interfacial issues arises with Ni-rich NCM cathodes. Thus, the initial focus of my Ph. D. was to develop an ALD-based surface coating method for the ready-to-use cathode sheets, which otherwise is impossible to coat with other coating methods. I have successfully developed an ALD-based Al_2O_3 coating approach and applied on ready-to-use cathodes resulting in a better electrochemical performance of LIBs (Publication 1). Thereafter, my research focus has been broadened to develop new solution-based coating methods for Al_2O_3 based coating material on NCM powder (Publication II). Furthermore, I have investigated the effect of high-temperature treatment on Al_2O_3 based coating and its effect on the electrochemical performance of the NCM has been studied (Publication III). I continued the development of new coating methods which can be applied in ASSBs, I applied a $Li_4Ti_5O_{12}$-based coating dry-processed coating method on NCM powder used as a cathode material in ASSBs. Due to the coating the performance of the ASSB could be significantly improved (Publication IV). For the last part of my Ph. D. research, I have investigated the influence of high-temperature treatment on dry-processed Al_2O_3 coating and its effect on the electrochemical performance of NCM based ASSB. The following four peer-reviewed represents the basis of this Ph.D. thesis.

3.1 Publication I: Optimized Atomic Layer Deposition of Homogeneous, Conductive Al_2O_3 Coatings for High-nickel NCM Containing Ready-to-Use Electrodes.

In my first publication, a new ALD-based Al_2O_3 coating process has been developed to improve the electrochemical performance of various Ni-rich NCM based ready-to-use electrodes. For the development of the coating process, various ALD parameters have been optimized to achieve homogenous coating on NCM based cathodes. After successful deposition of the coating layer, various structural characterization technique has been used to analyze the coating on the surface of cathode. The coating is found to be rather homogenous and thin. The coating layer is thin enough to retain the original conduction properties of the cathode.

The electrochemical characterization in terms of C-rate, long-term cycling, and electrochemical impedance spectroscopy (EIS) confirmed the improvement of the long-term cycling performance for the coated cathodes as compared to uncoated ones without a negative impact on the C-rate performance. The beneficial effect of the coating layer can be attributed to a reduced SEI formation and charge transfer resistance during long-term cycling.Post-mortem analysis of the cycled cathodes reveals that the coating itself is stable during cycling and the coating layer effectively prevents particle cracking during cycling.

I designed the concept and performed the experiments of this publication under the supervision of Dr. M. T. Elm and Dr. S. P. Culver. I wrote the manuscript, which was corrected by all five co-authors. High-resolution SEM images have been taken by Shamail Ahmad. AFM images have been taken by Miguel Wiche. Dr. S. P. Culver contributed to scientific discussions. Reprinted with permission from Physical Chemistry Chemical Physics. Copyright 2018 Elsevier.

R. S. Negi, S. P. Culver, M. Wiche, S. Ahmed, K. Volz, M. T. Elm, Optimized atomic layer deposition of homogeneous, conductive Al_2O_3 coatings for high-nickel NCM containing ready-to-use. *Physical Chemistry Chemical Physics* **2021**, 23 (11), 6725-6737

PCCP

ROYAL SOCIETY OF CHEMISTRY

PAPER

View Article Online
View Journal | View Issue

Cite this: *Phys. Chem. Chem. Phys.*, 2021, **23**, 6725

Optimized atomic layer deposition of homogeneous, conductive Al_2O_3 coatings for high-nickel NCM containing ready-to-use electrodes†

Rajendra S. Negi,[a] Sean P. Culver,[b] Miguel Wiche,[a] Shamail Ahmed,[c] Kerstin Volz[c] and Matthias T. Elm *[abd]

Atomic layer deposition (ALD) derived ultrathin conformal Al_2O_3 coating has been identified as an effective strategy for enhancing the electrochemical performance of Ni-rich $LiNi_xCo_yMn_zO_2$ (NCM; $0 \leq x, y, z < 1$) based cathode active materials (CAM) in Li-ion batteries. However, there is still a need to better understand the beneficial effect of ALD derived surface coatings on the performance of NCM based composite cathodes. In this work, we applied and optimized a low-temperature ALD derived Al_2O_3 coating on a series of Ni-rich NCM-based (NCM622, NCM71.51.5 and NCM811) ready-to-use composite cathodes and investigated the effect of coating on the surface conductivity of the electrode as well as its electrochemical performance. A highly uniform and conformal coating was successfully achieved on all three different cathode compositions under the same ALD deposition conditions. All the coated cathodes were found to exhibit an improved electrochemical performance during long-term cycling under moderate cycling conditions. The improvement in the electrochemical performance after Al_2O_3 coating is attributed to the suppression of parasitic side reactions between the electrode and the electrolyte during cycling. Furthermore, conductive atomic force microscopy (C-AFM) was performed on the electrode surface as a non-destructive technique to determine the difference in surface morphology and conductivity between uncoated and coated electrodes before and after cycling. C-AFM measurements on pristine cathodes before cycling allow clear separation between the conductive carbon additives and the embedded NCM secondary particles, which show an electrically insulating behavior. More importantly, the measurements reveal that the ALD-derived Al_2O_3 coating with an optimized thickness is thin enough to retain the original conduction properties of the coated electrodes, while thicker coating layers are insulating resulting in a worse cycling performance. After cycling, the surface conductivity of the coated electrodes is maintained, while in the case of uncoated electrodes the surface conductivity is completely suppressed confirming the formation of an insulating cathode electrolyte interface due to the parasitic side reactions. The results not only show the possibilities of C-AFM as a non-destructive evaluation of the surface properties, but also reveal that an optimized coating, which preserves the conductive properties of the electrode surface, is a crucial factor for stabilising the long-term battery performance.

Received 11th December 2020,
Accepted 20th February 2021

DOI: 10.1039/d0cp06422j

rsc.li/pccp

1. Introduction

The fast-growing development of electric vehicles (EVs) and hybrid electric vehicles (HEVs) has drawn extensive interest in the area of rechargeable lithium-ion battery (LIB) research for achieving a higher energy density and a long cycle life.[1,2] At present, the most commonly used cathode materials (such as $LiCoO_2$) are considered to be a limiting factor for developing high capacity LIBs because of their relatively low lithium utilization (*i.e.*, <60%) and severe degradation during continuous cycling.[2–4] Among all, $LiNi_xCo_yMn_zO_2$ (NCM; $0 \leq x, y, z < 1$) as

[a] *Center for Materials Research (LaMa), Justus Liebig University Giessen, Heinrich-Buff-Ring 16, 35392 Giessen, Germany*
[b] *Institute of Physical Chemistry, Justus Liebig University Giessen, Heinrich-Buff-Ring 17, 35392 Giessen, Germany. E-mail: matthias.elm@phys.chemie.uni-giessen.de*
[c] *Materials Science Centre and Faculty of Physics, Philipps University Marburg, Hans-Meerwein-Strasse 6, 35043 Marburg, Germany*
[d] *Institute of Experimental Physics I, Justus Liebig University Giessen, Heinrich-Buff-Ring 16, 35392 Giessen, Germany*

† Electronic supplementary information (ESI) available. See DOI: 10.1039/d0cp06422j

cathode active materials pioneered by Liu *et al.*[5] have attracted the highest interest due to their high capacity (*e.g.*, *ca.* 200 mA h g^{-1} for $LiNi_{0.8}Co_{0.1}Mn_{0.1}O_2$),[6] longer cycling stability[7] and low cost. However, these materials show severe capacity fading at higher working voltage (>4.3 V) due to lattice structural instabilities which lead to surface reconstruction of the cathode material caused by a layered to spinel-like phase transformation.[7–10] Also at a lower working voltage (<4.3 V), there is significant capacity degradation in NCM based cathodes due to parasitic side reactions between the electrode and electrolyte interface.[11] For example, the small amount of moisture present on the surface of NCM can react with $LiPF_6$ in the electrolyte to produce contaminants like HF which is known to be responsible for capacity fading during cycling.[12–14] These issues associated with NCM based CAM hinder its potential application in EVs and HEVs. Thus, the interfacial interactions between NCM and the liquid electrolyte play a crucial role in the electrochemical performance of LIBs.[15]

In the past few years, researchers have demonstrated that bulk doping and surface modification of NCM can overcome the aforementioned issues.[16–18] Modification of NCM using surface coating is found to be effective in improving the cycling performance by preventing the direct physical interaction of the electrolyte with the cathode and thus mitigating the side reactions at the interface.[19–22] Several surface coating materials and coating approaches have been applied to different CAM, which have been found to be effective in enhancing the cycling performance as collectively summarized in recent review articles.[23–25] Surface coating performed *via* conventional wet-chemical approaches[26–31] was found to be effective in improving the cell performance, but there is no precise control over the coating thickness, uniformity and surface coverage.[32] In addition, these coating approaches usually require post-heat treatment which is not suitable for coating ready-to-use composite electrodes (*i.e.* due to the decomposition of PVDF at >150 °C).[33] In contrast, atomic layer deposition (ALD) based coatings have many advantages over conventional wet-chemical approaches (*i.e.* uniform and conformal coating along with precise control over coating thickness) and can be performed at relatively low temperatures, allowing coatings to be applied directly on ready-to-use composite electrodes.[13,33–36] Furthermore, ALD is a suitable method to achieve homogeneous coatings even for highly porous materials with pore sizes in the nanometer range.[37–41] In surface coated ready-to-use composite electrodes, all constituents (*i.e.* CAM, binder and conductive carbon) are covered by the coating and thus prevent the direct physical contact of the cathode with the electrolyte. Apart from this, all the original conduction pathways formed between the constituents in the electrodes remain unaffected. Thus, better electron and Li-ion transport properties can be expected compared to electrodes prepared from coated powder CAM.[13,34]

In view of coating materials, various metal oxides and fluorides, such as Al_2O_3,[42,43] TiO_2,[30,44] ZnO,[44] SiO_2,[29] CeO_2,[45–47] and AlF_3[48,49] have been investigated. Among these, Al_2O_3 is by far considered as the most prominent coating material, which is widely used in both research and industry. Most of the reports on ALD based Al_2O_3 coatings have been published on LCO and NCM powders,[34,50–55] and there are only few reports on ALD based Al_2O_3 coatings on ready-to-use electrodes mostly in case of NCM based CAM.[36,56] However, in all of these reports the deposition parameters were optimized for only one composition of NCM (*i.e.*, either NCM523,[36,56] or NCM622[21]). Considering a wide range of NCM compositions, it is crucial to develop and optimize an ALD based Al_2O_3 coating technique which can be applied to a wide range of NCM compositions to enhance the electrochemical performance in LIBs.

In this study, we optimized an ALD-based Al_2O_3 coating technique, applied the coating on a series of ready-to-use composite electrodes (*i.e.*, NCM622, NCM71.51.5 and NCM811), and examined the effect of Al_2O_3 coating on the electrochemical performance of these electrodes in LIBs. Conductive AFM (C-AFM) measurements on the electrode surface were performed in order to gain a better understanding of the beneficial effect of the coating on the electrochemical cycling behavior. AFM measurement has been proven to be a powerful, non-destructive method to provide local information on the structural, chemical or conduction properties of battery electrodes at the nanoscale[57–61] and to study the formation of solid–electrolyte interfaces.[62–64] In this work, C-AFM measurements on the coated cathodes reveal that, on one hand, a sufficiently thin coating does not affect the electrical conductivity of the cathode surface and, on the other hand, the electrical and structural properties are maintained due to the coating even during cycling. Thus, this work offers an optimized oxide coating for a series of Ni-rich cathodes using ALD, which improves the electrochemical performance of various Ni-rich electrodes for lithium-ion batteries not only by preventing the direct contact between cathode and electrolyte, but also by retaining the electrical surface conductivity of the cathode. Furthermore, we show that the ALD-derived coating preserves the structural and electrical properties of the surface during cycling, while in case of the uncoated electrodes the formation of the cathode/electrolyte interface completely suppressed the electrical conductivity at the surface.

2. Experimental

2.1. Electrode preparation

Three kinds of electrodes using different Ni-rich NCM compositions as active materials (*i.e.* NCM622, NCM71.51.5 and NCM811) were prepared. For the electrode preparation, the corresponding Ni-rich NCM secondary particles (90 wt%), conductive carbon (Super P, 5 wt%) and 5 wt% solution of polyvinylidene fluoride (Solef PVDF 6020) binder were suspended in *N*-methyl-2-pyrrolidone (NMP, Sigma-Aldrich) and mixed for 24 h. The resulting cathode mixtures were cast on Al-foil using a doctor blade and dried under vacuum at 120 °C. The cathodes were calendared at 90 psi and dried again at 120 °C under vacuum overnight before transferring to the glovebox.

2.2. Al_2O_3 coating

ALD-based Al_2O_3 coating was performed directly on the as-prepared cathodes using a SUNALE R-200 Advanced (Picosun; Finland)

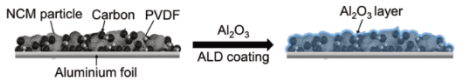

Fig. 1 Schematic illustration of ALD-based Al_2O_3 coating on NCM based ready-to-use composite electrodes.

reactor at 120 °C. The low reaction temperature was used to prevent PVDF decomposition (<150 °C). Trimethylaluminum (TMA, Sigma-Aldrich) and water (H_2O) were used as precursors for the deposition of Al_2O_3 coating. The pulse time for both precursors was 10 s, N_2 was purged in between two consecutive pulses for 60 s to ensure the complete removal of unreacted excess precursor and reaction by-products. Five cycles of Al_2O_3 were coated on the series of Ni-rich NCM based (NCM622, NCM71.51.5, and NCM811) ready-to-use composite cathodes for comparison (Fig. 1).

2.3. Electrochemical investigation

For electrochemical investigations, CR-2032 coin cells (MTI Corporation) were assembled in an argon-filled glovebox (oxygen and water levels of less than 1 ppm) using pre-dried materials. Half-cells were assembled using Pristine-/Coated-NCM (12 mm) as the cathode, lithium foil (Rockwood Lithium GmbH, 14 mm) as the anode, Celgard-2500 (16 mm) as the separator, and an electrolyte solution (50 μL, 1.0 M $LiPF_6$ in 1 : 1 by weight ethylene carbonate (EC)/ethyl methyl carbonate (EMC) purchased by Sigma-Aldrich (LP50)). Electrochemical investigations were performed using a multichannel battery cycler (MACCOR Inc., USA) at 25 °C after equilibration for 2 h. The coin cells were cycled between 3.0 and 4.3 V at 0.5C (1C = 160 mA $g_{NCM622}{}^{-1}$, 160 mA $g_{NCM71.51.5}{}^{-1}$, 200 mA $g_{NCM811}{}^{-1}$) after the C-rate capability tests at different discharge current densities (0.1C, 0.3C, 0.5C, 1C, 2C, and 4C). All coin cell data are averaged from three independent cells (for both pristine- and coated-cathodes).

2.4. Material characterization

The morphology and microstructure of the Al_2O_3 coating were investigated using a "Merlin" scanning electron microscope (SEM) from Zeiss (accelerating voltage = 5 kV, accelerating current = 1500 pA). The homogeneity of the Al_2O_3 coating was investigated by electron-dispersive X-ray spectroscopy (EDX) using an X-Max detector (Oxford Instruments, accelerating voltage = 5 kV, and accelerating current = 1500 pA). X-ray photoelectron spectroscopy (XPS) measurements were performed on the Al_2O_3 coated cathodes before and after cycling, using a PHI 5000 Versaprobe II Scanning ESCA microprobe (Physical Electronics, pressure $\sim 10^{-8}$ Pa). A monochromatic, micro focusing Al Kα X-ray source was used. The samples were sputtered for 90 s before the XPS data were collected in order to remove surface contaminants. Survey spectra were measured with a pass energy of 93.9 eV and high-resolution spectra with a pass energy of 23.5 eV. For calibration, the C 1s line at 284.8 eV was used as standard. CasaXPS software was used for evaluating the spectra. Structural characterization of the pristine and coated electrodes was performed using X-ray diffraction (XRD, Bruker) with Cu Kα radiation. The surface topology and conductivity of the electrodes were investigated by atomic force microscopy (AFM) using a Bruker Dimension Icon instrument (*Multimode* 8). All AFM measurements were operated in PeakForce TUNA mode which provides simultaneous mapping of the topography and the current using the TUNA module. In the conductive-AFM mode (C-AFM) the back side of the electrode is biased to a set voltage and a conductive tip is used. When the AFM tip comes in contact with the electrode surface, a current flows between the sample and the tip, if the sample is conductive. Depending on the cathode, imaging of the flowing current was done using a bias between 500 mV and 1100 mV to prevent damage to the tip. Platinum/iridium-coated tips were used during the analysis. All AFM image processing was done with the Nanoscope Analysis 1.9 software.

3. Results & discussion

3.1. Characterization of Al_2O_3-coated Ni-rich NCM

In this work, an optimal, low-temperature ALD derived coating method has been developed in order to coat Al_2O_3 on different $LiNi_xCo_yMn_zO_2$ (NCM; $0 \leq x, y, z < 1$) based ready-to-use cathodes for LIBs. Initially, the ALD process was optimized on a Si substrate, which allowed to determine the growth rate of Al_2O_3 (~1.0 Å per cycle) as shown in Fig. S1a (ESI†). These optimized process parameters have been directly applied to NCM based ready-to-use cathodes as stated in the experimental section to obtain electrodes with different thicknesses of the coating layer. Thereafter, these electrodes were tested regarding the electrochemical cycling stability as shown in Fig. S1b (ESI†), in which a coating thickness of 2–4 nm was found to show the best performance in the long-term stability tests and thus has been used for further studies. To confirm the successful Al_2O_3 coating on the electrodes, the Al 2p XPS spectra were collected for both the pristine and coated cathodes. As shown in Fig. 2a, the coated sample shows a sharp peak at 74.7 eV, which can be attributed to Al 2p[65] thereby verifying the successful Al_2O_3 coating. Furthermore, no Al peak is observed for the pristine cathode as expected. The XRD patterns of the pristine and coated cathodes are also provided in Fig. 2b. Here, a typical pattern of the layered α-$NaFeO_2$ structure is observed[66] confirming that the Al_2O_3 coating did not negatively alter the NCM structure. Moreover, no additional reflections can be observed for Al_2O_3, which is likely due to both the amorphous nature of the coating and the low weight fraction of the coating on the surface.

High magnification SEM images of the pristine and coated NCM71.51.5 cathodes are shown in Fig. 3. The polydisperse NCM secondary particles have a spherical morphology with sizes ranging from 2 to 10 μm and are composed of primary particles with diameters varying between 200 and 500 nm. Three different Ni-rich NCM cathodes (*i.e.*, NCM622,

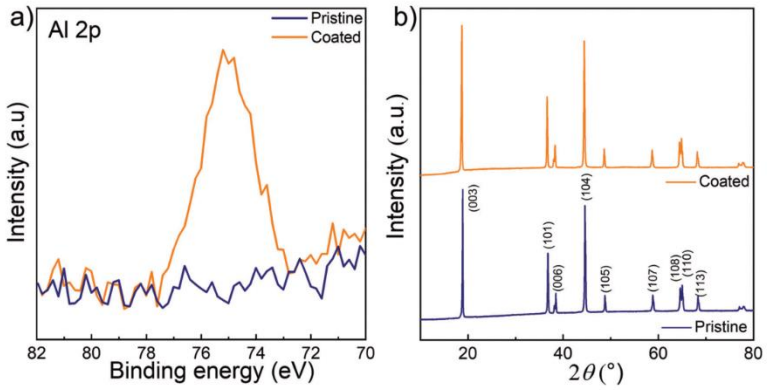

Fig. 2 (a) Al 2p XPS spectra and (b) XRD patterns of pristine and Al_2O_3 coated NCM71.51.5 electrodes.

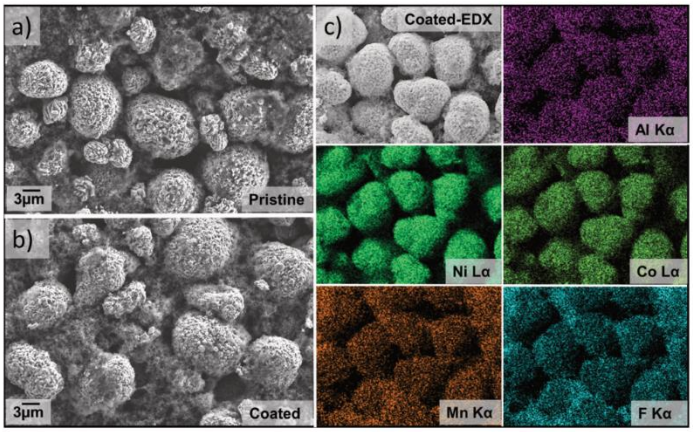

Fig. 3 SEM images of (a) pristine and (b) Al_2O_3 coated NCM71.51.5 electrodes. (c) SEM-EDX mapping of Al_2O_3 coated NCM71.51.5 electrodes confirming the homogeneous coating using ALD.

NCM71.51.5, and NCM811) were used for the ALD derived Al_2O_3 coating and the additional SEM images of the other cathodes can be found in the ESI† (Fig. S2). Importantly, no change in the morphology of the cathodes is found after the coating. EDX mapping of the coated NCM71.51.5 cathodes illustrates the homogeneous distribution of Al on the cathode surface (Fig. 3c), confirming the uniformity of the Al_2O_3 coating and indicating that all cathode components (*e.g.*, NCM, carbon and binder) are covered by Al_2O_3. Comparable results are observed for all three different Ni-rich NCM cathode compositions (see ESI,† Fig. S2). The F Kα EDX map corresponds to the distribution of PVDF (binder) in the cathode.

High-resolution cross-sectional SEM images of Al_2O_3 coated NCM particles using 40 ALD cycles (2–4 nm) are shown in Fig. 4. Notably, a thin tungsten layer ($W–e^-$) was first deposited on the coated NCM71.51.5 electrodes using an electron beam, followed by a thick tungsten layer (W–Ga) deposited using a Ga-ion beam. The tungsten layer was deposited to protect the surface from damage during focused ion beam (FIB) preparation. The dark contrast between the NCM primary particles and the $W–e^-$ layer in Fig. 4a shows that the particle surface has been coated homogeneously with the Al_2O_3 layer. This is further confirmed by high-magnification SEM images shown in Fig. 4b and c from different regions of the secondary particle surface.

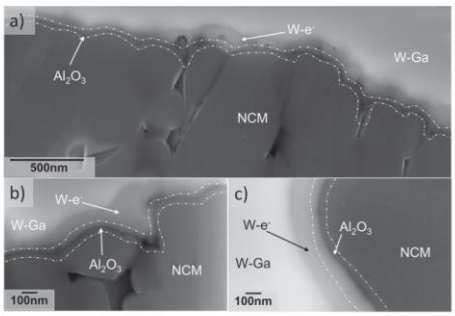

Fig. 4 High-resolution SEM images of Al_2O_3 coated NCM71.51.5 (40ALD) electrodes (a) at large field-of-view showing the homogeneous coating of the secondary particle surface and (b and c) at relatively higher magnifications from different regions of secondary particle surfaces.

The thickness of the coating layer is estimated to vary between 2 and 4 nm, which is in agreement with the expected value of about 2–4 nm according to the determined growth rate of Al_2O_3 (Fig. S1a, ESI†). All of the abovementioned characterization techniques confirm that a homogeneous, uniform Al_2O_3 coating has been successfully deposited on the electrodes.

AFM images of pristine and coated electrodes before cycling are shown in Fig. 5. The topography of the electrode surface is shown in Fig. 5a and c for the pristine and the coated electrode, respectively. In both cases, the NCM secondary particles can clearly be observed as spherical particles embedded in the mixture of conductive carbon and binder. A correlation of the C-AFM measurements shown in Fig. 5b reveals that an electrical current is only detectable in the areas, where carbon is found, while the surface of the NCM secondary particles is found to be rather electronically insulating.[60] This is expected, as the electronic conductivity of carbon is much higher than those of the mixed conducting NCM material. Interestingly, also for the coated NCM electrodes, a flowing current is detectable in the carbon regions of the surface, *i.e.*, the surface conductivity of the electrode is still maintained after coating with a thin Al_2O_3 layer. Coating of the electrode with a 20 nm thick Al_2O_3 layer completely suppresses the electronic surface conductivity (see ESI,† Fig. S3), *i.e.*, the coating is electronically insulating as expected for Al_2O_3. Thus, the electronic properties of the coating layer are strongly affected by its thickness, as recently also observed for ceria and titania coatings on ZrO_2-based oxides.[40,67] Thus, the measurements clearly confirm that the Al_2O_3 coating layer is thin enough to maintain conduction pathways along and across the surface, which is beneficial for the electrochemical performance of the coated electrodes. In addition, it can be seen that there is no change in the surface morphology after coating and the different constituents of the cathode composite (*e.g.*, NCM secondary particles and carbon) are still clearly distinguishable.

3.2. Electrochemical characterization

In order to investigate the influence of coating on the electrochemical performance of the high-Ni NCM cathodes, Li|LP50|NCM half-cells were assembled. The cells were initially galvanostatically cycled from 0.1C to 4C in order to analyze the effect of coating on the C-rate performance. The same cells were subsequently cycled at 0.5C for long-term cycling stability tests. As shown in Fig. 6, the C-rate capability of both the pristine and coated cathodes is found to be similar at all charge/discharge rates within the experimental error range. This indicates that modifying the surface of the cathode with Al_2O_3 does not appear to negatively influence the C-rate performance, which suggests that besides the preserved electronic conductivity the coating layer also possesses sufficient ionic conductivity to facilitate the desired Li-ion diffusion behavior. Typically, various factors,

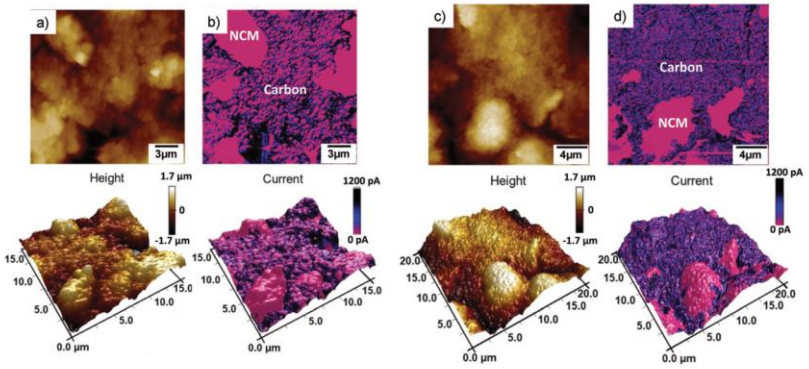

Fig. 5 AFM images of NCM71.51.5 electrodes (a and b) before and (c and d) after coating. In both cases, the insulating secondary NCM particles can clearly be distinguished from the electronically conductive carbon–binder mixture.

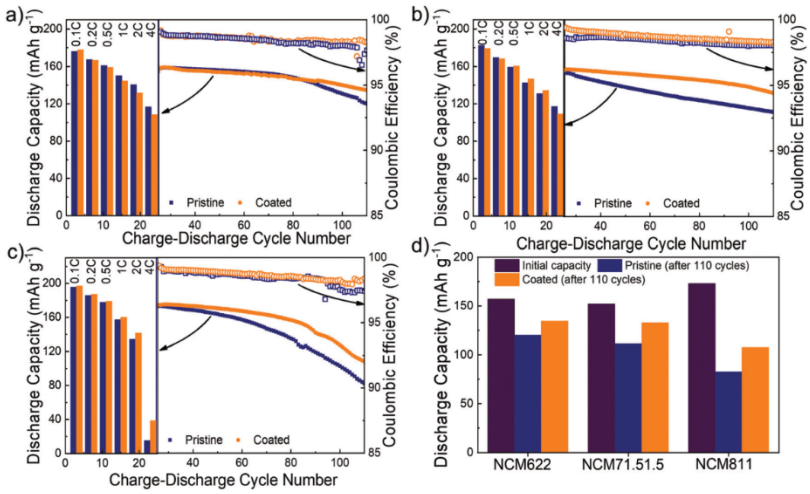

Fig. 6 Half-cell rate capability and long-term cycling stability of pristine and coated (a) NCM622 (b) NCM71.51.5 and (c) NCM811 cathodes. (d) Comparisons of capacity retention for pristine NCM and coated NCM for all three configurations.

such as coating thickness, porosity, homogeneity, and coating amount, significantly affect the C-rate performance, especially, when the NCM particles themselves are coated. In our case, the coating layer is just present on the surface of the electrode and all NCM particles below the surface are unaffected by the coating, which in turn preserves the original conduction pathways inside the cathode. It should also be noted that despite several reports showing an improvement in the C-rate performance after Al_2O_3 coating based on wet-chemical synthesis,[31,43,68] most of the reports on ALD[21,36,56,69] based Al_2O_3 coatings on powder or ready-to-use NCM electrodes showed a similar or worse C-rate performance compared to that of the pristine cathodes. Thus, additional studies related to the influence of coating temperature and coating thickness are required to obtain a complete understanding of the coating on the C-rate performance in ALD coated, ready to use cathodes.

After the C-rate test, the same cells were tested for long-term cycling performance and were cycled at 25 °C with a rate of 0.5C between 3.0 and 4.3 V. Fig. 6a–c compares the cycling performance and coulombic efficiencies of the pristine cathodes with those of the coated cathodes for all three compositions of Ni-rich NCM used in this study. It can be seen that the coated cathode exhibits higher cycling stability as compared to the pristine cathode after 110 cycles. In all three cases, the coated cathodes exhibit an improved long-term cycling performance with higher coulombic efficiencies compared to that of the pristine NCM cathodes. As shown in Fig. 6d, the capacity retention is improved by 9.1% for NCM622, 14% for NCM71.51.5 and 14.4% for NCM811 after 110 cycles. Notably, the higher coulombic efficiencies indicate that the coating effectively inhibits the deleterious side reactions taking place at the cathode/electrolyte interface. It is well known that NCM with a higher Ni content shows a much faster electrochemical decay due to a reduced interfacial stability. As NCM622 has the lowest Ni content, it shows the lowest capacity decay during long term cycling. Consequently, the effect of Al_2O_3 coating on the long-term cycling stability becomes noticeable only at higher cycle numbers (after approximately 80 cycles) as compared to the other two NCM compositions.

As all three different NCM configurations show an improvement upon coating, further detailed studies have been restricted to the NCM71.51.5 cathode and are discussed thoroughly in the following sections. Similar results are observed for NCM622 and NCM811, which can be found in the ESI† (Fig. S4). The initial charge–discharge profiles of pristine and coated cathodes cycled between 3.0 V and 4.3 V at the rate of 0.1C are compared and are shown in Fig. S5 (ESI†). The pristine cathode (183.06 mA h g^{-1}) shows a slightly higher initial discharge capacity as compared to the coated cathode (179.36 mA h g^{-1}). The slight decrease in capacity during the first few cycles of the coated cathode is attributed due to the additional resistance arised by the thin Al_2O_3 coatings and possibly due to the lithiation of the alumina layer during initial cycling.[70,71] Furthermore, it can be seen in Fig. 7 that the decrease in initial capacity due to the coating is compensated by the improved capacity retention and coulombic efficiency in the following cycles at 0.1C as compared to the pristine cathode. It can also be seen that the coated cathode has a higher overpotential during the first cycle compared to the pristine one, which again is attributed to the additional resistance arising from the thin Al_2O_3 layer. Nevertheless, the coated cathodes show no polarization in contrast to the pristine cathodes during further

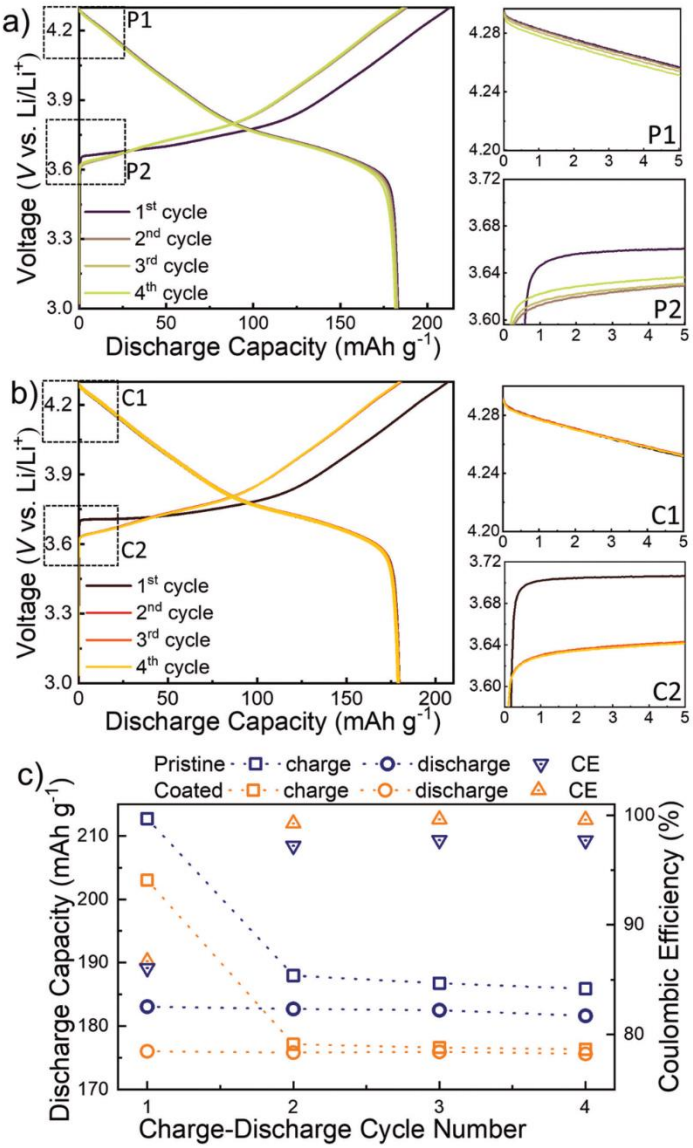

Fig. 7 Galvanostatic charge–discharge curves of first four cycles at 0.1C for (a) pristine cathode and (b) coated cathode. (c) Comparison of initial four charge–discharge cycles at 0.1C for pristine and coated cathodes.

cycling (Fig. 7a and b; P1, P2 *vs.* C1, C2), which further suggests the lithiation of the alumina layer and an improvement of the ionic transport properties of the coating layer. The exact values shown in Fig. 7c reveal that the stability of the coated cathode

has slightly improved compared to the pristine cathode during the initial formation step at 0.1C, which in turn suggests that the coated cathode is more stable against parasitic side reactions occurring at the electrode/electrolyte interface.

Fig. 8a and b compares the voltage *versus* capacity profile of different cycles of the pristine and the coated cathodes. A continuous polarization arises at the beginning of different charge–discharge cycles in both cases and the pristine cathode shows a much higher polarization as compared to the coated cathode during long-term cycling. The exact values of the voltage change of the pristine and coated cathodes during cycling are compared in Fig. 8c. It can be seen that the coated cathode is much more stable than the pristine one. This is attributed to the coating, which prevents the side reactions from taking place at the electrode/electrolyte interface leading to severe capacity degradation in Ni-rich NCM cathodes.[72] Impurities, *e.g.*, adsorbed H_2O on the surface of NCM, can accelerate the decomposition of the electrolyte, thereby releasing HF and inactive LiF phases.[73] These side reactions increase the charge transfer resistance,[74] as the reaction products (*e.g.*, LiF)

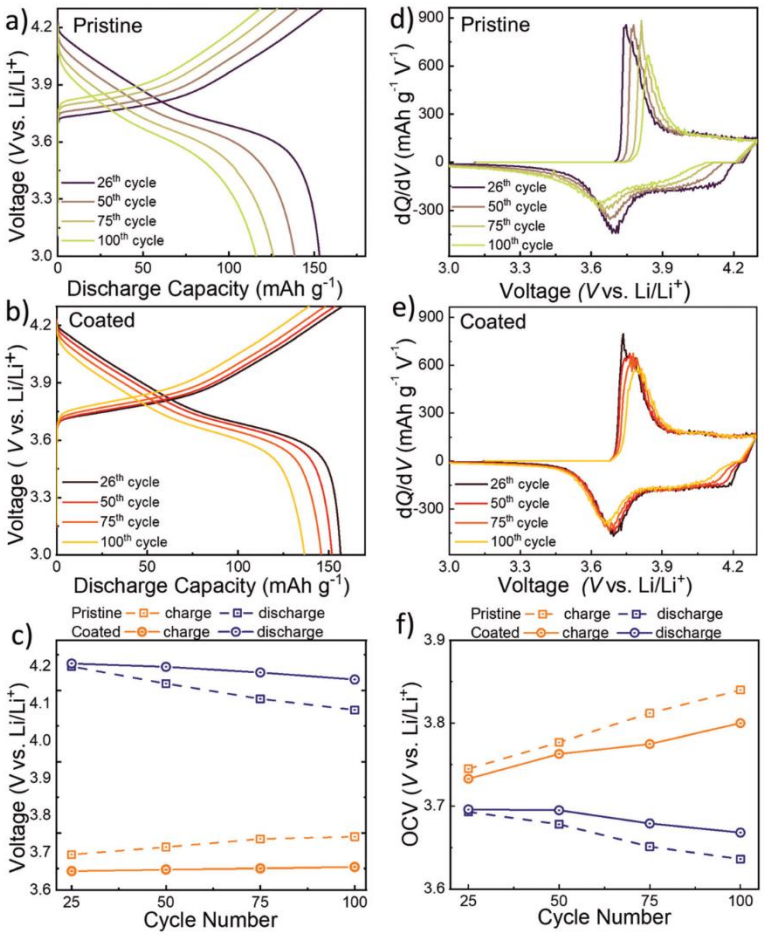

Fig. 8 Galvanostatic charge–discharge curves of (a) pristine and (b) coated NCM cycled at 0.5C after the C-rate test. (c) Comparison of voltage at the beginning of different cycles for pristine and coated NCM. Differential capacity plots for (d) pristine and (e) coated NCM cycled at 0.5C. (f) Comparison of the open-circuit voltage (OCV) change during cycling for pristine and coated NCM.

are highly resistive to Li-ion migration.[75] The formation of such a high resistive cathode/electrolyte interface (CEI) results in a higher polarization and severe capacity fading. The coating at the electrode surface prevents the direct physical contact between NCM and electrolyte and thus effectively suppresses the side reactions at the CEI.[76,77]

It should be noted that the ALD precursor for alumina (*i.e.* trimethylaluminium) is also a good H_2O scrubber, which can eliminate surface H_2O present on NCM and in-turn prevents electrolyte-related side reactions from taking place.[78,79] The higher capacity retention of the coated cathode can therefore also be due to the removal of H_2O from the electrode surface during the coating process, preventing side reactions and inhibiting HF formation.[22] The slightly lower initial coulombic efficiency of the pristine cathodes compared to that of the coated ones further indicates that more side reactions occur between the pristine cathode surfaces and the electrolyte. Also the higher polarization during cycling for the pristine cathodes compared to the coated cathodes signifies more pronounced parasitic side reactions at the surface.[80,81]

To further investigate the polarization of the cells during cycling, the differential capacity plots (dQ/dV) of the pristine and coated cathodes are shown in Fig. 8d and e, respectively. The redox peaks in the dQ/dV plots indicate the plateaus in the charge–discharge curves shown in Fig. 8a and b. It is found that the oxidation peak shifts to higher values and the reduction peak shifts to lower values during cycling, which indicates the polarization in the cell. Fig. 8f compares the OCV values of the pristine and coated cathodes, which also confirm a larger shift in the redox peaks of the pristine cathode, *i.e.*, the oxidation peak shifts to higher voltage and the reduction peak shifts to lower voltage, as compared to the coated cathode. This further corroborates the assumption that more side reactions occur at the surface of the pristine cathodes compared to the coated ones.[80]

3.3. Post-mortem characterization

During the electrochemical cycling, the stability of NCM based cathodes is also expressed in terms of the morphological integrity of the secondary particles. Microcracks in the NCM secondary particles are considered as one of the main causes for capacity fading. These microcracks are induced by electrochemical stress inside the particles caused by a volume change during lithiation/delithiation, parasitic side reactions generating a thick CEI layer, and the generation of new phases with larger lattice parameters. In our case, we consider the coating to be effective against the side reaction at the interface, which in turn might be also beneficial to maintain the secondary particle integrity. In order to investigate the effect of coating on the structural stability of the cathodes and the stability of the Al_2O_3 coating, electrochemically cycled electrodes were analyzed using SEM-EDX and C-AFM.

As shown in Fig. 9, the pristine cathode exhibits severe particle cracking as also confirmed by cross sectional SEM images shown in Fig. S6 (ESI†). Although the cracking likely improves the chemical diffusion of lithium and the charge transfer kinetics in the NCM particles due to an increase in the electrochemically active surface area,[82] it is also considered to be harmful for the electrochemical stability of LIBs as the new surface area also interacts with the electrolyte resulting in additional side reactions at the surface accompanied by a decrease in cycling performance.[83] In contrast to the uncoated cathode, the morphology of the particles of the coated cathode is maintained, which hinders the increase in surface area being in contact with the liquid electrolyte. A comparison of the high magnification SEM-EDX images of the coated cathode before and after cycling shown in Fig. 9c reveals that the Al_2O_3 layer is homogeneously distributed over the cathode even after long-term cycling, which shows that the Al_2O_3 coating is highly stable.

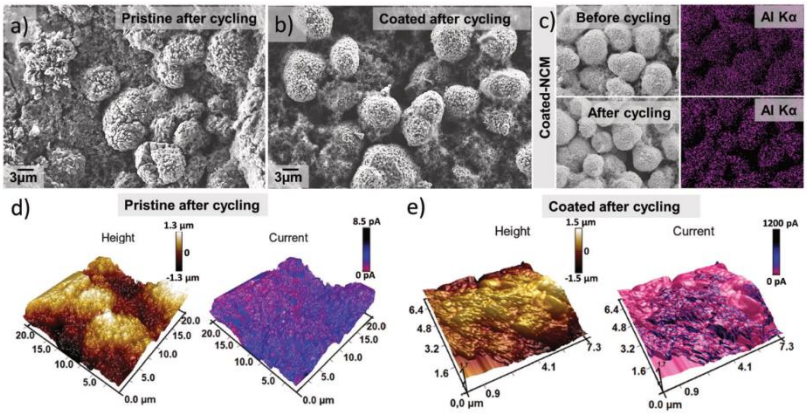

Fig. 9 SEM images of NCM71.51.5 electrodes (a) before, and (b) after cycling, (c) SEM-EDX mapping of Al before and after cycling. C-AFM image of NCM71.51.5 electrodes (d) pristine, and (e) coated, after cycling.

Fig. 9d and e show the C-AFM measurements of the pristine and coated electrodes after cycling, respectively. It can be seen that nearly no current signal is detectable, *i.e.*, the surface conductivity of the pristine sample vanishes completely after cycling. This confirms the formation of an insulating CEI in case of the pristine cathode, which impedes the charge transfer at the interface leading to the observed capacity fading. In case of the coated sample, a comparable current signal similar to that prior to cycling is detected. The surface conductivity is nearly unaffected still showing the NCM secondary particles embedded in a conductive carbon/binder matrix. Thus, the C-AFM results support the assumption that the Al_2O_3 coating is highly stable against electrochemical cycling and prevents CEI formation by suppressing the side reactions occurring at the interface.

4. Conclusions

In this work, the surface of different Ni-rich NCM cathodes was modified by Al_2O_3 using an optimized ALD process. C-AFM measurements of the pristine and coated cathodes before cycling reveal that the Al_2O_3 coating is sufficiently thin to maintain the electrical surface conductivity of the cathode. Improvements of capacity retention and coulombic efficiencies are observed for all three coated cathode compositions due to the coating. The improved electrochemical performance confirms that surface modification using the ALD techniques can significantly mitigate the detrimental side reactions at the electrode/electrolyte interface and thus improve the cycling stability of Ni-rich NCM based cathodes. The post-mortem analysis clearly shows that the Al_2O_3 coating is stable during electrochemical cycling and successfully inhibits deleterious side reactions and particle cracking. This is also supported by post-mortem C-AFM measurements, which reveal the formation of an insulating CEI resulting in a nearly complete suppression of the cathode surface conductivity and consequently impeding charge transfer at the interface. The results clearly indicate that applying conformal coatings using an optimized ALD coating technique can improve the structural and electrochemical integrity of Ni-rich NCM based ready-to-use cathodes as long as the charge transfer at the interface is preserved. The results could be a significant step towards considering Ni-rich NCM based high energy cathodes for practical applications in EVs/HEVs using conformal surface modification with ALD.

Conflicts of interest

The authors declare no competing financial interests.

Acknowledgements

R. S. N. and M. T. E. thank the German Federal Ministry of Education and Research (BMBF) for the funding of the NanoMatFutur project NiKo (03XP0093). S. C. gratefully acknowledges the Alexander von Humboldt Foundation for financial support through a Postdoctoral Fellowship.

References

1 K. Yang, L. Z. Fan, J. Guo and X. Qu, Significant improvement of electrochemical properties of AlF_3-coated $LiNi_{0.5}Co_{0.2}Mn_{0.3}O_2$ cathode materials, *Electrochim. Acta*, 2012, **63**, 363–368.
2 J. Tarascon and M. Armand, Issues and challenges facing rechargeable lithium batteries, *Nature*, 2001, **414**, 359–367.
3 L. Croguennec and M. R. Palacin, Recent achievements on inorganic electrode materials for lithium-ion batteries, *J. Am. Chem. Soc.*, 2015, **137**, 3140–3156.
4 K. Edström, T. Gustafsson and J. O. Thomas, The cathode–electrolyte interface in the Li-ion battery, *Electrochim. Acta*, 2004, **50**, 397–403.
5 Z. Liu, A. Yu and J. Y. Lee, Synthesis and characterization of $LiNi_{1-x-y}Co_xMn_yO_2$ as the cathode materials of secondary lithium batteries, *J. Power Sources*, 1999, **81**, 416–419.
6 K.-S. Lee, S.-T. Myung, K. Amine, H. Yashiro and Y.-K. Sun, Structural and Electrochemical Properties of Layered $LiNi_{1-2x}Co_xMn_xO_2$ (x = 0.1–0.3) Positive Electrode Materials for Li-Ion Batteries, *J. Electrochem. Soc.*, 2007, **154**, A971.
7 L. De Biasi, A. O. Kondrakov, H. Geßwein, T. Brezesinski, P. Hartmann and J. Janek, Between Scylla and Charybdis: Balancing among Structural Stability and Energy Density of Layered NCM Cathode Materials for Advanced Lithium-Ion Batteries, *J. Phys. Chem. C*, 2017, **121**, 26163–26171.
8 D. Wang, X. Li, Z. Wang, H. Guo, Y. Xu, Y. Fan and J. Ru, Role of zirconium dopant on the structure and high voltage electrochemical performances of $LiNi_{0.5}Co_{0.2}Mn_{0.3}O_2$ cathode materials for lithium ion batteries, *Electrochim. Acta*, 2016, **188**, 48–56.
9 A. Banerjee, K. H. Park, J. W. Heo, Y. J. Nam, C. K. Moon, S. M. Oh, S. T. Hong and Y. S. Jung, Na_3SbS_4: A Solution Processable Sodium Superionic Conductor for All-Solid-State Sodium-Ion Batteries, *Angew. Chem., Int. Ed.*, 2016, **55**, 9634–9638.
10 S. K. Jung, H. Gwon, J. Hong, K. Y. Park, D. H. Seo, H. Kim, J. Hyun, W. Yang and K. Kang, Understanding the degradation mechanisms of $LiNi_{0.5}Co_{0.2}Mn_{0.3}O_2$ cathode material in lithium ion batteries, *Adv. Energy Mater.*, 2014, **4**, 1–7.
11 D. Aurbach, Y. Talyosef, B. Markovsky, E. Markevich, E. Zinigrad, L. Asraf, J. S. Gnanaraj and H. J. Kim, Design of electrolyte solutions for Li and Li-ion batteries: a review, *Electrochim. Acta*, 2004, **50**, 247–254.
12 T. Kawamura, S. Okada and J. ichi Yamaki, Decomposition reaction of $LiPF_6$-based electrolytes for lithium ion cells, *J. Power Sources*, 2006, **156**, 547–554.
13 X. Li, J. Liu, X. Meng, Y. Tang, M. N. Banis, J. Yang, Y. Hu, R. Li, M. Cai and X. Sun, Significant impact on cathode performance of lithium-ion batteries by precisely controlled metal oxide nanocoatings via atomic layer deposition, *J. Power Sources*, 2014, **247**, 57–69.
14 S. F. Lux, J. Chevalier, I. T. Lucas and R. Kostecki, HF formation in $LiPF_6$-based organic carbonate electrolytes, *Electrochem. Lett.*, 2013, **2**, 121–123.
15 M. Hirayama, K. Sakamoto, T. Hiraide, D. Mori, A. Yamada, R. Kanno, N. Sonoyama, K. Tamura and J. Mizuki,

Fig. 9d and e show the C-AFM measurements of the pristine and coated electrodes after cycling, respectively. It can be seen that nearly no current signal is detectable, *i.e.*, the surface conductivity of the pristine sample vanishes completely after cycling. This confirms the formation of an insulating CEI in case of the pristine cathode, which impedes the charge transfer at the interface leading to the observed capacity fading. In case of the coated sample, a comparable current signal similar to that prior to cycling is detected. The surface conductivity is nearly unaffected still showing the NCM secondary particles embedded in a conductive carbon/binder matrix. Thus, the C-AFM results support the assumption that the Al_2O_3 coating is highly stable against electrochemical cycling and prevents CEI formation by suppressing the side reactions occurring at the interface.

4. Conclusions

In this work, the surface of different Ni-rich NCM cathodes was modified by Al_2O_3 using an optimized ALD process. C-AFM measurements of the pristine and coated cathodes before cycling reveal that the Al_2O_3 coating is sufficiently thin to maintain the electrical surface conductivity of the cathode. Improvements of capacity retention and coulombic efficiencies are observed for all three coated cathode compositions due to the coating. The improved electrochemical performance confirms that surface modification using the ALD techniques can significantly mitigate the detrimental side reactions at the electrode/electrolyte interface and thus improve the cycling stability of Ni-rich NCM based cathodes. The post-mortem analysis clearly shows that the Al_2O_3 coating is stable during electrochemical cycling and successfully inhibits deleterious side reactions and particle cracking. This is also supported by post-mortem C-AFM measurements, which reveal the formation of an insulating CEI resulting in a nearly complete suppression of the cathode surface conductivity and consequently impeding charge transfer at the interface. The results clearly indicate that applying conformal coatings using an optimized ALD coating technique can improve the structural and electrochemical integrity of Ni-rich NCM based ready-to-use cathodes as long as the charge transfer at the interface is preserved. The results could be a significant step towards considering Ni-rich NCM based high energy cathodes for practical applications in EVs/HEVs using conformal surface modification with ALD.

Conflicts of interest

The authors declare no competing financial interests.

Acknowledgements

R. S. N. and M. T. E. thank the German Federal Ministry of Education and Research (BMBF) for the funding of the NanoMatFutur project NiKo (03XP0093). S. C. gratefully acknowledges the Alexander von Humboldt Foundation for financial support through a Postdoctoral Fellowship.

References

1 K. Yang, L. Z. Fan, J. Guo and X. Qu, Significant improvement of electrochemical properties of AlF_3-coated $LiNi_{0.5}Co_{0.2}Mn_{0.3}O_2$ cathode materials, *Electrochim. Acta*, 2012, **63**, 363–368.
2 J. Tarascon and M. Armand, Issues and challenges facing rechargeable lithium batteries, *Nature*, 2001, **414**, 359–367.
3 L. Croguennec and M. R. Palacin, Recent achievements on inorganic electrode materials for lithium-ion batteries, *J. Am. Chem. Soc.*, 2015, **137**, 3140–3156.
4 K. Edström, T. Gustafsson and J. O. Thomas, The cathode–electrolyte interface in the Li-ion battery, *Electrochim. Acta*, 2004, **50**, 397–403.
5 Z. Liu, A. Yu and J. Y. Lee, Synthesis and characterization of $LiNi_{1-x-y}Co_xMn_yO_2$ as the cathode materials of secondary lithium batteries, *J. Power Sources*, 1999, **81**, 416–419.
6 K.-S. Lee, S.-T. Myung, K. Amine, H. Yashiro and Y.-K. Sun, Structural and Electrochemical Properties of Layered $LiNi_{1-2x}Co_xMn_xO_2$ (x = 0.1–0.3) Positive Electrode Materials for Li-Ion Batteries, *J. Electrochem. Soc.*, 2007, **154**, A971.
7 L. De Biasi, A. O. Kondrakov, H. Geßwein, T. Brezesinski, P. Hartmann and J. Janek, Between Scylla and Charybdis: Balancing among Structural Stability and Energy Density of Layered NCM Cathode Materials for Advanced Lithium-Ion Batteries, *J. Phys. Chem. C*, 2017, **121**, 26163–26171.
8 D. Wang, X. Li, Z. Wang, H. Guo, Y. Xu, Y. Fan and J. Ru, Role of zirconium dopant on the structure and high voltage electrochemical performances of $LiNi_{0.5}Co_{0.2}Mn_{0.3}O_2$ cathode materials for lithium ion batteries, *Electrochim. Acta*, 2016, **188**, 48–56.
9 A. Banerjee, K. H. Park, J. W. Heo, Y. J. Nam, C. K. Moon, S. M. Oh, S. T. Hong and Y. S. Jung, Na_3SbS_4: A Solution Processable Sodium Superionic Conductor for All-Solid-State Sodium-Ion Batteries, *Angew. Chem., Int. Ed.*, 2016, **55**, 9634–9638.
10 S. K. Jung, H. Gwon, J. Hong, K. Y. Park, D. H. Seo, H. Kim, J. Hyun, W. Yang and K. Kang, Understanding the degradation mechanisms of $LiNi_{0.5}Co_{0.2}Mn_{0.3}O_2$ cathode material in lithium ion batteries, *Adv. Energy Mater.*, 2014, **4**, 1–7.
11 D. Aurbach, Y. Talyosef, B. Markovsky, E. Markevich, E. Zinigrad, L. Asraf, J. S. Gnanaraj and H. J. Kim, Design of electrolyte solutions for Li and Li-ion batteries: a review, *Electrochim. Acta*, 2004, **50**, 247–254.
12 T. Kawamura, S. Okada and J. ichi Yamaki, Decomposition reaction of $LiPF_6$-based electrolytes for lithium ion cells, *J. Power Sources*, 2006, **156**, 547–554.
13 X. Li, J. Liu, X. Meng, Y. Tang, M. N. Banis, J. Yang, Y. Hu, R. Li, M. Cai and X. Sun, Significant impact on cathode performance of lithium-ion batteries by precisely controlled metal oxide nanocoatings via atomic layer deposition, *J. Power Sources*, 2014, **247**, 57–69.
14 S. F. Lux, J. Chevalier, I. T. Lucas and R. Kostecki, HF formation in $LiPF_6$-based organic carbonate electrolytes, *Electrochem. Lett.*, 2013, **2**, 121–123.
15 M. Hirayama, K. Sakamoto, T. Hiraide, D. Mori, A. Yamada, R. Kanno, N. Sonoyama, K. Tamura and J. Mizuki,

41 M. F. Zscherp, J. Glaser, C. Becker, A. Beyer, P. Cop, J. Schörmann, K. Volz and M. T. Elm, Epitaxial Growth and Structural Characterization of Ceria Deposited by Atomic Layer Deposition on High-Surface Porous Yttria-Stabilized Zirconia Thin Films, *Cryst. Growth Des.*, 2020, **20**, 2194–2201.

42 J. Cho, Y. J. Kim and B. Park, Novel $LiCoO_2$ Cathode Material with Al_2O_3 Coating for a Li Ion Cell, *Chem. Mater.*, 2000, **4**, 3788–3791.

43 J. Y. Liao and A. Manthiram, Surface-modified concentration-gradient Ni-rich layered oxide cathodes for high-energy lithium-ion batteries, *J. Power Sources*, 2015, **282**, 429–436.

44 C. C. Wang, J. W. Lin, Y. H. Yu, K. H. Lai, K. F. Chiu and C. C. Kei, Electrochemical and Structural Investigation on Ultra-thin ALD ZnO and TiO_2 Coated Lithium-Rich Layered Oxide Cathodes, *ACS Sustainable Chem. Eng.*, 2018, **6**, 16941–16950.

45 S. Dong, Y. Zhou, C. Hai, J. Zeng, Y. Sun, Y. Shen, X. Li, X. Ren, G. Qi, X. Zhang and L. Ma, Ultrathin CeO_2 coating for improved cycling and rate performance of Ni-rich layered $LiNi_{0.7}Co_{0.2}Mn_{0.1}O_2$ cathode materials, *Ceram. Int.*, 2019, **45**, 144–152.

46 P. Yan, J. Zheng, X. Zhang, R. Xu, K. Amine, J. Xiao, J. G. Zhang and C. M. Wang, Atomic to Nanoscale Investigation of Functionalities of an Al_2O_3 Coating Layer on a Cathode for Enhanced Battery Performance, *Chem. Mater.*, 2016, **28**, 857–863.

47 Y. Xu, X. Li, Z. Wang, H. Guo, W. Peng and W. Pan, The enhanced high cut-off voltage electrochemical performances of $LiNi_{0.5}Co_{0.2}Mn_{0.3}O_2$ by the CeO_2 modification, *Electrochim. Acta*, 2016, **219**, 49–60.

48 J. Zheng, M. Gu, J. Xiao, B. J. Polzin, P. Yan, X. Chen, C. Wang and J. G. Zhang, Functioning mechanism of AlF_3 coating on the Li- and Mn-rich cathode materials, *Chem. Mater.*, 2014, **26**, 6320–6327.

49 H. H. Sun, J. Y. Hwang, C. S. Yoon, A. Heller and C. B. Mullins, Capacity Degradation Mechanism and Cycling Stability Enhancement of AlF_3-Coated Nanorod Gradient $Na[Ni_{0.65}Co_{0.08}Mn_{0.27}]O_2$ Cathode for Sodium-Ion Batteries, *ACS Nano*, 2018, **12**, 12912–12922.

50 Y. Oh, D. Ahn, S. Nam and B. Park, The effect of Al_2O_3-coating coverage on the electrochemical properties in $LiCoO_2$ thin films, *J. Solid State Electrochem.*, 2010, **14**, 1235–1240.

51 Y. J. Kim, J. Cho, T.-J. Kim and B. Park, Suppression of Cobalt Dissolution from the $LiCoO_2$ Cathodes with Various Metal-Oxide Coatings, *J. Electrochem. Soc.*, 2003, **150**, 1723.

52 D. Mohanty, K. Dahlberg, D. M. King, L. A. David, A. S. Sefat, D. L. Wood, C. Daniel, S. Dhar, V. Mahajan, M. Lee and F. Albano, Modification of Ni-Rich FCG NMC and NCA Cathodes by Atomic Layer Deposition: Preventing Surface Phase Transitions for High-Voltage Lithium-Ion Batteries, *Sci. Rep.*, 2016, **6**, 1–16.

53 D. H. K. Jackson and T. F. Kuech, Electrochemical effects of annealing on atomic layer deposited Al_2O_3 coatings on $LiNi_{0.5}Co_{0.2}Mn_{0.3}O_2$, *J. Power Sources*, 2017, **365**, 61–67.

54 S. Fang, D. Jackson, M. L. Dreibelbis, T. F. Kuech and R. J. Hamers, Anode-originated SEI migration contributes to formation of cathode-electrolyte interphase layer, *J. Power Sources*, 2018, **373**, 184–192.

55 A. M. Wise, C. Ban, J. N. Weker, S. Misra, A. S. Cavanagh, Z. Wu, Z. Li, M. S. Whittingham, K. Xu, S. M. George and M. F. Toney, Effect of Al_2O_3 Coating on Stabilizing $LiNi_{0.4}Mn_{0.4}Co_{0.2}O_2$ Cathodes, *Chem. Mater.*, 2015, **27**, 6146–6154.

56 Y. Shi, M. Zhang, D. Qian and Y. S. Meng, Ultrathin Al_2O_3 Coatings for Improved Cycling Performance and Thermal Stability of $LiNi_{0.5}Co_{0.2}Mn_{0.3}O_2$ Cathode Material, *Electrochim. Acta*, 2016, **203**, 154–161.

57 W. Li, A. Dolocan, P. Oh, H. Celio, S. Park, J. Cho and A. Manthiram, Dynamic behaviour of interphases and its implication on high-energy-density cathode materials in lithium-ion batteries, *Nat. Commun.*, 2017, **8**, 1–10.

58 J. Zhu, L. Lu and K. Zeng, Nanoscale Mapping of Lithium-Ion Diffusion in a Cathode within an All-Solid-State Lithium-Ion Battery by Advanced Scanning Probe Microscopy Techniques, *ACS Nano*, 2013, **7**, 1666–1675.

59 H. Kang, J. Lee, T. Rodgers, J.-H. Shim and S. Lee, Electrical Conductivity of Delithiated Lithium Cobalt Oxides: Conductive Atomic Force Microscopy and Density Functional Theory Study, *J. Phys. Chem. C*, 2019, **123**, 17703–17710.

60 J. S. Terreblanche, D. L. Thompson, I. M. Aldous, J. Hartley, A. P. Abbott and K. S. Ryder, Experimental Visualization of Commercial Lithium Ion Battery Cathodes: Distinguishing Between the Microstructure Components Using Atomic Force Microscopy, *J. Phys. Chem. C*, 2020, **124**, 14622–14631.

61 N. Balke, S. Jesse, A. N. Morozovska, E. Eliseev, D. W. Chung, Y. Kim, L. Adamczyk, R. E. García, N. Dudney and S. V. Kalinin, Nanoscale mapping of ion diffusion in a lithium-ion battery cathode, *Nat. Nanotechnol.*, 2010, **5**, 749–754.

62 S.-K. Jeong, M. Inaba, T. Abe and Z. Ogumi, Surface Film Formation on Graphite Negative Electrode in Lithium-Ion Batteries: AFM Study in an Ethylene Carbonate-Based Solution, *J. Electrochem. Soc.*, 2001, **148**, 989.

63 S.-K. Jeong, M. Inaba, R. Mogi, Y. Iriyama, T. Abe and Z. Ogumi, Surface Film Formation on a Graphite Negative Electrode in Lithium-Ion Batteries: Atomic Force Microscopy Study on the Effects of Film-Forming Additives in Propylene Carbonate Solutions, *Langmuir*, 2001, **17**, 8281–8286.

64 S. Leroy, F. Blanchard, R. Dedryvère, H. Martinez, B. Carré, D. Lemordant and D. Gonbeau, Surface film formation on a graphite electrode in Li-ion batteries: AFM and XPS study, *Surf. Interface Anal.*, 2005, **37**, 773–781.

65 H. M. Cheng, F. M. Wang, J. P. Chu, R. Santhanam, J. Rick and S. C. Lo, Enhanced cycleabity in lithium ion batteries: Resulting from atomic layer depostion of Al_2O_3 or TiO_2 on $LiCoO_2$ electrodes, *J. Phys. Chem. C*, 2012, **116**, 7629–7637.

66 T. Li, X. Li, Z. Wang and H. Guo, A short process for the efficient utilization of transition-metal chlorides in lithium-ion batteries: A case of $Ni_{0.8}Co_{0.1}Mn_{0.1}O_{1.1}$and $LiNi_{0.8}Co_{0.1}Mn_{0.1}O_2$, *J. Power Sources*, 2017, **342**, 495–503.

67 P. Cop, E. Celik, K. Hess, Y. Moryson, P. Klement, M. T. Elm and B. M. Smarsly, Atomic Layer Deposition of Nanometer-Sized CeO_2 Layers in Ordered Mesoporous ZrO_2 Films and Their Impact on the Ionic/Electronic Conductivity, *ACS Appl. Nano Mater.*, 2020, **3**, 10757–10766.

68 S. Hildebrand, C. Vollmer, M. Winter and F. M. Schappacher, Al_2O_3, SiO_2 and TiO_2 as Coatings for safer $LiNi_{0.80}Co_{0.15}Al_{0.05}O_2$ cathodes: Electrochemical performance and thermal analysis by accelerating rate calorimetry, *J. Electrochem. Soc.*, 2017, **164**, A2190–A2198.

69 J.-T. Lee, F.-M. Wang, C.-S. Cheng, C.-C. Li and C.-H. Lin, Low-temperature atomic layer deposited Al_2O_3 thin film on layer structure cathode for enhanced cycleability in lithium-ion batteries, *Electrochim. Acta*, 2010, **55**, 4002–4006.

70 S. C. Jung and Y. K. Han, How do Li atoms pass through the Al_2O_3 coating layer during lithiation in Li-ion batteries, *J. Phys. Chem. Lett.*, 2013, **4**, 2681–2685.

71 Y. Liu, N. S. Hudak, D. L. Huber, S. J. Limmer, J. P. Sullivan and J. Y. Huang, In situ transmission electron microscopy observation of pulverization of aluminum nanowires and evolution of the thin surface Al_2O_3 layers during lithiation-delithiation cycles, *Nano Lett.*, 2011, **11**, 4188–4194.

72 X. H. Liu, L. Q. Kou, T. Shi, K. Liu and L. Chen, Excellent high rate capability and high voltage cycling stability of Y_2O_3-coated $LiNi_{0.5}Co_{0.2}Mn_{0.3}O_2$, *J. Power Sources*, 2014, **267**, 874–880.

73 L. Li, Z. Chen, Q. Zhang, M. Xu, X. Zhou, H. Zhu and K. Zhang, A hydrolysis-hydrothermal route for the synthesis of ultrathin $LiAlO_2$-inlaid $LiNi_{0.5}Co_{0.2}Mn_{0.3}O_2$ as a high-performance cathode material for lithium ion batteries, *J. Mater. Chem. A*, 2015, **3**, 894–904.

74 X. Xiong, D. Ding, Y. Bu, Z. Wang, B. Huang, H. Guo and X. Li, Enhanced electrochemical properties of a $LiNiO_2$-based cathode material by removing lithium residues with $(NH_4)_2HPO_4$, *J. Mater. Chem. A*, 2014, **2**, 11691–11696.

75 J. S. Gnanaraj, E. Zinigrad, M. D. Levi, D. Aurbach and M. Schmidt, A comparison among $LiPF_6$, $LiPF_3(CF_2CF_3)_3$ (LiFAP), and $LiN(SO_2CF_2CF_3)_2$ (LiBETI) solutions: electrochemical and thermal studies, *J. Power Sources*, 2003, **119**, 799–804.

76 L. J. Fu, H. Liu, C. Li, Y. P. Wu, E. Rahm, R. Holze and H. Q. Wu, Surface modifications of electrode materials for lithium ion batteries, *Solid State Sci.*, 2006, **8**, 113–128.

77 J. Cho, Y. J. Kim and B. Park, $LiCoO_2$ Cathode Material That Does Not Show a Phase Transition from Hexagonal to Monoclinic Phase, *J. Electrochem. Soc.*, 2001, **148**, 1110.

78 R. L. Puurunen, Surface chemistry of atomic layer deposition: A case study for the trimethylaluminum/water process, *J. Appl. Phys.*, 2005, **97**, 121301.

79 S. M. George, Atomic layer deposition: An overview, *Chem. Rev.*, 2010, **110**, 111–131.

80 J. Shim, R. Kostecki, T. Richardson, X. Song and K. A. Striebel, Electrochemical analysis for cycle performance and capacity fading of a lithium-ion battery cycled at elevated temperature, *J. Power Sources*, 2002, **112**, 222–230.

81 R. Jorn, R. Kumar, D. P. Abraham and G. A. Voth, Atomistic modeling of the electrode-electrolyte interface in Li-ion energy storage systems: Electrolyte structuring, *J. Phys. Chem. C*, 2013, **117**, 3747–3761.

82 R. Ruess, S. Schweidler, H. Hemmelmann, G. Conforto, A. Bielefeld, D. A. Weber, J. Sann, M. T. Elm and J. Janek, Influence of NCM Particle Cracking on Kinetics of Lithium-Ion Batteries with Liquid or Solid Electrolyte, *J. Electrochem. Soc.*, 2020, **167**, 100532.

83 W. Liu, P. Oh, X. Liu, S. Myeong, W. Cho and J. Cho, Countering Voltage Decay and Capacity Fading of Lithium-Rich Cathode Material at 60 °C by Hybrid Surface Protection Layers, *Adv. Energy Mater.*, 2015, **5**, 1–11.

3.2 Publication II: Enhancing the Electrochemical Performance of $LiNi_{0.70}Co_{0.15}Mn_{0.15}O_2$ Cathodes Using a Practical Solution-Based Al_2O_3 Coating

As demonstrated in publication I, ALD-based Al_2O_3 coatings can improve the electrochemical performance of Ni-rich NCM based cathodes. However, the ALD-based coating process is rather expensive and not quite suitable for industrial applications. Thus, using the basic knowledge of ALD-based coating method, we developed a rather cheap, easy and simple solution-based Al_2O_3 coating method.

Taking inspiration from the ALD coating mechanism for Al_2O_3, a solution-based coating method has been developed which makes use of the absorbed water at the NCM surface. Trimethylaluminium (TMA) acts as coating precursor. The NCM is mixed with TMA solution, which results in an Al_2O_3 coating on the NCM powder. No post-annealing step is involved. Structural analysis of the coated samples reveals the successful deposition of a homogenous and very thin Al_2O_3 coating on the surface of NCM. Electrochemical analysis shows a significantly improved long-term cycling performance of the coated NCM as compared to pristine NCM. The coated NCM also exhibits a lower impedance growth over long-term cycling suggesting much better prevention of the SEI formation as compared to pristine NCM. In addition, Post-mortem analysis of the cycled cathode reveals that the coating prevents particle cracking during cycling.

The concept and experiments for this publication have been designed and performed by myself under the supervision of Dr. M. T. Elm and Dr.T. Brezesinski. I wrote the manuscript and corrected by all co-authors. TEM images have been taken by A. Mazilkin. Dr. S. P. Culver contributed to scientific discussions. Reprinted with permission from Physical Chemistry Chemical Physics. Copyright 2018 Elsevier.

R. S. Negi, S. P. Culver, A. Mazilkin, T. Brezesinski, M. T. Elm, Enhancing the Electrochemical Performance of $LiNi_{0.70}Co_{0.15}Mn_{0.15}O_2$ Cathodes Using a Practical Solution-Based Al_2O_3 Coating. *ACS Applied Materials & Interfaces* **2020**, 12 (28), 31392-31400

ACS APPLIED MATERIALS & INTERFACES

www.acsami.org Research Article

Enhancing the Electrochemical Performance of $LiNi_{0.70}Co_{0.15}Mn_{0.15}O_2$ Cathodes Using a Practical Solution-Based Al_2O_3 Coating

Rajendra S. Negi, Sean P. Culver, Andrey Mazilkin, Torsten Brezesinski, and Matthias T. Elm*

Cite This: ACS Appl. Mater. Interfaces 2020, 12, 31392−31400 Read Online

ACCESS | Metrics & More | Article Recommendations | Supporting Information

ABSTRACT: Ni-rich $Li[Ni_xCo_yMn_{1-x-y}]O_2$ (NCM) cathode materials have attracted great research interest owing to their high energy density and relatively low cost. However, capacity fading because of parasitic side reactions, mainly occurring at the interface with the electrolyte, still hinders widespread application in advanced Li-ion batteries (LIBs). Surface modification via coating is a feasible approach to tackle this issue. Nevertheless, achieving uniform coatings is challenging, especially when using wet chemistry methods. In this work, a protective alumina shell on NCM701515 (70% Ni) was prepared through the reaction of surface-active −OH groups with trimethylaluminum as the precursor. The coated NCM701515 shows significantly improved capacity retention over uncoated (pristine) NCM701515. Part of the reason is the lower impedance buildup during cycling due to the effective suppression of adverse side reactions and secondary particle fracture. Taken together, the solution-based coating strategy described herein offers an easy way to apply surface treatment to stabilize Ni-rich NCM cathode materials in next-generation LIBs.

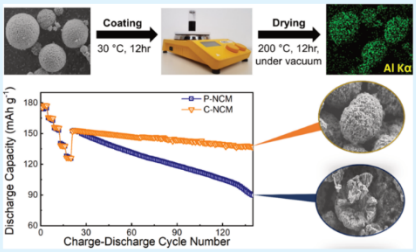

KEYWORDS: *Li-ion battery, Ni-rich NCM cathode, Al_2O_3 coating, wet chemistry, atomic layer deposition, surface protection*

INTRODUCTION

The rapid development of electric vehicles (EVs) and hybrid EVs (HEVs) has led to significant research efforts into rechargeable Li-ion batteries (LIBs), primarily aiming at achieving improved energy density and cycle life.[1,2] Advanced LIBs are also critical to the sustainable development of EVs and HEVs (by minimizing their environmental impact).[3−5] In the electromobility area, one of the major challenges to be tackled is the limited driving range, which is directly related to the gravimetric (W h kg^{-1}) and volumetric energy densities (W h L^{-1}) of LIBs.[2,6] The cathode material partly accounts for the attainable energy density. Various cathode materials such as $LiCoO_2$ (LCO),[7,8] $LiMn_2O_4$,[9,10] $LiFePO_4$,[11,12] and layered $Li[Ni_xCo_yMn_{1-x-y}]O_2$ (NCM)[13−17] have been employed commercially in LIBs. Among them, NCM is considered one of the most promising positive electrode materials for next-generation LIBs because of its relatively high energy density as well as lower cost and higher thermal stability than LCO.[5,18−20]

In recent years, new configurations of NCM-based cathode materials have been developed by increasing the Ni content to achieve improved energy densities at lower cost.[13,19,21,22] For example, NCM523 (50% Ni)[23,24] and NCM622 (60% Ni)[15] are actively used in battery applications for EVs and HEVs.[2] As mentioned previously, increasing the Ni content increases the attainable specific capacity for a given voltage window. However, it concurrently decreases the Mn and Co contents, leading to lower thermal and electrochemical stability (intrinsic structural instability).[25,26] Besides, residual water and alkali compounds (LiOH and Li_2O) present on the NCM surface are known to react with the supporting salt, resulting in an increase in cell resistance, among others.[27−30] Moreover, the electrochemical decomposition of surface contaminants[31,32] and/or reaction between the electrolyte and the surface species lead to the evolution of O_2, CO_2, and CO,[33,34] which exerts a negative effect on the cell performance. Overall, the reactive (and sensitive) nature of Ni-rich NCM toward the ambient atmosphere during storage and processing determines its surface properties,[35] which in turn strongly affect the cyclability.[30,36] In addition, in the delithiated state, the highly reactive NCM (containing tetravalent Ni) can oxidize the electrolyte, eventually leading to the formation of a detrimental surface layer, the so-called cathode solid−electrolyte interphase (cSEI), and gas evolution.[35,37] Hence, in order to improve the electrochemical performance of especially Ni-rich NCM

Received: April 8, 2020
Accepted: June 5, 2020
Published: June 5, 2020

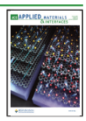

https://dx.doi.org/10.1021/acsami.0c06484
ACS Appl. Mater. Interfaces 2020, 12, 31392−31400

cathode materials in LIBs, surface modification seems indispensable.[38−40]

Surface modification via coating on powder or ready-to-use cathodes has been found promising because it effectively stabilizes the interface between the electrode and the electrolyte, thereby lowering the likelihood of parasitic side reactions during cycling.[17,41−43] The coating apparently can also partly prevent surface phase transformation from layered to a rock-salt or disordered spinel-like structure.[44,45] Various metal fluorides (e.g., LiF[46] and $LiAlF_4$[47]), metal oxides (e.g., CeO_2,[43] TiO_2,[7,48] ZrO_2,[41] and Al_2O_3[49,50]), and metal phosphates (e.g., $LiMgPO_4$,[51] $LiFePO_4$,[52] and Li_3PO_4[53]) have been tested as coating materials and shown to have a positive influence on the cyclability and stability of LIBs. In particular, Al_2O_3[17,36,50,54,55] has been most commonly applied to the cathode material because of its low cost and highly effective nature as a protective coating.

With respect to the coating process of Al_2O_3, two routes are usually explored, wet chemistry[56,57] and atomic layer deposition (ALD).[55,58] The wet-chemical route is considered to be simpler, cheaper, and easier for upscaling. However, there is virtually no control over the coating quality (thickness and homogeneity), and it also requires post heat-treatment.[56,59] For example, alkoxide-based coating approaches typically involve the use of (polar) protic solvents such as H_2O or ethanol[60,61] which may promote the generation of deleterious lithium residuals on the NCM surface (note that surface contaminants have a negative impact on the cyclability).[28,53] Additionally, post annealing at elevated temperatures may result in ion migration and cation mixing, which also deteriorates the cell performance.[23,59] In contrast, ALD has the advantage of precise control over thickness and homogeneity, but the process itself is rather complex and expensive.

The ALD-derived Al_2O_3 coating process is well-established in the literature.[62,63] Usually, it combines two steps, consisting of half-reactions using trimethylaluminum (TMA) and H_2O. In the first step, the surface-active −OH groups react with the TMA precursor. In the second step, H_2O reacts with TMA to complete the whole process.[62] Such ALD-derived Al_2O_3 coatings have been successfully applied to NCM powder and practical cathodes.[17,49]

In this work, we use the fundamentals of the ALD process to develop a facile and cost-effective, low-temperature wet-chemical-based alumina coating method to modify the surface of NCM701515 (70% Ni). Specifically, it makes use of surface-active −OH groups (from LiOH and adsorbed H_2O) to dry and coat the NCM cathode material in a single treatment step in solution.[64] Detailed structural characterization combined with electrochemical analysis reveals that using this approach, a thin and uniform coating can be achieved, which not only consumes unfavorable surface residuals, but also prevents particle fracture and stabilizes the interface between the cathode and the electrolyte, thereby leading to considerable improvements in cycling performance.

■ EXPERIMENTAL SECTION

Surface Modification of Ni-Rich NCM. The Al_2O_3 coating was prepared via a solution route. For the coating, TMA solution (0.279 mL, 2 M in toluene; Sigma-Aldrich) was diluted using anhydrous toluene (15 mL; Sigma-Aldrich) and stirred for 1 h. The diluted TMA solution (5 ml) was then added to $LiNi_{0.70}Co_{0.15}Mn_{0.15}O_2$ (NCM701515, 5 g; Gelon LIB) and stirred at 30 °C for 12 h. The final dispersion was filtered and washed with anhydrous toluene (20 mL) to remove unreacted TMA. The recovered (coated) powder was dried in a vacuum at 200 °C overnight before transferring it to the glove box.

Material Characterization. The particle morphology, microstructure, and electrode topography along with the elemental composition of pristine (P-NCM) and coated (C-NCM) samples were investigated by scanning electron microscopy (SEM, MERLIN with 7 kV accelerating voltage and 3000 pA current; Zeiss) coupled with energy dispersive X-ray (EDX) spectroscopy (X-Max detector; Oxford Instruments). X-ray photoelectron spectroscopy (XPS) was performed using a monochromatic Al Kα radiation on a PHI 5000 VersaProbe II Scanning ESCA microprobe ($\sim 10^{-8}$ Pa pressure; Physical Electronics). Survey spectra were recorded with a pass energy of 93.9 eV and, for high-resolution spectra, a pass energy of 23.5 eV was used. The structural characterization of pristine and coated powder was done by X-ray diffraction (XRD; Bruker) with Cu Kα radiation. The water content before and after coating was determined by Karl-Fischer titration. Transmission electron microscopy (TEM) was performed on an FEI Titan 80-300 aberration corrected transmission electron microscope at 300 kV. Samples for TEM investigation were prepared using an FEI STRATA 400 S dual beam facility, with the Ga-ion beam operating at 30 kV, followed by polishing at 2 kV to improve the surface quality.

Electrode Preparation. The solution of polyvinylidene fluoride binder (5 wt %, Solef PVDF 6020; Solvay) was prepared in *N*-methyl-2-pyrrolidone (NMP; Sigma-Aldrich). For the electrode preparation, either P-NCM or C-NCM (90 wt %) was mixed with conductive carbon black (5 wt %, Super P; TIMCAL) and suspended in the binder solution (5 wt %). Additional NMP was added and the solution was stirred overnight to achieve the desired viscosity. The resultant solution was then cast onto Al foil using a doctor blade. The as-prepared cathode sheets were calendared at 90 psi and dried at 120 °C in a vacuum (24 h) before transferring them to the glove box for further measurements.

Electrochemical Testing. For the electrochemical testing, coin cells (CR2032; MTI Corporation) with the P-NCM or C-NCM cathode (12 mm) and Li foil anode (14 mm; Rockwood Lithium GmbH) were assembled using Celgard2500 (16 mm; Celgard) as the separator and LP50 (1 M $LiPF_6$ in 1/1 wt/wt ethylene carbonate/ethyl methyl carbonate, 50 μL; Sigma-Aldrich) as the electrolyte. The areal loading was 10.4−10.8 $mg_{NCM701515}$ cm^{-2}. All of the electrochemical testing was done using a multichannel battery cycler (MACCOR, Inc.). The coin cells were cycled in a constant current (CC) mode in the voltage range between 3.0 and 4.3 V at 25 °C. A specific current of 160 mA g^{-1} was defined at the 1C rate. Initially, the cells were tested at various C-rates ranging from 0.1 to 2C, each for four cycles. For the long-term cycling, the same cells were cycled at 0.5C after the C-rate test under the same conditions. Electrochemical impedance spectroscopy (EIS) on P-NCM and C-NCM in a charged state (4.3 V) was performed using an electrochemical workstation (VMP300; BioLogic) in the frequency range of 100 kHz to 10 mHz. For high accuracy, the data presented are averaged from at least three cells.

Post-Mortem Characterization. For the post-mortem characterization, the coin cells were carefully disassembled inside the glove box after long-term cycling. The recovered electrodes were washed with dimethyl carbonate (~200 μL) and dried. SEM and FIB-SEM analyses were performed to monitor the effect of coating on the structural stability of the NCM701515 secondary particles.

■ RESULTS & DISCUSSION

Characterization of Al_2O_3-Coated Ni-Rich NCM. Inspired by the fundamental chemistry utilized in ALD methods for generating protective oxide coatings on cathode materials, in this work, TMA was reacted with the surface-adsorbed moisture on NCM701515 in order to achieve a thin Al_2O_3 coating.[28,64] More specifically, the solution-based approach involves mixing the cathode material with TMA in

https://dx.doi.org/10.1021/acsami.0c06484
ACS Appl. Mater. Interfaces 2020, 12, 31392−31400

cathode materials in LIBs, surface modification seems indispensable.[38−40]

Surface modification via coating on powder or ready-to-use cathodes has been found promising because it effectively stabilizes the interface between the electrode and the electrolyte, thereby lowering the likelihood of parasitic side reactions during cycling.[17,41−43] The coating apparently can also partly prevent surface phase transformation from layered to a rock-salt or disordered spinel-like structure.[44,45] Various metal fluorides (e.g., LiF[46] and $LiAlF_4$[47]), metal oxides (e.g., CeO_2,[43] TiO_2,[7,48] ZrO_2,[41] and Al_2O_3[49,50]), and metal phosphates (e.g., $LiMgPO_4$,[51] $LiFePO_4$,[52] and Li_3PO_4[53]) have been tested as coating materials and shown to have a positive influence on the cyclability and stability of LIBs. In particular, Al_2O_3[17,36,50,54,55] has been most commonly applied to the cathode material because of its low cost and highly effective nature as a protective coating.

With respect to the coating process of Al_2O_3, two routes are usually explored, wet chemistry[56,57] and atomic layer deposition (ALD).[55,58] The wet-chemical route is considered to be simpler, cheaper, and easier for upscaling. However, there is virtually no control over the coating quality (thickness and homogeneity), and it also requires post heat-treatment.[56,59] For example, alkoxide-based coating approaches typically involve the use of (polar) protic solvents such as H_2O or ethanol[60,61] which may promote the generation of deleterious lithium residuals on the NCM surface (note that surface contaminants have a negative impact on the cyclability).[28,53] Additionally, post annealing at elevated temperatures may result in ion migration and cation mixing, which also deteriorates the cell performance.[23,59] In contrast, ALD has the advantage of precise control over thickness and homogeneity, but the process itself is rather complex and expensive.

The ALD-derived Al_2O_3 coating process is well-established in the literature.[62,63] Usually, it combines two steps, consisting of half-reactions using trimethylaluminum (TMA) and H_2O. In the first step, the surface-active −OH groups react with the TMA precursor. In the second step, H_2O reacts with TMA to complete the whole process.[62] Such ALD-derived Al_2O_3 coatings have been successfully applied to NCM powder and practical cathodes.[17,49]

In this work, we use the fundamentals of the ALD process to develop a facile and cost-effective, low-temperature wet-chemical-based alumina coating method to modify the surface of NCM701515 (70% Ni). Specifically, it makes use of surface-active −OH groups (from LiOH and adsorbed H_2O) to dry and coat the NCM cathode material in a single treatment step in solution.[64] Detailed structural characterization combined with electrochemical analysis reveals that using this approach, a thin and uniform coating can be achieved, which not only consumes unfavorable surface residuals, but also prevents particle fracture and stabilizes the interface between the cathode and the electrolyte, thereby leading to considerable improvements in cycling performance.

■ EXPERIMENTAL SECTION

Surface Modification of Ni-Rich NCM. The Al_2O_3 coating was prepared via a solution route. For the coating, TMA solution (0.279 mL, 2 M in toluene; Sigma-Aldrich) was diluted using anhydrous toluene (15 mL; Sigma-Aldrich) and stirred for 1 h. The diluted TMA solution (5 ml) was then added to $LiNi_{0.70}Co_{0.15}Mn_{0.15}O_2$ (NCM701515, 5 g; Gelon LIB) and stirred at 30 °C for 12 h. The final dispersion was filtered and washed with anhydrous toluene (20 mL) to remove unreacted TMA. The recovered (coated) powder was dried in a vacuum at 200 °C overnight before transferring it to the glove box.

Material Characterization. The particle morphology, microstructure, and electrode topography along with the elemental composition of pristine (P-NCM) and coated (C-NCM) samples were investigated by scanning electron microscopy (SEM, MERLIN with 7 kV accelerating voltage and 3000 pA current; Zeiss) coupled with energy dispersive X-ray (EDX) spectroscopy (X-Max detector; Oxford Instruments). X-ray photoelectron spectroscopy (XPS) was performed using a monochromatic Al Kα radiation on a PHI 5000 VersaProbe II Scanning ESCA microprobe (~10^{-8} Pa pressure; Physical Electronics). Survey spectra were recorded with a pass energy of 93.9 eV and, for high-resolution spectra, a pass energy of 23.5 eV was used. The structural characterization of pristine and coated powder was done by X-ray diffraction (XRD; Bruker) with Cu Kα radiation. The water content before and after coating was determined by Karl-Fischer titration. Transmission electron microscopy (TEM) was performed on an FEI Titan 80-300 aberration corrected transmission electron microscope at 300 kV. Samples for TEM investigation were prepared using an FEI STRATA 400 S dual beam facility, with the Ga-ion beam operating at 30 kV, followed by polishing at 2 kV to improve the surface quality.

Electrode Preparation. The solution of polyvinylidene fluoride binder (5 wt %, Solef PVDF 6020; Solvay) was prepared in *N*-methyl-2-pyrrolidone (NMP; Sigma-Aldrich). For the electrode preparation, either P-NCM or C-NCM (90 wt %) was mixed with conductive carbon black (5 wt %, Super P; TIMCAL) and suspended in the binder solution (5 wt %). Additional NMP was added and the solution was stirred overnight to achieve the desired viscosity. The resultant solution was then cast onto Al foil using a doctor blade. The as-prepared cathode sheets were calendared at 90 psi and dried at 120 °C in a vacuum (24 h) before transferring them to the glove box for further measurements.

Electrochemical Testing. For the electrochemical testing, coin cells (CR2032; MTI Corporation) with the P-NCM or C-NCM cathode (12 mm) and Li foil anode (14 mm; Rockwood Lithium GmbH) were assembled using Celgard2500 (16 mm; Celgard) as the separator and LP50 (1 M $LiPF_6$ in 1/1 wt/wt ethylene carbonate/ethyl methyl carbonate, 50 μL; Sigma-Aldrich) as the electrolyte. The areal loading was 10.4−10.8 $mg_{NCM701515}$ cm^{-2}. All of the electrochemical testing was done using a multichannel battery cycler (MACCOR, Inc.). The coin cells were cycled in a constant current (CC) mode in the voltage range between 3.0 and 4.3 V at 25 °C. A specific current of 160 mA g^{-1} was defined at the 1C rate. Initially, the cells were tested at various C-rates ranging from 0.1 to 2C, each for four cycles. For the long-term cycling, the same cells were cycled at 0.5C after the C-rate test under the same conditions. Electrochemical impedance spectroscopy (EIS) on P-NCM and C-NCM in a charged state (4.3 V) was performed using an electrochemical workstation (VMP300; BioLogic) in the frequency range of 100 kHz to 10 mHz. For high accuracy, the data presented are averaged from at least three cells.

Post-Mortem Characterization. For the post-mortem characterization, the coin cells were carefully disassembled inside the glove box after long-term cycling. The recovered electrodes were washed with dimethyl carbonate (~200 μL) and dried. SEM and FIB-SEM analyses were performed to monitor the effect of coating on the structural stability of the NCM701515 secondary particles.

■ RESULTS & DISCUSSION

Characterization of Al_2O_3-Coated Ni-Rich NCM. Inspired by the fundamental chemistry utilized in ALD methods for generating protective oxide coatings on cathode materials, in this work, TMA was reacted with the surface-adsorbed moisture on NCM701515 in order to achieve a thin Al_2O_3 coating.[28,64] More specifically, the solution-based approach involves mixing the cathode material with TMA in

https://dx.doi.org/10.1021/acsami.0c06484
ACS Appl. Mater. Interfaces 2020, 12, 31392−31400

toluene, where the latter is allowed to react with the hydroxyl species inherent to NCM until the surface is fully passivated, driving off methane as a reaction product and resulting in the formation of a conformal Al_2O_3 protective layer (Figure 1). Although toluene is toxic and flammable, it is one of the most suitable solvents for the TMA precursor. Moreover, it can be recovered during the drying process and thus reused.

In order to confirm the suggested reaction mechanism, Karl-Fischer titration was performed before and after the coating process. The pristine material exhibited >1600 ppm of H_2O. The water level decreased to below 600 ppm after TMA exposure (Figure 2a), thereby confirming the consumption of moisture during the coating process. In order to prove the presence of the alumina coating, XPS analysis was performed on both the pristine (P-NCM) and coated (C-NCM) NCM powders (see also Figure S1 of the Supporting Information). Notably, the Al 2p signature (~74 eV) can only be found in the case of C-NCM (Figure 2b), which is consistent with reports available in the literature.[7] XRD data for P-NCM and C-NCM are shown in Figure 2c. Both patterns are in good agreement with the layered structure of NCM, belonging to the $R\bar{3}m$ space group, indicating that the coating process does not induce any structural changes to the cathode material. Importantly, there are no new reflections appearing that can be assigned to the alumina, which is due to both the amorphous nature and low weight fraction of coating on the surface.[65] Additionally, given the relatively low temperature employed in the coating process (≤ 200 °C, Figure 1), no interdiffusion between the active material and the coating, involving either Al^{3+} or transition metal ions,[59] is to be expected.

The morphology of P-NCM and C-NCM from SEM imaging is shown in Figure 3a,b, respectively. The P-NCM exhibits spherical secondary particles that are 8−10 μm in diameter and are composed of primary particles ranging from 200 to 400 nm in size. The C-NCM particles show no significant change in the morphology after the coating process. The EDX elemental mapping of C-NCM indicates the conformal distribution of Al over the entirety of the surface, confirming that the coating is indeed homogenous (Figure 3c). To further probe the distribution of coating on the NCM, a line-scan was performed across the length of a secondary particle. The results of such measurement are shown in Figure S2 of the Supporting Information.

High-angle annular dark-field scanning TEM (HAADF-STEM) was performed on the C-NCM to determine the uniformity of the coating layer. Figure 4a shows Al_2O_3 as a dark layer between Pt and NCM because of the lower Z value of Al, thereby confirming the presence of Al_2O_3 on the top surface with a thickness of ~6 nm. The TEM−EDX mapping results in Figure 4b further support the presence of Al. The Al_2O_3 coating layer seems rather uniformly distributed over the surface. Nonetheless, some (minor) nonuniformity would not be very surprising, as the distribution of surface −OH groups, which are required for successful coating, may not be even. In agreement with XRD and expectations, the Al_2O_3 surface coating is of an amorphous nature. This is evident both from the high-resolution (HR) TEM imaging data and from the fast Fourier transform (FFT) pattern of the coating layer (see Figure 4c,d), with the latter showing only an amorphous halo.

Electrochemical Characterization. In order to investigate the influence of coating on the cyclability, electrochemical measurements were performed using a Li|LP50|P-/C-NCM half-cell configuration. Figure 5a shows a comparison of

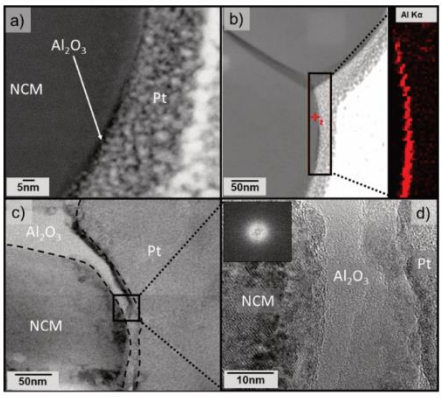

Figure 4. (a,b) STEM-HAADF micrographs and the Al map of coated NCM701515. (c,d) Corresponding HRTEM micrographs. The inset in (d) is an FFT pattern of the coating layer.

the rate capability of P-NCM and C-NCM from 0.1 to 2C at 25 °C in the voltage window of 3.0 to 4.3 V versus Li^+/Li. Notably, the rate performance of both the P-NCM and C-NCM cells was found to be similar, demonstrating that surface modification does not negatively affect the kinetics. While the C-NCM cells showed an initial resistance slightly higher than that of the P-NCM cells (see the section on EIS below), it had no immediate effect on the rate capability. This result thus suggests that the rate performance depends on various factors such as the coating morphology and thickness or test cell configuration, to name a few. Although literature reports have shown improvements in rate capability upon coating the cathode material,[49,66] there are also others revealing similar or worse performance than the uncoated material.[67−69] Hence, in order to gain a better understanding of the impact of the coating layer on the rate performance, additional studies are required. In addition, one must keep in mind that the coating was done at low temperature and the amorphous structure of the protective surface layer also affects the associated Li^+ transport properties and therefore the kinetics.

Next, the same cells were investigated for their long-term cycling stability. To this end, coin cells with P-NCM and C-NCM were galvanostatically cycled at a rate of 0.5C. As shown in Figure 5b, C-NCM exhibits higher capacity retention (~90%) as compared to P-NCM (~60%) after 130 cycles, indicating that the coating improved the stability considerably. The better retention is mainly attributed to effectively mitigating side reactions at the cathode/electrolyte interface, as the coating provides a physical barrier between the two component materials. The coating layer also serves to consume the surface-active species, which is considered to be the primary cause of parasitic reactions at the surface.[28] Nevertheless, these side reactions still persist to some degree and are known to generate HF, which can etch the cathode material (corrosion). Accordingly, another beneficial function of the coating is to act as an HF scavenger, thereby preventing severe cathode degradation.

A comparison of the first four charge/discharge curves for the P-NCM and C-NCM cells at 0.1C rate is shown in Figure

https://dx.doi.org/10.1021/acsami.0c06484
ACS Appl. Mater. Interfaces 2020, 12, 31392−31400

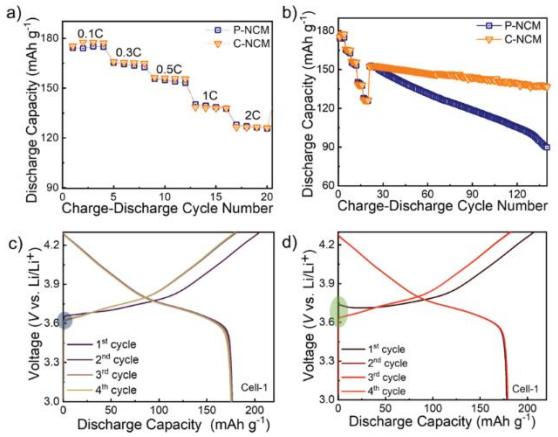

Figure 5. Comparison of (a) rate capability and (b) long-term cycling performance at 0.5C (following the rate test) of pristine and coated NCM701515-based LIB cells. Voltage profiles of the first four cycles for (c) P-NCM (cell-1) and (d) C-NCM (cell-1) at 0.1C. All data are averaged from at least three independent cells; the original data are shown in Figures S3 and S4 of the Supporting Information.

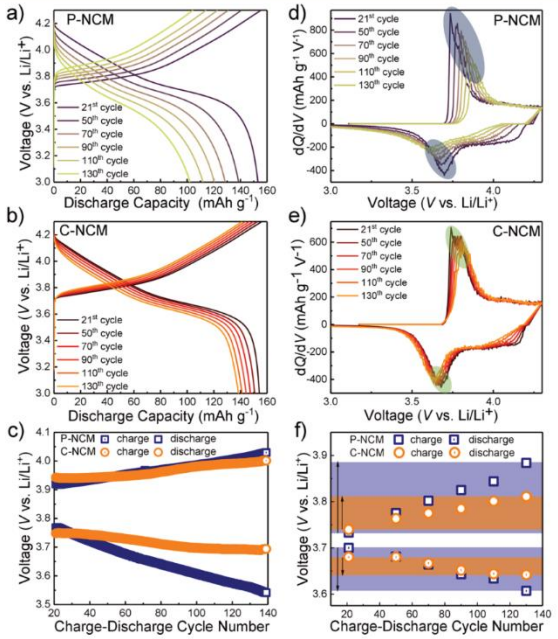

Figure 6. Voltage profiles at 0.5C for the long-term cycling of (a) pristine and (b) coated NCM701515-based LIB cells and (d,e) corresponding differential capacity plots. Comparison of (c) mean voltage and (f) overpotential evolution for P-NCM and C-NCM during cycling.

https://dx.doi.org/10.1021/acsami.0c06484
ACS Appl. Mater. Interfaces 2020, 12, 31392−31400

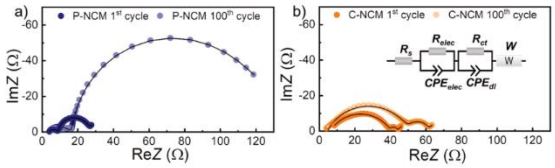

Figure 7. Nyquist plots of the electrochemical impedance measured in the fully charged state (4.3 V) for (a) pristine and (b) coated NCM701515 after the 1st and 100th cycles.

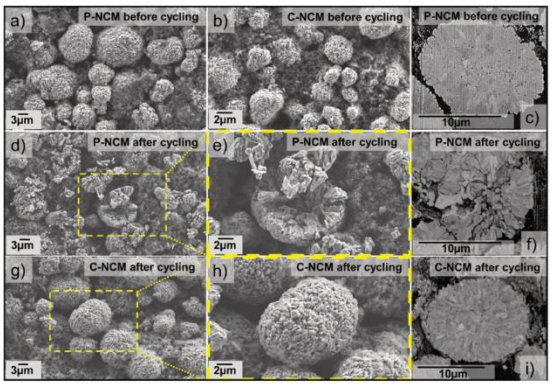

Figure 8. Top view SEM micrographs of (a) P-NCM and (b) C-NCM cathodes and (c) cross-sectional micrograph of a P-NCM secondary particle before cycling. Top view and cross-sectional SEM micrographs of (d–f) P-NCM and (g–i) C-NCM after 100 cycles.

5c,d, respectively. Both reveal similar profiles with the exception of the initial cycle. Compared to P-NCM, the C-NCM cells exhibit a larger overpotential in the beginning of the first charge cycle, which we attribute to the higher initial resistance of the coating layer. However, in the following cycles, the curves for C-NCM closely resemble those of P-NCM (see also differential capacity plots in Figure S5 of the Supporting Information).

Figure 6a,b shows the charge/discharge curves of the cells containing P-NCM and C-NCM during long-term cycling. P-NCM shows a much faster capacity fading than C-NCM. In addition, there is a continuous increase in polarization with cycling in both cases, evident from the potential rise during charge and the potential drop during discharge. This polarization can be ascribed to side reactions between the cathode and the electrolyte, among others.[35] Figure 6c shows the evolution of the mean charge/discharge voltage with cycling. A higher polarization is observed for P-NCM as compared to C-NCM. This result suggests that the coating effectively prevents contact between the NCM701515 and the electrolyte, thereby inhibiting side reactions and cSEI formation. This is further supported by the differential capacity plots shown in Figure 6d,e. The peaks in the dQ/dV curves correspond to the plateaus in the charge/discharge profiles. As seen in Figure 6f, the redox peaks for P-NCM exhibit a much more pronounced shift than those for C-NCM between the 20th and 130th cycles (from 3.73 to 3.88 vs 3.74 to 3.81 V during charge and from 3.70 to 3.60 vs 3.67 to 3.63 V during discharge). Apart from the shift, the redox peaks for P-NCM continuously broaden with cycling, which we attribute to the deterioration of the cathode/electrolyte interface as well as the continuous formation of a deactivated oxide surface layer.

In order to better understand the effect of coating on the electrochemical activity, EIS measurements were conducted on the P-NCM and C-NCM cells. Figure 7a,b shows the measured data in the fully charged state (4.3 V) after the 1st and 100th cycles at 25 °C. The Nyquist plots are composed of a semicircle in the high-frequency region, corresponding to the resistance associated with Li^+ migration in the electrode (R_{elec}), a semicircle in the medium-frequency region, corresponding to the charge-transfer resistance (R_{ct}) at the electrode/electrolyte interface, and the Warburg element W in the low-frequency region is related to Li-ion diffusion.[70,71] Note that the small interruption in the beginning of the Nyquist plots in the high-frequency region can be assigned to the resistance of the liquid electrolyte (R_s), which is similar in both cases. The equivalent circuit used for fitting is shown in the inset of Figure 7b. For C-NCM, the high-frequency semicircle and therefore R_{elec} is increased by a factor of ~6 because of the coating with Al_2O_3. However, the beneficial effect of the coating layer is clearly evident after the 100th cycle. For P-NCM, R_{ct} completely dominates the overall cell resistance, while C-NCM exhibits a much smaller R_{ct} growth during cycling. This is in agreement with the faster capacity decay in the case of P-NCM. The lower R_{ct} for C-NCM can be explained by the fact that the coating protects the electrode surface and therefore reduces the cSEI formation, which in turn decreases the electrode polarization upon repeated cycling. The coating not only affects the charge-

https://dx.doi.org/10.1021/acsami.0c06484
ACS Appl. Mater. Interfaces 2020, 12, 31392–31400

transfer resistance at the electrode/electrolyte interface but also the change in resistance R_{elec} of the electrode itself. For P-NCM, R_{elec} is increased by a factor of ~2 after the 100th cycle, which we attribute to the cracking of the NCM701515 secondary particles (see section on the post-mortem characterization below). For C-NCM, the electrode resistance is only increased by ~20%, indicating that the coating also stabilizes the particles and somewhat inhibits particle fracture. These results provide clear evidence that the coating helps to stabilize the cell impedance and maintain better charge transfer during long-term cycling, which ultimately improves the performance.

Post-Mortem Characterization. In order to study the effect of coating on the structural stability, electrochemically cycled cathodes were analyzed in some more detail via SEM. Figure 8 shows top view SEM micrographs obtained on both P-NCM and C-NCM before and after cycling along with the corresponding cross sections. The uncycled cathodes (Figure 8a–c) serve as a kind of baseline, as the secondary particles may be deformed already through the application of external pressure during the course of electrode preparation (calendaring). As seen in Figure 8a,b, mechanically induced particle deformation can be ruled out. According to cross-sectional SEM, the same holds true for internal cracking prior to cycling (Figure 8c). However, after 100 cycles, P-NCM (Figure 8d–f) shows severe particle fracture, probably accelerating side reactions at the newly exposed surfaces, thereby increasing capacity decay. In contrast, for the cycled C-NCM (Figure 8g–i), no such crack formation was detected. This suggests that the coating acts as a robust physical barrier, in agreement with the EIS results, while providing more structural stability to the cathode material, all of which greatly enhances the cell cyclability.

■ CONCLUSIONS

Herein, we have demonstrated the positive effect that alumina surface coating has on the electrochemical performance of Ni-rich NCM. High-quality coating layers were achieved using a facile low-temperature solution-based route, drawing inspiration from the chemistry employed in ALD approaches. Detailed structural and chemical analyses indicated that the coating is uniform, and Karl-Fischer titration measurements confirmed the consumption of surface-adsorbed water. Interestingly, the rate capability (after the initial cycle) was not negatively affected, despite the insulating nature of the coating. Moreover, the C-NCM cells showed significantly improved long-term cycling performance compared to the uncoated NCM. EIS analysis confirmed the better cyclability; the impedance buildup was much lower than for cells using pristine NCM. Post-mortem analysis via SEM indicated that the P-NCM cathodes suffer from severe secondary particle fracture. In contrast, the C-NCM cathodes showed negligible cracking.

Taken together, the improvement in the performance of the coated Ni-rich NCM can be ascribed to the effective protection against adverse side reactions. The alumina coating acts as a kind of shield and prevents direct contact between the active electrode material and the electrolyte, which in turn inhibits surface degradation and significantly enhances the cyclability and stability of high-loading LIB cells. Overall, the strategy of using an −OH group-assisted wet-chemical coating approach opens up a new avenue for modifying the cathode surface in a simple and cost effective way.

■ ASSOCIATED CONTENT

Supporting Information

The Supporting Information is available free of charge at https://pubs.acs.org/doi/10.1021/acsami.0c06484.

XPS survey spectra, SEM−EDX line scan, long-term cycling performances, voltage profiles, and differential capacity plots (PDF)

■ AUTHOR INFORMATION

Corresponding Author

Matthias T. Elm − *Center for Materials Research (LaMa), Institute of Physical Chemistry, and Institute of Experimental Physics I, Justus Liebig University Giessen, 35392 Giessen, Germany*; orcid.org/0000-0001-7014-5772; Email: matthias.elm@phys.chemie.uni-giessen.de

Authors

Rajendra S. Negi − *Center for Materials Research (LaMa), Justus Liebig University Giessen, 35392 Giessen, Germany*

Sean P. Culver − *Institute of Physical Chemistry, Justus Liebig University Giessen, 35392 Giessen, Germany*

Andrey Mazilkin − *Institute of Nanotechnology, Karlsruhe Institute of Technology (KIT), 76344 Eggenstein-Leopoldshafen, Germany*

Torsten Brezesinski − *Institute of Nanotechnology, Karlsruhe Institute of Technology (KIT), 76344 Eggenstein-Leopoldshafen, Germany*; orcid.org/0000-0002-4336-263X

Complete contact information is available at: https://pubs.acs.org/10.1021/acsami.0c06484

Notes

The authors declare no competing financial interest.

■ ACKNOWLEDGMENTS

R.S.N. and M.T.E. thank the German Federal Ministry of Education and Research (BMBF) for the funding of the NanoMatFutur project NiKo (03XP0093). S.P.C. gratefully acknowledges the Alexander von Humboldt Foundation for financial support through a postdoctoral fellowship. Karlsruhe Nano Micro Facility (KNMF), a Helmholtz Research Infrastructure at Karlsruhe Institute of Technology (KIT), is acknowledged for TEM.

■ REFERENCES

(1) Blomgren, G. E. The Development and Future of Lithium Ion Batteries. *J. Electrochem. Soc.* **2017**, *164*, A5019−A5025.

(2) Schmuch, R.; Wagner, R.; Hörpel, G.; Placke, T.; Winter, M. Performance and Cost of Materials for Lithium-Based Rechargeable Automotive Batteries. *Nat. Energy* **2018**, *3*, 267−278.

(3) Yan, P.; Zheng, J.; Liu, J.; Wang, B.; Cheng, X.; Zhang, Y.; Sun, X.; Wang, C.; Zhang, J.-G. Tailoring Grain Boundary Structures and Chemistry of Ni-Rich Layered Cathodes for Enhanced Cycle Stability of Lithium-Ion Batteries. *Nat. Energy* **2018**, *3*, 600−605.

(4) Sun, Y.-K.; Myung, S.-T.; Park, B.-C.; Prakash, J.; Belharouak, I.; Amine, K. High-Energy Cathode Material for Long-Life and Safe Lithium Batteries. *Nat. Mater.* **2009**, *8*, 320−324.

(5) Croguennec, L.; Palacin, M. R. Recent Achievements on Inorganic Electrode Materials for Lithium-Ion Batteries. *J. Am. Chem. Soc.* **2015**, *137*, 3140−3156.

(6) Placke, T.; Kloepsch, R.; Dühnen, S.; Winter, M. Lithium Ion, Lithium Metal, and Alternative Rechargeable Battery Technologies: The Odyssey for High Energy Density. *J. Solid State Electrochem.* **2017**, *21*, 1939−1964.

(7) Cheng, H.-M.; Wang, F.-M.; Chu, J. P.; Santhanam, R.; Rick, J.; Lo, S.-C. Enhanced Cycleabity in Lithium Ion Batteries: Resulting from Atomic Layer Depostion of Al_2O_3 or TiO_2 on $LiCoO_2$ Electrodes. *J. Phys. Chem. C* **2012**, *116*, 7629−7637.
(8) Zhang, W.; Richter, F. H.; Culver, S. P.; Leichtweiss, T.; Lozano, J. G.; Dietrich, C.; Bruce, P. G.; Zeier, W. G.; Janek, J. Degradation Mechanisms at the $Li_{10}GeP_2S_{12}/LiCoO_2$ Cathode Interface in an All-Solid-State Lithium-Ion Battery. *ACS Appl. Mater. Interfaces* **2018**, *10*, 22226−22236.
(9) Saat, G.; Balci, F. M.; Alsaç, E. P.; Karadas, F.; Dag, Ö. Molten Salt Assisted Self-Assembly: Synthesis of Mesoporous $LiCoO_2$ and $LiMn_2O_4$ Thin Films and Investigation of Electrocatalytic Water Oxidation Performance of Lithium Cobaltate. *Small* **2018**, *14*, 1701913.
(10) Ben, L.; Yu, H.; Chen, B.; Chen, Y.; Gong, Y.; Yang, X.; Gu, L.; Huang, X. Unusual Spinel-to-Layered Transformation in $LiMn_2O_4$ Cathode Explained by Electrochemical and Thermal Stability Investigation. *ACS Appl. Mater. Interfaces* **2017**, *9*, 35463−35475.
(11) Zhu, Y. G.; Du, Y.; Jia, C.; Zhou, M.; Fan, L.; Wang, X.; Wang, Q. Unleashing the Power and Energy of $LiFePO_4$-Based Redox Flow Lithium Battery with a Bifunctional Redox Mediator. *J. Am. Chem. Soc.* **2017**, *139*, 6286−6289.
(12) Wang, X.; Feng, Z.; Huang, J.; Deng, W.; Li, X.; Zhang, H.; Wen, Z. Graphene-Decorated Carbon-Coated $LiFePO_4$ Nanospheres as a High-Performance Cathode Material for Lithium-Ion Batteries. *Carbon* **2018**, *127*, 149−157.
(13) de Biasi, L.; Kondrakov, A. O.; Geßwein, H.; Brezesinski, T.; Hartmann, P.; Janek, J. Between Scylla and Charybdis: Balancing Among Structural Stability and Energy Density of Layered NCM Cathode Materials for Advanced Lithium-Ion Batteries. *J. Phys. Chem. C* **2017**, *121*, 26163−26171.
(14) Kim, A.-Y.; Strauss, F.; Bartsch, T.; Teo, J. H.; Hatsukade, T.; Mazilkin, A.; Janek, J.; Hartmann, P.; Brezesinski, T. Stabilizing Effect of a Hybrid Surface Coating on a Ni-Rich NCM Cathode Material in All-Solid-State Batteries. *Chem. Mater.* **2019**, *31*, 9664−9672.
(15) Neudeck, S.; Walther, F.; Bergfeldt, T.; Suchomski, C.; Rohnke, M.; Hartmann, P.; Janek, J.; Brezesinski, T. Molecular Surface Modification of NCM622 Cathode Material Using Organophosphates for Improved Li-Ion Battery Full-Cells. *ACS Appl. Mater. Interfaces* **2018**, *10*, 20487−20498.
(16) Binder, J. O.; Culver, S. P.; Pinedo, R.; Weber, D. A.; Friedrich, M. S.; Gries, K. I.; Volz, K.; Zeier, W. G.; Janek, J. Investigation of Fluorine and Nitrogen as Anionic Dopants in Nickel-Rich Cathode Materials for Lithium-Ion Batteries. *ACS Appl. Mater. Interfaces* **2018**, *10*, 44452−44462.
(17) Neudeck, S.; Mazilkin, A.; Reitz, C.; Hartmann, P.; Janek, J.; Brezesinski, T. Effect of Low-Temperature Al_2O_3 ALD Coating on Ni-Rich Layered Oxide Composite Cathode on the Long-Term Cycling Performance of Lithium-Ion Batteries. *Sci. Rep.* **2019**, *9*, 5328.
(18) Radin, M. D.; Hy, S.; Sina, M.; Fang, C.; Liu, H.; Vinckeviciute, J.; Zhang, M.; Whittingham, M. S.; Meng, Y. S.; Van der Ven, A. Narrowing the Gap between Theoretical and Practical Capacities in Li-Ion Layered Oxide Cathode Materials. *Adv. Energy Mater.* **2017**, *7*, 1602888.
(19) Andre, D.; Kim, S.-J.; Lamp, P.; Lux, S. F.; Maglia, F.; Paschos, O.; Stiaszny, B. Future Generations of Cathode Materials: An Automotive Industry Perspective. *J. Mater. Chem. A* **2015**, *3*, 6709−6732.
(20) de Biasi, L.; Schwarz, B.; Brezesinski, T.; Hartmann, P.; Janek, J.; Ehrenberg, H. Chemical, Structural, and Electronic Aspects of Formation and Degradation Behavior on Different Length Scales of Ni-Rich NCM and Li-Rich HE-NCM Cathode Materials in Li-Ion Batteries. *Adv. Mater.* **2019**, *31*, 1900985.
(21) Myung, S.-T.; Maglia, F.; Park, K.-J.; Yoon, C. S.; Lamp, P.; Kim, S.-J.; Sun, Y.-K. Nickel-Rich Layered Cathode Materials for Automotive Lithium-Ion Batteries: Achievements and Perspectives. *ACS Energy Lett.* **2017**, *2*, 196−223.
(22) Schweidler, S.; de Biasi, L.; Garcia, G.; Mazilkin, A.; Hartmann, P.; Brezesinski, T.; Janek, J. Investigation into Mechanical Degradation and Fatigue of High-Ni NCM Cathode Material: A Long-Term Cycling Study of Full Cells. *ACS Appl. Energy Mater.* **2019**, *2*, 7375−7384.
(23) Han, B.; Paulauskas, T.; Key, B.; Peebles, C.; Park, J. S.; Klie, R. F.; Vaughey, J. T.; Dogan, F. Understanding the Role of Temperature and Cathode Composition on Interface and Bulk: Optimizing Aluminum Oxide Coatings for Li-Ion Cathodes. *ACS Appl. Mater. Interfaces* **2017**, *9*, 14769−14778.
(24) Su, Y.; Cui, S.; Zhuo, Z.; Yang, W.; Wang, X.; Pan, F. Enhancing the High-Voltage Cycling Performance of $LiNi_{0.5}Mn_{0.3}Co_{0.2}O_2$ by Retarding Its Interfacial Reaction with an Electrolyte by Atomic-Layer-Deposited Al_2O_3. *ACS Appl. Mater. Interfaces* **2015**, *7*, 25105−25112.
(25) Konishi, H.; Yuasa, T.; Yoshikawa, M. Thermal Stability of $Li_{1-y}Ni_xMn_{(1-x)/2}Co_{(1-x)/2}O_2$ Layer-Structured Cathode Materials Used in Li-Ion Batteries. *J. Power Sources* **2011**, *196*, 6884−6888.
(26) Wu, L.; Nam, K.-W.; Wang, X.; Zhou, Y.; Zheng, J.-C.; Yang, X.-Q.; Zhu, Y. Structural Origin of Overcharge-Induced Thermal Instability of Ni-Containing Layered-Cathodes for High-Energy-Density Lithium Batteries. *Chem. Mater.* **2011**, *23*, 3953−3960.
(27) Noh, H.-J.; Youn, S.; Yoon, C. S.; Sun, Y.-K. Comparison of the Structural and Electrochemical Properties of Layered $Li[Ni_xCo_yMn_z]O_2$ (x = 1/3, 0.5, 0.6, 0.7, 0.8 and 0.85) Cathode Material for Lithium-Ion Batteries. *J. Power Sources* **2013**, *233*, 121−130.
(28) Cho, D.-H.; Jo, C.-H.; Cho, W.; Kim, Y.-J.; Yashiro, H.; Sun, Y.-K.; Myung, S.-T. Effect of Residual Lithium Compounds on Layer Ni-Rich $Li[Ni_{0.7}Mn_{0.3}]O_2$. *J. Electrochem. Soc.* **2014**, *161*, A920−A926.
(29) Xiong, X.; Wang, Z.; Yue, P.; Guo, H.; Wu, F.; Wang, J.; Li, X. Washing Effects on Electrochemical Performance and Storage Characteristics of $LiNi_{0.8}Co_{0.1}Mn_{0.1}O_2$ as Cathode Material for Lithium-Ion Batteries. *J. Power Sources* **2013**, *222*, 318−325.
(30) Jung, R.; Morasch, R.; Karayaylali, P.; Phillips, K.; Maglia, F.; Stinner, C.; Shao-Horn, Y.; Gasteiger, H. A. Effect of Ambient Storage on the Degradation of Ni-Rich Positive Electrode Materials (NMC811) for Li-Ion Batteries. *J. Electrochem. Soc.* **2018**, *165*, A132−A141.
(31) Hatsukade, T.; Schiele, A.; Hartmann, P.; Brezesinski, T.; Janek, J. Origin of Carbon Dioxide Evolved during Cycling of Nickel-Rich Layered NCM Cathodes. *ACS Appl. Mater. Interfaces* **2018**, *10*, 38892−38899.
(32) Renfrew, S. E.; McCloskey, B. D. Residual Lithium Carbonate Predominantly Accounts for First Cycle CO_2 and CO Outgassing of Li-Stoichiometric and Li-Rich Layered Transition-Metal Oxides. *J. Am. Chem. Soc.* **2017**, *139*, 17853−17860.
(33) Kim, Y. Encapsulation of $LiNi_{0.5}Co_{0.2}Mn_{0.3}O_2$ with a Thin Inorganic Electrolyte Film to Reduce Gas Evolution in the Application of Lithium Ion Batteries. *Phys. Chem. Chem. Phys.* **2013**, *15*, 6400−6405.
(34) Kim, Y.; Cho, J. Lithium-Reactive $Co_3(PO_4)_2$ Nanoparticle Coating on High-Capacity $LiNi_{0.8}Co_{0.16}Al_{0.04}O_2$ Cathode Material for Lithium Rechargeable Batteries. *J. Electrochem. Soc.* **2007**, *154*, A495−A499.
(35) Liu, W.; Oh, P.; Liu, X.; Lee, M.-J.; Cho, W.; Chae, S.; Kim, Y.; Cho, J. Nickel-Rich Layered Lithium Transition-Metal Oxide for High-Energy Lithium-Ion Batteries. *Angew. Chem., Int. Ed.* **2015**, *54*, 4440−4457.
(36) Riley, L. A.; Van Atta, S.; Cavanagh, A. S.; Yan, Y.; George, S. M.; Liu, P.; Dillon, A. C.; Lee, S.-H. Electrochemical Effects of ALD Surface Modification on Combustion Synthesized $LiNi_{1/3}Mn_{1/3}Co_{1/3}O_2$ as a Layered-Cathode. *J. Power Sources* **2011**, *196*, 3317−3324.
(37) Qian, Y.; Niehoff, P.; Börner, M.; Grützke, M.; Mönnighoff, X.; Behrends, P.; Nowak, S.; Winter, M.; Schappacher, F. M. Influence of Electrolyte Additives on the Cathode Electrolyte Interphase (CEI) Formation on $LiNi_{1/3}Mn_{1/3}Co_{1/3}O_2$ in Half Cells with Li Metal Counter Electrode. *J. Power Sources* **2016**, *329*, 31−40.
(38) Armand, M.; Tarascon, J.-M. Building Better Batteries. *Nature* **2008**, *451*, 652−657.

https://dx.doi.org/10.1021/acsami.0c06484
ACS Appl. Mater. Interfaces 2020, 12, 31392−31400

(39) Shi, J.-L.; Xiao, D.-D.; Ge, M.; Yu, X.; Chu, Y.; Huang, X.; Zhang, X.-D.; Yin, Y.-X.; Yang, X.-Q.; Guo, Y.-G.; Gu, L.; Wan, L.-J. High-Capacity Cathode Material with High Voltage for Li-Ion Batteries. *Adv. Mater.* **2018**, *30*, 1705575.
(40) Shi, J.-L.; Xiao, D.-D.; Zhang, X.-D.; Yin, Y.-X.; Guo, Y.-G.; Gu, L.; Wan, L.-J. Improving the Structural Stability of Li-Rich Cathode Materials via Reservation of Cations in the Li-Slab for Li-Ion Batteries. *Nano Res.* **2017**, *10*, 4201−4209.
(41) Hwang, B.-J.; Hu, S.-K.; Chen, C.-H.; Chen, C.-Y.; Sheu, H.-S. In-Situ XRD Investigations on Structure Changes of ZrO_2-Coated $LiMn_{0.5}Ni_{0.5}O_2$ Cathode Materials during Charge. *J. Power Sources* **2007**, *174*, 761−765.
(42) Kim, J. W.; Travis, J. J.; Hu, E.; Nam, K.-W.; Kim, S. C.; Kang, C. S.; Woo, J.-H.; Yang, X.-Q.; George, S. M.; Oh, K. H.; Cho, S.-J.; Lee, S.-H. Unexpected High Power Performance of Atomic Layer Deposition Coated $Li[Ni_{1/3}Mn_{1/3}Co_{1/3}]O_2$ Cathodes. *J. Power Sources* **2014**, *254*, 190−197.
(43) Dong, S.; Zhou, Y.; Hai, C.; Zeng, J.; Sun, Y.; Shen, Y.; Li, X.; Ren, X.; Qi, G.; Zhang, X.; Ma, L. Ultrathin CeO_2 Coating for Improved Cycling and Rate Performance of Ni-Rich Layered $LiNi_{0.7}Co_{0.2}Mn_{0.1}O_2$ Cathode Materials. *Ceram. Int.* **2019**, *45*, 144−152.
(44) Jung, S.-K.; Gwon, H.; Hong, J.; Park, K.-Y.; Seo, D.-H.; Kim, H.; Hyun, J.; Yang, W.; Kang, K. Understanding the Degradation Mechanisms of $LiNi_{0.5}Co_{0.2}Mn_{0.3}O_2$ Cathode Material in Lithium Ion Batteries. *Adv. Energy Mater.* **2014**, *4*, 1300787.
(45) Zhang, X.-D.; Shi, J.-L.; Liang, J.-Y.; Yin, Y.-X.; Zhang, J.-N.; Yu, X.-Q.; Guo, Y.-G. Suppressing Surface Lattice Oxygen Release of Li-Rich Cathode Materials via Heterostructured Spinel $Li_4Mn_5O_{12}$ Coating. *Adv. Mater.* **2018**, *30*, 1801751.
(46) Zhao, T.; Li, L.; Chen, R.; Wu, H.; Zhang, X.; Chen, S.; Xie, M.; Wu, F.; Lu, J.; Amine, K. Design of Surface Protective Layer of LiF/FeF_3 Nanoparticles in Li-Rich Cathode for High-Capacity Li-Ion Batteries. *Nano Energy* **2015**, *15*, 164−176.
(47) Xie, J.; Sendek, A. D.; Cubuk, E. D.; Zhang, X.; Lu, Z.; Gong, Y.; Wu, T.; Shi, F.; Liu, W.; Reed, E. J.; Cui, Y. Atomic Layer Deposition of Stable $LiAlF_4$ Lithium Ion Conductive Interfacial Layer for Stable Cathode Cycling. *ACS Nano* **2017**, *11*, 7019−7027.
(48) Chen, Y.; Zhang, Y.; Chen, B.; Wang, Z.; Lu, C. An Approach to Application for $LiNi_{0.6}Co_{0.2}Mn_{0.2}O_2$ Cathode Material at High Cutoff Voltage by TiO_2 Coating. *J. Power Sources* **2014**, *256*, 20−27.
(49) Shi, Y.; Zhang, M.; Qian, D.; Meng, Y. S. Ultrathin Al_2O_3 Coatings for Improved Cycling Performance and Thermal Stability of $LiNi_{0.5}Co_{0.2}Mn_{0.3}O_2$ Cathode. *Electrochim. Acta* **2016**, *203*, 154−161.
(50) Lee, J.-T.; Wang, F.-M.; Cheng, C.-S.; Li, C.-C.; Lin, C.-H. Low-Temperature Atomic Layer Deposited Al_2O_3 Thin Film on Layer Structure Cathode for Enhanced Cycleability in Lithium-Ion Batteries. *Electrochim. Acta* **2010**, *55*, 4002−4006.
(51) Liu, W.; Oh, P.; Liu, X.; Myeong, S.; Cho, W.; Cho, J. Countering Voltage Decay and Capacity Fading of Lithium-Rich Cathode Material at 60 °C by Hybrid Surface Protection Layers. *Adv. Energy Mater.* **2015**, *5*, 1500274.
(52) Zheng, F.; Yang, C.; Xiong, X.; Xiong, J.; Hu, R.; Chen, Y.; Liu, M. Nanoscale Surface Modification of Lithium-Rich Layered-Oxide Composite Cathodes for Suppressing Voltage Fade. *Angew. Chem., Int. Ed.* **2015**, *54*, 13058−13062.
(53) Jo, C.-H.; Cho, D.-H.; Noh, H.-J.; Yashiro, H.; Sun, Y.-K.; Myung, S. T. An Effective Method to Reduce Residual Lithium Compounds on Ni-Rich $Li[Ni_{0.6}Co_{0.2}Mn_{0.2}]O_2$ Active Material Using a Phosphoric Acid Derived Li_3PO_4 Nanolayer. *Nano Res.* **2015**, *8*, 1464−1479.
(54) Jackson, D. H. K.; Kuech, T. F. Electrochemical Effects of Annealing on Atomic Layer Deposited Al_2O_3 Coatings on $LiNi_{0.5}Mn_{0.3}Co_{0.2}O_2$. *J. Power Sources* **2017**, *365*, 61−67.
(55) Seok Jung, Y.; Cavanagh, A. S.; Yan, Y.; George, S. M.; Manthiram, A. Effects of Atomic Layer Deposition of Al_2O_3 on the $Li[Li_{0.20}Mn_{0.54}Ni_{0.13}Co_{0.13}]O_2$ Cathode for Lithium-Ion Batteries. *J. Electrochem. Soc.* **2011**, *158*, A1298−A1302.
(56) Zhou, A.; Liu, Q.; Wang, Y.; Wang, W.; Yao, X.; Hu, W.; Zhang, L.; Yu, X.; Li, J.; Li, H. Al_2O_3 Surface Coating on $LiCoO_2$ through a Facile and Scalable Wet-Chemical Method towards High-Energy Cathode Materials Withstanding High Cutoff Voltages. *J. Mater. Chem. A* **2017**, *5*, 24361−24370.
(57) Liao, J.-Y.; Manthiram, A. Surface-Modified Concentration-Gradient Ni-Rich Layered Oxide Cathodes for High-Energy Lithium-Ion Batteries. *J. Power Sources* **2015**, *282*, 429−436.
(58) Mohanty, D.; Dahlberg, K.; King, D. M.; David, L. A.; Sefat, A. S.; Wood, D. L.; Daniel, C.; Dhar, S.; Mahajan, V.; Lee, M.; Albano, F. Modification of Ni-Rich FCG NMC and NCA Cathodes by Atomic Layer Deposition: Preventing Surface Phase Transitions for High-Voltage Lithium-Ion Batteries. *Sci. Rep.* **2016**, *6*, 26532.
(59) Han, B.; Key, B.; Lapidus, S. H.; Garcia, J. C.; Iddir, H.; Vaughey, J. T.; Dogan, F. From Coating to Dopant: How the Transition Metal Composition Affects Alumina Coatings on Ni-Rich Cathodes. *ACS Appl. Mater. Interfaces* **2017**, *9*, 41291−41302.
(60) Liu, W.; Li, X.; Xiong, D.; Hao, Y.; Li, J.; Kou, H.; Yan, B.; Li, D.; Lu, S.; Koo, A.; Adair, K.; Sun, X. Significantly Improving Cycling Performance of Cathodes in Lithium Ion Batteries: The Effect of Al_2O_3 and $LiAlO_2$ Coatings on $LiNi_{0.6}Co_{0.2}Mn_{0.2}O_2$. *Nano Energy* **2018**, *44*, 111−120.
(61) Xu, M.; Chen, Z.; Li, L.; Zhu, H.; Zhao, Q.; Xu, L.; Peng, N.; Gong, L. Highly Crystalline Alumina Surface Coating from Hydrolysis of Aluminum Isopropoxide on Lithium-Rich Layered Oxide. *J. Power Sources* **2015**, *281*, 444−454.
(62) Puurunen, R. L. Surface Chemistry of Atomic Layer Deposition: A Case Study for the Trimethylaluminum/Water Process. *J. Appl. Phys.* **2005**, *97*, 121301.
(63) George, S. M. Atomic Layer Deposition: An Overview. *Chem. Rev.* **2010**, *110*, 111−131.
(64) Neudeck, S.; Strauss, F.; Garcia, G.; Wolf, H.; Janek, J.; Hartmann, P.; Brezesinski, T. Room Temperature, Liquid-Phase Al_2O_3 Surface Coating Approach for Ni-Rich Layered Oxide Cathode Material. *Chem. Commun.* **2019**, *55*, 2174−2177.
(65) Li, T.; Li, X.; Wang, Z.; Guo, H. A Short Process for the Efficient Utilization of Transition-Metal Chlorides in Lithium-Ion Batteries: A Case of $Ni_{0.8}Co_{0.1}Mn_{0.1}O_{1.1}$ and $LiNi_{0.8}Co_{0.1}Mn_{0.1}O_2$. *J. Power Sources* **2017**, *342*, 495−503.
(66) Gan, Q.; Qin, N.; Zhu, Y.; Huang, Z.; Zhang, F.; Gu, S.; Xie, J.; Zhang, K.; Lu, L.; Lu, Z. Polyvinylpyrrolidone-Induced Uniform Surface-Conductive Polymer Coating Endows Ni-Rich Li-$Ni_{0.8}Co_{0.1}Mn_{0.1}O_2$ with Enhanced Cyclability for Lithium-Ion Batteries. *ACS Appl. Mater. Interfaces* **2019**, *11*, 12594−12604.
(67) Shang, G.; Tang, Y.; Lai, Y.; Wu, J.; Yang, X.; Li, H.; Peng, C.; Zheng, J.; Zhang, Z. Enhancing Structural Stability unto 4.5 V of Ni-Rich Cathodes by Tungsten-Doping for Lithium Storage. *J. Power Sources* **2019**, *423*, 246−254.
(68) Cho, W.; Kim, S.-M.; Song, J. H.; Yim, T.; Woo, S.-G.; Lee, K.-W.; Kim, J.-S.; Kim, Y.-J. Improved Electrochemical and Thermal Properties of Nickel Rich $LiNi_{0.6}Co_{0.2}Mn_{0.2}O_2$ Cathode Materials by SiO_2 Coating. *J. Power Sources* **2015**, *282*, 45−50.
(69) Hildebrand, S.; Vollmer, C.; Winter, M.; Schappacher, F. M. Al_2O_3, SiO_2 and TiO_2 as Coatings for Safer $LiNi_{0.8}Co_{0.15}Al_{0.05}O_2$ Cathodes: Electrochemical Performance and Thermal Analysis by Accelerating Rate Calorimetry. *J. Electrochem. Soc.* **2017**, *164*, A2190−A2198.
(70) Yan, G.; Li, X.; Wang, Z.; Guo, H.; Wang, J.; Peng, W.; Hu, Q. Effects of 1-Propylphosphonic Acid Cyclic Anhydride as an Electrolyte Additive on the High Voltage Cycling Performance of Graphite/$LiNi_{0.5}Co_{0.2}Mn_{0.3}O_2$ Battery. *Electrochim. Acta* **2015**, *166*, 190−196.
(71) Liu, X.; Li, H.; Yoo, E.; Ishida, M.; Zhou, H. Fabrication of $FePO_4$ Layer Coated $LiNi_{1/3}Co_{1/3}Mn_{1/3}O_2$: Towards High-Performance Cathode Materials for Lithium Ion Batteries. *Electrochim. Acta* **2012**, *83*, 253−258.

https://dx.doi.org/10.1021/acsami.0c06484
ACS Appl. Mater. Interfaces 2020, 12, 31392−31400

3.3 Publication III: Insights into the Positive Effect of Post-Annealing on the Electrochemical Performance of Al_2O_3-Coated Ni-Rich NCM Cathodes for Lithium-Ion Batteries

In publication II, we have developed a new solution based Al_2O_3 coating approach for Ni-rich NCM based cathodes, which results in an improved long-term cycling performance, but no positive effect on the C-rate performance has been observed. However, for the commercialization of Ni-rich NCM based cathodes for next generation battery systems improvements of the C-rate performance is required along with cycling performance. Keeping that in mind, an additional annealing step has been added to the coating method. The recovered powder obtained after the coating process has been annealed at high-temperatures under oxygen. Structural analysis of the samples reveal that the annealing step has no effect on the structural properties of NCM particles. However, significant changes of the structural properties of the coating layer are observed. NMR studies reveal the diffusion of Li^+ inside the coating layer during annealing, resulting in the formation of mixed $Al_2O_3/LiAlO_2$ composite layer. This has been further confirmed by XPS. The Li^+ diffusion inside the coating layer results in significant improvement in the coating conductivity, as confirmed by EIS analysis. The increase in conductivity of the coating layer, improves electrochemical performance of the NCM in-terms of C-rate capabilities and long-term cycling. In addition, the mixed coating layer is found to be effective against parasitic side reaction at the interface between electrode and electrolyte resulting in a lower impedance rise over long-term cycling as confirmed by EIS analysis. Furthermore, post-mortem analysis of the cycled cells reveal that the coating is also effective against the particle fracture.

The concept and experiments for this publication have been designed and performed by myself under the supervision of Dr. M. T. Elm. The manuscript was written by me and corrected by all co-authors. NMR analysis has been taken by R. Staglich. E. Celik and R. Pan contributed to the scientific discussions. Reprinted with permission from ACS Applied Energy Materials 2021.

R. S. Negi, E. Celik, R. Pan, R. Stäglich, J. Senker, M. T. Elm, Insights into the positive effect of post-annealing on the electrochemical performance of Al_2O_3 coated Ni-Rich NCM cathode for lithium-ion batteries, ACS Appl. Energy Mater. **2021**, 4, 4, 3369–338

ACS APPLIED ENERGY MATERIALS

www.acsaem.org Article

Insights into the Positive Effect of Post-Annealing on the Electrochemical Performance of Al_2O_3-Coated Ni-Rich NCM Cathodes for Lithium-Ion Batteries

Rajendra S. Negi, Erdogan Celik, Ruijun Pan, Robert Stäglich, Jürgen Senker, and Matthias T. Elm*

Cite This: https://doi.org/10.1021/acsaem.0c03135 Read Online

ACCESS | Metrics & More | Article Recommendations | Supporting Information

ABSTRACT: Ni-rich $Li(Ni_{1-x-y}Co_xMn_y)O_2$-based cathodes still suffer from low cycling stability, which arises from capacity fading and impedance rise due to parasitic side reactions at the interface. Surface coatings have shown promising results in stabilizing the cathode surface and improving the cycling stability. However, a comprehensive understanding on the beneficial effect of the coating is still missing. In this paper, we used a solution-based technique to coat Ni-rich $Li(Ni_{0.70}Co_{0.15}Mn_{0.15})O_2$ with a thin Al_2O_3 layer followed by post-annealing at 600 °C. Electrochemical characterization shows a drastic improvement of the cathode's cycling stability due to the coating. After post-annealing, the cycling stability is even further improved, accompanied with its C-rate performance. Structural characterization confirms that annealing results in the formation of an amorphous $Al_2O_3/LiAlO_2$ coating layer, which exhibits increased lithium-ion conductivity compared to the Al_2O_3 coating. More importantly, temperature-dependent impedance measurements reveal that the coatings do not affect the activation energy of the charge transport, which guarantees a sufficient electronic conductivity between the secondary NCM particles in the cathode. Thus, the $Al_2O_3/LiAlO_2$ layer not only inhibits direct contact between electrode and electrolyte, preventing side reactions and stabilizes the performance, but also facilitates conductive pathways for lithium ions while preserving the electronic connectivity between cathode's particles, leading to a low interfacial resistance and excellent rate capability. The results show the importance of providing a sufficiently high electrical conductivity accompanied with low activation energies in coating layers for both ions and electrons, which needs to be considered in design strategies for next-generation lithium-ion batteries.

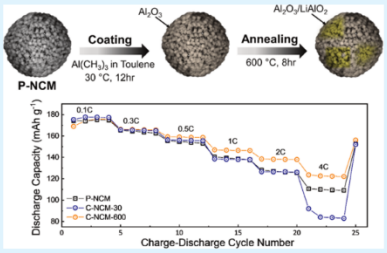

KEYWORDS: *Li-ion battery, Al_2O_3 coating, NCM cathode, annealing, ^{27}Al NMR, EIS*

1. INTRODUCTION

The groundbreaking research during the 1980s led to the commercialization of the first Li-ion battery (LIB) by Sony in 1991[1,2] with the configuration of lithium cobalt oxide (LCO) as cathode and graphite as anode materials.[3,4] In LIBs, LCO has been demonstrated as one of the most promising materials of choice due to its high theoretical specific capacity (~274 mA h g^{-1}) and an easy synthesis process.[5−7] However, its low practical capacity (135 mA h g^{-1}) is inadequate to achieve high gravimetric densities required to fulfill the demand for long-range electric vehicles (EVs) or hybrid electric vehicles (HEVs).[8,9] Much research effort has been devoted to develop high-energy-density cathodes in the past decade. NCM-based cathodes with a general formula of $Li(Ni_{1-x-y}Co_xMn_y)O_2$ have attracted much attention since their first synthesis by Dahn et al.[10] due to their high energy densities (~220 mA h g^{-1}) and relatively low synthesis cost.[11−14]

For NCM-based cathodes, it is well known that the increase in nickel (Ni) content leads to higher achievable capacities in the same operating voltage range ($Li(Ni_{0.33}Co_{0.33}Mn_{0.33})O_2$ (NCM111) ~155 mA h g^{-1} vs $Li(Ni_{0.8}Co_{0.1}Mn_{0.1})O_2$ (NCM811) ~190 mA h g^{-1}, when charging to 4.3 V),[15] since Ni(II)/Ni(III) and Ni(III)/Ni(IV) are the main redox pairs contributing to the overall capacity. Moreover, increasing the Ni content is also beneficial from economic and environmental aspects, since Ni is cheaper and less toxic than cobalt.[16,17] However, increasing the Ni content in NCM also results in intrinsic problems, such as poor cycling stability and serious safety issues, due to the high reactivity of Ni(IV) with the electrolyte and an oxygen release at charged states.[18−22] It is also reported that trace amounts of moisture at the NCM surface react with the electrolyte and produce HF,

Received: December 16, 2020
Accepted: March 8, 2021

https://doi.org/10.1021/acsaem.0c03135
ACS Appl. Energy Mater. XXXX, XXX, XXX−XXX

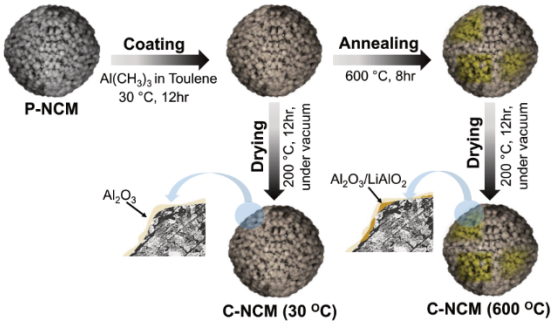

Figure 1. Schematic representation of the coating process of Ni-rich NCM.

which deteriorates the NCM surface by forming an insulating LiF layer, leading to exacerbated electrochemical performances.[13,23−26]

To address the aforementioned problems with Ni-rich NCM cathodes, surface coating using different materials, e.g., Al_2O_3, TiO_2, ZnO, and ZrO_2, has been proposed[27−32] to protect the surface of NCM from reacting with HF and inhibit the parasitic side reactions at the cathode−electrolyte interface.[33,34] Al_2O_3 is one of the most widely employed coating materials; however, it is an electronic insulator ($\sim 10^{-8}$ S cm^{-1}) and has an extremely low Li diffusivity. Thus, an Al_2O_3 coating generally increases the interfacial resistance and results in a reduced rate capability.[35−37] In contrast, a $LiAlO_2$-based coating shows excellent Li conductivity due to partially occupied Li sites. Therefore, $LiAlO_2$ or mixed $Al_2O_3/LiAlO_2$ coatings can not only stabilize the cathode−electrolyte interface but also improve the rate capability,[19,33,35,38,39] making them a promising coating material for Ni-rich NCM cathodes. However, Al_2O_3 as well as $LiAlO_2$ coating layers exhibit comparably high activation energies for lithium-ion diffusion of about 0.71 and 0.54 eV,[35] respectively, which limits an efficient lithium-ion transport. Furthermore, the electronic conductivity between the NCM particles may be severely hindered due to the electronically insulating properties of the coating layers.[37,40]

In this work, we successfully prepared an $Al_2O_3/LiAlO_2$ coating for Ni-rich NCM particles using a low-temperature wet-chemical-based alumina coating method followed by post-annealing. As reported in our previous study,[41] the coating method takes advantage of surface-active −OH groups, which dry and coat the NCM cathode material in a single step, leading to a significant enhancement of the cycling performance. Here, we show that post-annealing of the Al_2O_3 layer at 600 °C for 8 h results in an even further improvement of the long-term cycling accompanied with a significantly enhanced rate performance of the NCM cathode. Several structural and electrochemical characterization techniques have been applied to analyze the transformation of the Al_2O_3 layer to an amorphous $Al_2O_3/LiAlO_2$ layer upon high-temperature treatment. We reveal that the lithium diffusion into Al_2O_3 (as confirmed by structural characterization) is accompanied with a significant improvement of the lithium-ion conductivity of the coating layer, which is clearly confirmed by impedance spectroscopy. Furthermore, we show that the coating barely affects the activation energy for the charge transport preserving a sufficient electronic conductivity between the single NCM particles, which form the single cathodes. As annealing does not change the structural properties of the NCM, the enhancement of the electrochemical performance can therefore directly be related to the improved electrical properties of the $Al_2O_3/LiAlO_2$ coating layer. The findings in this paper will help to better understand how the coating process and post-annealing influence the coating properties and the electrochemical performances of the coated cathodes, which is among the most critical issues in the development of coatings for high-energy-density cathodes.

2. EXPERIMENTAL SECTION

2.1. Surface Coating of Ni-Rich NCM with Al_2O_3. Commercially available NCM 7/1.5/1.5 (NCM701515) powder was used as a raw material, denoted as pristine NCM (P-NCM) in the following. For the coating, a solution route was used. First, trimethylaluminum (TMA, 0.279 mL, 2 M in toluene; Sigma-Aldrich) was diluted by adding anhydrous toluene (15 mL; Sigma-Aldrich) and stirred to get a homogeneous solution. Then, NCM powder (5 g; Gelon LIB) was added into the diluted TMA solution (5 mL) and the mixture was continuously stirred at 30 °C overnight (12 h).[41] This wet-chemical-based coating method takes advantage of surface-active −OH groups (from LiOH and adsorbed H_2O) that dry and coat the NCM cathode material in a single treatment step in solution, as previously reported.[28,41,42] The mixture was filtered and washed using toluene and then dried under vacuum at 200 °C overnight (12 h), which was later transferred to an argon-filled glovebox. The obtained coated NCM powder was divided into two batches. Batch-1 (C-NCM-30) of the coated powder was used as a cathode material without further treatment. Batch-2 (C-NCM-600) was further annealed at 600 °C for 8 h to modify the Al_2O_3 coating and investigate its effect on the electrochemical performance. A schematic of the coating process is shown in Figure 1.

2.2. Structural Characterization. The morphology of the NCM701515 particles and the coating were investigated using high-resolution scanning electron microscopy (HRSEM, Merlin, Zeiss). The accelerating voltage and current were set to 7 kV and 3000 pA, respectively. Electron-dispersive X-ray (EDX) spectroscopy investigation was performed using an X-Max detector (Oxford Instruments) equipped to the HRSEM. The samples were directly transferred from the glovebox to the HRSEM chamber using a transfer module (Kammrath & Weiss GmbH) to prevent air exposure.

Powder X-ray diffraction (XRD, Bruker) was performed on synthesized samples using Cu Kα radiation source in a 2θ range of 10−80°. X-ray photoelectron spectroscopy (XPS) measurements were

https://doi.org/10.1021/acsaem.0c03135
ACS Appl. Energy Mater. XXXX, XXX, XXX−XXX

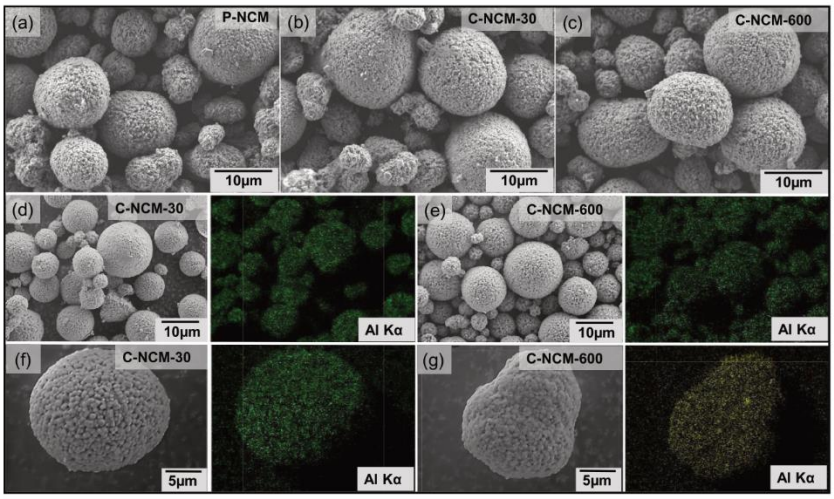

Figure 2. SEM images of the NCM701515 powders: (a) P-NCM, (b) C-NCM-30, and (c) C-NCM-600. EDX mapping of Al_2O_3-coated powders: (d, f) C-NCM-30 and (e, g) C-NCM-600.

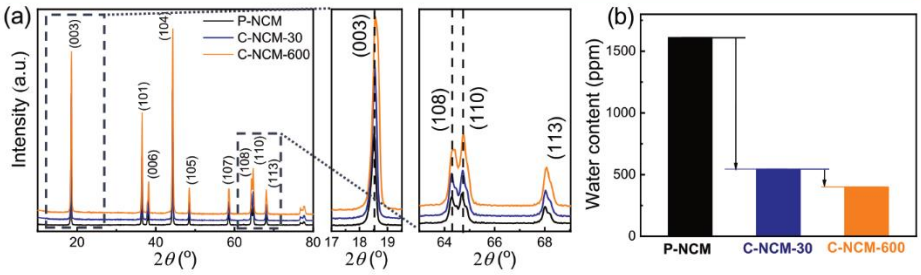

Figure 3. Comparison of (a) XRD patterns and (b) water content values obtained by KF titration.

done using monochromatic Al Kα radiation (PHI 5000 Versaprobe II Scanning ESCA microprobe, Physical Electronics) at a pressure of ~10^{-8} Pa. For the survey scan and detailed spectra, pass energies of 93.9 and 23.5 eV were used, respectively. The synthesized samples were directly transferred to the XPS chamber using the transfer module. All data calibration and analysis were done using CasaXPS. All spectra were calibrated to the corresponding carbon peak (C 1s, 284.8 eV). Karl−Fischer titration (KF titration) was performed on all samples to determine their water content.

Solid-state NMR studies of ^{27}Al were performed on a Bruker AvanceIII HD spectrometer with an external magnetic field of 14.1 T, which corresponds to a Larmor frequency of ν_0 = 156.43 MHz. The measurements were performed in a 1.9 mm HXY MAS triple-resonance probe with commercial ZrO_2 rotors using a spinning speed of 30 kHz. For single-pulse (SP) acquisition, a nutation frequency of 25 kHz with a pulse length of 1 μs was utilized, with a recycling delay of 0.5 s. Between 455k and 470k scans have been accumulated. The FID was processed with an exponential line broadening of 500 Hz. The spectra were referenced to an aqueous solution of $Al(NO_3)_3$ adjusted to a pH of 0.

2.3. Cell Assembly. Electrode sheets were prepared by mixing the NCM (90 wt %) powder with carbon black (5 wt %, Super P) and poly(vinyl difluoride) (5 wt %, Solef PVDF 6020) in *N*-methyl-2-pyrrolidone (NMP, Sigma-Aldrich). The slurry was stirred with a magnetic stirrer overnight (12 h) to get a homogeneous mixing. The prepared slurry was then casted onto aluminum foil and dried under vacuum overnight (12 h). Electrode disks (12 mm) were punched from the prepared sheet, calendered at 90 psi, and dried under vacuum at 120 °C for 12 h. Coin cells were prepared using CR2032-type cases; Li foil (14 mm) was used as the anode, Celgard 2500 (16 mm, Celgard) as the separator, and LP50 (50 μL, Sigma-Aldrich) as the electrolyte. The areal loading was 10.4−10.8 $mg_{NCM701515}$ cm^{-2}.

2.4. Cell Cycling. All cells were cycled using a MACCOR Series 4300 (Tulsa) multichannel battery cycler. All cells were electrochemically tested between 3.0 and 4.3 V vs Li^+/Li at 25 °C. Initially, for the rate test, the cells were cycled from 0.1C to 4C (1C means fully charging/discharging the cell in 1 h), each for four cycles between 3.0 and 4.3 V vs Li^+/Li. Subsequently, for a long-term cycling test, the same cells were cycled at 0.5C in the same voltage range. For calculating the capacities and specific currents, masses of active material in the individual cathodes were considered.

https://doi.org/10.1021/acsaem.0c03135
ACS Appl. Energy Mater. XXXX, XXX, XXX−XXX

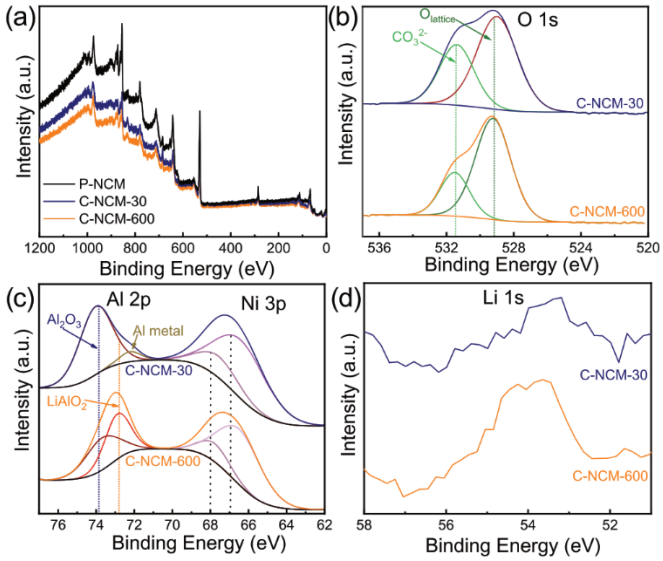

Figure 4. Comparison of (a) survey XPS of P-NCM, C-NCM-30, and C-NCM-600 and (b–d) detailed XPS spectra of C-NCM-30 and C-NCM-600.

2.5. Electrochemical Impedance Spectroscopy (EIS). To investigate the effect of annealing on the total conductivity of the NCM powder, temperature-dependent (−100 to −60 °C) electrochemical impedance spectroscopy (EIS) measurements were performed using a Novocool Cryosystem setup on hand-pressed NCM pellets. For the impedance measurements, ionically blocking electrodes were used (stainless steel). The spectra were acquired between 100 mHz and 1 GHz. EIS was also performed on cells with uncoated and coated NCM cathodes in the fully charged state (4.3 V) on a VMP300 potentiostat (BioLogic) between 10 mHz and 100 kHz at room temperature.

3. RESULTS AND DISCUSSION

3.1. Characterization of the Al_2O_3-Coated NCM. The morphology of the as-received and coated NCM powders was analyzed by HRSEM, as shown in Figure 2. As can be seen in Figure 2a–c, the pristine and coated samples show a similar morphology, which confirms that the coating process has no significant impact on the morphology of the NCM particles. The secondary particles are spherical in shape having a diameter of 5–15 μm and are composed of submicron and nanosized primary particles (Figure S1). The EDX mappings (Figure 2d–g) show an even distribution of aluminum, indicating a uniform and conformal coating of Al_2O_3 on the NCM surface. As reported in our recent work, high-resolution transmission electron microscopy confirm the homogeneous coating of the NCM particles with an amorphous Al_2O_3 layer with a thickness of about 6 nm (Figure S2).[41] EDX analysis of the annealed powders also shows that high-temperature annealing has no drastic influence on the distribution and homogeneity of the coating layer.

The XRD analysis (Figure 3a) confirms that all NCM samples have the crystalline layered structure of $LiCoO_2$ (space group $R\text{-}3m$).[39,43] No peak shift is observed for the coated samples. Furthermore, both coated and heat-treated samples show no additional peaks, which indicate the presence of Al_2O_3 or $LiAlO_2$ due to the small thicknesses, low contents, and amorphous nature of the coating layers.[44] Rietveld refinement was performed to estimate changes of the lattice due to the coating. The obtained values of the lattice parameters a and c are listed in Table S1 in the SI. For the pristine and the coated samples, a c/a ratio of 4.94 is obtained, which confirms a well-defined layered structure.[45] After annealing, the c/a ratio and the unit cell volume slightly increases. The increase of the cell volume indicates a possible loss of lithium in the NCM[33] due to lithium diffusion into the Al_2O_3 coating.

Karl–Fischer titration was performed on the NCM powders before and after coating. As shown in Figure 3b, the water content is significantly reduced after coating for both C-NCM-30 and C-NCM-600 compared to P-NCM, which confirms that surface-active −OH groups (from surface-absorbed H_2O and LiOH) are consumed during the coating process. The slight reduction of the water content of C-NCM-600 compared to C-NCM-300 is probably due to the annealing step at 600 °C. The reduction of surface-active −OH groups is assumed to be beneficial for the long-term cycling performance of the coated NCM cathodes, as surface-active −OH groups have significant side effects on the electrochemical performance of NCM-based cathodes.[23,26,46]

XPS measurements were carried out to further analyze the influence of coating and the effect of heat treatment on the coating layer and the NCM powder. The survey spectrum of P-

https://doi.org/10.1021/acsaem.0c03135
ACS Appl. Energy Mater. XXXX, XXX, XXX−XXX

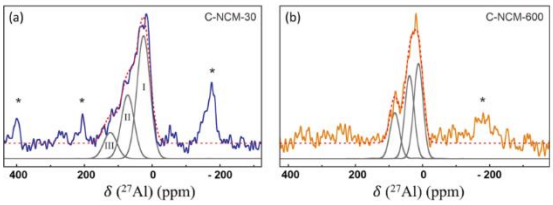

Figure 5. Diamagnetic region of (a) the ^{27}Al NMR spectra of C-NCM-30 (left, blue) and (b) C-NCM-600 (right, orange). The spectra were deconvoluted with three quadrupole shapes (gray) with typical tensor values for six-, five-, and four-fold aluminum oxygen coordinations. (Rotational side bands are indicated by an asterisk).

NCM (Figure 4a) indicates the presence of Ni, Co, Mn, and O without any other elements. However, on the surface of C-NCM-30 and C-NCM-600, the characteristic peak of Al 2p is detected (see also Figure S3), which proves the successful coating of Al_2O_3 on the NCM surface. Detailed spectra were recorded for O, Al, and Li along with Ni and C. As shown in Figure S4 (SI), no significant change is observed for the Ni 2p and C 1s peaks. For the pristine NCM, the O 1s signal comprises two signals. The signal located at 529.3 eV is assigned to the lattice oxygen of NCM, while that at 531.2 eV matches well with the CO_3^{2-} binding energy of Li_2Co_3.[47] After annealing, the CO_3^{2-} peak intensity reduces significantly due to the removal of the carbonates. Of particular interest is the binding energy region between 50 and 80 eV (Figure 4c,d) as it includes the Li 1s and Al 2p core levels. The Al 2p peak shows a significant shift (approximately 1 eV) to lower binding energies after the heat treatment. Further deconvolution reveals that C-NCM-30 shows only one major peak at a binding energy of 73.9 eV corresponding to Al atoms in an oxygen environment, such as Al_2O_3 and $Al(OH)_3$,[44] and one minor peak at 72 eV corresponding to metallic Al resulting from unwanted side products during the coating process. After the heat treatment, the Al 2p peak splits into two peaks, one at a binding energy of 73.9 eV and the other at a lower binding energy of 72.8 eV corresponding to the binding energy of Al^{3+} in $LiAlO_2$, as reported by Tang et al.,[48] indicating the conversion of the Al_2O_3 coating layer to a more conductive $Al_2O_3/LiAlO_2$ layer after the heat treatment.[33] Furthermore, as XPS is a surface-sensitive technique, the peak intensity of an element represents its overall amount at the surface. The increased Li 1s peak intensity for the coated sample after heat treatment therefore also suggests the formation of $LiAlO_2$ caused by Li diffusion from the NCM particles into the Al_2O_3 coating layer during annealing at 600 °C.

To get deeper insight into the structural properties of the $Al_2O_3/LiAlO_2$ layer formed during annealing, NMR spectroscopic measurements were performed. Due to the relatively low temperature during heat treatment and since XPS data do not reveal any evidence for aluminum diffusion into the NCM bulk material, we focus on the diamagnetic region for the ^{27}Al NMR spectroscopic experiments. To reduce the influence of quadrupolar couplings and paramagnetic interactions on the lineshape, all spectra were acquired at high magnetic fields (B_0 = 14.01 T). The diamagnetic region of ^{27}Al MAS NMR spectra (Figure 5) for C-NCM-30 and C-NCM-600 show a broad signal group, which spans −5 to 120 ppm demonstrating that the Al atoms in the coated layer exhibit environments with six (Figure 5, I), five (Figure 5, II), and four (Figure 5, III) oxygen neighbors.[49] Deconvolutions with typical quadrupolar lineshapes for these three environments require broad distributions reflected in large line broadenings (Table 1) typical for a multitude of defects and distortions and an amorphous character of the Al-containing layers for both systems. Nevertheless, significant lineshape changes occur for C-NCM-600. First, the line broadening decreases markedly by roughly 2 kHz, indicating an increasing short-range order of the Al-containing layer. This is in line with the highfield shift for the penta-coordinated Al atoms, suggesting that these environments approach a six-fold coordination. Second, the resonance assigned to Al in tetrahedral coordinations is highfield shifted by roughly 40 ppm approaching the chemical shift reported for $LiAlO_2$.[50] In addition, the proportion for the tetrahedral Al environments increases by roughly 10%. We thus expect that two processes occur upon annealing. (i) Defects and distortions are partially removed, which should decrease the probability to observe Al in four- and five-fold coordinations. (ii) Nevertheless, the proportion of Al in environments typical for $LiAlO_2$ increases, hinting toward a diffusion of Li from the NCM phase into the Al-containing layer, thus stabilizing these particular environments.

Table 1. Relevant Refinement Parameters (δ_{iso}: Isotropic Chemical Shift, C_Q: Quadrupolar Coupling Constant, η_Q: Anisotropy of the Electric Field Gradient Tensor, GB: Gaussian Line Broadening) for the Deconvolutions of the ^{27}Al MAS NMR Spectra of C-NCM-30 and C-NCM-600[a]

	C-NCM-30			C-NCM-600		
	six-fold	five-fold	four-fold	six-fold	five-fold	four-fold
δ_{iso}/ppm	30	76	132	17	42	91
GB/kHz	7.0	7.0	7.0	5.0	5.0	5.0
integral/au	57.7	29.8	12.5	48.1	27.3	24.6

[a]For the resonances representing the six-, five-, and four-fold coordinations, CQ and h pairs of 4.5 MHz/0.3, 3.8 MHz/0.4, and 5.5 MHz/0.7 were used and kept constant. δ_{iso} and the relative intensities were refined freely. For GB, one parameter was used for the three lineshapes.

Conductivity measurement of the uncoated and coated powder can be very useful to determine how coating influences the intrinsic conduction properties of the bare NCM particles. Temperature-dependent EIS measurements were performed on all three samples, and their representative impedance spectra are shown in Figure 6a–c. The impedance of the uncoated NCM powder (Figure 6a) reveals that at least two transport processes contribute to the impedance of the

https://doi.org/10.1021/acsaem.0c03135
ACS Appl. Energy Mater. XXXX, XXX, XXX−XXX

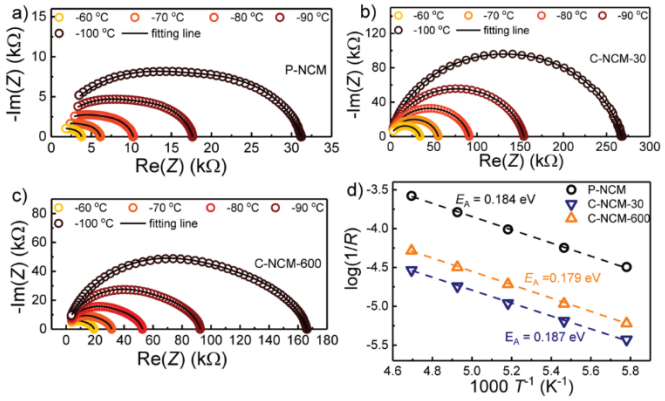

Figure 6. Temperature-dependent EIS spectra of (a) P-NCM, (b) C-NCM-30, and (c) C-NCM-600 pellets. (d) Arrhenius plots of the conductance revealing that the coating has a negligible effect on the activation energy of the transport process in the cathode materials.

powder, resulting in the deviations from a single semicircle behavior as typically observed for NCM pellets using ion-blocking electrodes.[51,52] Although it is possible that the high-frequency process represents the transport in the particles and the lower-frequency process corresponds to the interface resistance between the single NCM particles of the powder, it is more likely that the two transport processes correspond to the electronic and ionic conductivities as NCM is a mixed ion-electronic conductor. As reported, the first semicircle arises from the geometrical capacitance connected in parallel to the total resistance of the NCM powder, which comprises the electronic and ionic resistance. At low frequencies, the ionic transport is blocked and only the electronic conductivity contributes to the transport represented by the second semicircle.[51−53] The electronic resistance is therefore given by the intercept of the impedance with the real part axis in the Nyquist plot. A comparable behavior is also found for the coated powder samples, as shown in Figure 6b,c. A comparison of the total impedance of the three samples shows that the P-NCM powder (Figure 6a) has the lowest impedance, i.e., the highest electronic conductivity, among the three samples. This is expected as coating the powder with Al_2O_3 (Figure 6b) increases the impedance due to the lower electronic and ionic conductivity of the Al_2O_3 coating layer. The Al_2O_3 coating acts as a blocking barrier between the single NCM particles of the powder, resulting in a large interface resistance dominating the overall impedance spectra. However, it is worth noting that the impedance of the post-annealed sample C-NCM-600 (Figure 6c) is significantly decreased and therefore shows a higher conductivity than the C-NCM-30 sample. Since the conductivity includes contribution from the NCM powder and the coating material, it is reasonable to conclude that the increase in conductivity mainly results from a decrease of the interface resistance of the coating material due to the formation of $LiAlO_2$, which exhibits a higher ionic conductivity compared to Al_2O_3.[54] To get further insight into the effect of coating on the charge transport in the cathode, the temperature dependence of the electronic resistance of NCM powder material is plotted in an Arrhenius representation in Figure 6d. The electronic resistance of the uncoated NCM powder shows the expected linear behavior due to the hopping transport of the electrons. The extracted activation energy of $E_A \approx 0.18$ eV is also in good agreement with values from the literature for highly lithiated NCM of comparable composition, confirming the assumption of an electronic transport process.[51,55] Interestingly, also the coated samples reveal a comparable activation energy, although the activation energy of amorphous Al_2O_3 or $LiAlO_2$ is expected to be significantly higher.[40] These results show that despite the homogeneous coating, the electronic transport between NCM particles is barely affected, which is probably due to the thin coating thickness.

3.2. Electrochemical Characterization. It is well known that if a battery is run at higher currents (i.e., higher C-rates), the overpotential of the battery increases due to increased resistance losses (IR drop) and polarization effects in the electrodes, which results in decreased charge/discharge capacities. To evaluate the effect of coating on the electrochemical performance of NCM, all samples were cycled at various C-rates (0.1C to 4C, a specific current of 160 mA g^{-1} was defined at the 1C rate) within the voltage range of 3.0−4.3 V vs Li$^+$/Li. For each C-rate, four cycles were performed before the same cell was subjected to long-term cycling tests at 0.5C. Figure 7a compares the discharge capacities of the different NCM cathodes prepared with C-rates increasing from 0.1C to 4C. As can be seen, the initial capacities at 0.1C are comparable for all three NCM cathodes. However, an effect of the surface modification is clearly notable at higher C-rates. Although the effect of coating on the C-rate performance for C-NCM-30 is nearly negligible up to 2C, C-NCM-30 shows a much lower capacity at 4C than P-NCM. In contrast, C-NCM-600 shows a significant improvement in the C-rate performance at higher C-rates (above 0.5C) compared to both P-NCM and C-NCM-30. Figure 7b,c shows the corresponding discharge profiles of P-NCM and C-NCM-600 at different C-rates. C-NCM-600 exhibits a lower overpotential and retains higher discharge capacities at all C rates than P-NCM. To understand the difference between C-NCM-600 and P-NCM, the corresponding differential capacity plots were analyzed,

https://doi.org/10.1021/acsaem.0c03135
ACS Appl. Energy Mater. XXXX, XXX, XXX−XXX

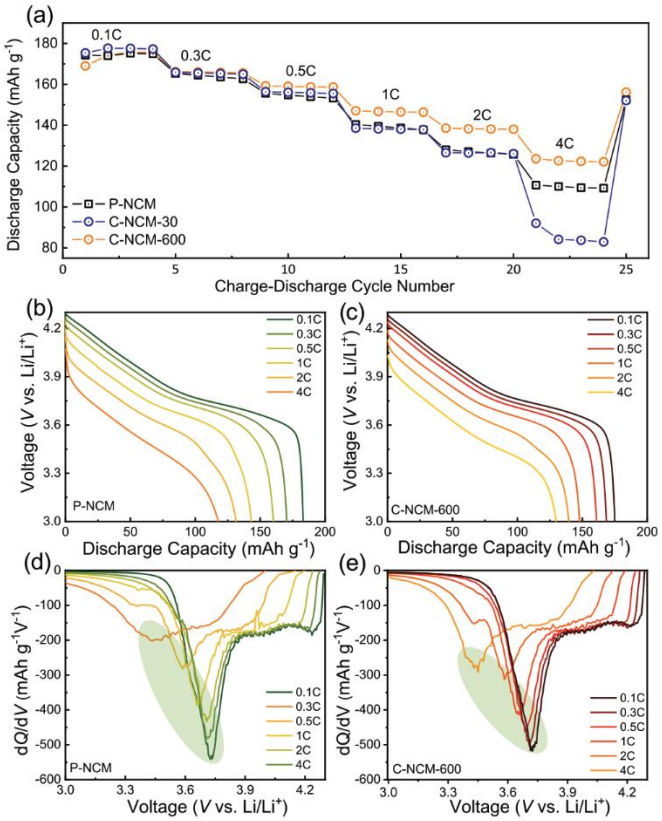

Figure 7. (a) Comparison of rate capabilities at different discharge rates between 0.1C and 4C at 25 °C. Charge−discharge voltage profiles at different C-rates for (b) P-NCM and (c) C-NCM-600 and corresponding differential capacity plots of (d) P-NCM and (e) C-NCM-600.

which are shown in Figure 7d,e. Besides a similar behavior at low C-rates, it can be seen that (i) the shoulder at high voltages shrinks more significantly for P-NCM than for C-NCM-600 with increasing C-rates, which suggests that Li intercalation/deintercalation is better maintained in C-NCM-600; (ii) the potential shift of the minimum is less pronounced for C-NCM-600, which indicates that C-NCM-600 shows a lower overpotential than P-NCM.[37,56] The observations in the C-rate test can be well understood when considering the results from the total conductivity measurements of the three NCM pellets (Figure 6). Since the coating layer of the C-NCM-30 cathode contains only Al_2O_3 with a low electronic and ionic conductivity, C-NCM-30 is expected to have a high interfacial resistance when used as a cathode in a cell. Since the coating layer is sufficiently thin, it does not hinder Li diffusion between NCM and electrolyte to a notable extent at lower C-rates. However, at higher C-rates (e.g., 4C), the resistive properties of the Al_2O_3 layer become a limiting factor, resulting in higher overpotentials and lower capacities than P-NCM. In the case of C-NCM-600, a mixed $Al_2O_3/LiAlO_2$ coating layer at the NCM particle surface was formed during annealing at 600 °C, which is expected to have a higher Li conductivity than the Al_2O_3 layer. Consequently, Li^+ transfer between NCM and the electrolyte is possible, explaining the improved rate capability of C-NCM-600 compared to C-NCM-30. The mixed $Al_2O_3/LiAlO_2$ coating layer on C-NCM600 also prevents side reactions at the cathode−electrolyte interface (e.g., electrolyte decomposition, LiF formation due to HF attack)[57] and thus hinders the formation of an insulting cathode−electrolyte interface (CEI). In fact, this explains why C-NCM-600 also shows the best long-term cycling performance among the three cathodes as shown in Figures S5 and 8a, which will be discussed in detail below. The improvement of the electrochemical performance of C-NCM-30 compared to P-NCM was discussed thoroughly in our previous publica-

https://doi.org/10.1021/acsaem.0c03135
ACS Appl. Energy Mater. XXXX, XXX, XXX−XXX

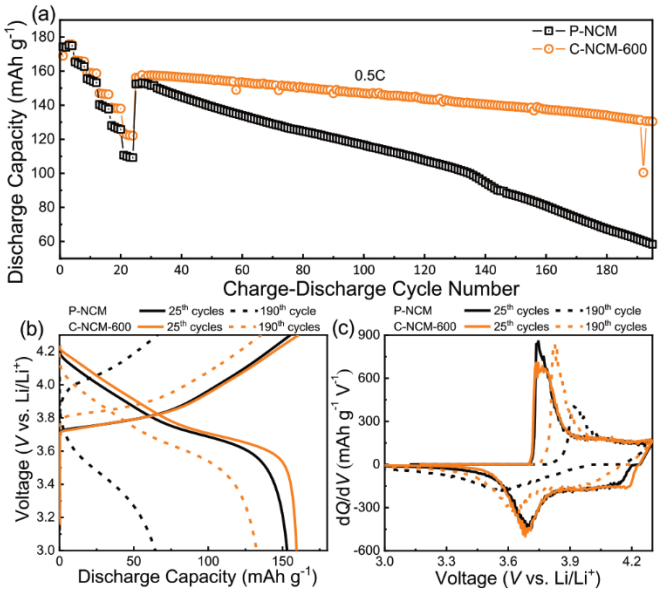

Figure 8. (a) Comparison of long-term cycling performances of P-NCM and C-NCM-600. (b) Charge−discharge profiles of P-NCM and C-NCM-600 on the 25th and 190th cycles, along with (c) the corresponding differential capacity plots. The long-term cycling comparison of P-NCM with C-NCM-30 is shown in Figure S4 and has been discussed in our previous publication.[41]

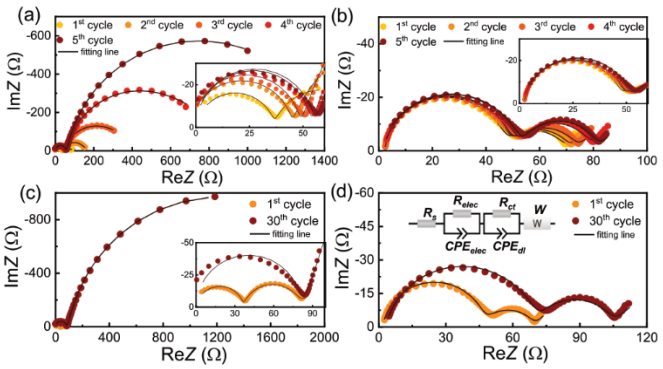

Figure 9. Nyquist plots of the electrochemical impedance measurements performed at the fully charged state (4.3 V) of (a) P-NCM and (b) C-NCM-600 during the initial five cycles. Nyquist plots of (c) P-NCM and (d) C-NCM-600 after the 1st and 30th cycles.

tion.[41] Therefore, we will focus on the electrochemical performance of P-NCM and C-NCM-600 in the following.

Figure 8a shows the long-term cycling performances of the P-NCM and C-NCM-600 cells at 0.5C after the C-rate test. It can be seen that the discharge capacity of P-NCM decreases rapidly from 153.5 to 58.9 mA h g^{-1} after 190 cycles with a capacity retention of only 38.3%. Such a low cycling stability of P-NCM is attributed primarily to the poor structural stability and severe parasitic side reactions occurring at the surface of NCM.[32,58,59] In contrast, C-NCM-600 shows a significantly improved cycling performance with a much higher capacity retention of 83.3% after the same number of charge−discharge cycles. Apparently, the protective $Al_2O_3/LiAlO_2$ coating layer acts as an effective protective barrier at the interface against

https://doi.org/10.1021/acsaem.0c03135
ACS Appl. Energy Mater. XXXX, XXX, XXX−XXX

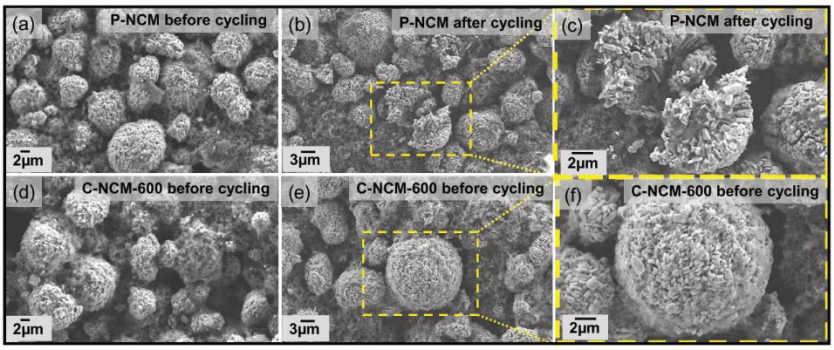

Figure 10. SEM images of (a) P- and (d) C-NCM-600 electrodes before cycling. (b, c) Surface of the P-NCM electrode after cycling. (e, f) Surface of the C-NCM-600 electrode after cycling.

parasitic reactions. In addition, the $LiAlO_2$ layer also provides a conduction pathway for Li^+ to diffuse during the charge/discharge process. The charge−discharge profiles of P-NCM and C-NCM-600 at the beginning and end of the long-term cycling test (25^{th} and 190^{th} cycles including the C-rate test) along with the corresponding differential capacity plots are shown in Figure 8b,c. C-NCM-600 exhibits a much smaller polarization increase than P-NCM during the long-term cycling test, and the differential capacity peaks are much sharper for C-NCM-600 during the 190^{th} cycle. As for the C-rate tests, these findings also indicate a more stable interface and a better preserved Li^+ diffusion pathway through the coating as usually the formation of the highly resistive CEI is responsible for the capacity fading and polarization increase along with the diminishing of the peak sharpness and intensity.[57] All of these observations support that the Al_2O_3/$LiAlO_2$ composite coating layer is very effective in stabilizing the surface of the Ni-rich NCM and thus the electrochemical performance during long-term cycling.

To further understand the effect of the Al_2O_3/$LiAlO_2$ coating on the long-term cycling of the coated Ni-rich NCM, EIS measurements were performed on P-NCM and C-NCM-600 as a function of cycle number. The results are shown in Figure 9. The samples were cycled between 3.0 and 4.3 V vs Li^+/Li at 0.5C, and EIS measurements were performed at the fully charged state (4.3 V) of every cycle. Fitting of the Nyquist plots was done using the equivalent circuit shown in Figure 9d. Here, R_s represented the internal ohmic resistance of the cell, which involves the resistances from the electrolyte and other components of the cell, corresponding to the intercept on the real axis at the high-frequency region. The mid-frequency (MF) semicircle is assigned to the resistance of the NCM electrode (R_{Elec}) as the impedance agrees with the results obtained for the corresponding NCM pellets (Figure 6). Finally, the low-frequency (LF) semicircle is attributed to charge transfer resistance (R_{ct}) at the surface of NCM.[60−62] As shown in Figure 9a, the value of R_{Elec} for the P-NCM slowly increases with increasing cycling number and almost doubles after the initial five cycles. On the contrary, R_{Elec} for C-NCM-600 is much more stable and remains nearly constant during the initial five cycles (Figure 9b), which suggests that the cathode interface is much more stable during cycling due to the presence of the protective Al_2O_3/$LiAlO_2$ coating. The R_{ct} values for both materials increase with cycling number. However, the rate of increase of R_{ct} is much more pronounced for P-NCM than that for C-NCM-600. After 30 cycles, the R_{ct} value for C-NCM-600 is distinctly smaller than that for P-NCM, whose R_{ct} increases by nearly a factor of 10. The increase of R_{ct} during cycling also confirms the formation of a CEI due to side reactions at the electrode/electrolyte interface.[63,64] The stabilized R_{Elec} and the significantly smaller R_{ct} for C-NCM-600 further confirm the beneficial effect of the Al_2O_3/$LiAlO_2$ coating layer in preventing side reactions.

3.3. Postmortem Characterization. Postmortem analysis was performed on cells before and after the long-term cycling test as apart from mechanical-induced deformation during electrode preparation, electrochemical-induced deformation (e.g., cathode volume changes, crack formation, and new phase formation during the delithiation/lithiation) also takes place inside of the secondary particles. The deformations increase the active surface area[59] and thus accelerate side reaction, which finally leads to poor cycling performance of NCM.[65] Figure 10 shows the SEM images of the cycled cells. The SEM images for both P-NCM and C-NCM-600 (Figure 10a,d, respectively) show no cracking of the NCM secondary particles before cycling. On the other hand, severe exfoliation and cracking can be observed after cycling in the case of P-NCM, which is one reason for the loss of irreversible capacity during cycling and also for the increase of R_{Elec} during cycling observed in the EIS measurements. However, in the case of C-NCM-600, the structure is well maintained and almost no cracking is observed after cycling. Thus, postmortem analysis also confirms that the coating effectively prevents the surface deterioration and protects the structural integrity of the NCM secondary particles, which is also seen in the FIB cross-sectional images of both samples after cycling (Figure S6).

4. CONCLUSIONS

In this work, we report on the beneficial effect of a thin Al_2O_3/$LiAlO_2$ coating on Ni-rich NCM cathodes for LIBs resulting in improved electrochemical performance compared to Al_2O_3-coated samples. The Al_2O_3/$LiAlO_2$ coating of NCM was achieved by a straightforward and scalable solution-based

https://doi.org/10.1021/acsaem.0c03135
ACS Appl. Energy Mater. XXXX, XXX, XXX−XXX

approach followed by a high-temperature heat treatment under oxygen. NMR analysis reveals the diffusion of Li^+ into the Al_2O_3 layer during the heat treatment, resulting in the formation of an amorphous $Al_2O_3/LiAlO_2$ composite layer, which has been also confirmed using XPS analyses. In addition, XRD and SEM measurements showed no significant changes in the reflection peaks of NCM as well as no observable change in the morphology. During heat treatment, lithium diffusion into Al_2O_3 is accompanied with a significant improvement of the lithium-ion conductivity of the coating layer, as confirmed by the EIS study. After heat treatment, the coated NCM reveals an increased conductivity, giving rise to a significantly improved C-rate and cycling performance compared to P-NCM and even to coated, but nonannealed C-NCM-30. The improvement in the electrochemical performance can therefore directly be related to the increase in ionic conductivity of the coating layer, as the structural properties of the NCM remain unaffected by the annealing. The multifunctional $Al_2O_3/LiAlO_2$ coating isolates the direct contact between the electrode and the electrolyte, preventing side reactions, and stabilizes the electrochemical performance of the coated cathode. Furthermore, the $Al_2O_3/LiAlO_2$ coating not only facilitates conductive and well-defined Li diffusion pathways but also preserves electronic conductivity between the NCM particles in the cathode, leading to a low interfacial resistance and excellent rate capability. Thus, the $Al_2O_3/LiAlO_2$ coating formed by annealing of Al_2O_3-coated NCM provides a beneficial synergy to improve the electrochemical performance of Ni-rich NCM701515 cathode materials.

■ ASSOCIATED CONTENT

Supporting Information

The Supporting Information is available free of charge at https://pubs.acs.org/doi/10.1021/acsaem.0c03135.

Lattice constants from Rietveld refinement, SEM micrograph, high-resolution transmission electron microscopy (HR-TEM), XPS spectra, long-term electrochemical cycling performances, and cross-sectional SEM micrographs (PDF)

■ AUTHOR INFORMATION

Corresponding Author

Matthias T. Elm − *Center for Materials Research (ZfM), Justus-Liebig-University Giessen, D-35392 Giessen, Germany; Institute of Physical Chemistry, Justus-Liebig-University Giessen, D-35392 Giessen, Germany; Institute of Experimental Physics I, Justus Liebig University Giessen, 35392 Giessen, Germany;* orcid.org/0000-0001-7014-5772; Email: matthias.elm@phys.chemie.uni-giessen.de

Authors

Rajendra S. Negi − *Center for Materials Research (ZfM), Justus-Liebig-University Giessen, D-35392 Giessen, Germany*

Erdogan Celik − *Center for Materials Research (ZfM), Justus-Liebig-University Giessen, D-35392 Giessen, Germany*

Ruijun Pan − *Center for Materials Research (ZfM), Justus-Liebig-University Giessen, D-35392 Giessen, Germany; Institute of Physical Chemistry, Justus-Liebig-University Giessen, D-35392 Giessen, Germany;* orcid.org/0000-0002-6301-4771

Robert Stäglich − *Inorganic Chemistry III and Northern Bavarian NMR Centre, University of Bayreuth, D-95440 Bayreuth, Germany*

Jürgen Senker − *Inorganic Chemistry III and Northern Bavarian NMR Centre, University of Bayreuth, D-95440 Bayreuth, Germany;* orcid.org/0000-0002-7278-7952

Complete contact information is available at: https://pubs.acs.org/10.1021/acsaem.0c03135

Notes

The authors declare no competing financial interest.

■ ACKNOWLEDGMENTS

R.S.N. and M.T.E. thank the German Federal Ministry of Education and Research (BMBF) for funding the Nano-MatFutur project NiKo (03XP0093). R.S. and J.S. gratefully acknowledge financial support of the German Science Foundation (DFG) within the SFB 840 project C1.

■ REFERENCES

(1) Nishi, Y. Performance of the First Lithium Ion Battery and Its Process Technology. In *Lithium Ion Batteries*, 2007; pp 181−198.

(2) Johnson, B. A.; White, R. E. Characterization of Commercially Available Lithium-Ion Batteries. *J. Power Sources* **1998**, *70*, 48−54.

(3) Winter, M.; Besenhard, J. O.; Spahr, M. E.; Novák, P. Insertion Electrode Materials for Rechargeable Lithium Batteries. *Adv. Mater.* **1998**, *10*, 725−763.

(4) Goodenough, J. B.; Kim, Y. Challenges for Rechargeable Li Batteries. *Chem. Mater.* **2010**, *22*, 587−603.

(5) Mizushima, K.; Jones, P. C.; Wiseman, P. J.; Goodenough, J. B. $LixCoO_2$ (0<x<-1): A New Cathode Material for Batteries of High Energy Density. *Mater. Res. Bull.* **1980**, *15*, 783−789.

(6) Delmas, C.; Fouassier, C.; Hagenmuller, P. Structural Classification and Properties of the Layered Oxides. *Phys. B+C* **1980**, *99*, 81−85.

(7) Cho, J.; Kim, Y. J.; Kim, T. J.; Park, B. Zero-Strain Intercalation Cathode for Rechargeable Li-Ion Cell. *Angew. Chemie* **2001**, *40*, 3367−3369.

(8) Chen, Z.; Dahn, J. R. Methods to Obtain Excellent Capacity Retention in $LiCoO_2$ Cycled to 4.5 V. *Electrochim. Acta* **2004**, *49*, 1079−1090.

(9) Cho, J.; Kim, G. Enhancement of Thermal Stability of $LiCoO_2$ by $LiMn_2O_4$ Coating. *Electrochem. Solid-State Lett.* **1999**, *2*, 253−255.

(10) Lu, Z.; MacNeil, D. D.; Dahn, J. R. Layered Cathode Materials $Li[Ni_xLi_{(1/3-2x/3)}Mn_{(2/3-x/3)}]O_2$ for Lithium-Ion Batteries. *Electrochem. Solid-State Lett.* **2001**, *4*, A191−A194.

(11) Yabuuchi, N.; Ohzuku, T. Novel Lithium Insertion Material of $LiCo_{1/3}Ni_{1/3}Mn_{1/3}O_2$ for Advanced Lithium-Ion Batteries. *J. Power Sources* **2003**, *119−121*, 171−174.

(12) Shi, J.-L.; Xiao, D. D.; Ge, M.; Yu, X.; Chu, Y.; Huang, X.; Zhang, X. D.; Yin, Y. X.; Yang, X. Q.; Guo, Y. G.; et al. High-Capacity Cathode Material with High Voltage for Li-Ion Batteries. *Adv. Mater.* **2018**, *30*, No. 1705575.

(13) Noh, H.-J.; Youn, S.; Yoon, C. S.; Sun, Y. K. Comparison of the Structural and Electrochemical Properties of Layered $Li[Ni_xCo_yMn_z]O_2$ (x = 1/3, 0.5, 0.6, 0.7, 0.8 and 0.85) Cathode Material for Lithium-Ion Batteries. *J. Power Sources* **2013**, *233*, 121−130.

(14) Kim, J.; Lee, H.; Cha, H.; Yoon, M.; Park, M.; Cho, J. Prospect and Reality of Ni-Rich Cathode for Commercialization. *Adv. Energy Mater.* **2018**, *8*, No. 1702028.

(15) Andre, D.; Kim, S. J.; Lamp, P.; Lux, S. F.; Maglia, F.; Paschos, O.; Stiaszny, B. Future Generations of Cathode Materials: An Automotive Industry Perspective. *J. Mater. Chem. A* **2015**, *3*, 6709−6732.

(16) Schipper, F.; Erk, C.; Chesneau, F. F.; Aurbach, D.; Shin, J.-Y.; Erickson, E. M. Review—Recent Advances and Remaining Challenges

for Lithium Ion Battery Cathodes. *J. Electrochem. Soc.* **2017**, *164*, A6220−A6228.
(17) Nitta, N.; Wu, F.; Lee, J. T.; Yushin, G. Li-Ion Battery Materials: Present and Future. *Mater. Today* **2015**, *18*, 252−264.
(18) Wu, Y.; Li, M.; Wahyudi, W.; Sheng, G.; Miao, X.; Anthopoulos, T. D.; Huang, K. W.; Li, Y.; Lai, Z. Performance and Stability Improvement of Layered NCM Lithium-Ion Batteries at High Voltage by a Microporous Al_2O_3 Sol-Gel Coating. *ACS Omega* **2019**, *4*, 13972−13980.
(19) Dong, S.; Zhou, Y.; Hai, C.; Zeng, J.; Sun, Y.; Shen, Y.; Li, X.; Ren, X.; Qi, G.; Zhang, X.; et al. Ultrathin CeO_2 Coating for Improved Cycling and Rate Performance of Ni-Rich Layered $LiNi_{0.7}Co_{0.2}Mn_{0.1}O_2$ Cathode. *Ceram. Int.* **2019**, *45*, 144−152.
(20) Han, B.; Key, B.; Lapidus, S. H.; Garcia, J. C.; Iddir, H.; Vaughey, J. T.; Dogan, F. From Coating to Dopant: How the Transition Metal Composition Affects Alumina Coatings on Ni-Rich Cathodes. *ACS Appl. Mater. Interfaces* **2017**, *9*, 41291−41302.
(21) Konishi, H.; Yuasa, T.; Yoshikawa, M. Thermal Stability of $Li_{1-y}Ni_xMn_{(1-x)/2}Co_{(1-x)/2}O_2$ Layer-Structured Cathode Materials Used in Li-Ion Batteries. *J. Power Sources* **2011**, *196*, 6884−6888.
(22) Wu, L.; Nam, K. W.; Wang, X.; Zhou, Y.; Zheng, J. C.; Yang, X. Q.; Zhu, Y. Structural Origin of Overcharge-Induced Thermal Instability of Ni-Containing Layered-Cathodes for High-Energy-Density Lithium Batteries. *Chem. Mater.* **2011**, *23*, 3953−3960.
(23) Cho, D.-H.; Jo, C.-H.; Cho, W.; Kim, Y.-J.; Yashiro, H.; Sun, Y.-K.; Myung, S.-T. Effect of Residual Lithium Compounds on Layer Ni-Rich $Li[Ni_{0.7}Mn_{0.3}]O_2$. *J. Electrochem. Soc.* **2014**, *161*, A920−A926.
(24) Lebens-Higgins, Z. W.; Sallis, S.; Faenza, N. V.; Badway, F.; Pereira, N.; Halat, D. M.; Wahila, M.; Schlueter, C.; Lee, T. L.; Yang, W.; et al. Evolution of the Electrode-Electrolyte Interface of $LiNi_{0.8}Co_{0.15}Al_{0.05}O_2$ Electrodes Due to Electrochemical and Thermal Stress. *Chem. Mater.* **2018**, *30*, 958−969.
(25) Zhou, A.; Liu, Q.; Wang, Y.; Wang, W.; Yao, X.; Hu, W.; Zhang, L.; Yu, X.; Li, J.; Li, H. Al_2O_3 Surface Coating on $LiCoO_2$ through a Facile and Scalable Wet-Chemical Method towards High-Energy Cathode Materials Withstanding High Cutoff Voltages. *J. Mater. Chem. A* **2017**, *5*, 24361−24370.
(26) Jung, R.; Morasch, R.; Karayaylali, P.; Phillips, K.; Maglia, F.; Stinner, C.; Shao-Horn, Y.; Gasteiger, H. A. Effect of Ambient Storage on the Degradation of Ni-Rich Positive Electrode Materials (NMC811) for Li-Ion Batteries. *J. Electrochem. Soc.* **2018**, *165*, A132−A141.
(27) Lee, J. T.; Wang, F. M.; Cheng, C. S.; Li, C. C.; Lin, C. H. Low-Temperature Atomic Layer Deposited Al_2O_3 Thin Film on Layer Structure Cathode for Enhanced Cycleability in Lithium-Ion Batteries. *Electrochim. Acta* **2010**, *55*, 4002−4006.
(28) Neudeck, S.; Strauss, F.; Garcia, G.; Wolf, H.; Janek, J.; Hartmann, P.; Brezesinski, T. Room Temperature, Liquid-Phase Al_2O_3 Surface Coating Approach for Ni-Rich Layered Oxide Cathode Material. *Chem. Commun.* **2019**, *55*, 2174−2177.
(29) Neudeck, S.; Walther, F.; Bergfeldt, T.; Suchomski, C.; Rohnke, M.; Hartmann, P.; Janek, J.; Brezesinski, T. Molecular Surface Modification of NCM622 Cathode Material Using Organophosphates for Improved Li-Ion Battery Full-Cells. *ACS Appl. Mater. Interfaces* **2018**, *10*, 20487−20498.
(30) Chen, Y.; Zhang, Y.; Chen, B.; Wang, Z.; Lu, C. An Approach to Application for LiNi0.6Co0.2Mn 0.2O_2 Cathode Material at High Cutoff Voltage by TiO_2 Coating. *J. Power Sources* **2014**, *256*, 20−27.
(31) Zhang, X.; Belharouak, I.; Li, L.; Lei, Y.; Elam, J. W.; Nie, A.; Chen, X.; Yassar, R. S.; Axelbaum, R. L. Structural and Electrochemical Study of Al_2O_3 and TiO_2 Coated $Li_{1.2}Ni_{0.13}Mn_{0.54}Co_{0.13}O_2$ Cathode Material Using ALD. *Adv. Energy Mater.* **2013**, *3*, 1299−1307.
(32) Hwang, B.-J.; Hu, S. K.; Chen, C. H.; Chen, C. Y.; Sheu, H. S. In-Situ XRD Investigations on Structure Changes of ZrO_2-Coated $LiMn_{0.5}Ni_{0.5}O_2$ Cathode Materials during Charge. *J. Power Sources* **2007**, *174*, 761−765.
(33) Han, B.; Paulauskas, T.; Key, B.; Peebles, C.; Park, J. S.; Klie, R. F.; Vaughey, J. T.; Dogan, F. Understanding the Role of Temperature and Cathode Composition on Interface and Bulk: Optimizing Aluminum Oxide Coatings for Li-Ion Cathodes. *ACS Appl. Mater. Interfaces* **2017**, *9*, 14769−14778.
(34) Sun, H. H.; Hwang, J. Y.; Yoon, C. S.; Heller, A.; Mullins, C. B. Capacity Degradation Mechanism and Cycling Stability Enhancement of AlF_3-Coated Nanorod Gradient $Na[Ni_{0.65}Co_{0.08}Mn_{0.27}]O_2$ Cathode for Sodium-Ion Batteries. *ACS Nano* **2018**, *12*, 12912−12922.
(35) Park, J. S.; Meng, X.; Elam, J. W.; Hao, S.; Wolverton, C.; Kim, C.; Cabana, J. Ultrathin Lithium-Ion Conducting Coatings for Increased Interfacial Stability in High Voltage Lithium-Ion Batteries. *Chem. Mater.* **2014**, *26*, 3128−3134.
(36) Li, X.; Liu, J.; Banis, M. N.; Lushington, A.; Li, R.; Cai, M.; Sun, X. Atomic Layer Deposition of Solid-State Electrolyte Coated Cathode Materials with Superior High-Voltage Cycling Behavior for Lithium Ion Battery Application. *Energy Environ. Sci.* **2014**, *7*, 768−778.
(37) Li, X.; Liu, J.; Meng, X.; Tang, Y.; Banis, M. N.; Yang, J.; Hu, Y.; Li, R.; Cai, M.; Sun, X. Significant Impact on Cathode Performance of Lithium-Ion Batteries by Precisely Controlled Metal Oxide Nanocoatings via Atomic Layer Deposition. *J. Power Sources* **2014**, *247*, 57−69.
(38) Liu, W.; Li, X.; Xiong, D.; Hao, Y.; Li, J.; Kou, H.; Yan, B.; Li, D.; Lu, S.; Koo, A.; et al. Significantly Improving Cycling Performance of Cathodes in Lithium Ion Batteries: The Effect of Al_2O_3 and $LiAlO_2$ Coatings on $LiNi_{0.6}Co_{0.2}Mn_{0.2}O_2$. *Nano Energy* **2018**, *44*, 111−120.
(39) Chen, C.; Yao, W.; He, Q.; Ashuri, M.; Kaduk, J.; Liu, Y.; Shaw, L. Tunable $LiAlO_2/Al_2O_3$ Coating through a Wet-Chemical Method to Improve Cycle Stability of Nano-$LiCoO_2$. *ACS Appl. Energy Mater.* **2019**, *2*, 3098−3113.
(40) Hu, Y.; Ruud, A.; Miikkulainen, V.; Norby, T.; Nilsen, O.; Fjellvåg, H. Electrical Characterization of Amorphous $LiAlO_2$ Thin Films Deposited by Atomic Layer Deposition. *RSC Adv.* **2016**, *6*, 60479−60486.
(41) Negi, R.; Culver, S. P.; Mazilkin, A.; Brezesinski, T.; Elm, M. T. Enhancing the Electrochemical Performance of $Li-Ni_{0.70}Co_{0.15}Mn_{0.15}O_2$ Cathodes Using a Practical Solution-Based Al_2O_3 Coating. *ACS Appl. Mater. Interfaces* **2020**, *12*, 31392−31400.
(42) Neudeck, S.; Mazilkin, A.; Reitz, C.; Hartmann, P.; Janek, J.; Brezesinski, T. Effect of Low-Temperature Al_2O_3 ALD Coating on Ni-Rich Layered Oxide Composite Cathode on the Long-Term Cycling Performance of Lithium-Ion Batteries. *Sci. Rep.* **2019**, *9*, No. 5328.
(43) Okubo, M.; Hosono, E.; Kim, J.; Enomoto, M.; Kojima, N.; Kudo, T.; Zhou, H.; Honma, I. Nanosize Effect on High-Rate Li-Ion Intercalation in $LiCoO_2$ Electrode. *J. Am. Chem. Soc.* **2007**, *129*, 7444−7452.
(44) Zhu, W.; Gao, L.; Liu, T.; Xie, Z.; Huang, X.; Zhao, J.; Bu, L.; Tian, K.; Wang, Y.; Wang, H. Ultrathin Al_2O_3 Coating on $LiNi_{0.8}Co_{0.1}Mn_{0.1}O_2$ Cathode Material for Enhanced Cycleability at Extended Voltage Ranges. *Coatings* **2019**, *9*, 92.
(45) Xiong, X.; Wang, Z.; Yue, P.; Guo, H.; Wu, F.; Wang, J.; Li, X. Washing Effects on Electrochemical Performance and Storage Characteristics of $LiNi_{0.8}Co_{0.1}Mn_{0.1}O_2$ as Cathode Material for Lithium-Ion Batteries. *J. Power Sources* **2013**, *222*, 318−325.
(46) Tang, W.; Chen, Z.; Xiong, F.; Chen, F.; Huang, C.; Gao, Q.; Wang, T.; Yang, Z.; Zhang, W. An Effective Etching-Induced Coating Strategy to Shield $LiNi_{0.8}Co_{0.1}Mn_{0.1}O_2$ Electrode Materials by $LiAlO_2$. *J. Power Sources* **2019**, *412*, 246−254.
(47) Qiu, B.; Zhang, M.; Wu, L.; Wang, J.; Xia, Y.; Qian, D.; Liu, H.; Hy, S.; Chen, Y.; An, K.; et al. Gas−Solid Interfacial Modification of Oxygen Activity in Layered Oxide Cathodes for Lithium-Ion Batteries. *Nat. Commun.* **2016**, *7*, No. 12108.
(48) Tang, W.; Chen, Z.; Xiong, F.; Chen, F.; Huang, C.; Gao, Q.; Wang, T.; Yang, Z.; Zhang, W. An Effective Etching-Induced Coating Strategy to Shield LiNi0.8Co0.1Mn0.1O2 Electrode Materials by LiAlO2. *J. Power Sources* **2019**, *412*, 246−254.
(49) Vinod Chandran, C.; Kirschhock, C. E. A.; Radhakrishnan, S.; Taulelle, F.; Martens, J. A.; Breynaert, E. Alumina: Discriminative

https://doi.org/10.1021/acsaem.0c03135
ACS Appl. Energy Mater. XXXX, XXX, XXX−XXX

Analysis Using 3D Correlation of Solid-State NMR Parameters. *Chem. Soc. Rev.* **2019**, 134−156.
(50) Müller, D.; Gessner, W.; Scheler, G. Chemical Shift and Quadrupole Coupling of the 27Al NMR Spectra of $LiAlO_2$ Polymorphs. *Polyhedron* **1983**, *2*, 1195−1198.
(51) Wang, S.; Yan, M.; Li, Y.; Vinado, C.; Yang, J. Separating Electronic and Ionic Conductivity in Mix-Conducting Layered Lithium Transition-Metal Oxides. *J. Power Sources* **2018**, *393*, 75−82.
(52) Zahnow, J.; Bernges, T.; Wagner, A. C.; Bohn, N.; Binder, J. R.; Zeier, W. G.; Elm, M. T.; Janek, J. Impedance Analysis of NCM Cathode Materials − Electronic and Ionic Partial Conductivity and the Influence of Microstructure. *ACS Appl. Energy Mater.* **2021**, *4*, 1335−1345.
(53) Burkhardt, S.; Friedrich, M. S.; Eckhardt, J. K.; Wagner, A. C.; Bohn, N.; Binder, J. R.; Chen, L.; Elm, M. T.; Janek, J.; Klar, P. J. Charge Transport in Single NCM Cathode Active Material Particles for Lithium-Ion Batteries Studied under Well-Defined Contact Conditions. *ACS Energy Lett.* **2019**, *4*, 2117−2123.
(54) Liu, W.; Li, X.; Xiong, D.; Hao, Y.; Li, J.; Kou, H.; Yan, B.; Li, D.; Lu, S.; Koo, A.; et al. Significantly Improving Cycling Performance of Cathodes in Lithium Ion Batteries: The Effect of Al_2O_3 and $LiAlO_2$ Coatings on $LiNi_{0.6}Co_{0.2}Mn_{0.2}O_2$. *Nano Energy* **2018**, *44*, 111−120.
(55) Amin, R.; Chiang, Y.-M. Characterization of Electronic and Ionic Transport in $Li_{1-x}Ni_{0.33}Mn_{0.33}Co_{0.33}O_2$ (NMC333) and $Li_{1-x}Ni_{0.50}Mn_{0.20}Co_{0.30}O_2$ (NMC523) as a Function of Li Content. *J. Electrochem. Soc.* **2016**, *163*, A1512−A1517.
(56) Laskar, M. R.; Jackson, D. H. K.; Xu, S.; Hamers, R. J.; Morgan, D.; Kuech, T. F. Atomic Layer Deposited MgO: A Lower Overpotential Coating for Li[Ni0.5Mn0.3Co0.2]O_2 Cathode. *ACS Appl. Mater. Interfaces* **2017**, *9*, 11231−11239.
(57) Liu, W.; Oh, P.; Liu, X.; Lee, M. J.; Cho, W.; Chae, S.; Kim, Y.; Cho, J. Nickel-Rich Layered Lithium Transition-Metal Oxide for High-Energy Lithium-Ion Batteries. *Angew. Chem., Int. Ed.* **2015**, *54*, 4440−4457.
(58) Kim, J. W.; Travis, J. J.; Hu, E.; Nam, K. W.; Kim, S. C.; Kang, C. S.; Woo, J. H.; Yang, X. Q.; George, S. M.; Oh, K. H.; et al. Unexpected High Power Performance of Atomic Layer Deposition Coated $Li[Ni_{1/3}Mn_{1/3}Co_{1/3}]O_2$ Cathodes. *J. Power Sources* **2014**, *254*, 190−197.
(59) Ruess, R.; Schweidler, S.; Hemmelmann, H.; Conforto, G.; Bielefeld, A.; Weber, D. A.; Sann, J.; Elm, M. T.; Janek, J. Influence of NCM Particle Cracking on Kinetics of Lithium-Ion Batteries with Liquid or Solid Electrolyte. *J. Electrochem. Soc.* **2020**, *167*, No. 100532.
(60) Zhang, S. S. The Effect of the Charging Protocol on the Cycle Life of a Li-Ion Battery. *J. Power Sources* **2006**, *161*, 1385−1391.
(61) Wu, F.; Zhang, X.; Zhao, T.; Li, L.; Xie, M.; Chen, R. Multifunctional $AlPO_4$ Coating for Improving Electrochemical Properties of Low-Cost $Li[Li_{0.2}Fe_{0.1}Ni_{0.15}Mn_{0.55}]O_2$ Cathode Materials for Lithium-Ion Batteries. *ACS Appl. Mater. Interfaces* **2015**, *7*, 3773−3781.
(62) Li, X.; Xu, Y. Novel Method to Enhance the Cycling Performance of Spinel $LiMn_2O_4$. *Electrochem. Commun.* **2007**, *9*, 2023−2026.
(63) Xu, Y.-D.; Xiang, W.; Wu, Z.-G.; Xu, C.-L.; Li, Y.-C.; Guo, X.-D.; Lv, G- P.; Peng, X.; Zhong, B.-H. Improving Cycling Performance and Rate Capability of Ni-Rich $LiNi_{0.8}Co_{0.1}Mn_{0.1}O_2$ Cathode Materials by $Li_4Ti_5O_{12}$ Coating. *Electrochim. Acta* **2018**, *268*, 358−365.
(64) Huang, B.; Li, X.; Wang, Z.; Guo, H.; Xiong, X.; Wang, J. A Novel Carbamide-Assistant Hydrothermal Process for Coating Al_2O_3 onto $LiMn_{1.5}Ni_{0.5}O_4$ Particles Used for Cathode Material of Lithium-Ion Batteries. *J. Alloys Compd.* **2014**, *583*, 313−319.
(65) Tsai, P. C.; Wen, B.; Wolfman, M.; Choe, M. J.; Pan, M. S.; Su, L.; Thornton, K.; Cabana, J.; Chiang, Y. M. Single-Particle Measurements of Electrochemical Kinetics in NMC and NCA Cathodes for Li-Ion Batteries. *Energy Environ. Sci.* **2018**, *11*, 860−871.

https://doi.org/10.1021/acsaem.0c03135
ACS Appl. Energy Mater. XXXX, XXX, XXX−XXX

3.4 Publication IV: Stabilizing the Cathode/Electrolyte Interface Using a Dry-Processed Lithium Titanate Coating for All-Solid-State-Batteries

The successful development of coating strategies for liquid electrolyte-based Li-ion batteries during the course of this Ph.D. work further motivated me to take the next step and work on the development of coating strategies for all-solid-state Li-ion batteries (ASSB) systems. Due to their improved safety and high theoretical energy density, ASSBs are considered the future of next-generation energy storage systems. However, the interfacial instability between the solid electrolyte (SE) and the cathode materials still hinders their application for next generation. Thus, surface coating strategies for ASSBs are considered to be beneficial as in case of LIBs. In this publication, we have developed a new LTO based dry-coating approach for Ni-rich NCM based cathodes. No post-annealing step has been involved during or after the coating process. Structural analysis of the recovered coated powder reveals the successful deposition of a really homogenous and well-distributed LTO coating on the surface of NCM. The electrochemical analysis demonstrates the improvement of the C-rate and long-term cycling performance of the coated NCM as compared to pristine NCM in ASSBs. The coated NCM also shows much lower impedance growth during first cycle along with a lower impedance after 100 cycles during long-term cycling. The results suggest that the coating effectively prevents SEI formation.

The concept and experiments for this publication have been designed and performed by myself under the supervision of Prof. J. Janek, Dr. R. Takata, Dr. F. Schmidt, and Dr. M.T. Elm. The manuscript was written by me and corrected by all co-authors. P. Minnmann helped in performing the electrochemical test. TEM images have been taken by S. Ahmad. Dr. R. Pann and Dr. M. Herzog contributed to the scientific discussions.

R. S. Negi, P. Minnmann, R. Pan, S. Ahmed, M. Herzog, K. Volz, R. Takata, F. Schmidt, J. Janek, and M. T. Elm, Stabilizing the cathode/electrolyte interface using a dry-processed lithium titanate coating for all-solid-state-batteries, ACS Chem. Mater. **2021**, 33 (17), 6713–6723

CHEMISTRY OF MATERIALS

pubs.acs.org/cm Article

Stabilizing the Cathode/Electrolyte Interface Using a Dry-Processed Lithium Titanate Coating for All-Solid-State Batteries

Rajendra S. Negi, Philip Minnmann, Ruijun Pan, Shamail Ahmed, Marcel J. Herzog, Kerstin Volz, Ryo Takata, Franz Schmidt, Jürgen Janek, and Matthias T. Elm*

Cite This: https://doi.org/10.1021/acs.chemmater.1c01123 Read Online

ACCESS | Metrics & More | Article Recommendations | Supporting Information

ABSTRACT: Considering the high theoretical energy density and improved safety, thiophosphate-based all-solid-state batteries (ASSBs) have become one of the most promising candidates for next-generation energy storage systems. However, the intrinsic electrochemical instability of thiophosphate-based solid electrolytes in contact with oxide-based cathodes results in rapid capacity fading and has driven the need of protective cathode coatings. In this work, for the first time, a fumed lithium titanate (LTO) powder-based coating has been applied to Ni-rich oxide-based cathode active material (CAM) using a newly developed dry-coating process. The LTO cathode coating has been tested in thiophosphate-based ASSBs. It exhibits a significantly improved C-rate performance along with superior long-term cycling stability. The improved electrochemical performance is attributed to a reduced interfacial resistance between coated cathode and solid electrolyte as deduced from in-depth electrochemical impedance spectroscopy analysis. These results open up a new, facile dry-coating route to fabricate effective protective CAM coatings to enable long-life ASSBs. This nondestructive coating process with no post-heat-treatment approach is expected to simplify the coating process for a wide range of coatings and cathode materials, resulting in much improved cathode/electrolyte interfacial stability and electrochemical performance of ASSBs.

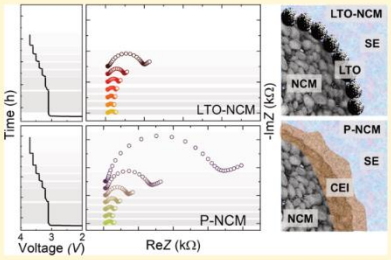

1. INTRODUCTION

The development of all-solid-state batteries (ASSBs) is among one of the most active research areas in the field of electrochemical energy storage in the current decade because of their potential to provide higher energy density, much improved safety (i.e., reduced flammability of solid electrolyte), and the possibility to use high-capacity metal anodes compared to those of conventional lithium-ion batteries.[1−4] The development of solid-state electrolytes (SSEs) for ASSBs has been rapidly accelerated during the last decade,[3] and their performance is largely determined by the ionic conductivity of SSEs.[5−7] Initially, NASICON[8,9] and garnet-type[10] oxides have been considered as feasible SSEs for ASSBs due to their high ionic conductivities (10^{-3} S cm^{-1}). However, to obtain a sufficient contact between cathode active material (CAM) and SSE, these electrolytes require a high-temperature sintering step, which inevitably results in unwanted side reactions and in turn results in a high interfacial resistance.[8,10] In addition, they have reached their practical limits in terms of ionic conductivity[11,12] and have been used only for all-solid-state micro batteries, e.g., thin-film-type batteries.[13,14] For the development of large-scale ASSBs, thiophosphate-based SSEs are considered as one of the most promising candidates, as these exhibit much higher ionic conductivities at room temperature (RT).[15−17] Furthermore, thiophosphate-based electrolytes possess good elasticity and softness, which allows the formation of intimate interfacial contacts between the CAM and SSE via a simple mechanical pressing at RT, resulting in excellent electrochemical performance at the test cell scale.[18−22]

Despite these advantages, thiophosphate-based SSEs suffer from the issue of interfacial instability with CAM (specifically oxide-based cathodes).[23−26] The interfacial reaction between CAM and SSE results in an undesirable interfacial layer, disturbing the transfer of Li ions and electrons.[22,27,28] This layer increases the resistance at the electrode−electrolyte interface, resulting in a significant capacity fade and poor C-rate performance.[22,29−31] This interfacial instability is one of the main scientific concerns limiting the commercialization of thiophosphate-based ASSBs. Addressing this issue, considerable research effort has been made to enhance the interfacial stability between the CAM and SSE.

Received: April 1, 2021
Revised: August 5, 2021

Surface modification of CAMs by coating with various stable oxides has been suggested to improve the interfacial stability by preventing the direct physical contact between CAM and SSE.[32,33] Most research on CAM coatings in thiophosphate-based ASSBs has been focused on exploring lithiated metal oxides such as $LiNbO_3$,[29,34−36] Li_2ZrO_3,[37−40] and $Li_3B_{11}O_{18}$ (LBO).[39] Such surface coatings have been successfully applied and studied on CAMs for LIBs, resulting in better cycling life and C-rate performance by reducing the unwanted side reactions between CAM and liquid electrolyte.[4,41−43] Surface coatings for inorganic SSE-based ASSBs are still at a very early stage, and most of the studies have been carried out with $LiCoO_2$-based CAM.[33] New surface coatings materials for $LiNi_{1-x-y}Co_xMn_yO_2$ (NCM)-based ASSBs are still under exploration, as the development of optimized coatings is a crucial step in improving the performance of NCM-based ASSBs.[33]

The most commonly used coating methods are solvent-based (wet chemical, sol−gel) and require a subsequent annealing or drying step.[33−36,44] This results in rather complex, time-consuming, and expensive coating processes, making them unfavorable for large-scale industrial application. In addition, the use of organic solvent during the coating process further increases environmental concerns.[35−37] Other coating methods, such as atomic layer deposition (ALD) have been found to provide very thin and conformal coatings,[45,46] but show major drawbacks in terms of a low throughput and expensive operating costs.[33] Thus, a rather simple, cost-effective, and easily scalable coating method is required.

In this work, a new dry-coating process using fumed $Li_4Ti_5O_{12}$ powder has been developed and was successfully applied on the surface of NCM-based CAM particles for thiophosphate-based ASSBs. Structural characterization confirms the successful coating of homogeneous LTO on NCM surface. Furthermore, electrochemical characterization shows a much improved C-rate and long-term cycling performance of the coated NCM compared to uncoated samples. The presented dry-coating process opens up a new route to fabricate effective protective CAM coatings to enable long-life ASSBs.

2. EXPERIMENTAL SECTION

2.1. Surface Modification of Ni-Rich NCM by LTO Using a Dry-Coating Process. For the current study, commercial $LiNi_{0.70}Co_{0.15}Mn_{0.15}$ (NCM70151S, Linyi Gelon LIB Co.) powder has been used as the cathode active material and nanostructured fumed $Li_4Ti_5O_{12}$ (VP LTO, Evonik Operations GmbH) powder has been employed as coating material in a dry-coating process. The fumed LTO coating has been prepared by a flame hydrolysis process resulting in agglomerated LTO particles with a high specific surface area (47 $m^2\ g^{-1}$). Figure S1 (Supporting Information, SI) shows a scanning electron microscopy (SEM) image and the X-ray diffraction (XRD) pattern of the fumed LTO agglomerates. The agglomerates built during the synthesis, in which the nuclei formed by the flame process bond chemically together to form a three-dimensional (3D) nanostructure with a high degree of branching. To carry out the dry-coating process, a lab-scale high-energy Somakon mixer MP-GL (Somakon Verfahrenstechnik UG) has been used. For the dry-coating process, the NCM powder was mixed with different weight ratios of nanostructured LTO (0.5, 1, and 2 wt %) in the high-energy mixer initially at 500 rpm (speed of the rotor) for 1 min to get a well-distributed mixture. Thereafter, the mixing intensity was increased to 2000 rpm for a time period of 6 min. The powder was collected and dried under vacuum at 200 °C overnight (12 h) before being transferred to an argon-filled glovebox.

2.2. Materials Characterization. The particle morphology, topography, and microstructure together with the elemental composition of uncoated (P-NCM) and coated (LTO) samples were investigated using scanning electron microscopy (SEM, Merlin, Zeiss) at an accelerating voltage of 7 kV and an accelerating current of 3000 pA, combined with energy-dispersive X-ray spectroscopy (EDS, X-Max-Extreme detector, Oxford Instruments). Powder X-ray diffraction (XRD) patterns for P-NCM and LTO were collected using an Empyrean XRD (Panalytical) system with Cu Kα radiation. Focused-ion beam (FIB-SEM) analysis of the coated NCM powder was done using a XEIA Xe-plasma FIB (TESCAN). The XPS measurements were carried out using a PHI5000 Versa Probe II (Physical Electronics GmbH) with Al anode. To avoid air exposure, the samples were transferred to the analysis chamber using a transfer module filled with argon gas. The pass energy of the analyzer was set at 93.9 eV for the survey spectra and at 23.5 eV for the detailed spectra. The chamber pressure was maintained below 10^{-7} Pa.

Transmission electron microscope (TEM) samples were prepared using a JEOL JIB-4601 focused-ion beam/scanning electron microscope (FIB/SEM). Pt and W coatings are deposited prior to FIB milling to protect the surface during FIB sample preparation using a Ga ion beam. A thin Pt layer is coated with a Leica EM ACE600 sputter coater prior to loading the sample to the SEM/FIB. The tungsten layer is deposited in the FIB setup. First, a thin W layer is deposited using electron beam followed by a relatively thick W layer using Ga ion beam evaporation. Scanning TEM (STEM) high-angle angular dark-field (HAADF) imaging and energy-dispersive spectroscopy (EDS) were performed using a double Cs-corrected JEOL 2200-FS microscope. The microscope was operated at 200 kV and TEM imaging was done at 300 kV using a JEOL 3010 TEM. Precession electron nano-beam diffraction (PENBD) data sets acquisition and analysis were done using ASTAR system from NanoMegas installed at JEOL 3010 TEM. The data were acquired using the precession angle of 0.25° with a step size of 7 nm. The beam resolution was about 10 nm. At each scan point, 15 precessions were averaged. The PENBD data sets were analyzed with the ASTAR software package to find the best agreement between experimental data and the reference library of simulated diffraction patterns.

2.3. Electrode Preparation and Cell Assembly. The composite cathodes (CC) contained pristine or coated NCM70151S, Li_6PS_5Cl (LPSCl, NEI Corporation), and vapor-grown carbon fibers (VGCFs, Sigma-Aldrich, Inc., iron-free). Initially, NCM and LPS powders were mixed in a mass ratio of 70:30 (volume ratio 47:53) and then an additional 3 wt % of VGCF was added (exact mass ratio 68:29.1:2.9 (NCM/LPS/VGCF)). The composite cathode was then hand-ground in an agate mortar for 15 min. For the cell assembly, the composite cathode mixture was prepared always freshly. All of the cell tests were performed with an in-house (pellet-type) cell casing.[24,27] For cell assembly, a poly(ether ether ketone) (PEEK) cylinder (inner diameter: 10 mm) was closed from one side using a stainless steel stamp. 60 mg of LPSCl was added into the cylinder and uniformly distributed followed by manual compression by hand. Afterward, 12 mg of CC was added to one side of the SSE and distributed uniformly. The whole stack was pressed uniaxially at 30 kN (380 MPa) for 3 min, resulting in a pellet of 430 μm thickness (ca. 400 μm SSE and approximately 30 μm cathode composite). On the other side of the pellet, first, an indium foil (In, chemPUR GmbH, 9 mm) with 125 μm thickness and then lithium foil (Li, Albermarle (Rockwood Lithium GmbH), 6 mm) with 120 μm thickness were placed and closed with another stainless steel stamp. The whole-cell assembly was then closed and an external frame was used around the cell casing during the whole electrochemical testing applying a constant pressure of ∼50 MPa.

2.4. Electrochemical Testing. For the electrochemical testing, VMP-300 (Biologic) and MACCOR potentiostats/galvanostats were used. The C-rate tests and the long-term cycling tests were performed with MACCOR instruments, while the impedance measurements were performed with VMP-300 instruments. The cells were cycled in the voltage window between 2.0 and 3.7 V (vs InIInLi), corresponding to approximately 2.6−4.3 V vs Li^+/Li at 25 °C (1C = 200 mA g^{-1}).

https://doi.org/10.1021/acs.chemmater.1c01123
Chem. Mater. XXXX, XXX, XXX−XXX

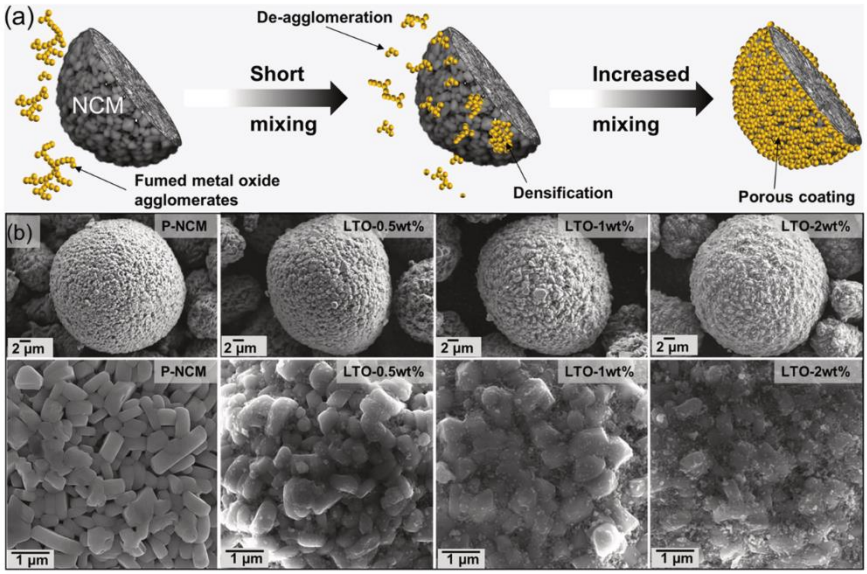

Figure 1. (a) Schematic representation of the dry-coating process of Ni-rich NCM with fumed $Li_4Ti_5O_{12}$ powder. (b) SEM images of pristine and LTO-coated samples.

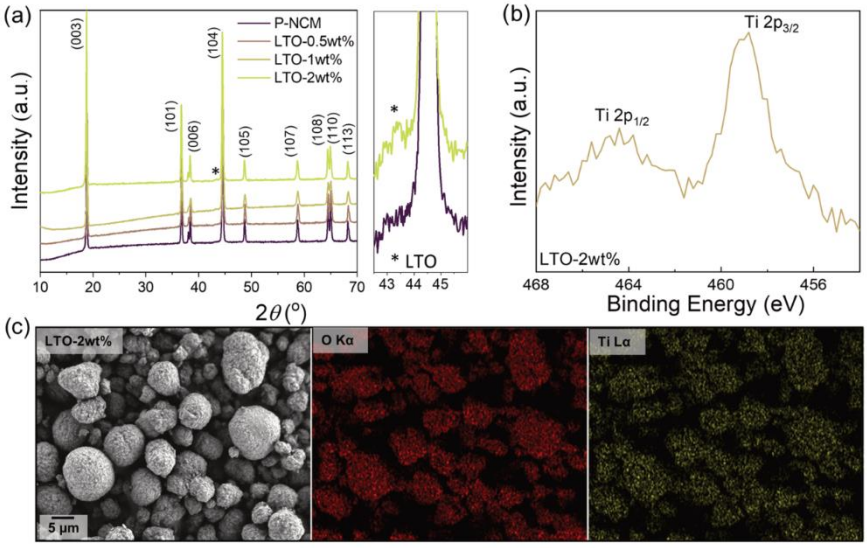

Figure 2. Comparison of (a) X-ray diffraction patterns (XRD patterns are shifted in intensity for a better comparison), (b) high-resolution Ti 2p XPS spectrum, and (c) EDS mapping of coated NCM particles.

For the C-rate tests, the cells were cycled at different C-rates up to 2C [i.e., 0.1C (3 cycles), 0.25C (3 cycles), 0.5C (3 cycles), 1C (5 cycles), 2C (5 cycles)]. For the long-term cycling, the cells were cycled initially at 0.1C for one cycle and then at 0.25C for the consequent

https://doi.org/10.1021/acs.chemmater.1c01123
Chem. Mater. XXXX, XXX, XXX−XXX

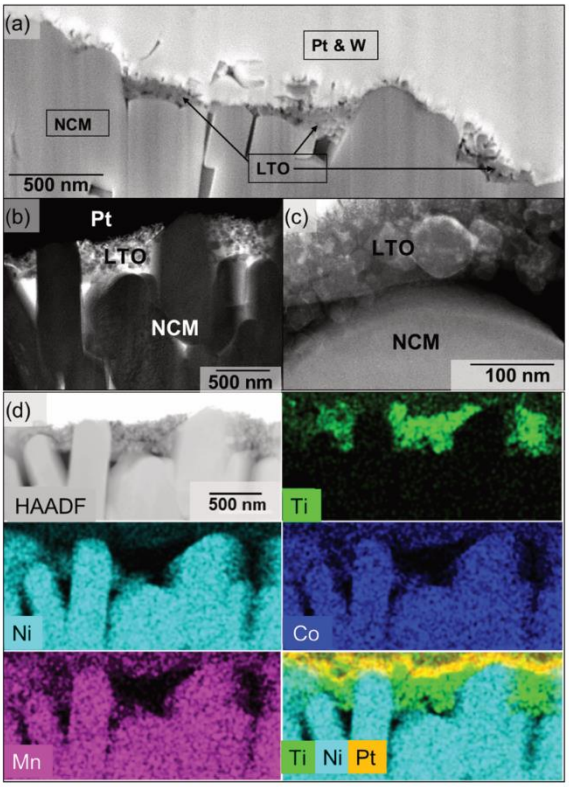

Figure 3. (a) FIB-SEM cross-sectional image of LTO-2 wt % sample, at a large field of view, showing well-distributed LTO particles on the NCM secondary particle surface. (b) High-magnification TEM-bright field (BF) and (c) STEM-HAADF images of a secondary particle surface. (d) STEM-HAADF image and the corresponding EDS maps showing the distribution of Ti, Ni, Co, Mn, and Pt.

cycles up to 100 cycles. All electrochemical data are averaged from three independent cells (for pristine and coated cathodes). Electrochemical impedance measurements (EIS) were performed using a VMP-300 potentiostat on the cycled cells after the 1st and 100th cycles. All EIS measurements were performed in a frequency range between 7 MHz and 50 mHz, applying a 10 mV AC bias. For state of charge (SOC)-dependent EIS measurements during the initial cycles, the same parameters were used.

3. RESULTS AND DISCUSSION

3.1. Dry-Coating Method. The main principle of the coating process using fumed nanostructured $Li_4Ti_5O_{12}$ (LTO) is shown in Figure 1a. The NCM secondary particles act as host particles and the sub-micron-sized LTO particles act as guest particles. During the first step of the coating process, the fumed LTO de-agglomerates into smaller aggregates and interacts with the cathode surface. The smaller aggregates exhibit a high surface area and a very strong adhesion to the cathode surface. During the second step, at a given mixing rotation, significant densification and coalescence of the smaller aggregates is achieved on the cathode surface, resulting in a continuous and adhesive coating layer. No post-heat treatment is used during the process, which is beneficial for industrial application. As very strong forces act on the material during mixing due to the high speed of the rotor, a complete coating is obtained in a short processing time (less than 10 min). The mixing time and intensity are crucial parameters of the dry-coating process. A lower mixing time or intensity results in incomplete coatings due to insufficient energy to break up the agglomerates. A higher mixing intensity, on the other hand, results in breakage of the secondary NCM particles.

3.2. Characterization of LTO-Coated NCM. A schematic illustration of the dry-coating process with fumed $Li_4Ti_5O_{12}$ powder is shown in Figure 1a. As described in the Experimental Section, the nanostructured LTO powder was mixed with NCM powder in different weight ratios and mixed with a in-house mixer to achieve homogeneous coatings. The SEM images in Figure 1b show a comparison of P-NCM with LTO-coated NCM samples (0.5, 1, and 2 wt %). The surface of the secondary P-NCM particles is clean and the primary

https://doi.org/10.1021/acs.chemmater.1c01123
Chem. Mater. XXXX, XXX, XXX−XXX

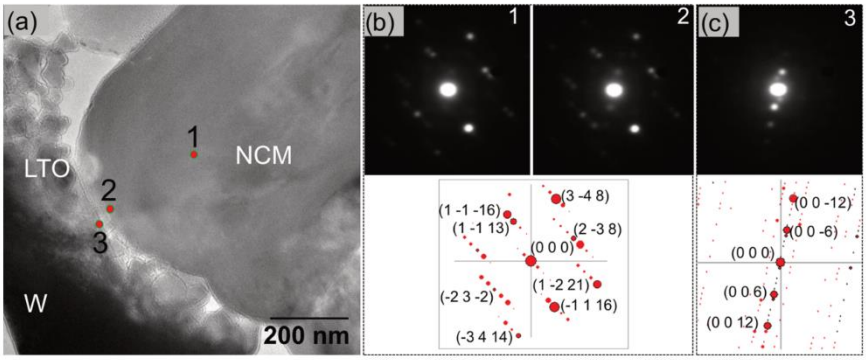

Figure 4. (a) TEM image showing the LTO particles on the surface of the primary NCM particle. (b, c) PENBD patterns from points 1, 2, and 3 marked in (a); on the bottom of the diffraction patterns are the best matches from the library of the simulated diffraction patterns from NCM701515 and LTO crystal structures. The zone axis is found to be around 6.80° off from the $[\bar{3}20]$ direction of the crystal structure for NCM and the $[\bar{7}50]$ direction for LTO. SPED-VDF images obtained from corresponding NCM and LTO particles are shown in Figure S2 (Supporting Information).

particles are visible. The coated NCM surface looks much different compared to that of the P-NCM and the grains are mostly covered by coating material. Furthermore, the coating coverage gets more homogeneous with increasing the coating material loading as more and more grains are covered by increasing the loading, i.e., with 2 wt % LTO most of the NCM particle surface is covered, while for 0.5 wt % LTO is mainly agglomerated at the grain boundaries of the NCM primary particles. The higher coverage of LTO on NCM particle surface is expected to result in a significant electrochemical stability enhancement, as LTO should prevent the electrochemical degradation at the NCM/LPS interface.

To inspect the influence of coating on the crystal structure of NCM, powder XRD was performed on both pristine and coated samples as shown in Figure 2a. All main reflections attributed to NCM are unaltered by the dry-coating process as expected.[47] However, only the (004) peak related to LTO is observed in the case of LTO-2 wt %[48] as the most intensive (111) peak of LTO at 18.4° (Figure S1) is overlapping with the (003) peak of NCM. To get information on the composition of the coating, Ti 3d XPS spectra were collected on both P-NCM and LTO-2 wt % samples. As shown in Figure 2b, the LTO-2 wt % sample exhibits sharp lines at 458.4 and 464.2 eV corresponding to the Ti $2p_{3/2}$ and Ti $2p_{1/2}$ lines of LTO, verifying the successful coating with LTO. In addition, the SEM−EDS images in Figure 2c show a continuous distribution of the Ti signals over the NCM particles, confirming the homogeneity of the coating layer obtained by the dry-coating process described in this study.

The coating layer is expected to be located only on the NCM surface as a dry-coating method without a post-heat-treatment step was used. However, as the resolution in SEM is limited TEM analysis was performed on the LTO-2 wt % sample to obtain detailed information about the coating layer. Figure 3a shows that the LTO particles of the coating are well distributed at a large field of view. Figure 3b,c displays high-magnification TEM and STEM images of the LTO particles on the surface of NCM. The LTO particles are crystalline in nature as expected. Figure 3d shows EDS elemental distribution maps. The Ti signal characteristic for the LTO coating reveals that the particle distribution is restricted to the secondary particle surface. No selective segregation of any specific transition metal was observed as also evident in the Ni, Co, and Mn distribution maps.

An additional TEM image of a secondary particle's surface covered with LTO is shown in Figure 4a. To analyze the crystal structure of the LTO coating and the NCM particles in more detail, precession electron nano-beam diffraction (PENBD) patterns are acquired from the marked area in Figure 4a. Figure 4b shows diffraction patterns from the bulk and surface of NCM's primary particle marked in Figure 4a. The diffraction patterns from points "1" and "2" are matched with NCM701515 from the library of simulated diffraction patterns using the ASTAR software package.[49−52] Both diffraction patterns from the surface and the bulk show the layered NCM structure. In addition, the diffraction pattern show some extra and faint reflection due to an overlap of the NCM surface with the LTO particles, which is in most cases unavoidable due to beam resolution in this mode. Finally, Figure 4c shows the diffraction pattern from an LTO particle (marked with point "3" in Figure 4a). This diffraction can be matched with the LTO structure from the library of simulated diffraction patterns and confirms that the LTO particles of the coating are crystalline. SPED-virtual dark-field (VDF) images of the NCM and LTO particles from the corresponding diffraction spots shown in Figure 4b,c are shown in Figure S2 (Supporting Information). All of the TEM results confirm that the LTO coating is well distributed on the NCM surface. Combined with the EDS results shown in Figure 3d the structural analysis reveal that the LTO coating is crystalline in nature. No specific segregation of any transition metal or any change of the NCM surface structure compared to the bulk is observed. However, atomic-level surface reconstruction and doping resulting from the LTO particle coating is difficult to observe, if any, due to the projection effect of the TEM at the surface. High-resolution imaging at the surface is also very challenging not only due to the projection effect but also due to difficulties in finding the correct zone axis at that position.

https://doi.org/10.1021/acs.chemmater.1c01123
Chem. Mater. XXXX, XXX, XXX−XXX

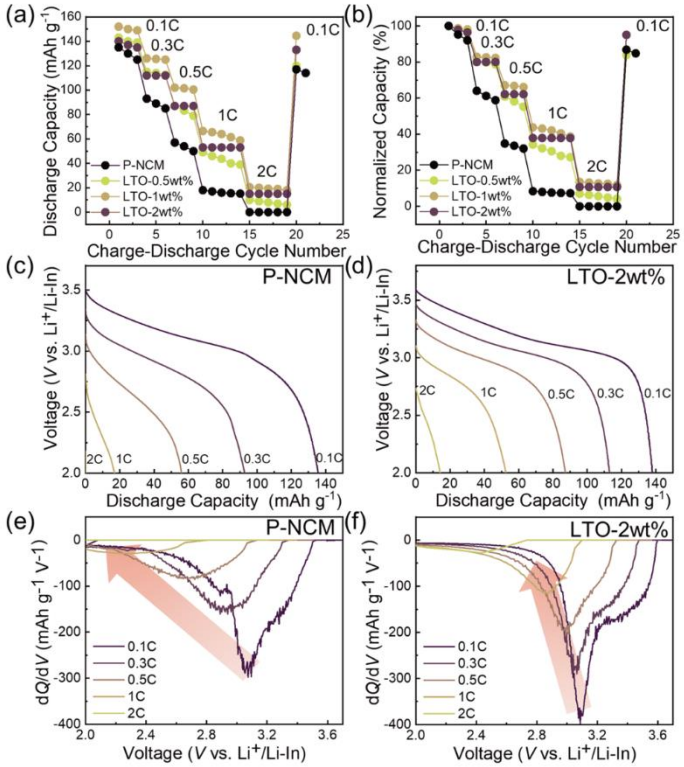

Figure 5. Comparison of (a) rate capabilities and (b) the corresponding normalized capacity plot for P-NCM and LTO-coated samples. Comparison of charge/discharge voltage profiles and the corresponding differential capacity plots of (c, e) P-NCM and (d, f) LTO-2 wt % cells at different C-rates.

However, it is unlikely that atomic-level surface reconstruction or doping took place during coating, as the dry-coating process involves only mechanical mixing at room temperature without applying any post-heat-treatment step.

3.3. Electrochemical Characterization. The electrochemical performance of the pristine NCM and LTO-coated NCM cathodes was evaluated in ASSBs with an active material loading of 8.15 mg cm^{-2}, LPSCl as the SSE, and InlInLi as the anode. Figure 5a shows the comparison of the discharge capacities of the cells with composite cathodes, i.e., P-NCM, LTO-0.5 wt %, LTO-1 wt %, and LTO-2 wt %, at different C-rates (0.1, 0.25, 0.5, 1 and 2C) in the voltage range between 2.0 and 3.7 V (vs InlInLi). All LTO-coated samples show an improved C-rate performance compared to the P-NCM irrespective of the C-rate, revealing the positive effect of the LTO coating on the C-rate performance in ASSBs. The best performance is observed for the LTO-1 wt % and LTO-2 wt % samples as can be seen in the corresponding normalized plots (Figure 5b). Furthermore, LTO-2 wt % seems to be rather stable in progressive cycles of the same C-rate, while for the other samples a slight decrease in capacity with increasing cycle number is observed. Thus, LTO-2 wt % was chosen for further electrochemical characterizations. To further demonstrate the positive effect of LTO coatings on the C-rate performance, the discharge curves of the P-NCM and LTO-2 wt % coated samples at different C-rates are presented in Figure 5c–f with the corresponding differential capacity plots. As shown in Figure 5c,d, the increase in overpotential with increasing C-rate is much higher for the P-NCM than for the LTO-2 wt % sample, suggesting a lower cell impedance of the latter. Furthermore, the differential capacity plots (Figure 5e,f) reveal that (i) with increasing C-rate, the shrinkage of the shoulder in the higher-voltage range is much more pronounced for P-NCM than for LTO-2 wt %, suggesting a better Li intercalation/deintercalation kinetics for LTO-2 wt %; (ii) the potential shift over the C-rate is less pronounced for LTO-2 wt %, indicating that LTO-2 wt % maintains a lower overpotential compared to P-NCM. The improved C-rate performance for LTO-2 wt % can therefore be attributed to the coating, which most likely prevents side reactions at the cathode/electrolyte interface (i.e., electrolyte decomposition, formation of sulfate and phosphate species).[53] It therefore

https://doi.org/10.1021/acs.chemmater.1c01123
Chem. Mater. XXXX, XXX, XXX−XXX

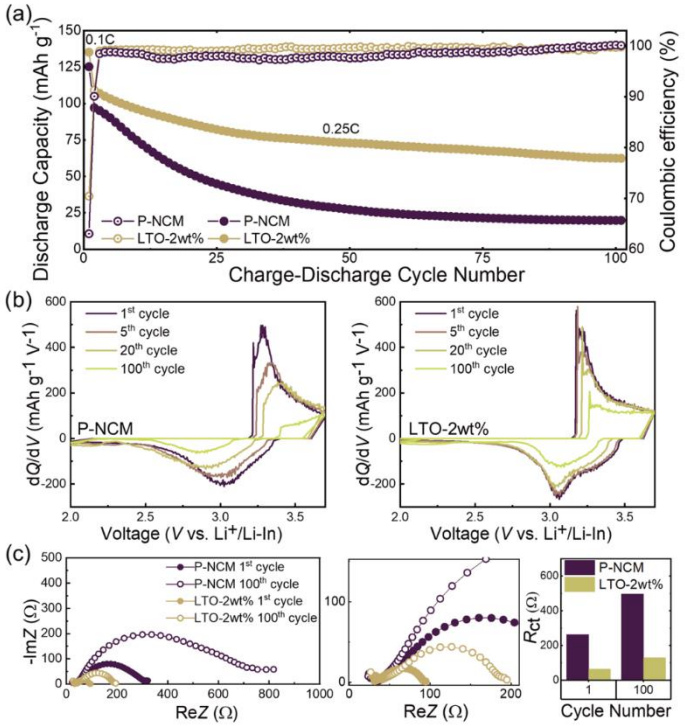

Figure 6. Comparison of (a) long-term cycling capabilities at 0.25C of P-NCM- and LTO-2 wt %-based cells, comparison of differential capacity plot at different cycles for long-term cycling of (b) P-NCM and LTO-2 wt %. Comparison of Nyquist plots corresponding to (c) P-NCM and LTO-2 wt % after the 1st and 100th cycles along with fitted results for the charge transfer resistance at an open-circuit voltage (OCV) of 3.1 V.

inhibits the formation of an insulating cathode-electrolyte interface (CEI) upon cycling, which hinders lithium-ion exchange at the interface. This assumption is well supported by state of charge (SOC) dependent impedance analysis shown in Figure 7, as during the first cycle, other capacity fading issues such as cracking and contact loss are expected to be less significant.[54] Thus, the difference in the impedance can be assumed to arise mainly from the different surface reactivity of the pristine and coated cells. In fact, this also explains why the LTO-2 wt % has a better long-term cycling performance compared to P-NCM, which is discussed in more detail in the following.

For the long-term cycling stability test, additional P-NCM and LTO-2 wt % samples were cycled at 0.25C at 25 °C between 2.0 and 3.7 V. As shown in Figure 6a, the P-NCM shows worse long-term cycling stability compared to LTO-2 wt %. The P-NCM retains only 16% capacity, while for LTO-2 wt % a significantly enhanced capacity retention of 48% is obtained after 100 cycles. Furthermore, the corresponding Coulombic efficiency (CE) plot (Figure S3a) reveals over 99% CE for the LTO-2 wt % during 100 cycles, while the P-NCM exhibits a much lower CE. In addition, the charge/discharge profile of the first cycle is shown in Figure S3b (Supporting Information) for both P-NCM and LTO-2 wt %. For P-NCM, initial specific charge and discharge capacities of 198 and 124 mAh g^{-1} are found, respectively, giving a CE of 63%, while for the LTO-2 wt %, a CE of 70% is obtained with the respective charge/discharge capacities of 190 and 135 mAh g^{-1}. These results provide the first indication that the LTO coating is helpful for the suppression of undesired side reactions at the CEI in the ASSBs.

To further evaluate the long-term properties of the LTO coating, selected differential capacity plots during 100 cycles are presented in Figure 6b, which show that the peak corresponding to the lithiation/delithiation redox reaction is much sharper in the case of LTO-2 wt % along with a smaller peak shift compared to P-NCM after the same number of cycles. In addition, the charge/discharge plots (Figure S3c,d) reveal that the LTO-2 wt % exhibit a much smaller polarization rise than P-NCM during long-term cycling. In accordance with the C-rate tests, these results hint at an improved stability of the interface and also a better preserved Li diffusion pathway in the case of the coated samples, as it is well known that the formation of a resistive CEI is the main cause for capacity fading and polarization rise accompanied with a reduction in peak sharpness and intensity.[24,27] All of these results support

https://doi.org/10.1021/acs.chemmater.1c01123
Chem. Mater. XXXX, XXX, XXX−XXX

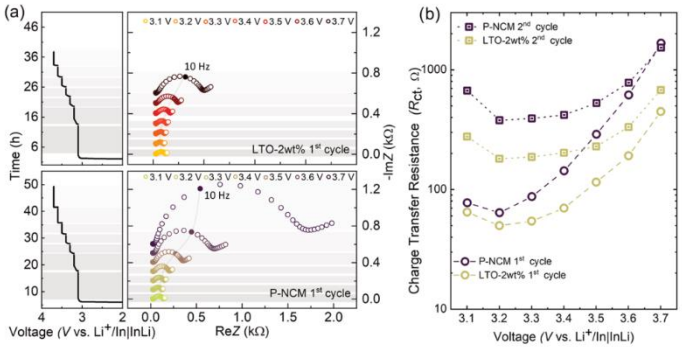

Figure 7. (a) First-cycle charge profile (left) of P-NCM and LTO-2 wt % cells at 0.1C showing current interruptions corresponding to the periods for stabilizing the potential and performing the EIS measurement during charge (right). (b) Potential-dependent charge transfer resistance for the first two cycles of composite cathodes employing P-NCM and LTO-2 wt % as active material. A typical U-shape of R_{ct} with increasing voltage is observed with a strong increase at higher potentials. In both cycles, R_{ct} of the coated active material is smaller than the value of the pristine one, indicating a suppression of the interfacial reaction by the applied coating.

the assumption that the applied LTO-based coating is very effective in stabilizing the NCM/LPSCl interface and thus improves the electrochemical performance of NCM and LPS-based ASSBs.

To further elucidate the influence of the LTO coating on the performance of ASSBs and to confirm that the improved performance is attributed to a stabilized NCM/LPS interface, EIS measurements have been performed on full cells containing P-NCM and LTO-2 wt % composite cathodes during long-term cycling. Additionally, the impedance evolution at different states of charge during the initial two cycles has been investigated, which allows to determine the interfacial processes in SSBs and to determine the contribution of the cathode-electrolyte interface to the total impedance of the cell.[24,27] For a comparison of the long-term cycling EIS, the impedance was measured at an open-circuit potential of 3.1 V after the 1st and 100th cycles, respectively. To ensure equal conditions, a constant potential step was applied after the constant-current discharge, to equilibrate the Li concentrations within the CAM particles by diffusion. The equivalent circuit as well as the respective physiochemical processes contributing to the impedance are described in the Supporting Information (SI Figure S4).

The change of the cell impedance during long-term cycling is displayed in Figure 6c. Comparing the impedance spectra obtained after the 1st and 100th cycles, a clear increase in the impedance is observed for both the pristine and the coated NCM-containing cells. However, the increase is significantly larger for the pristine NCM cells. Especially the low-frequency impedance contribution increases, as visible in the corresponding Bode plots (SI Figure S5). Furthermore, Figure 6c shows the charge transfer resistance, R_{ct}, determined from the impedance spectra, after 1st and 100th cycle for both pristine and coated cells. The massive increase in R_{ct} for the P-NCM sample indicates a strong degradation reaction at the SSE-NCM interface due to the oxidation of solid electrolyte during the first cycles.[27] However, applying the coating not only decreases the initial resistance but also leads to a less pronounced resistance increase over the cycle number, further confirming that the coating reduces the interfacial decomposition of the SSE and hinders the growth of the CEI, which improves the stability in cycling behavior.

Because oxidation reactions of the electrolyte leading to the formation of an insulating CEI typically take place at higher potentials during cycling,[24,27,53] the interfacial resistance evolution was investigated for varying the open-circuit voltage (OCV). Figure 7a shows the growth of the impedance during charging, which is much more pronounced for P-NCM than for LTO-2 wt %. From the impedance measured at different voltages, the SOC-dependent charge transfer resistance R_{ct} is determined for the first and second charge cycles as shown in Figure 7b. With increasing voltage R_{ct} increases with a typical U-shape behavior, i.e., while a slight decrease of R_{ct} is observed, when the voltage is increased from 3.1 to 3.2 V, a significant increase in R_{ct} is found for further increasing voltage, especially during the first cycle. During the second charge cycle, the resistance starts with a lower value than the one reached at high voltages during the first cycle, revealing that the increase in R_{ct} is partly reversible. As the reversible increase in resistance is related to the SOC of the cathode, it is typically attributed to the decreasing concentration of Li in the active material during charging.[27] However, the main contribution of the increasing charge transfer resistance during the first cycle is irreversible, confirming the occurrence of interfacial degradation reaction at higher potentials.[27] Comparing the behavior of the P-NCM and the LTO-2 wt % sample, both start with nearly the same initial resistance at a potential of 3.1 V. However, the increase in resistance at higher voltages is much more pronounced for the P-NCM cells compared to the coated ones. While at a low potential, the charge transfer resistance of the coated NCM corresponds to 98% of that of the P-NCM, it only reaches 13% of the P-NCM value at the potential of 3.7 V. This clearly reveals a significantly more stable interface and the suppression of the formation of an ion-blocking layer caused by SSE oxidation and transition-metal diffusion.[39] Comparing the first and second cycles, it can be seen, that also for the LTO-2 wt % sample some of the resistance increase observed in the first cycle is not completely recovered. We attribute this to a degradation reaction between the coating layer and the SSE, or to degradation reactions

https://doi.org/10.1021/acs.chemmater.1c01123
Chem. Mater. XXXX, XXX, XXX−XXX

between uncovered NCM areas and the SSE as the coating is not completely covering the surface of the CAM. Nonetheless, the resistance is much lower for the coated active material, confirming the beneficial effect of the LTO coating in stabilizing the SSE-CAM interface, which is responsible for the much more stable cycling performance.

4. CONCLUSIONS

Thiophosphate-based ASSBs using oxide-based cathodes with protective CAM coatings show an improved electrochemical performance due to the stabilization of the electrode−electrolyte interface. Various coatings have been previously applied and tested, usually via solvent-based processes. In this work, a dry-processed, fumed LTO powder-based coating has been successfully applied to NCM-based CAM. Using SOC-dependent EIS measurements, it is demonstrated that the CAM/SSE interface of the ASSBs is significantly stabilized by hindering oxidation reactions and the formation of an insulating CEI, resulting in an improved C-rate and cycling performance. Thus, this work introduces a new and straightforward approach of interfacial modification for high-performance ASSBs and demonstrates the promising future of dry-coating processes and fumed LTO powder-based coatings toward better-performing ASSBs.

■ ASSOCIATED CONTENT

Supporting Information

The Supporting Information is available free of charge at https://pubs.acs.org/doi/10.1021/acs.chemmater.1c01123.

SEM image and XRD pattern of the fumed LTO coating, SPED virtual dark-field (VDF) image of an NCM primary particle, Coulombic efficiency (CE) plot at 0.25C and first-cycle charge/discharge voltage profile of P-NCM- and LTO-2 wt %-based cells, equivalent circuit used for fitting, table of obtained fitting parameters, and Bode plots after the 1st and 100th cycles of P-NCM and LTO-2 wt % (PDF)

■ AUTHOR INFORMATION

Corresponding Author

Matthias T. Elm − *Center for Materials Research (LaMa) Justus Liebig University Giessen, D-35392 Giessen, Germany; Institute of Physical Chemistry, Justus Liebig University Giessen, D-35392 Giessen, Germany; Institute of Experimental Physics I, Justus Liebig University Giessen, D-35392 Giessen, Germany;* orcid.org/0000-0001-7014-5772; Email: matthias.elm@phys.chemie.uni-giessen.de

Authors

Rajendra S. Negi − *Center for Materials Research (LaMa) Justus Liebig University Giessen, D-35392 Giessen, Germany*

Philip Minnmann − *Institute of Physical Chemistry, Justus Liebig University Giessen, D-35392 Giessen, Germany*

Ruijun Pan − *Institute of Physical Chemistry, Justus Liebig University Giessen, D-35392 Giessen, Germany*

Shamail Ahmed − *Materials Science Centre and Faculty of Physics, Philipps University Marburg, 35043 Marburg, Germany*

Marcel J. Herzog − *Evonik Operations GmbH, 63457 Hanau, Germany*

Kerstin Volz − *Materials Science Centre and Faculty of Physics, Philipps University Marburg, 35043 Marburg, Germany*

Ryo Takata − *Evonik Operations GmbH, 63457 Hanau, Germany*

Franz Schmidt − *Evonik Operations GmbH, 63457 Hanau, Germany*

Jürgen Janek − *Center for Materials Research (LaMa) Justus Liebig University Giessen, D-35392 Giessen, Germany; Institute of Physical Chemistry, Justus Liebig University Giessen, D-35392 Giessen, Germany;* orcid.org/0000-0002-9221-4756

Complete contact information is available at: https://pubs.acs.org/10.1021/acs.chemmater.1c01123

Notes

The authors declare no competing financial interest.

■ ACKNOWLEDGMENTS

R.S.N. and M.T.E. thank the German Federal Ministry of Education and Research (BMBF) for the funding of the NanoMatFutur project NiKo (03XP0093). P.M., J.J., S.A., and K.V. acknowledge financial support by BMBF with the cluster of competence FestBatt (project 0XP0177A and project 03XP0176C).

■ REFERENCES

(1) Janek, J.; Zeier, W. G. A Solid Future for Battery Development. *Nat. Energy* **2016**, *1*, No. 16141.

(2) Thackeray, M. M.; Wolverton, C.; Isaacs, E. D. Electrical Energy Storage for Transportation—Approaching the Limits of, and Going beyond, Lithium-Ion Batteries. *Energy Environ. Sci.* **2012**, *5*, 7854−7863.

(3) Kato, Y.; Hori, S.; Saito, T.; Suzuki, K.; Hirayama, M.; Mitsui, A.; Yonemura, M.; Iba, H.; Kanno, R. High-Power All-Solid-State Batteries Using Sulfide Superionic Conductors. *Nat. Energy* **2016**, *1*, No. 16030.

(4) Etacheri, V.; Marom, R.; Elazari, R.; Salitra, G.; Aurbach, D. Challenges in the Development of Advanced Li-Ion Batteries: A Review. *Energy Environ. Sci.* **2011**, *4*, 3243−3262.

(5) Buschmann, H.; Dölle, J.; Berendts, S.; Kuhn, A.; Bottke, P.; Wilkening, M.; Heitjans, P.; Senyshyn, A.; Ehrenberg, H.; Lotnyk, A.; et al. Structure and Dynamics of the Fast Lithium Ion Conductor "$Li_7La_3Zr_2O_{12}$". *Phys. Chem. Chem. Phys.* **2011**, *13*, 19378−19392.

(6) Busche, M. R.; Weber, D. A.; Schneider, Y.; Dietrich, C.; Wenzel, S.; Leichtweiss, T.; Schröder, D.; Zhang, W.; Weigand, H.; Walter, D.; et al. In Situ Monitoring of Fast Li-Ion Conductor $Li_7P_3S_{11}$ Crystallization Inside a Hot-Press Setup. *Chem. Mater.* **2016**, *28*, 6152−6165.

(7) Murugan, R.; Thangadurai, V.; Weppner, W. Fast Lithium Ion Conduction in Garnet-Type $Li_7La_3Zr_2O_{12}$. *Angew. Chem., Int. Ed.* **2007**, *46*, 7778−7781.

(8) Fergus, J. W. Ion Transport in Sodium Ion Conducting Solid Electrolytes. *Solid State Ionics* **2012**, *227*, 102−112.

(9) Gromov, O. G.; Kunshina, G. B.; Kuz'min, A. P.; Kalinnikov, V. T. Ionic Conductivity of Solid Electrolytes Based on $Li_{1.3}Al_{0.3}Ti_{1.7}(PO_4)_3$. *Russ. J. Appl. Chem.* **1996**, *69*, 385−388.

(10) Yoon, S. A.; Oh, N. R.; Yoo, A. R.; Lee, H. G.; Lee, H. C. Preparation and Characterization of Ta-Substituted $Li_7La_3Zr_{2-x}O_{12}$ Garnet Solid Electrolyte by Sol-Gel Processing. *J. Korean Ceram. Soc.* **2017**, *54*, 278−284.

(11) Imanishi, N.; Hasegawa, S.; Zhang, T.; Hirano, A.; Takeda, Y.; Yamamoto, O. Lithium Anode for Lithium-Air Secondary Batteries. *J. Power Sources* **2008**, *185*, 1392−1397.

(12) Nagata, K.; Nanno, T. All Solid Battery with Phosphate Compounds Made through Sintering Process. *J. Power Sources* **2007**, *174*, 832−837.
(13) Lethien, C.; Zegaoui, M.; Roussel, P.; Tilmant, P.; Rolland, N.; Rolland, P. A. Micro-Patterning of LiPON and Lithium Iron Phosphate Material Deposited onto Silicon Nanopillars Array for Lithium Ion Solid State 3D Micro-Battery. *Microelectron. Eng.* **2011**, *88*, 3172−3177.
(14) Fleutot, B.; Pecquenard, B.; Le Cras, F.; Delis, B.; Martinez, H.; Dupont, L.; Guy-Bouyssou, D. Characterization of All-Solid-State Li/LiPONB/TiOS Microbatteries Produced at the Pilot Scale. *J. Power Sources* **2011**, *196*, 10289−10296.
(15) Liu, Z.; Fu, W.; Payzant, E. A.; Yu, X.; Wu, Z.; Dudney, N. J.; Kiggans, J.; Hong, K.; Rondinone, A. J.; Liang, C. Anomalous High Ionic Conductivity of Nanoporous β-Li_3PS_4. *J. Am. Chem. Soc.* **2013**, *135*, 975−978.
(16) Hayamizu, K.; Aihara, Y. Lithium Ion Diffusion in Solid Electrolyte $(Li_2S)_7(P_2S_5)_3$ Measured by Pulsed-Gradient Spin-Echo 7Li NMR Spectroscopy. *Solid State Ionics* **2013**, *238*, 7−14.
(17) Tatsumisago, M.; Hama, S.; Hayashi, A.; Morimoto, H.; Minami, T. New Lithium Ion Conducting Glass-Ceramics Prepared from Mechanochemical Li_2S-P_2S_5 Glasses. *Solid State Ionics* **2002**, *154*, 635−640.
(18) Kim, D. H.; Oh, D. Y.; Park, K. H.; Choi, Y. E.; Nam, Y. J.; Lee, H. A.; Lee, S. M.; Jung, Y. S. Infiltration of Solution-Processable Solid Electrolytes into Conventional Li-Ion-Battery Electrodes for All-Solid-State Li-Ion Batteries. *Nano Lett.* **2017**, *17*, 3013−3020.
(19) Kamaya, N.; Homma, K.; Yamakawa, Y.; Hirayama, M.; Kanno, R.; Yonemura, M.; Kamiyama, T.; Kato, Y.; Hama, S.; Kawamoto, K.; et al. A Lithium Superionic Conductor. *Nat. Mater.* **2011**, *10*, 682−686.
(20) Rangasamy, E.; Liu, Z.; Gobet, M.; Pilar, K.; Sahu, G.; Zhou, W.; Wu, H.; Greenbaum, S.; Liang, C. An Iodide-Based $Li_7P_2S_8I$ Superionic Conductor A New Stoichiometric Phase Is Formed. Upon Mixing LiI with Li_3PS_4 and Subsequent Heat Treatment, a New Phase. *J. Am. Chem. Soc* **2015**, *137*, 1384−1387.
(21) Seino, Y.; Ota, T.; Takada, K.; Hayashi, A.; Tatsumisago, M. A Sulphide Lithium Super Ion Conductor Is Superior to Liquid Ion Conductors for Use in Rechargeable Batteries. *Energy Environ. Sci.* **2014**, *7*, 627−631.
(22) Sakuda, A.; Hayashi, A.; Tatsumisago, M. Interfacial Observation between $LiCoO_2$ Electrode and Li_2S-P_2S_5 Solid Electrolytes of All-Solid-State Lithium Secondary Batteries Using Transmission Electron Microscopy. *Chem. Mater.* **2010**, *22*, 949−956.
(23) Zhang, W.; Schröder, D.; Arlt, T.; Manke, I.; Koerver, R.; Pinedo, R.; Weber, D. A.; Sann, J.; Zeier, W. G.; Janek, J. (Electro)Chemical Expansion during Cycling: Monitoring the Pressure Changes in Operating Solid-State Lithium Batteries. *J. Mater. Chem. A* **2017**, *5*, 9929−9936.
(24) Zhang, W.; Weber, D. A.; Weigand, H.; Arlt, T.; Manke, I.; Schröder, D.; Koerver, R.; Leichtweiss, T.; Hartmann, P.; Zeier, W. G.; et al. Interfacial Processes and Influence of Composite Cathode Microstructure Controlling the Performance of All-Solid-State Lithium Batteries. *ACS Appl. Mater. Interfaces* **2017**, *9*, 17835−17845.
(25) Zhu, Y.; He, X.; Mo, Y. Origin of Outstanding Stability in the Lithium Solid Electrolyte Materials: Insights from Thermodynamic Analyses Based on First-Principles Calculations. *ACS Appl. Mater. Interfaces* **2015**, *7*, 23685−23693.
(26) Wenzel, S.; Randau, S.; Leichtweiß, T.; Weber, D. A.; Sann, J.; Zeier, W. G.; Janek, J. Direct Observation of the Interfacial Instability of the Fast Ionic Conductor $Li_{10}GeP_2S_{12}$ at the Lithium Metal Anode. *Chem. Mater.* **2016**, *28*, 2400−2407.
(27) Koerver, R.; Aygün, I.; Leichtweiß, T.; Dietrich, C.; Zhang, W.; Binder, J. O.; Hartmann, P.; Zeier, W. G.; Janek, J. Capacity Fade in Solid-State Batteries: Interphase Formation and Chemomechanical Processes in Nickel-Rich Layered Oxide Cathodes and Lithium Thiophosphate Solid Electrolytes. *Chem. Mater.* **2017**, *29*, 5574−5582.
(28) Tian, Y.; Shi, T.; Richards, W. D.; Li, J.; Kim, J. C.; Bo, S.-H.; Ceder, G. Compatibility Issues between Electrodes and Electrolytes in Solid-State Batteries. *Energy Environ. Sci.* **2017**, *10*, 1150−1166.
(29) Zhang, W.; Richter, F. H.; Culver, S. P.; Leichtweiss, T.; Lozano, J. G.; Dietrich, C.; Bruce, P. G.; Zeier, W. G.; Janek, J. Degradation Mechanisms at the $Li_{10}GeP_2S_{12}/LiCoO_2$ Cathode Interface in an All-Solid-State Lithium-Ion Battery. *ACS Appl. Mater. Interfaces* **2018**, *10*, 22226−22236.
(30) Xu, L.; Tang, S.; Cheng, Y.; Wang, K.; Liang, J.; Liu, C.; Cao, Y.-C.; Wei, F.; Mai, L. Interfaces in Solid-State Lithium Batteries. *Joule* **2018**, *2*, 1991−2015.
(31) Nolan, A. M.; Zhu, Y.; He, X.; Bai, Q.; Mo, Y. Computation-Accelerated Design of Materials and Interfaces for All-Solid-State Lithium-Ion Batteries. *Joule* **2018**, *2*, 2016−2046.
(32) Xiao, Y.; Miara, L. J.; Wang, Y.; Ceder, G. Computational Screening of Cathode Coatings for Solid-State Batteries. *Joule* **2019**, *3*, 1252−1275.
(33) Culver, S. P.; Koerver, R.; Zeier, W. G.; Janek, J. On the Functionality of Coatings for Cathode Active Materials in Thiophosphate-Based All-Solid-State Batteries. *Adv. Energy Mater.* **2019**, *9*, No. 1900626.
(34) Oh, G.; Hirayama, M.; Kwon, O.; Suzuki, K.; Kanno, R. Bulk-Type All Solid-State Batteries with 5 V Class $LiNi_{0.5}Mn_{1.5}O_4$ Cathode and $Li_{10}GeP_2S_{12}$ Solid Electrolyte. *Chem. Mater.* **2016**, *28*, 2634−2640.
(35) Park, K. H.; Oh, D. Y.; Choi, Y. E.; Nam, Y. J.; Han, L.; Kim, J.-Y.; Xin, H.; Lin, F.; Oh, S. M.; Jung, Y. S. Solution-Processable Glass LiI-Li_4SnS_4 Superionic Conductors for All-Solid-State Li-Ion Batteries. *Adv. Mater.* **2016**, *28*, 1874−1883.
(36) Kim, A. Y.; Strauss, F.; Bartsch, T.; Teo, J. H.; Hatsukade, T.; Mazilkin, A.; Janek, J.; Hartmann, P.; Brezesinski, T. Stabilizing Effect of a Hybrid Surface Coating on a Ni-Rich NCM Cathode Material in All-Solid-State Batteries. *Chem. Mater.* **2019**, *31*, 9664−9672.
(37) Lee, J. W.; Park, Y. J. Enhanced Cathode/Sulfide Electrolyte Interface Stability Using an Li_2ZrO_3 Coating for All-Solid-State Batteries. *J. Electrochem. Sci. Technol.* **2018**, *9*, 176−183.
(38) Ito, S.; Fujiki, S.; Yamada, T.; Aihara, Y.; Park, Y.; Kim, T. Y.; Baek, S. W.; Lee, J. M.; Doo, S.; Machida, N. A Rocking Chair Type All-Solid-State Lithium Ion Battery Adopting Li_2O-ZrO_2 Coated $LiNi_{0.8}Co_{0.15}Al_{0.05}O_2$ and a Sulfide Based Electrolyte. *J. Power Sources* **2014**, *248*, 943−950.
(39) Zhang, Y.; Tian, Y.; Xiao, Y.; Miara, L. J.; Aihara, Y.; Tsujimura, T.; Shi, T.; Scott, M. C.; Ceder, G. Direct Visualization of the Interfacial Degradation of Cathode Coatings in Solid State Batteries: A Combined Experimental and Computational Study. *Adv. Energy Mater.* **2020**, *10*, No. 1903778.
(40) Strauss, F.; Teo, J. H.; Maibach, J.; Kim, A.-Y.; Mazilkin, A.; Janek, J.; Brezesinski, T. Li_2ZrO_3-Coated NCM622 for Application in Inorganic Solid-State Batteries: Role of Surface Carbonates in the Cycling Performance. *ACS Appl. Mater. Interfaces* **2020**, *12*, 57146−57154.
(41) Meng, X.; Yang, X.-Q.; Sun, X. Emerging Applications of Atomic Layer Deposition for Lithium-Ion Battery Studies. *Adv. Mater.* **2012**, *24*, 3589−3615.
(42) Negi, R. S.; Culver, S. P.; Mazilkin, A.; Brezesinski, T.; Elm, M. T. Enhancing the Electrochemical Performance of Li-$Ni_{0.70}Co_{0.15}Mn_{0.15}O_2$ Cathodes Using a Practical Solution-Based Al_2O_3 Coating. *ACS Appl. Mater. Interfaces* **2020**, *12*, 31392−31400.
(43) Kim, J.; Lee, H.; Cha, H.; Yoon, M.; Park, M.; Cho, J. Prospect and Reality of Ni-Rich Cathode for Commercialization. *Adv. Energy Mater.* **2018**, *8*, No. 1702028.
(44) Negi, R. S.; Celik, E.; Pan, R.; Stäglich, R.; Senker, J.; Elm, M. T. Insights into the Positive Effect of Post-Annealing on the Electrochemical Performance of Al_2O_3-Coated Ni-Rich NCM Cathodes for Lithium-Ion Batteries. *ACS Appl. Energy Mater.* **2021**, *4*, 3369−3380.
(45) Hemmelmann, H.; Dinter, J. K.; Elm, M. T. Thin Film NCM Cathodes as Model Systems to Assess the Influence of Coating Layers

https://doi.org/10.1021/acs.chemmater.1c01123
Chem. Mater. XXXX, XXX, XXX−XXX

on the Electrochemical Performance of Lithium Ion Batteries. *Adv. Mater. Interfaces* **2021**, *8*, No. 2002074.
(46) Negi, R. S.; Culver, S. P.; Wiche, M.; Ahmed, S.; Volz, K.; Elm, M. T. Optimized Atomic Layer Deposition of Homogeneous, Conductive Al_2O_3 Coatings for High-Nickel NCM Containing Ready-to-Use Electrodes. *Phys. Chem. Chem. Phys.* **2021**, *23*, 6725−6737.
(47) Hwang, B. J.; Hu, S. K.; Chen, C. H.; Chen, C. Y.; Sheu, H. S. In-Situ XRD Investigations on Structure Changes of ZrO_2-Coated $LiMn_{0.5}Ni_{0.5}O_2$ Cathode Materials during Charge. *J. Power Sources* **2007**, *174*, 761−765.
(48) Zhang, M.; Hu, G.; Wu, L.; Peng, Z.; Du, K.; Cao, Y. A Facile Approach to Enhance High-Cutoff Voltage Cycle Stability of $LiNi_{0.5}Co_{0.2}Mn_{0.3}O_2$ Cathode Materials Using Lithium Titanium Oxide. *Electrochim. Acta* **2017**, *232*, 80−88.
(49) Rauch, E. F.; Portillo, J.; Nicolopoulos, S.; Bultreys, D.; Rouvimov, S.; Moeck, P. Automated Nanocrystal Orientation and Phase Mapping in the Transmission Electron Microscope on the Basis of Precession Electron Diffraction. *Z. Kristallogr.* **2010**, *225*, 103−109.
(50) Rauch, E. F.; Véron, M. Methods for Orientation and Phase Identification of Nano-Sized Embedded Secondary Phase Particles by 4D Scanning Precession Electron Diffraction. *Acta Crystallogr., Sect. B: Struct. Sci., Cryst. Eng. Mater.* **2019**, *75*, 505−511.
(51) Mu, X.; Kobler, A.; Wang, D.; Chakravadhanula, V. S. K.; Schlabach, S.; Szabó, D. V.; Norby, P.; Kübel, C. Comprehensive Analysis of TEM Methods for $LiFePO_4$/$FePO_4$ Phase Mapping: Spectroscopic Techniques (EFTEM, STEM-EELS) and STEM Diffraction Techniques (ACOM-TEM). *Ultramicroscopy* **2016**, *170*, 10−18.
(52) Lee, S. Y.; Park, G. S.; Jung, C.; Ko, D. S.; Park, S. Y.; Kim, H. G.; Hong, S. H.; Zhu, Y.; Kim, M. Revisiting Primary Particles in Layered Lithium Transition-Metal Oxides and Their Impact on Structural Degradation. *Adv. Sci.* **2019**, *6*, No. 1800843.
(53) Walther, F.; Koerver, R.; Fuchs, T.; Ohno, S.; Sann, J.; Rohnke, M.; Zeier, W. G.; Janek, J. Visualization of the Interfacial Decomposition of Composite Cathodes in Argyrodite-Based All-Solid-State Batteries Using Time-of-Flight Secondary-Ion Mass Spectrometry. *Chem. Mater.* **2019**, *31*, 3745−3755.
(54) Ruess, R.; Schweidler, S.; Hemmelmann, H.; Conforto, G.; Bielefeld, A.; Weber, D. A.; Sann, J.; Elm, M. T.; Janek, J. Influence of NCM Particle Cracking on Kinetics of Lithium-Ion Batteries with Liquid or Solid Electrolyte. *J. Electrochem. Soc.* **2020**, *167*, No. 100532.

https://doi.org/10.1021/acs.chemmater.1c01123
Chem. Mater. XXXX, XXX, XXX−XXX

3.5 Publication V: A Dry-Processed $Al_2O_3/LiAlO_2$ Coating for Stabilizing the Cathode/Electrolyte Interface in High-Ni NCM-Based All-Solid-State Batteries

As known from our previous work on annealing (publication III), we have successfully understood that the annealing step during the coating can be crucial for improving the electrochemical performance of NCM based cathodes. Thus, keeping that in mind, additional annealing step is added to the dry-processed Al_2O_3 based coating for NCM based cathodes used in ASSBs. The annealing seems to improve various expects of the coating. Structural analysis revealed that no observable changes have been observed in the NCM. However, various significant structural changes in the coating have been observed. SEM and TEM studies showed that the coating layer becomes thin, dense and homogenous after annealing resulting in an improved interfacial property between NCM and the coating layer. BET studies further supported the loss of porosity in the coating layer. XPS studies revealed the inter-diffusion of Li^+ inside the coating layer during annealing, resulting in an $Al_2O_3/LiAlO_2$ composite coating layer, as observed in our previous publication (publication III). The improvement in various properties resulted in improved electrochemical performance of the NCM both, in-terms of C-rate and long-term cycling. The following observation suggested that annealing step could be very crucial for the development of coating strategies for ASSBs

The concept and experiments for this publication have been designed and performed by myself and Y. Yusim under the supervision of Dr. M. T. Elm and Dr. A. Henss. The manuscript was written by me, Y. Yusim, and corrected by all co-authors. TEM analysis has been taken by S. Ahmad. Dr. R. Pan contributed to the scientific discussions. Just accepted Advanced Materials Interfaces 2021

R. S. Negi, Y. Yusim, R. Pan, S. Ahmed, K. Volz, R. Takata, F.Schmidt, A. Henss and M. T. Elm, A dry-processed $Al_2O_3/LiAlO_2$ coating for stabilizing the cathode/electrolyte interface in high-Ni NCM-based all-solid-state batteries

A dry-processed $Al_2O_3/LiAlO_2$ coating for stabilizing the cathode/electrolyte interface in high-Ni NCM-based all-solid-state batteries

Rajendra S. Negi[a,=], Yuriy Yusim[b,=], Ruijun Pan[a,b,c*], Shamail Ahmed[d], Kerstin Volz[d], Ryo Takata[e], Franz Schmidt[e], Anja Henss[a,b*] and Matthias T. Elm[a,b,f*]

[a]*Center for Materials Research (LaMa), Justus Liebig University Giessen, Heinrich-Buff-Ring 16, 35392 Giessen, Germany*

[b]*Institute of Physical Chemistry, Justus Liebig University Giessen, Heinrich-Buff-Ring 17, 35392 Giessen, Germany*

[c]*Materials Science and Engineering Program and Texas Materials Institute, University of Texas at Austin, Austin, TX, 78712 USA*

[d]*Materials Science Centre and Faculty of Physics, Philipps University Marburg, Hans-Meerwein-Strasse 6, 35043 Marburg, Germany*

[e]*Evonik Operations GmbH, Rodenbacher Chaussee 4, 63457 Hanau, Germany*

[f]*Institute of Experimental Physics I, Justus Liebig University Giessen, Heinrich-Buff-Ring 16, 35392 Giessen, Germany*

=These authors contributed equally to this work

Abstract

Due to their high theoretical energy densities and superior safety, thiophosphate-based all-solid-state batteries (ASSBs) are considered as promising power source for electric vehicles. However, for large-scale industrial applications, interfacial degradation between high-voltage cathode active materials (CAMs) and solid-state electrolytes (SSEs) needs to be overcome with a simple, cost-effective solution. Surface coatings, which prevent the direct physical contact between CAM and SSE and in turn stabilize the interface, are considered as promising approach to solve this issue. In this work, an $Al_2O_3/LiAlO_2$ coating for $Li(Ni_{0.70}Co_{0.15}Mn_{0.15})O_2$ (NCM) has been tested for ASSBs. The coating is obtained from a recently developed dry coating process followed by post-annealing at 600 °C. Structural characterization reveals that the heat treatment results in the formation of a dense $Al_2O_3/LiAlO_2$ coating layer. Electrochemical evaluations confirm that the annealing induced structural changes are beneficial for ASSB. Cells containing $Al_2O_3/LiAlO_2$-coated NCM show a significant improvement of the rate capability and long-term cycling performance compared to those assembled from Al_2O_3-coated and uncoated cathodes. Moreover, EIS analysis shows a decreased cell impedance after cycling indicating a reduced interfacial degradation for the $Al_2O_3/LiAlO_2$-coated electrode. The results

highlight a promising low-cost and scalable CAM coating process, enabling large-scale cathode coating for next-generation ASSBs.

1. Introduction

All-solid-state batteries (ASSBs) are one of the most promising approaches to achieving electrical energy storage and transport electrification goals.[1-3] In comparison to state-of-the-art liquid electrolyte containing lithium-ion batteries (LIBs), ASSBs provide an improved safety due to the non-flammability of the solid-state electrolytes (SSEs) along with the possibility to achieve higher energy density when using a lithium metal anode.[4] So far, several SSEs with high ionic conductivity have been discovered for ASSBs.[4,5] Among them, oxide-based SSEs including garnet ceramics (e.g. $Li_7La_3Zr_2O_{12}$ (LLZO))[6], perovskites (e.g. $Li_{1+x}Al_xTi_{2-x}(PO_4)_3$ (LATP))[7], and thiophosphate-based SSEs (TSSEs)[8] including $Li_{10}GeP_2S_{12}$ (LGPS) are considered as promising candidates for practical applications.[9] Oxide-based SSEs require high-temperature sintering (> 700 °C) to achieve sufficient interfacial contact between SSEs and cathode active materials (CAMs) due to their hard mechanical properties. Unfortunately, the heat treatment causes irreversible degradation reactions at the electrolyte-electrode interface resulting in increased interfacial resistances.[10-12] In contrast, thiophosphate-based SSEs are rather soft and, thus, provide good interfacial contact to CAMs. Furthermore, they exhibit high ionic conductivities of above 20 mS cm^{-1} at room temperature[3,13] making them more attractive for application in ASSBs.[14]

Despite several advantages of TSSEs, several remaining challenges have to be addressed on the way to large-scale industrial application of ASSBs, such as interfacial stability issues[15,16] between high voltage CAMs and TSSEs. Ni-rich $LiNi_{1-x-y}Co_xMn_yO_2$ (NCM) CAMs are commonly accepted as the state-of-the-art high energy density CAMs for ASSBs with high specific capacities and high working voltages combined with mature industrial-scale production.[17,18] However, inside the cell, NCMs and TSSEs form a cathode-electrolyte interphase (CEI) consisting of degradation products of both.[19] Various studies suggest that the formed CEI layer between CAM and SSE is responsible for long-term capacity fading and limited operational life.[20,15,21] Therefore, research efforts are dedicated to improve the interfacial stability between CAMs and TSSEs.

Surface coating is well established strategy to enhance the interfacial stability between CAM and SSE by preventing direct physical contact. For NCM-CAM, oxide-based coatings such as $LiNbO_3$[22-24], $Li_4Ti_5O_{12}$[23], Li_2O-ZrO_2[25], HfO_2[26], and $Li_3B_{11}O_{18}$[27] have been reported to improve the electrochemical performance of ASSBs, as they effectively prevent or reduce detrimental

side reactions at the NCM/SSE interface. In conventional LIBs, Al_2O_3-based coatings have been considered as promising coatings due to their effectiveness against side reactions and low synthesis cost.[28-31] However, they are not well explored in ASSBs yet.[32-35] Although Al_2O_3-based coatings enhance the interfacial stability, the rate capability could not be improved significantly, primarily due to the ionically and electronically insulating nature of the coating.[36] In contrast, $LiAlO_2$ provides good lithium-ion transport properties due to partially occupied Li sites.[37] This means that $LiAlO_2$ or mixed Al_2O_3/$LiAlO_2$ coating layers stabilize the CAM/SSE interface effectively without significantly increasing the interfacial resistance.[38,39] Thus, $LiAlO_2$ based coatings could be promising candidates to improve the overall performance of ASSBs.

Surface coatings on cathode materials using wet-chemical approaches[40], atomic layer deposition (ALD)[41], or spray coating procedures[23,42] are already successfully established in thiophosphate-based ASSBs.[43] However, wet-chemical approaches require additional drying steps that increase the energy costs and manufacturing time.[44] While the ALD technology provides thin coating layers with excellent conformity, it often requires toxic precursors and shows slow deposition rates.[33,45,46] With spray coating procedures, the manufacturing time can be reduced, but an expensive piece of instrument is needed.[43]

In order to reduce ecological and economic costs, a new dry coating procedure on CAM was recently introduced by Herzog et al.[33] It has been shown that by using a high energy mixer, fumed nanostructured Al_2O_3 physically absorb on the surface of NCM particles and form a porous Al_2O_3-coating layer, which significantly improves the electrochemical rate performance and capacity retention in liquid-based LIBs.[33]

In the study presented here, we modified the dry coating procedure by using an additional annealing step in order to make it more suitable for thiophosphate-based ASSBs, and to achieve a dry-processed Al_2O_3/$LiAlO_2$ coating for $Li(Ni_{0.70}Co_{0.15}Mn_{0.15})O_2$ (NCM701515) CAM. The high-temperature treatment is found to improve various aspects of the coating (such as better interface formation, reduced porosity, thickness, etc.), which altogether significantly improve the electrochemical performance of the NCM-based ASSBs in terms of the C-rate and long-term cycling performance. The full cells with coated NCM cathodes show a decreased interfacial impedance, which indicates a better interfacial stability between CAM and TSSE. Our results highlight that the low cost and simple dry coating process without any detrimental environmental solvents is a highly promising approach for the large-scale industrial coating of cathodes for next-generation ASSBs.

2. Experimental

Surface modification of Ni-rich NCM using an Al_2O_3-dry coating process

Commercial $Li(Ni_{0.70}Co_{0.15}Mn_{0.15})O_2$ (NCM701515, Linyi Gelon LIB. Co.) was used as CAM, and nanostructured fumed Al_2O_3 (Alu, Evonik Operation GmbH) powder was utilized as coating material during the dry-coating process. A lab-scale high-energy Somakon mixer MP-GL (Somakon Verfahrenstechnik UG) was used for mixing. Two different steps were performed for the dry-coating process. Initially, the CAM powder was well mixed with nanostructured Al_2O_3 (1 wt%) at 500 rpm for 1 min. Subsequently, the mixing intensity was raised to 2000 rpm for 6 min to achieve a well-distributed coating on the surface of CAM. Then, the powder obtained was divided into two batches. The first batch was dried and transferred into the glovebox for further use (denoted as Alu-NCM). The second batch was additionally annealed at 600 °C for 8 h to modify the coating layer. Subsequently, it was dried and transferred to the glovebox for further use (denoted as Alu-NCM600).

During the first step of the dry-coating process, the fumed nanostructured Al_2O_3 de-agglomerates into smaller aggregates and interacts with the cathode surface, resulting in smaller Al_2O_3 aggregates with very strong adhesion to the CAM surface. During the second step, at higher mixing rotation, desirable densification and coalescence of Al_2O_3 aggregates is achieved on the surface of the cathode, which results in a highly homogenous coating.

Materials characterization

The surface morphology and the elemental composition of the pristine and coated NCM was investigated with scanning electron microscopy (SEM, Merlin, Zeiss) at an accelerating voltage of 7 kV and a current of 3000 pA. Focussed-ion beam (FIB) cross-sections of the coated secondary particles were prepared by a dual-beam JEOL JIB-4601 FIB -SEM. First, a thin layer of platinum was deposited on the surfaces of the coated secondary particles via a Leica EM ACE600 sputter coater before loading them to the FIB-SEM. This is done to protect the coated surfaces of the secondary particles coming in direct contact with the electron beam during FIB cross-section preparation. On top of the thin platinum coating, thick carbon and tungsten protective layers were deposited, respectively, using a Ga-ion beam to further protect the surfaces from Ga-ion beam damage during FIB milling. The samples were milled down using a 30 kV Ga-ion beam to roughly about 200 nm and further thinned down using a 5 kV Ga-ion beam to electron transparency. A double Cs-corrected JEOL 2200-FS microscope was used for scanning TEM (STEM) high-angle annular dark-field (HAADF) imaging and energy dispersive spectroscopy (EDS). The microscope was operated at 200 kV.

Powder X-ray diffraction (XRD) diffractograms of pristine and coated NCM were obtained using an Empyrean XRD (Panalytical) system with Cu Kα radiation. The XPS analysis was performed using a PHI5000 Versa Probe II (Physical Electronics GmbH) with an Al anode. The pass energy of the analyzer was fixed at 23.5 eV to obtain the survey spectra and the detailed spectra. The chamber pressure was maintained below 10^{-7} Pa. Furthermore, Brunauer-Emmett-Teller (BET) analysis was performed on pristine and coated NCM in order to determine the porosity change after coating and heat treatment. Single point BET was performed using a MICROMERITICS TRISTAR 3000 with a nitrogen/helium flow (28.6% N_2). The samples were degassed for 20 min at 150 °C before the measurement.

Electrode Preparation

Composite cathode: The composite cathodes (CC) comprise the pristine or coated $Li(Ni_{0.70}Co_{0.15}Mn_{0.15})O_2$ (NCM701515), Li_6PS_5Cl (LPS, NEI Corporation), and vapor-grown carbon fibers (VGCFs, Sigma-Aldrich Inc., iron-free). At first, NCM and LPS powders have been mixed in a mass ratio of 70:30 (volume ratio 47:53). Then, 3 wt% of VGCF was additional added (exact mass ratio 68:29.1:2.9 (NCM: LPS:VGCF)) to the mixture. Finally, the resulting mixture was hand grounded using an agate mortar for 15 min.

Cell assembly: The composite cathode was prepared fresh before preparing the cells in order to avoid time-dependent side reactions. All the electrochemical tests were performed using an in-house (pellet type) cell casing.[15,16] For cell assembly, one side of the poly(ether-ether-ketone) (PEEK) cylinder (inner diameter: 10 mm) was closed using a stainless-steel stamp. 60 mg of LPS was uniformly put into the PEEK cylinder, followed by a manual hand compression. Subsequently, 12 mg of CC was added to one side of the pressed LPS and distributed uniformly. The whole stack was then pressed uniaxially at 30 kN (380 MPa) for a duration of 3 min, resulting in a pressed pellet with a thickness of 430 µm (400 µm SSE and 30 µm SSE). An indium foil (In, chemPUR GmbH, 9 mm (diameter), 125 µm (thickness)) and a lithium foil (Li, Albermarle (Rockwood Lithium GmbH), 9 mm (diameter), 120 µm (thickness))) were placed on the other side of the pellet as an anode. Then, the whole stack was closed using another stainless-steel stamp. Finally, the complete cell assembly was fully closed. During electrochemical characterization, an external frame under constant pressure of ~50 MPa was used around the cell casing.

Electrochemical characterization

For electrochemical characterization, MACCOR potentiostats/galvanostats and VMP-300 (Biologic) were used. The cycling tests (i.e., C-rate and long-term cycling tests) were performed on MACCOR, while the electrochemical impedance (EIS) measurements were performed on VMP-300. The cells were cycled in a voltage window of 2.0 and 3.7 V vs. In|InLi, corresponding to 2.6 - 4.3 V vs. Li^+/Li at 25 °C. For the C-rate tests, the cells were cycled up to 2 C, 1 C = 200 mA g^{-1} (3 cycles at 0.1 C, 3 cycles at 0.25 C, 3 cycles at 0.5 C, 5 cycles at 1 C) and 5 cycles at 2 C). For the long-term cycling, the cells were cycled at 0.1 C for one cycle, followed by 100 cycles at 0.25C. EIS measurements were performed after the 1st and 100th cycle. All EIS measurements were performed in the frequency range between 7 MHz and 50 mHz, applying a 10 mV AC bias. To ensure reproducibility, every electrochemical experiment was performed with two independent cells.

3. Results and discussion

3.1 Characterization of the Al_2O_3- and $Al_2O_3/LiAlO_2$-coated NCM

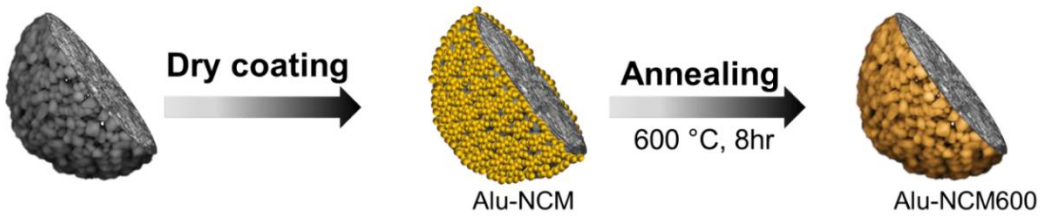

Figure 1. *Schematic illustration of the $Al_2O_3/LiAlO_2$ dry coating process of Ni-rich NCM for ASSBs.*

Figure 1 shows a schematic illustration of the dry coating process used to NCM secondary particles with $Al_2O_3/LiAlO_2$. As described in the experimental part, the Al_2O_3 powder was mixed with the NCM powder in a high-energy mixer to achieve an Al_2O_3 coating on the surface of the NCM secondary particles (denoted as Alu-NCM) in the first step. In the second step, the samples were annealed at 600 °C for 8h, resulting in the conversion of Al_2O_3 to $Al_2O_3/LiAlO_2$ (denoted as Alu-NCM600). The formation of $Al_2O_3/LiAlO_2$ is confirmed by XPS as will be discussed later. The principle of the dry coating process is described in detail by M. Herzog et al.[33] In brief, during high energy mixing, nanostructured fumed Al_2O_3 powder produced from flame hydrolysis is de-agglomerated into smaller aggregates with a high specific surface area. This ensures a good adhesion capability of the aggregates at the CAM surface, which is decisive for the formation of a complete and strongly adherent coating layer.[33] Due to the short

processing time, easy application and solvent-free nature, the dry coating process is a promising method for large-scale production at low costs.

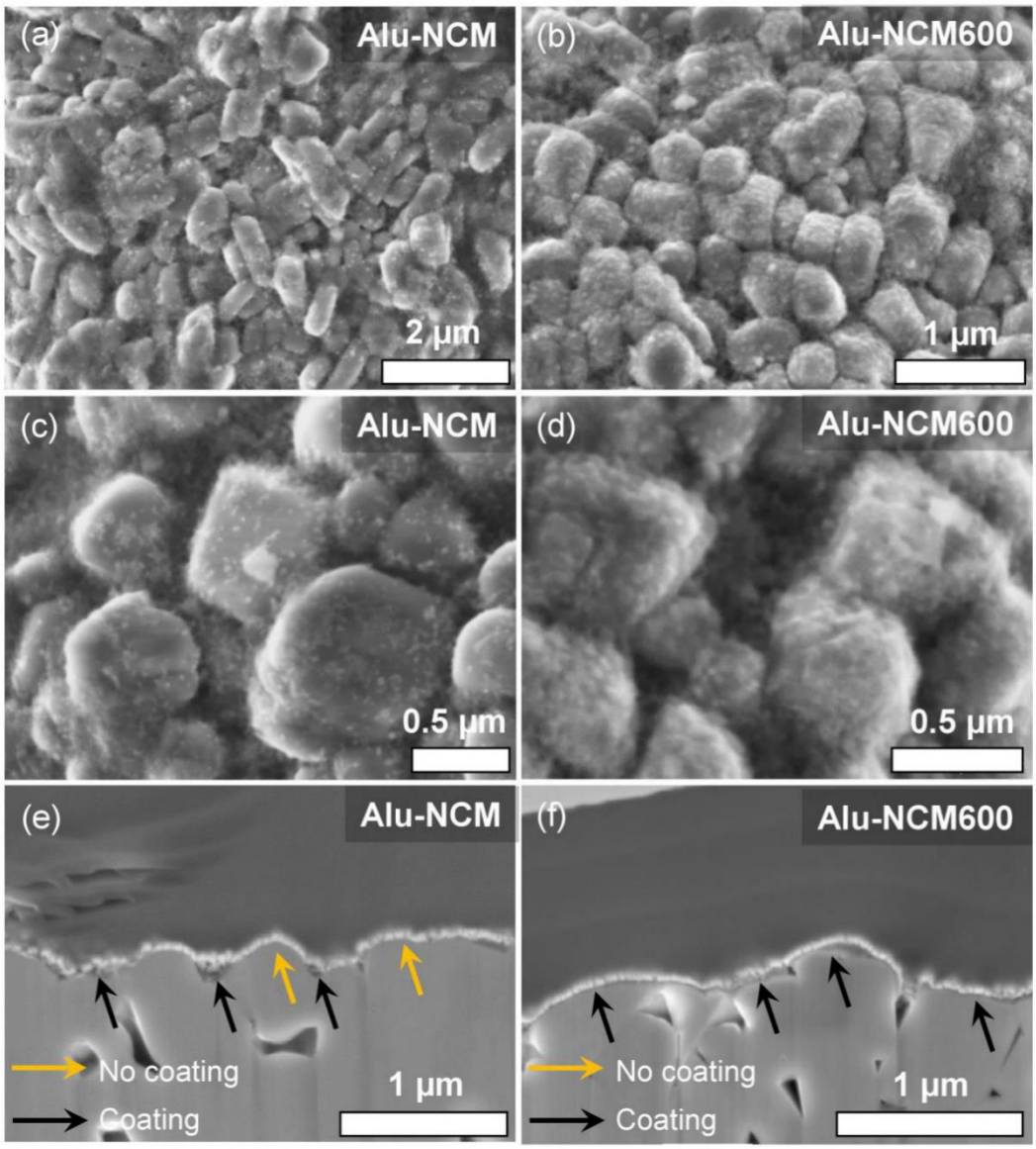

Figure 2. *SEM images of the coated NCM powder: (a, c) Alu-NCM and (b, d) Alu-NCM600. SEM cross-section images of coated NCM secondary particles: (e) Alu-NCM and (f) Alu-NCM600.*

The NCM-based CAM with an Al_2O_3 and $Al_2O_3/LiAlO_2$ coating layer was investigated by SEM. As shown in Figure S1, the secondary particles of the uncoated NCM are spherical in shape with a diameter of 5-15 µm composed of nano-sized primary particles. The SEM images in Figure 2 a) – d) show a comparison between Alu-NCM and Alu-NCM600. It can be seen that in both cases, the coated NCM reveals a narrow size distribution of the primary particles,

which agrees well with those of the uncoated NCM primary particles (see Figure S1). This indicates that the mixing intensity is strong enough to break the fumed Al_2O_3 agglomerates and to coat the secondary NCM particles while maintaining their structural integrity during the dry coating process.

However, the surface of non-annealed Alu-NCM shows significant differences compared to that of Alu-NCM600. After the coating, the Al_2O_3 looks inhomogeneously distributed with incomplete coverage of the NCM surface. In contrast, the coating seems to be fused after the annealing step, resulting in a very homogeneous and complete coverage of the NCM surface. FIB-SEM analysis was carried out to compare the cross-section of the NCM particles after coating and annealing. In Figure 2 e), the coating without annealing looks rough and is mainly accumulated in the gaps between neighboring primary NCM particles. However, as shown in Figure 2 f), the coating after annealing is much smoother and completely distributed over the surface, but the thickness varies slightly. Further SEM images of Alu-NCM and Alu-NCM600 with higher magnification are shown in Figure S2.

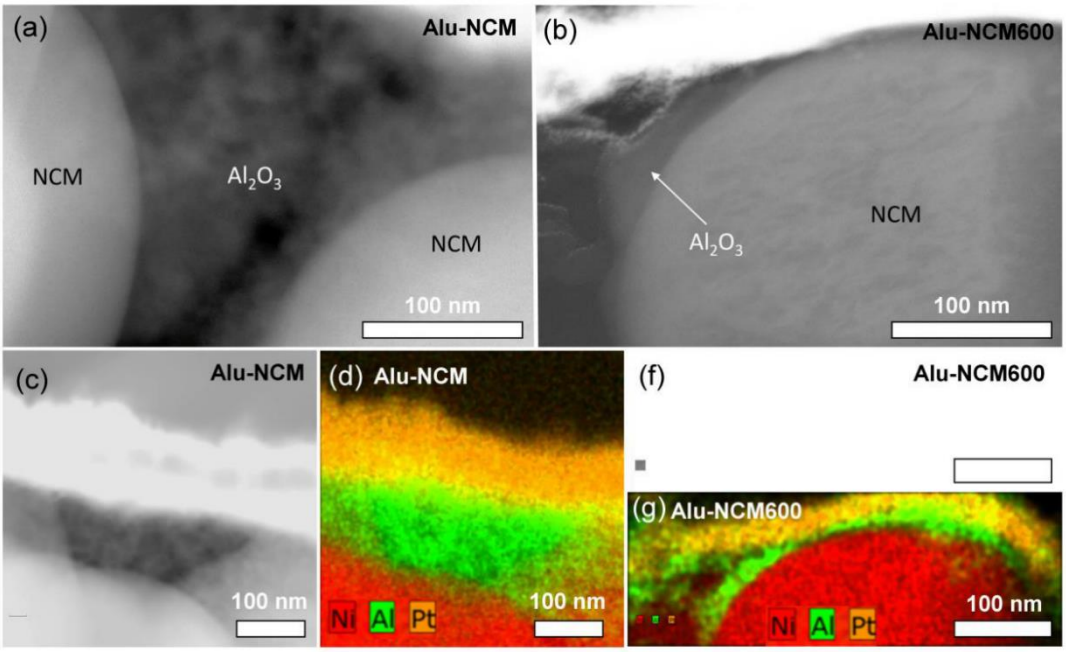

Figure 3. *TEM images of a cross-section of coated NCM701515: (a, c) Alu-NCM and (b, f) Alu-NCM600. STEM-EDS analysis of a cross-section of coated NCM701515 showing a three-color superposition image of Ni, Al, and Pt: (d) Alu-NCM and (g) Alu-NCM600.*

For a more detailed surface analysis, the microstructure of the coating layer was characterized by TEM in combination with EDS. As shown in Figure 3 a) and c), for Alu-NCM, the coating layer is highly porous as observed by M. Herzog et al.[33] Figure 3 a) shows that the gaps between

the primary NCM particles are completely filled with Al_2O_3, leaving the surface uncovered. On the other hand, in the case of Alu-NCM600 (Figure 3 b) and f)), the coating layer is less porous and much thinner after the annealing step. No structural changes of the NCM particles are observable. Only the structural properties of the coating are affected by the additional annealing step. EDS analysis confirms the drastic change of the coating thickness and porosity after annealing (Figure 3 d) and g)). As expected, there are no hints for the diffusion of aluminum into the CAM bulk phase observable for the non-annealed Alu-NCM sample, as no high-temperature step is involved in the coating process and aluminum diffusion is unlikely to occur at room temperature.[33] However, in case of Alu-NCM600 (Figure 3 g)) the possibility of inter-diffusion of a small Al amount into the CAM bulk structure during annealing cannot be excluded.[47] As reported in literature, the interdiffusion of Al between the CAM and the coating layer may enhance the overall stability of the CAM, and lead to improved cycling performance.[48] However, a detailed discussion of aluminum diffusion into the NCM bulk is beyond the scope of this study.

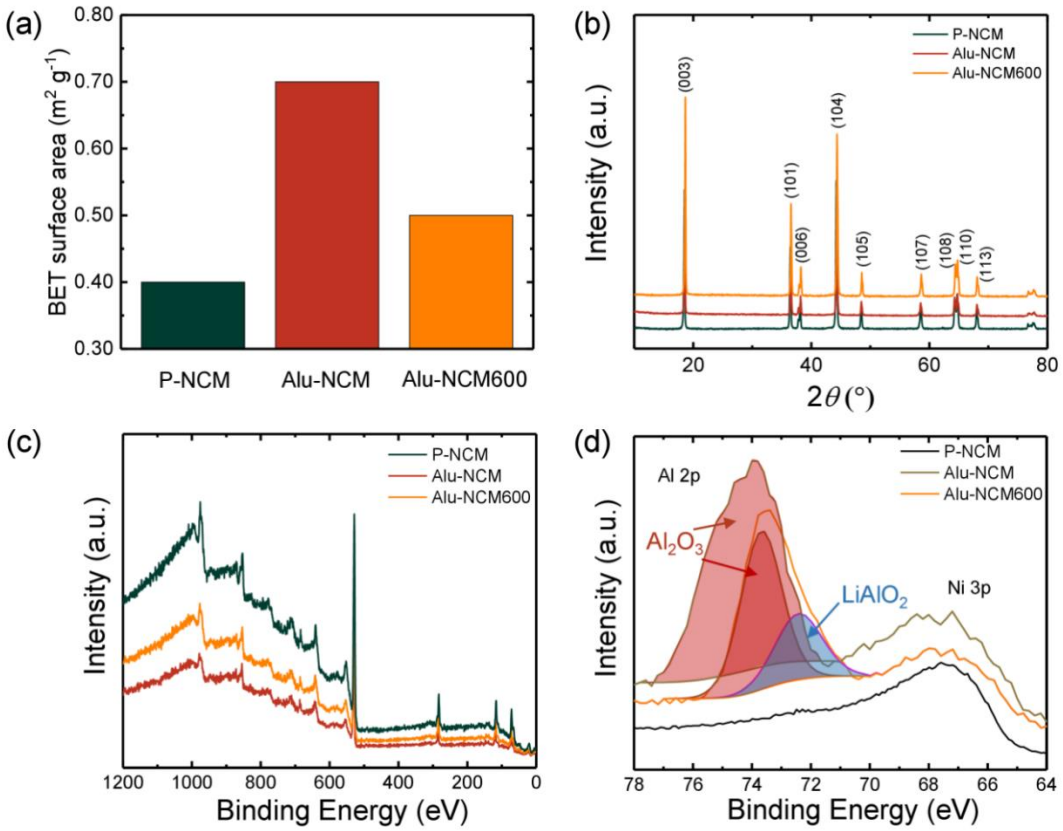

Figure 4. *Comparison of (a) Brunauer–Emmett–Teller (BET) measurements, (b) X-ray diffraction pattern, (c) survey XPS spectra, and (d) detailed XPS spectra of P-NCM, Alu-NCM, and Alu-NCM600.*

The porosity of the CAM particles after the coating was investigated by N_2 adsorption. The measurements were evaluated using the Brunauer–Emmett–Teller (BET) model. As shown in Figure 4 a), the uncoated NCM has a very low BET surface of 0.40 m^2 g^{-1}. After coating with fumed Al_2O_3, the BET surface area increases drastically to 0.70 m^2 g^{-1} (Alu-NCM sample), which is well expected due to the high porosity of the coating as observed by TEM measurements (Figure 3 c)). After the annealing step (Alu-NCM600 sample), the BET area is significantly decreased (0.50 m^2 g^{-1}). This confirms that the annealing step leads to a densification of the coating layer and a lower surface area.

Powder XRD measurements were carried out on P-NCM, Alu-NCM, and Alu-NCM600 samples to investigate the potential influence of the coating process on the crystal structure of NCM. As shown in Figure 4 b), the XRD patterns confirm that all NCM samples exhibit the same crystal structure of $LiCoO_2$ (space group *R*-3m). No peak shifts are observed, confirming that no significant bulk crystallographic defects are generated in the NCM structure during coating or the annealing step. In addition, both coated samples show no additional peaks belonging to Al_2O_3 due to the low amount of coating material, as observed in our previous study[38].

XPS measurements were carried out to investigate the coating composition and the effect of annealing on the structural properties of the coating layer. The NCM XPS analysis delivers quantitative element and compound-specific information with a detection limit of about 1 atom%.[49] The survey spectrum of P-NCM shown in Figure 4 c) confirms the presence of Ni, Co, Mn, and O without any additional elements apart from the carbon contamination at the NCM surface, which is commonly used as a calibration reference for XPS spectra.[50] In addition, the characteristic peak of Al 2p is detected on the surface of Alu-NCM and Alu-NCM600, which proves the existence of Al species on the surface of the coated NCM with Al_2O_3 (Figure 4 d). A detailed spectrum in the region between 78 and 64 eV is shown in Figure 4 d). It includes the Al 2p core levels and the Ni 3p peak. No peak shift is observed for the Ni 3p peak for all samples, which additionally confirms the structural stability of NCM during the coating and annealing processes. However, the presence of Ni implies that the coating is not completely covering the NCM surface or, alternatively, thinner than the typical probing depth of XPS of about 3 – 7 nm[51], as already indicated by the TEM measurements shown in Figure 3 f) and g). Deconvolution of the Al 2p peak (Figure 4 d)) reveals that Alu-NCM shows only one peak at a binding energy of 73.9 eV, which is distinctive for Al atoms in an oxygen environment, such as Al_2O_3 or $Al(OH)_3$.[34] However, after annealing a significant peak shift of Al 2p to lower binding energy is observed. The deconvolution confirms that the signal comprises two different

peaks. One at a binding energy 73.9 eV (corresponding to Al_2O_3 or $Al(OH)_3$)[51] and a second one at 72.8 eV, which is attributed to $LiAlO_2$ as observed by Tang et al.[52] The results confirm the conversion of an insulating Al_2O_3 coating into an ion conducting $Al_2O_3/LiAlO_2$ coating during heat treatment, as discussed in detail in previous studies.[38,39] The diffusion of Li^+ from NCM into the Al_2O_3 layer during the heat treatment is expected to result in the formation of conductive pathways for the Li^+ ions and thus an improvement of the ionic conductivity of the $Al_2O_3/LiAlO_2$ coating, as discussed in our previous study.[38]

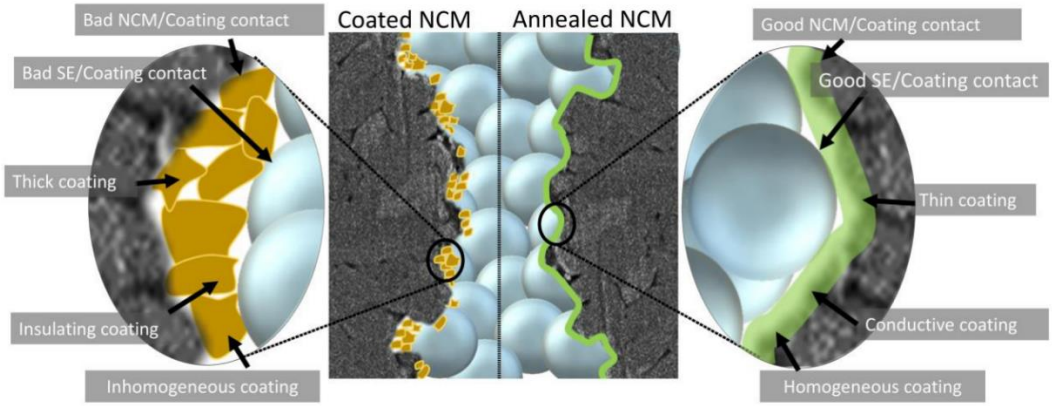

Figure 5. *Schematic representation comparing the differences in coating properties before and after annealing.*

The results reveal the tremendous effect of the annealing step on the structural properties of the coating layer, which are illustrated in Figure 5. The recently developed dry coating process enables the successful deposition of an Al_2O_3 coating on the surface of NCM particles. The coating is rather thick, porous, and inhomogeneous distributed on the surface of NCM. After annealing at 600 °C, various aspects of the coating morphology are improved. The coating becomes more homogenous (SEM, FIB-SEM), thinner (SEM, TEM), and exhibits a lower porosity, i.e., lower surface area as confirmed by TEM and BET. In addition, the diffusion of Li^+ into the coating results in the conversion from an insulating Al_2O_3 coating layer to $Al_2O_3/LiAlO_2$, which is known to exhibit an improved Li^+ conductivity. All these changes are expected to affect the electrochemical performance of NCM, as will be discussed in detail in the next section.

3.2. Electrochemical characterization

To elucidate the impact of the obtained microstructural and compositional differences of the two different coatings on the cell performance, we assembled and cycled ASSB cells at different

C-rates. The C-rate was varied between 0.1 C and 2 C, within the voltage window of 2.0 to 3.7 V (vs. In/InLi), exceeding the electrochemical stability window of thiophosphate-based SSEs (1.7- 2.3 V vs. Li^+/Li).[53] The rate capability tests and the long-term cycling stability were investigated for two independent cells in all three cases to ensure reproducibility of the results.

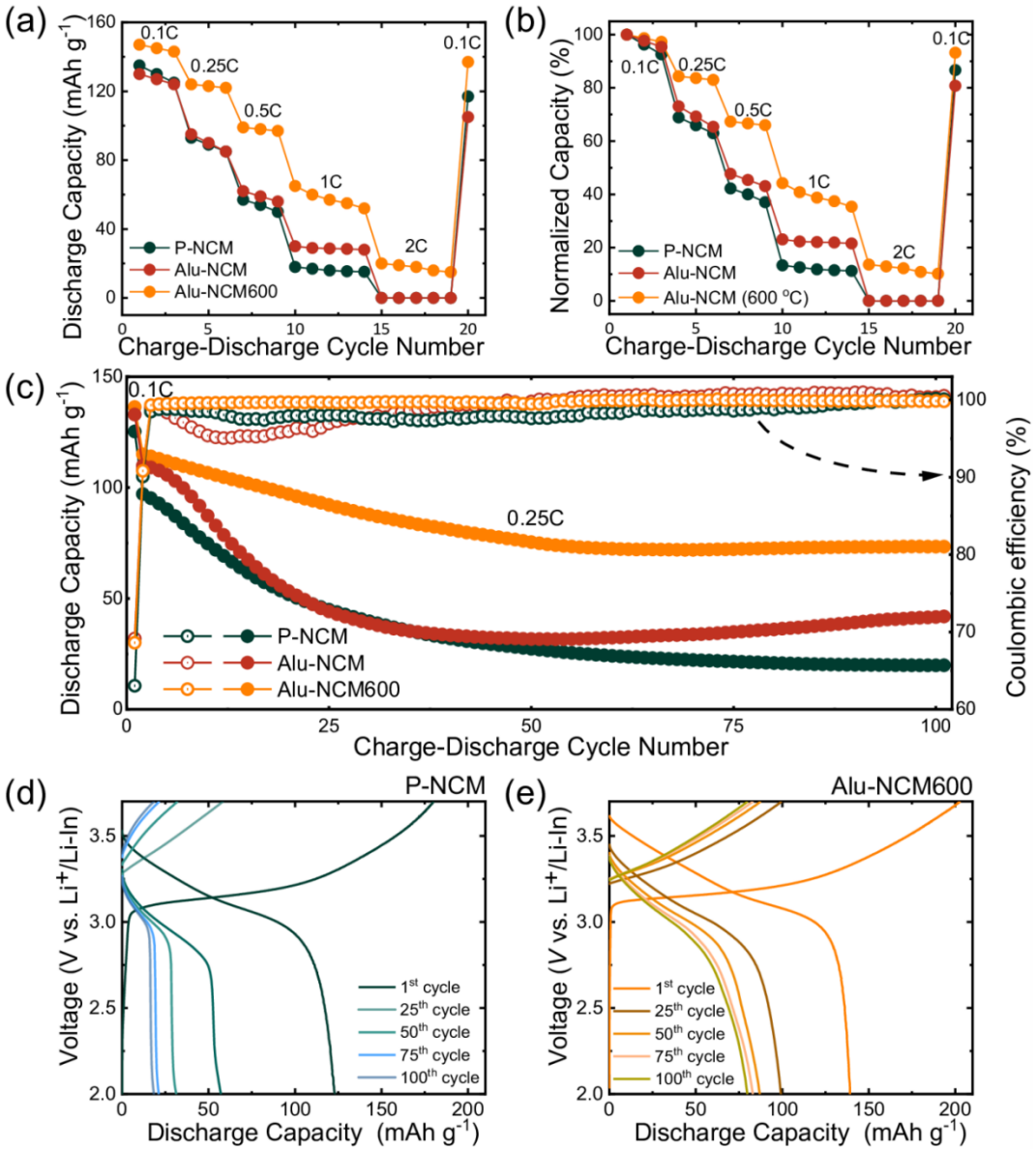

Figure 6. *Comparison of (a) rate capability and (b) corresponding normalized capacity plot of P-NCM, Alu-NCM, and Alu-NCM600. (c) Long-term cycling capability at 0.25 C of P-NCM, Alu-NCM, and Alu-NCM600. d), e) Charge-discharge voltage profiles of P-NCM and Alu-NCM600, respectively.*

Figure 6 a) shows the rate capability performance of the coated CAMs in comparison with the performance of the uncoated ones. For a better comparison, Figure 6 b) also shows the

normalized discharge capacity, i.e., the specific discharge capacity of each cell was normalized to the CAM mass and related to the initial specific discharge capacity. The initial specific discharge capacity of the P-NCM cells (136 mAh g^{-1}) is found significant lower compared to cells with liquid electrolytes (~180 mAh g^{-1})[33,38] indicating a higher interfacial degradation of the SSE than for cells with liquid electrolytes (as the achievable theoretical capacity of NCM is ~180 mAh g^{-1}) as reviewed by Jena et al.[54] The Alu-coated NCM material shows a slightly lower initial specific capacity (130 mAh g^{-1}) than the P-CAM. It indicates that the insulating nature of the Al_2O_3 coating along with its structural properties (such as porosity, insufficient contact area, interfacial degradation, etc.) limits the initial discharge capacity. In contrast, Alu-NCM600 shows a significantly higher initial specific discharge capacity (154 mAh g^{-1}). This is attributed to a lower interfacial resistance, either due to the higher Li^+ conductivity of the $Al_2O_3/LiAlO_2$ coating layer, an increased contact area, or improved interfacial stability (as discussed in the previous section). Furthermore, with increasing C-rate, the discharge capacity of Alu-NCM tends to be slightly superior to P-NCM, revealing the protective effect of the Al_2O_3 coating. However, at a C-rate of 2 C, both the P-NCM and the Alu-NCM samples exhibit no capacity, probably caused by a high internal cell resistance. However, a significant improvement of the C-rate performance in our ASSBs is observed for the Alu-NCM600 samples for all C-rate. In particular, Alu-NCM600 shows a discharge capacity of ~ 20 mAh g^{-1} even at 2 C. These results indicate that at high C-rates, a sufficient lithium-ion conductivity still persists in the $Al_2O_3/LiAlO_2$ coating layer, while in the case of the uncoated NCM, the formation of an insulating CEI caused by electrolyte degradation impedes lithium-ion exchange between electrode and electrolyte. Thus, the less porous and more conductive $Al_2O_3/LiAlO_2$ coating material in Alu-NCM600 enables a superior rate capability as compared to Al_2O_3-coated Alu-NCM samples. It is worth noting that the Al_2O_3-dry coating is very effective in improving the electrochemical performance of liquid electrolyte-based cells, as recently shown by Herzog et al.[33] One main reason is that the liquid electrolyte can penetrate into the highly porous Al_2O_3 coating, which facilitates the transport of lithium ions through the surface layer. In contrast, the solid electrolyte used in ASSBs is not able to reach the interior of the pores of the coating (Alu-NCM), i.e., the porous coating impedes lithium-ion transport between active material and electrolyte due to its insulating properties and the reduced contact area. Thus, the results highlight that effective coatings for ASSBs need to fulfill other demands regarding their structural properties than coatings used for liquid-electrolyte-based LIBs.

After the C-rate capability tests, the long-term cycling performance was investigated. Figure 6 c) compares the discharge capacity and the coulombic efficiency (CE) of pristine NCM, Alu-

NCM, and Alu-NCM600 for 100 cycles at 0.25 C in the voltage range between 2.0 and 3.7 V (vs. In/InLi). A significantly improved capacity retention is found for Alu-NCM600, which exhibits a discharge capacity of 75 mAh g^{-1} after 100 cycles implying capacity retention of 54% based on the first cycle capacity. In contrast, for the P-NCM sample, a capacity of only 25 mAh g^{-1}, i.e., capacity retention of 20%, is achieved. Furthermore, the corresponding CE of the Alu-NCM600 is superior compared to that of the uncoated sample. As shown in Figures 6 d) and e), the increase in overpotential is much higher for P-NCM than for Alu-NCM, indicating a more severe electrolyte degradation at the P-NCM surface. The Alu-NCM sample shows a similar behavior as P-NCM during long-term cycling. Although the Al_2O_3 coating certainly suppresses the electrolyte degradation at the NCM-electrolyte interface, its insulating nature, along with the rather worse coating properties, are responsible for a high interfacial resistance, which explains the poor cycling performance. However, the results confirm that the $Al_2O_3/LiAlO_2$ coating significantly improves the long-term cycle stability of NCM in ASSBs. The coating is expected to prevent side reactions between Li_6PS_5Cl and NCM, which lead to the formation of a highly resistive CEI consisting of sulfur and phosphorus pentasulfide oxidation products.[19]

To support this assumption, EIS measurements were carried out on ASSB cells containing P-NCM or Alu-NCM600 as EIS allows to distinguish between different processes in ASSBs and to determine their contribution to the total impedance of the cells.[15,16,55] As no drastic improvement of the cycling capability is found for the Alu-NCM samples, only P-NCM and Alu-NCM600 are investigated. The EIS measurements were performed at an open-circuit potential of 3.1 V (vs. In/InLi) after the 1st cycle and 100th cycle to determine the long-term impedance evolution. A constant potential step was included after constant-current discharge in order to achieve an equilibration of Li within the CAM particles by diffusion processes. This step is necessary to ensure comparability between P-NCM and Alu-NCM600 as the impedance of layered oxide cathode materials depends on the lithium content (SOC) of the electrode.[56] Comparing the impedance spectra after 1st and 100th cycles, displayed in Figure 7 a), a distinct increase of the impedance is observed for the pristine sample indicating a strong degradation reaction at the SSE/CAM interface due to the oxidation of the solid electrolyte.[16,21] The total impedance of the coated NCM cell is significantly lower after the 1st and 100th cycle, corroborating the protection function of the $Al_2O_3/LiAlO_2$ coating. The spectra were fitted using the transmission line model, which describes the impedance of porous electrodes considering SSE-filled pores.[57,58] Due to the presence of non-blocking conditions and negligible electronic conductivity, a Bisquert Open element[59] was used to fit the composite cathode impedance. The

equivalent circuit model, including the Bisquert open element, is described in more detail in Figure S3. The fitting reveals that the differences in the impedance are mainly caused by changes in the charge transfer resistance R_{CT}. The other fitting parameters, such as the anode contribution or the ionic resistance of the electrolyte, do not differ significantly for the different cells (see table S1 in the supporting information). The determined values of the charge transfer resistance R_{CT} after the 1st and 100th cycles for the pristine and coated samples are shown in Figure 7 b). As is evident, the charge transfer resistance of the Alu-NCM600-containing cell is significantly lower not only after the 1st but also after the 100th cycle. Moreover, the comparison with the other impedance values obtained from the fitting (Table S1) demonstrates that the impedance of the full cell is dominated by the charge transfer resistance of the composite cathode. The comparison of the R_{CT} values confirms that the $Al_2O_3/LiAlO_2$ coating layer significantly improves the interfacial stability by reducing oxidative interfacial decomposition of the SSE on the cathode side.

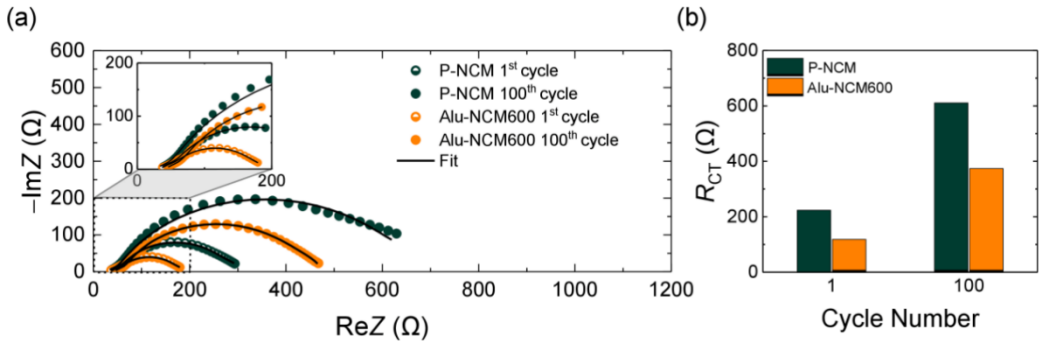

Figure 7. *Comparison of (a) Nyquist plots of the impedance of full cells containing P-NCM and Alu-NCM600 after the 1st and 100th cycle. (b) Corresponding charge transfer resistance R_{CT} measured at an open-circuit voltage of 3.1 V.*

4. Conclusions

In this study, we present a low-cost, straightforward and scalable dry coating process to modify the surface of Ni-rich NCM for thiophosphate-based ASSBs. A highly efficient $Al_2O_3/LiAlO_2$ coating is achieved by a high-energy mixing process followed by a high-temperature annealing step. While the Al_2O_3 coating shows a certain porosity after the coating process, the annealing step results in the formation of a dense and thin coating layer as confirmed by TEM and BET measurements. Furthermore, XPS analysis confirms that a mixed $Al_2O_3/LiAlO_2$ layer is formed during the heat treatment, while no significant changes in bulk NCM are observed. Electrochemical characterization demonstrates that the $Al_2O_3/LiAlO_2$ coating significantly

improves the electrochemical performance of NCM cathodes in LPS-based ASSBs. As the coating prevents the direct contact between CAM and thiophosphate-based SSE, interfacial degradation reactions responsible for the formation of an insulating CEI are reduced, as demonstrated by EIS analysis. Compared to the porous Al_2O_3 coating, the Al_2O_3/$LiAlO_2$ coating layer provides an improved rate capability and long-term cycling performance, including higher initial cycling capacity. Thus, the results present a highly effective dry coating method, which is suitable for large-scale processing of cathodes for next-generation ASSBs, excluding any solvent-related influences and costs.

Supporting Information

SEM images of pristine and coated samples, the equivalent circuit used for fitting after the first and 100^{th} cycle.

AUTHOR INFORMATION

=These authors contributed equally to this work

Corresponding Authors

*Email:
Matthias.elm@phys.chemie.uni-giessen.de (M. T. Elm)
Anja.Henss@phys.chemie.uni-giessen.de (A. Henss)
Ruijun.Pan@phys.chemie.uni-geissen.de (R. Pan)

Notes

The authors declare no competing financial interests.

Acknowledgments

R.S.N. and M.T.E. thank the German Federal Ministry of Education and Research (BMBF) for the funding of the NanoMatFutur project NiKo (03XP0093). S.A. and K.V. acknowledge the Federal Ministry of Education and Research (BMBF, Germany) within the cluster of competence FESTBATT (project 03XP0176D).

5. References

[1] G. E. Blomgren, *J. Electrochem. Soc.* **2017**, *164*, A5019-A5025.

[2] D. Liu, W. Zhu, Z. Feng, A. Guerfi, A. Vijh, K. Zaghib, *Mater. Sci. Eng. B* **2016**, *213*, 169.

[3] Y. Kato, S. Hori, T. Saito, K. Suzuki, M. Hirayama, A. Mitsui, M. Yonemura, H. Iba, R. Kanno, *Nat. Energy* **2016**, *1,* 16030.

[4] J. Janek, W. G. Zeier, *Nat. Energy* **2016**, *1,* 16141.

[5] J. M. Tarascon, M. Armand, *Nature* **2001**, *414*, 359.

[6] S. Ramakumar, C. Deviannapoorani, L. Dhivya, L. S. Shankar, R. Murugan, *Prog. Mater. Sci.* **2017**, *88*, 325.

[7] M. Monchak, T. Hupfer, A. Senyshyn, H. Boysen, D. Chernyshov, T. Hansen, K. G. Schell, E. C. Bucharsky, M. J. Hoffmann, H. Ehrenberg, *Inorg Chem* **2016**, *55*, 2941.

[8] N. Kamaya, K. Homma, Y. Yamakawa, M. Hirayama, R. Kanno, M. Yonemura, T. Kamiyama, Y. Kato, S. Hama, K. Kawamoto, A. Mitsui, *Nat. Mater.* **2011**, *10*, 682.

[9] T. Krauskopf, F. H. Richter, W. G. Zeier, J. Janek, *Chem. Rev.* **2020**, *120*, 7745.

[10] M. Bertrand, S. Rousselot, D. Aymé-Perrot, M. Dollé, *Mater. Adv.* **2021**, *2*, 2989.

[11] J.-H. Seo, H. Nakaya, Y. Takeuchi, Z. Fan, H. Hikosaka, R. Rajagopalan, E. D. Gomez, M. Iwasaki, C. A. Randall, *J. Eur. Ceram. Soc.* **2020**, *40*, 6241.

[12] A. Kim, S. Woo, M. Kang, H. Park, B. Kang, *Front. Chem.* **2020**, *8*, 468.

[13] S. V. Patel, S. Banerjee, H. Liu, P. Wang, P.-H. Chien, X. Feng, J. Liu, S. Ping Ong, Y.-Y. Hu, *Chem. Mater.* **2021**, *33*, 1435.

[14] M. Shoji, E. Jianfeng Cheng, T. Kimura, K. Kanamura, *J. Phys. D: Appl. Phys.* **2019**, *52*, 103001.

[15] W. Zhang, D. A. Weber, H. Weigand, T. Arlt, I. Manke, D. Schröder, R. Koerver, T. Leichtweiss, P. Hartmann, W. G. Zeier, J. Janek, *ACS Appl. Mater. Interfaces* **2017**, *9*, 17835.

[16] R. Koerver, I. Aygün, T. Leichtweiß, C. Dietrich, W. Zhang, J. O. Binder, P. Hartmann, W. G. Zeier, J. Janek, *Chem. Mater.* **2017**, *29*, 5574.

[17] P. Zou, Z. Lin, M. Fan, F. Wang, Y. Liu, X. Xiong, *Appl. Surf. Sci.* **2020**, *504*, 144506.

[18] X. Li, W. Peng, R. Tian, D. Song, Z. Wang, H. Zhang, L. Zhu, L. Zhang, *Electrochim. Acta* **2020**, *363*, 137185.

[19] D. H. S. Tan, E. A. Wu, H. Nguyen, Z. Chen, M. A. T. Marple, J.-M. Doux, X. Wang, H. Yang, A. Banerjee, Y. Shirley Meng, *ACS Energy Lett.* **2019**, *4*, 2418.

[20] S. Wang, R. Fang, Y. Li, Y. Liu, C. Xin, F. H. Richter, C.-W. Nan, *J. Materiomics* **2021**, *7*, 209.

[21] F. Walther, R. Koerver, T. Fuchs, S. Ohno, J. Sann, M. Rohnke, W. G. Zeier, J. Janek, *Chem. Mater.* **2019**, *31*, 3745.

[22] J. Zhang, H. Zhong, C. Zheng, Y. Xia, C. Liang, H. Huang, Y. Gan, X. Tao, W. Zhang, *J. Power Sources* **2018**, *391*, 73.

[23] K. Takada, N. Ohta, L. Zhang, K. Fukuda, I. Sakaguchi, R. Ma, M. Osada, T. Sasaki, *Solid State Ion.* **2008**, *179*, 1333.

[24] S. Yubuchi, S. Teragawa, K. Aso, K. Tadanaga, A. Hayashi, M. Tatsumisago, *J. Power Sources* **2015**, *293*, 941.

[25] S. Ito, S. Fujiki, T. Yamada, Y. Aihara, Y. Park, T. Young Kim, S.-W. Baek, J.-M. Lee, S. Doo, N. Machida, *J. Power Sources* **2014**, *248*, 943.

[26] D. Kitsche, Y. Tang, Y. Ma, D. Goonetilleke, J. Sann, F. Walther, M. Bianchini, J. Janek, T. Brezesinski, *ACS Appl. Energy Mater.* **2021**.
[27] Y.-Q. Zhang, Y. Tian, Y. Xiao, L. J. Miara, Y. Aihara, T. Tsujimura, T. Shi, M. C. Scott, G. Ceder, *Adv. Energy Mater.* **2020**, *10*, 1903778.
[28] J. Cho, Y. Jeong Kim, B. Park, *Chem. Mater.* **2000**, *12*, 3788.
[29] J.-Y. Liao, A. Manthiram, *J. Power Sources* **2015**, *282*, 429.
[30] R. S. Negi, S. P. Culver, A. Mazilkin, T. Brezesinski, M. T. Elm, *ACS Appl. Mater. Interfaces* **2020**, *12*, 31392.
[31] R. S. Negi, S. P. Culver, M. Wiche, S. Ahmed, K. Volz, M. T. Elm, *Phys. Chem. Chem. Phys.* **2021**, *23*, 6725.
[32] L. Liu, *Solid State Ion.* **2002**, *152-153*, 341.
[33] M. J. Herzog, N. Gauquelin, D. Esken, J. Verbeeck, J. Janek, *Energy Technol.* **2021**, *9*, 2100028.
[34] W. Zhu, X. Huang, T. Liu, Z. Xie, Y. Wang, K. Tian, L. Bu, H. Wang, L. Gao, J. Zhao, *Coatings* **2019**, *9*, 92.
[35] X. Wen, K. Liang, L. Tian, K. Shi, J. Zheng, *Electrochim. Acta* **2018**, *260*, 549.
[36] X. Li, J. Liu, M. Norouzi Banis, A. Lushington, R. Li, M. Cai, X. Sun, *Energy Environ. Sci.* **2014**, *7*, 768.
[37] A. Garcia, *Solid State Ion.* **1990**, *40-41*, 13.
[38] R. S. Negi, E. Celik, R. Pan, R. Stäglich, J. Senker, M. T. Elm, *ACS Appl. Energy Mater.* **2021**, *4*, 3369.
[39] B. Han, T. Paulauskas, B. Key, C. Peebles, J. Sun Park, R. F. Klie, J. T. Vaughey, F. Dogan, *ACS Appl. Mater. Interfaces* **2017**, *9*, 14769.
[40] G. Oh, M. Hirayama, O. Kwon, K. Suzuki, R. Kanno, *Chem. Mater.* **2016**, *28*, 2634.
[41] J. Ha Woo, J. E. Trevey, A. S. Cavanagh, Y. Seok Choi, S. Cham Kim, S. M. George, K. Hwan Oh, S.-H. Lee, *J. Electrochem. Soc.* **2012**, *159*, A1120-A1124.
[42] K. Takada, N. Ohta, L. Zhang, X. Xu, B. Thi Hang, T. Ohnishi, M. Osada, T. Sasaki, *Solid State Ion.* **2012**, *225*, 594.
[43] S. P. Culver, R. Koerver, W. G. Zeier, J. Janek, *Adv. Energy Mater.* **2019**, *9*, 1900626.
[44] W. Blake Hawley, J. Li, *J. Energy Storage* **2019**, *25*, 100862.
[45] R. L. Puurunen, *J. Appl. Physics* **2005**, *97*, 121301.
[46] C. Geng, S. Trussler, M. B. Johnson, N. Zaker, B. Scott, G. Botton, J. R. Dahn, *J. Electrochem. Soc.* **2020**, *167*, 110509.
[47] B. Han, B. Key, S. H. Lapidus, J. C. Garcia, H. Iddir, J. T. Vaughey, F. Dogan, *ACS Appl. Mater. Interfaces* **2017**, *9*, 41291.
[48] T. Teranishi, Y. Yoshikawa, M. Yoneda, A. Kishimoto, J. Halpin, S. O'Brien, M. Modreanu, I. M. Povey, *ACS Appl. Energy Mater.* **2018**, *1*, 3277.
[49] S.-K. Otto, Y. Moryson, T. Krauskopf, K. Peppler, J. Sann, J. Janek, A. Henss, *Chem. Mater.* **2021**, *33*, 859.
[50] de Fang, F. He, J. Xie, L. Xue, *J. Wuhan Univ. Technol. Mater. Sci. Edit.* **2020**, *35*, 711.
[51] H. Hemmelmann, J. K. Dinter, M. T. Elm, *Adv. Mater. Interfaces* **2021**, *8*, 2002074.
[52] W. Tang, Z. Chen, F. Xiong, F. Chen, C. Huang, Q. Gao, T. Wang, Z. Yang, W. Zhang, *J. Power Sources* **2019**, *412*, 246.
[53] Y. Zhu, X. He, Y. Mo, *ACS Appl. Mater. Interfaces* **2015**, *7*, 23685.
[54] A. Jena, Y. Meesala, S.-F. Hu, H. Chang, R.-S. Liu, *ACS Energy Lett.* **2018**, *3*, 2775.
[55] R.S. Negi, P. Minnmann, R. Pan, S. Ahmed, M. Herzog, K. Volz , R. Takata, F. Schmidt, J. Janek, M.T. Elm, *Chem. Mater.* **2021**, *Stabilizing the cathode/electrolyte*

interface using a novel dry-processed lithium titanate coating for all-solid-state-batteries, under review.
[56] R. Pan, D. Rau, Y. Moryson, J. Sann, J. Janek, *ACS Appl. Energy Mater.* **2020**, *3*, 6065.
[57] J. Moškon, M. Gaberšček, *J. Power Sources Advances* **2021**, *7*, 100047.
[58] N. Ogihara, S. Kawauchi, C. Okuda, Y. Itou, Y. Takeuchi, Y. Ukyo, *J. Electrochem. Soc.* **2012**, *159*, A1034-A1039.
[59] J. Bisquert, *Phys. Chem. Chem. Phys.* **2000**, *2*, 4185.

4. Conclusion and Outlook

Ni-rich NCM based cathodes are considered as one of the most promising cathode materials for next-generation LIBs. However, they suffer from fast capacity fading during electrochemical cycling due to an unstable interface in contact with the electrolyte. Modification of the cathodes via surface coating has shown promising results in mitigation of the undesired side reactions happening at the electrode-electrolyte interface. Since, the commonly applied coating methods are very complicated, costly, and time-consuming, the development of an easy, scalable, cheap and time-effective coating method is necessary in order to successfully use Ni-rich NCM in next-generation LIBs. In addition, a detailed understanding of the beneficial effect of the coating layer is still incomplete. Therefore, a comprehensive understanding of the ongoing mechanisms of the coating is necessary in order to optimize the properties of effective coatings for LIBs.

Thus, in this thesis, different simple and effective powder coating techniques for Ni-rich NCM based cathodes have been developed, which all improved the electrochemical performance of LIBs. In addition, detailed investigations have been performed on the coated NCM (before/after cycling), in order to elucidate the working principle of the coating layer during electrochemical cycling.

Three different types of coating methods (wet-chemical, ALD and dry-coating) have been developed during the course of this thesis. It is found that homogenous coating can also be achieved via a wet-chemical coating method. ALD-based coatings are found to be beneficial for coating ready-to-use cathodes, due to low coating temperature. Dry-process coating methods have also been successfully developed for NCM based coating powder, resulting in a very porous coating layer. It has been concluded that the most important physical parameter influencing the long-term cycling performance is the homogeneity of the coating layer and coating composition. In addition, post-annealing of the metal oxide coating is found beneficial for electrochemical performance of coated cathodes for bot LIBs and ASSBs.

Although various coating materials (Al_2O_3, CeO_2, TiO_2, $LiAlO_2$, $Li_4Ti_5O_{12}$, etc.) have been tested, yet the most suitable coating material has not been agreed upon for NCM based cathodes. Thus, keeping that in mind, in this thesis various coating materials (Al_2O_3, $LiAl_2O_3$ and $Li_4Ti_5O_{12}$) have been successfully coated and tested on NCM cathodes. All of these materials improved electrochemical performance of NCM based cathodes. In addition, influence of the post-heat treatment on the Al_2O_3 based coating and subsequently on the electrochemical performance of the NCM has been investigated and explained.

Although all the developed coating methods improved electrochemical performance, the best electrochemical performance in terms of C-rate performance, as well as long-term cycling, is achieved via lithiated metal oxide coatings on the NCM cathodes for LIBs as well as ASSBs. The result shows that lithiated metal oxide coatings could play a key role in commercialization of NCM based cathodes in next-generation LIBs.

In conclusion, various developed coating processes during this Ph.D. thesis are found to be very effective methods to protect the direct physical contact between the electrode and electrolyte, thus preventing the parasitic side reaction and improving the electrochemical

performance of NCM based cathodes. All these coating processes are very simple, fast, practical and easily scalable, as well as energy and cost-effective. In addition, all of these coating methods can be transferred to any type of NCM-based cathode. The developed dry-process coating method can also be transferred to various coating materials (e.g. TiO_2, ZrO_2). In addition, lithiated metal oxide coating has been found superior over metal oxide analog in terms of electrochemical performance. Thus, all these results in combination provide a solid base for further future research on coating or Ni-rich NCM.

In order to unveil the mechanism of how the metal oxide coatings (Al_2O_3, TiO_2) transport Li-ion during cycling, further in-depth investigations on structural properties of the coating layer and cathode are necessary. Furthermore, effect of surface impurities (e.g. LiOH, Li_2CO_3, Li_2O) on the performance of the coating layer should be studied, by coating and analyzing fresh and aged NCM. To prevent the formation of surface impurities after the coating process, all steps of coating procedure should be performed inside inert gas atmosphere. Furthermore, it should also be investigated if chemical reactions take place between the coating layer and the surface during the post-annealing step and how it affects the electrochemical performance of LIBs. In addition, further analysis is needed to elucidate if electrochemical reactions between coating and NCM take place during cycling These reactions may result in a conversion of the coating layer, which is not investigated yet.

The developed coating approaches may be transferred to other potential cathodes (e.g. Lithium-rich layered oxides (LLOs)) that can meet the high demands of next-generation LIBs. Surface coatings have already been found to improve the electrochemical performance of LLOs based cathodes. However, the exact mechanism regarding how the coating layer works is still under debate. Thus, it would be very interesting to investigate the influence of these rather simple coating methods on the cycling performance of LLOs based cathodes. If the coating process is successful and mitigates the deficiencies of LLOs based cathodes, the developed coating methods can definitely help in the commercialization of next-generation LIBs.

In addition, lithiated metal oxide coating agents also show promising results for cathodes in ASSBs. ASSBs are considered as an alternative for conventional liquid electrolyte-based LIBs. However, several issues need to be addressed before their successful commercialization. One issue that remains constant for both liquid and solid-state batteries is the highly reactive surface of the cathode. Thus, different concepts of surface modification successfully applied in LIBs may be transferred to ASSB. Initial investigation has already shown promising results in improving the electrochemical performance of the cathodes in ASSBs. However, more in-depth analysis is still needed to fully develop and understand the coatings for ASSBs.

5. References

1) J. B. Goodenough, K. S. Park, Journal of American Chemical Society 135 (2013) 1167 1176.

2) Greenband, Greenband: http://www.greenbang.com/peak-water-worries-energy-experts_22514.html (2013).

3) D. Mohindra, World Economic Forum: http://www.weforum.org/news/despite-rise-renewables-fossil-fuel-still-fastest-growing-energy-source?news=page (2013).

4) M. Caine, http://theenergycollective.com/markecaine/173971/new-energy-sources-possibilities-and-prospects (2013).

5) D. Johnson, SPIE: http://spie.org/x93835.xml (2013).

6) B. Scrosati, Nature 373 (1995), 557-558.

7) J.-M. Tarascon and M. Armand, Nature 414 (2001) 359-367. 39

8) J. B. Goodenough and Y. Kim, Chem. Mater. 22 (2010) 587-603.

9) J. B. Goodenough, Acc. Chem. Res. 46 (2013) 1053-1061.

10) Y. Nishi, Chem. Rec 1 (2001) 406-413.

11) H. H. Cheng, F. M. Wang, J. P. Chu, R. Santhanam, J. Rick, S. C. Lo, J. Phys. Chem. C 116 (2012) 7629−7637.

12) X. Wang, Z. Feng, J. Huang, W. Deng, X. Li, H. Zhang, Z. Wen, Carbon 127 (2018) 149−157

13) W. Zhang, F. H. Richter, S. P. Culver, T. Leichtweiss, J. G. Lozano, C. Dietrich, P. G. Bruce, W. G. Zeier, J. Janek, ACS Appl. Mater. Interfaces 10 (2018) 22226−22236.

14) Y. G. Zhu, Y. Du, C. Jia, M. Zhou, L. Fan, X. Wang, Q. Wang, J. Am. Chem. Soc. 139 (2017) 6286−6289.

15) G. Saat, F. M. Balci, E. P. Alsac, F. Karadas, O. Dag, Small 14 (2018) 1701913.

16) L. Ben, H. Yu, B. Chen, Y. Chen, Y. Gong, X. Yang, L. Gu, X. Huang, ACS Appl. Mater. Interfaces 9 (2017) 35463−35475.

17) L. Croguennec and M. R. Palacin, J. Am. Chem. Soc. 137(2015) 3140–3156.4

18) K. Edstrom, T. Gustafsson and J. O. Thomas, Electrochim. Acta 50 (2004) 397–403

19) D. Andre, S. J. Kim, P. Lamp, S. F. Lux, F. Maglia, O. Paschos, B. Stiaszny, J. Mater. Chem. A 3 (2015) 6709− 6732.

20) S. Myung, F. Maglia, K. Park, C. Yoon, P. Lamp, S. Kim, K. Sun, ACS Energy Lett. 2 (2017) 196−223.

21) D. Radin, S. Hy, M. Sina, C. Fang, H. Liu, J. Vinckeviciute, M. Zhang, M. Whittingham, Y. Meng, A. Van der Ven, Adv. Energy Mater. 7 (2017) 1602888.

22) R. Jung, R. Morasch, P. Karayaylali, K. Phillips, F. Maglia, C. Stinner, Y. Shao-Horn, A. Gasteiger, J. Electrochem. Soc. 165 (2018), 165, A132−A141.

23) H. Konishi, T. Yuasa, M. Yoshikawa, J. Power Sources 196 (2011) 6884−6888.

24) H. Cho, C. Jo, W. Cho, Y. Kim, H. Yashiro, Y. Sun, S. Myung , J. Electrochem. Soc. 161 (2014) A920−A926.

25) L. Wu, K. Nam, X. Wang, Y. Zhou, J. Zheng, X. Yang, Y. Zhu, Chem. Mater. 23 (2011) 3953−3960.

26) J. Noh, S. Youn, C. Yoon, Y. Sun, J. Power Sources 233 (2013) 121−130.

27) D. Cho, C. Jo, W. Cho, Y. Kim, H. Yashiro, Y. Sun, S. Myung, J. Electrochem. Soc. 161 (2014) A920−A926.

28) J. Shi, D. Xiao, M. Ge, X. Yu, Y. Chu, X. Huang, X. Zhang, Y. Yin, X. Yang, Y. Guo, L. Gu, L. Wan, Adv. Mater. 30 (2018) 1705575.

29) J. Shi, D. Xiao, X. Zhang, Y. Yin, Y. Guo, L. Gu, L. Wan, Nano Res. 10 (2017) 4201−4209.

30) J. Lee, F. Wang, C. Cheng, C. Li, C. Lin, Electrochim. Acta 55 (2010), 55, 4002−4006.

34) X. Zhang, I. Belharouak, L. Li, Y. Lei, J. Elam, A.Nie, X. Chen, R. Yassar, R.. Axelbaum, R. L., Adv. Energy Mater. 3 (2013) 1299−1307.

31) S. Neudeck, F. Strauss, G. Garcia, H. Wolf, J. Janek, P. Hartmann, T. Brezesinski, Chem. Commun. 55 (2019) 2174−2177.

33) Y. Chen, Y. Zhang, B. Chen, Z. Wang, C. Lu, J. Power Sources 256 (2014) 20−27.

32) S. Neudeck, F. Walther, T. Bergfeldt, C. Suchomski, M. Rohnke, P. Hartmann, P.; J. Janek, T. Brezesinski, ACS Appl. Mater. Interfaces 10 (2018) 20487−20498.

35) Wikipedia, The Free Encyclopedia, http://en.wikipedia.org/wiki/Lithium-ion_battery (2013).

36) M. Armand, J.-M. Tarascon, Nature 451 (2008) 652–657.

37) K. Ozawa, Solid State Ionics 69 (1994) 212–221.

38) M. C. Yang, Strategies to Improve the Electrochemical Performance of Li-Ion

Batteries, Dissertation, University of Floride (2012).

39) P. Guan, L. Zhou, Z. Yu, Y. Sun, Y. Liu, F. Wu, Y. Jiang, D. Chu, J. Energy Chem.

43 (2020) 220–235.

40) B. Xu, D. Qian, Z. Wang, Y. S. Meng, Mater. Sci. Eng. R Rep. 73 (2012) 51–65.

41) L.-X. Yuan, Z.-H. Wang, W.-X. Zhang, X.-L. Hu, J.-T. Chen, Y.-H. Huang, J. B.

Goodenough, Energy Environ. Sci. 4 (2011) 269–284.

42) R. A. Adams, A. Varma, V. G. Pol, Adv. Energy Mater. 9 (2019) 1900550.

43) T. Placke, R. Kloepsch, S. Dühnen, M. Winter, J. Solid State Electrochem. 21 (2017) 1939–1964.

44) S.-I. Lee, U.-H. Jung, Y.-S. Kim, M.-H. Kim, D.-J. Ahn, H.-S. Chun, Korean J. Chem.

Eng. 19 (2002) 638–644.

45) S. G. Stewart, J. Newman, J. Electrochem. Soc. 155 (2008) F13.

46) H. Hesse, M. Schimpe, D. Kucevic, A. Jossen, Energies 10 (2017) 2107.

47) S. Liang, W. Yan, X. Wu, Y. Zhang, Y. Zhu, H. Wang, Y. Wu, Solid State Ion. 318 (2018) 318, 2–18.

48) B. Xu, D. Qian, Z. Wang, Y. S. Meng, Mater. Sci. Eng. R Rep. 73 (2012) 51–65.

49) V. Ramadesigan, P. W. C. Northrop, S. De, S. Santhanagopalan, R. D. Braatz, V. R.

Subramanian, J. Electrochem. Soc. 159 (2012) R31–R45.

50) D. Aurbach, J. Power Sources 89 (2000) 206–218.

51) N. Nitta, F. X. Wu, J. T. Lee and G. Yushin, Mater. Today 18 (2015) 252-264.

52) J. Cabana, L. Monconduit, D. Larcher and M. R. Palacin, Adv. Mater. 22 (2010), E170-192.

53) M. S. Whittingh, Lithium Batteries and Cathode Materials. Chemical Reviews 104 (2004) 4271-4301.

54) N. H. Kwon, J. Conder, M. Srout, K. M. Fromm, Chim. Int. J. Chem. 73 (2019) 880–893.

55) C. Julien, A. Mauger , A. Vijh , K. Zaghib, Springer, Cham (2016) 201–268.

56) J. Xu, S. Dou, H. Liu, L. Dai, Nano Energy 2 (2013) 439 442

57) X. Wang, Y. Ding,Y. Deng, Z. Chen, Advanced Energy Materials 10 (2020) 1903864

58) J. M. Tarascon and M. Armand, Nature 414 (2001) 359-367.

59) M. R. Palacin, Chem. Soc. Rev. 38 (2009) 2565-2575.

60) P. G. Bruce, B. Scrosati and J. M. Tarascon, Angew. Chem. Int. Ed. 47 (2008) 2930-2946.

61) K. T. Lee, S. Jeong and J. Cho, Acc. Chem. Res. 46 (2013) 1161-1170.

62) M. S. Islam and C. A. Fisher Chem. Soc. Rev. 43 (2014) 185-204.

63) W. Liu, P. Oh, X. Liu, M.-J. Lee, W. Cho, S. Chae, Y. Kim, J. Cho, Angew. Chem. Int. Ed.54 (2015) 4440–4457.

64) A. Mauger, C. Julien, Ionics 20 (2014) 751–787.

65) L. de Biasi, B. Schwarz, T. Brezesinski, P. Hartmann, J. Janek, H. Ehrenberg, Adv. Mater. 2019, 31, 1900985.

66) G. E. Blomgren, J. Electrochem. Soc. 164 (2017) A5019–A5025.

67) X. Xiong, Z. Wang, G. Yan, H. Guo, X. Li, J. Power Sources 245 (2014) 183–193.

68) L. de Biasi, A. O. Kondrakov, H. Geßwein, T. Brezesinski, P. Hartmann, J. Janek, J. Phys. Chem. C 2017, 121, 26163–26171.

69) S.-K. Jung, H. Gwon, J. Hong, K.-Y. Park, D.-H. Seo, H. Kim, J. Hyun, W. Yang, K.

Kang, Adv. Energy Mater. 4 (2014) 1300787.

70) K.-S. Lee, S.-T. Myung, K. Amine, H. Yashiro, Y.-K. Sun, J. Electrochem. Soc. 154 (2007), A971.

71) B. Wu, J. Bi, Q. Liu, D. Mu, L. Wang, J. Fu, F. Wu, Electrochimica Acta 298 (2019) 609–615.

72) S.-M. Bak, E. Hu, Y. Zhou, X. Yu, S. D. Senanayake, S.-J. Cho, K.-B. Kim, K. Y. Chung, X.-Q. Yang, K.-W. Nam, ACS Appl. Mater. Interfaces 2014, 6, 22594–22601.

73) T. Li, X.-Z. Yuan, L. Zhang, D. Song, K. Shi, C. Bock, Electrochem. Energ. Rev. 2020, 3, 43–80.

74) J. Zheng, P. Yan, J. Zhang, M. H. Engelhard, Z. Zhu, B. J. Polzin, S. Trask, J. Xiao, C. Wang, J. Zhang, Nano Res. 10 (2017) 4221–4231.

75) S. Schweidler, L. de Biasi, G. Garcia, A. Mazilkin, P. Hartmann, T. Brezesinski, J. Janek, ACS Appl. Energy Mater. 2 (2019) 7375–7384.

76) Y. J. Kim, J. Cho, T.-J. Kim, B. Parka, J. Electrochem. Soc. 150 (2003) A1723–A1725.

77) J. L. Tebbe, A. M. Holder, C. B. Musgrave, ACS Appl. Mater. Interfaces 7 (2015) 24265– 24278.

78) Y. Liu, X.-J. Lin, Y.-G. Sun, Y.-S. Xu, B.-B. Chang, C.-T. Liu, A.-M. Cao, L.-J. Wa, Small 9 (2019) 1901019.

79) T. Ohzuku, A. Ueda, M. Nagayama, Y. Iwakoshi and H. Komori, Electrochim. Acta 38 (1993) 1159-1167.

80) G. G. Amatucci, J. Electrochem. Soc. 143 (1996), 1114.

81) Z. Chen, Z. Lu and J. R. Dahn, J. Electrochem. Soc. 149 (2002) A1604.

82) E. Rossen, J. Reimers and J. Dahn, Solid State Ionics 62 (1993) 53-60.

83) S. Kang, Solid State Ionics 120 (1999) 155-161.

84) Y. Shao-Horn, S. A. Hackney, A. J. Kahaian and M. M. Thackeray J. Solid State Chem. 168 (2002) 60-68.

85) H. Wang, J. Electrochem. Soc. 146 (1999) 473.

86) H. Gabrisch, R. Yazami and B. Fultz, J. Power Sources 119 (2003) 674-679.

87) J.-H. Shim, K.-S. Lee, A. Missyul, J. Lee, B. Linn, E. C. Lee and S. Lee, Chem. Mater., 27 (2015) 3273- 3279.

88) S. Muto, Y. Sasano, K. Tatsumi, T. Sasaki, K. Horibuchi, Y. Takeuchi and Y. Ukyo, J. Electrochem. Soc. 156 (2009) A371.

89) F. Lin, I. M. Markus, D. Nordlund, T. C. Weng, M. D. Asta, H. L. Xin and M. M. Doeff, Nat. Commun. 5 (2014) 3529.

90) R. Robert, C. Villevieille and P. Novák, J. Mater. Chem. A 2 (2014) 8589.

91) T. Nonaka, C. Okuda, Y. Seno, K. Koumoto and Y. Ukyo, Ceram. Int. 34 (2008) 859-862.

92) T. Nonaka, C. Okuda, Y. Seno, Y. Kondo, K. Koumoto and Y. Ukyo, J. Electrochem. Soc. 154 (2007) A353.

93) P. F. Yan, J. M. Zheng, D. P. Lv, Y. Wei, J. X. Zheng, Z. G. Wang, S. Kuppan, J. G. Yu, L. L. Luo, D. Edwards, M. Olszta, K. Amine, J. Liu, J. Xiao, F. Pan, G. Y. Chen, J. G. Zhang and C. M. Wang, Chem. Mater. 27 (2015) 5393-5401.

94) B.-B. Lim, S.-J. Yoon, K.-J. Park, C. S. Yoon, S.-J. Kim, J. J. Lee and Y.-K. Sun, Adv. Funct. Mater. 25 (2015) 4673-4680.

95) Y. K. Sun, Z. Chen, H. J. Noh, D. J. Lee, H. G. Jung, Y. Ren, S. Wang, C. S. Yoon, S. T. Myung and K. Amine, Nat. Mater. 11 (2012) 942-947.

96) A. K. Shukla, Q. M. Ramasse, C. Ophus, H. Duncan, F. Hage and G. Chen, Nat. Commun. 6 (2015) 8711.

97) S. H. Kang and M. M. Thackeray, J. Electrochem.Soc. 155 (2008) A269.

98) A. R. Armstrong, M. Holzapfel, P. Novak, C. S. Johnson, S. H. Kang, M. M. Thackeray and P. G. Bruce, J. Am. Chem. Soc. 128 (2006) 8694-8698.

99) D. Mohanty, A. S. Sefat, J. Li, R. A. Meisner, A. J. Rondinone, E. A. Payzant, D. P. Abraham, D. L. Wood III, and C. Daniel, Phys. Chem. Chem. Phys. 15 (2013) 19496-19509.

100) N. Yabuuchi, K. Yoshii, S. T. Myung, I. Nakai and S. Komaba, J. Am. Chem. Soc. 133 (2011) 4404-4419.

101) J. Zheng, P. Xu, M. Gu, J. Xiao, N. D. Browning, P. Yan, C. Wang and J.-G. Zhang, Chem. Mater. 27 (2015) 1381-1390.

102) M. Gu, A. Genc, I. Belharouak, D. Wang, K. Amine, S. Thevuthasan, D. R. Baer, J.-G. Zhang, N. D. Browning, J. Liu and C. Wang, Chem. Mater. 25 (2013) 2319-2326.

103) M. Gu, I. Belharouak, J. Zheng, H. Wu, J. Xiao, A. Genc, K. Amine, S. Thevuthasan, D. R. Baer, J. G. Zhang, N. D. Browning, J. Liu and C. Wang, ACS Nano 7 (2013) 760-767.

104) J. M. Tarascon, E. Wang, F. K. Shokoohi, W. R. Mckinnon and S. Colson, J. Electrochem. Soc. 138 (1991) 2859-2864.

105) Y. Shao-Horn, S. A. Hackney, A. J. Kahaian, K. D. Kepler, E. Skinner, J. T., J. Power Sources 81 (1999), 496-499.

106) K. Y. Chung, W.-S. Yoon, H. S. Lee, X.-Q. Yang, J. McBreen, B. H. Deng, X. Q. Wang, M. Yoshio, R. Wang, J. Gui and M. Okada, J. Power Sources 146 (2005) 226-231.

107) T. Eriksson, T. Gustafsson and J. O. Thomas, Electrochem. Solid St. 5 (2002) A35.

108) K. Y. Chung and K.-B. Kim, Electrochim. Acta, 49 (2004) 3327-3337.

109) R. Alcántara, M. Jaraba, P. Lavela, J. L. Tirado, P. Biensan, A. de Guibert, C. Jordy and J. P. Peres, Chem Mater. 15 (2003) 2376-2382.

110) K. Zhao, M. Pharr, J. J. Vlassak and Z. Suo, J. Appl. Phys. 108 (2010) 073517.

111) W. H. Woodford, Y.-M. Chiang and W. C. Carter, J. Electrochem. Soc. 157 (2010) A1052.

112) A. Ito, D. Li, Y. Sato, M. Arao, M. Watanabe, M. Hatano, H. Horie and Y. Ohsawa, J. Power Sources 195 (2010) 567-573.

113) D. J. Miller, C. Proff, J. G. Wen, D. P. Abraham and J. Bareño, Adv. Energy Mater., 3 (2013) 1098-1103.

114) K. Xu, Nonaqueous Liquid Electrolytes for Lithium-Based Rechargeable Batteries, Chem. Rev., 2004, 104, 4303-4418.

115) V. Aravindan, J. Gnanaraj, S. Madhavi and H. K. Liu, Lithium-Ion Conducting Electrolyte Salts for Lithium Batteries, Chemistry, 2011, 17, 14326-14346.

116) X. R. Zhang, R. Kostecki, T. J. Richardson, J. K. Pugh and P. N. Ross, J. Electrochem. Soc. 148 (2001) A1341-A1345.

117) M. Egashira, H. Takahashi, S. Okada and J. Yamaki, J. Power Sources 92 (2001) 267-271.

118) S. Shi, P. Lu, Z. Liu, Y. Qi, L. G. Hector, Jr., H. Li and S. J. Harris, J. Am. Chem. Soc. 134 (2012) 15476-15487.

119) Y. Kim, J. Mater. Sci. 48 (2013) 8547-8551.

120) M. Winter, Z. Phys. Chem. 223 (2009) 1395-1406.

121) K. L. Browning, L. Baggetto, R. R. Unocic, N. J. Dudney and G. M. Veith, J. Power Sources 239 (2013) 341-346.

122) D. Aurbach, B. Markovsky, G. Salitra, E. Markevich, Y. Talyossef, M. Koltypin, L. Nazar, B. Ellis and D. Kovacheva, J. Power Sources 165 (2007) 491-499.

123) J. B. Goodenough and Y. Kim, J. Power Sources 196 (2011) 6688-6694.

124) H. Bouayad, Z. Wang, N. Dupré, R. Dedryvère, D. Foix, S. Franger, J. F. Martin, L. Boutafa, S. Patoux, D. Gonbeau and D. Guyomard, J. Phys. Chem. C 118 (2014) 4634-4648.

125) X.-G. Sun, C. Liao, L. Baggetto, B. Guo, R. R. Unocic, G. M. Veith and S. Dai, J. Mater. Chem. A 2 (2014) 7606.

126) T. Kubota, M. Ihara, S. Katayama, H. Nakai and J. Ichikawa, J. Power Sources 207 (2012) 141-149.

127) A. von Cresce and K. Xu, J. Electrochem. Soc. 158 (2011) A337.

128) Z. Chen and K. Amine, Electrochem. Commun. 9 (2007) 703-707.

129) U. Heider, R. Oesten and M. Jungnitz, J. Power Sources 81 (1999) 119-122.

130) M. Hirayama, H. Ido, K. Kim, W. Cho, K. Tamura, J. Mizuki and R. Kanno, J. Am. Chem. Soc. 132 (2010) 15268-15276.

131) W. Choi and A. Manthiram, J. Electrochem. Soc. 153 (2006) A1760.

132) D. H. Jang, J. Electrochem. Soc. 143 (1996) 2204.

133) T. Aoshima, K. Okahara, C. Kiyohara and K. Shizuka, J. Power Sources 97 (2001) 377-380.

134) C. Zhan, J. Lu, A. Jeremy Kropf, T. Wu, A. N. Jansen, Y. K. Sun, X. Qiu and K. Amine Nat. Commun. 4 (2013) 2437.

135) J. Cho, Electrochem. Solid-State Lett. 3 (1999) 362.

136) J. Cho, Y. J. Kim, T.-J. Kim and B. Park, Angew. Chem. Int. Ed. 40 (2001) 3367-3369.

137) J. Cho, Y. J. Kim and B. Park, Chem. Mater. 12 (2000) 3788-3791.

138) Z. Chen and J. R. Dahn, Electrochem. Solid St. 5 (2002) A213.

139) Z. Chen and J. R. Dahn, Electrochem. Solid St. (6) 2003 A221.

140) Y. Cho, P. Oh and J. Cho, Nano Lett. 13 (2013) 1145-1152.

141) C. Kim, P. J. Phillips, L. Xu, A. Dong, R. Buonsanti, R. F. Klie and J. Cabana, Chem. Mater. 27 (2015) 394-399.

142) J. Lu, C. Zhan, T. Wu, J. Wen, Y. Lei, A. J. Kropf, H. Wu, D. J. Miller, J. W. Elam, Y. K. Sun, X. Qiu and K. Amine, Nat. Commun. 5 (2014) 5693.

143) R. J. Gummow, A. de Kock and M. M. Thackeray, Solid State Ionics 69 (1994) 59-67.

144) L. Xiong, Y. Xu, T. Tao, X. Du and J. Li, J. Mater. Chem. 21 (2011) 4937.

145) M.-S. Park, J.-W. Lee, W. Choi, D. Im, S.-G. Doo and K.-S. Park, J. Mater. Chem. 20 (2010) 7208.

146) F. Wu, N. Li, Y. Su, H. Lu, L. Zhang, R. An, Z. Wang, L. Bao and S. Chen, J. Mater. Chem. 22 (2012) 1489.

147) B. Han, T. Paulauskas, B. Key, C. Peebles, J. Park, R. Klie, J. Vaughey, and F. Dogan, ACS Appl. Mater. Interfaces 9 (2017) 14769−14778

148) I. Bloom, L. Trahey, A. Abouimrane, I. Belharouak, X. Zhang, Q. Wu, W. Lu, D. P. Abraham, M. Bettge, J. W. Elam, X. Meng, A. K. Burrell, C. Ban, R. Tenent, J. Nanda and N. Dudney, J. Power Sources 249 (2014) 509-514.

149) J. Zheng, M. Gu, J. Xiao, B. J. Polzin, P. Yan, X. Chen, C. Wang and J.-G. Zhang, Chem. Mater. 26 (2014) 6320-6327

150) C. Chen, W. Yao, Q. He, M. Ashuri, J. Kaduk, Y. Liu and L. Shaw, ACS Appl. Energy Mater. 2 (2019) 3098−3113.

151) Y. Shia, M. Zhanga,b, D. Qianb, Y. Shirley Meng, Electrochimica Acta 203 (2016) 154–161.

152) J. Leea, F. Wangb, C. Chengc, C. Lid, C. Lin, Electrochimica Acta 55 (2010) 4002–4006.

153) X. Zhang , I. Belharouak , L. Li , Y. Lei , J. W. Elam , A. Nie , X. Chen , R. S.Yassar, and R. L. Axelbaum, Adv. Energy Mater. 3 (2013) 1299–1307.

154) P. Yan, J. Zheng, X. Zhang, R. Xu, K. Amine, J. Xiao, J.-G. Zhang and C.-M. Wang, Chem. Mater. 28 (2016) 857-863.

155) K. Araki, N. Taguchi, H. Sakaebe, K. Tatsumi and Z. Ogumi, J. Power Sources 269 (2014) 236-243.

156) Y. Kim, G. M. Veith, J. Nanda, R. R. Unocic, M. Chi and N. J. Dudney, Electrochim. Acta. 56 (2011) 6573-6580.

157) S.-H. Lee, C. S. Yoon, K. Amine and Y.-K. Sun, J. Power Sources, 234 (2013) 201-207.

158) Y. Yang, X.-Z. Liao, Z.-F. Ma, B.-F. Wang, L. He and Y.-S. He, Electrochem. Commun.11 (2009) 1277-1280.

159) C. Wang, H. Wu, Z. Chen, M. T. McDowell, Y. Cui and Z. Bao, Nat. Chem. 5 (2013) 1042-1048.

160) Z. Wang, C. Wu, L. Liu, F. Wu, L. Chen and X. Huang, J. Electrochem. Soc. 149 (2002), A466.

161) K. W. Kim, S.-W. Lee, K.-S. Han, H. J. Chung and S. I. Woo, Electrochim. Acta 48 (2003), 4223-4231.

162) J. S. Kim, C. S. Johnson, J. T. Vaughey, S. A. Hackney, K. A. Walz, W. A. Zeltner, M. A. Anderson and M. M. Thackeray, J. Electrochem. Soc. 151 (2004) 151, A1755.

163) Y. K. Sun, K. J. Hong, J. Prakash and K. Amine, Electrochem. Commun., 4 (2002) 344-348.

164) Z. R. Zhang, H. S. Liu, Z. L. Gong and Y. Yang, J. Power Sources 129 (2004) 101-106.

165) K. Yang, L.-Z. Fan, J. Guo and X. Qu, Electrochim. Acta 63 (2012) 363-368.

166) Z. Yang, Q. Qiao and W. Yang, Electrochim. Acta 56 (2011) 4791-4796.

167) K.-S. Lee, S.-T. Myung, D.-W. Kim and Y.-K. Sun, J. Power Sources 196 (2011) 6974-6977.

168) J. M. Zheng, Z. R. Zhang, X. B. Wu, Z. X. Dong, Z. Zhu and Y. Yang, J. Electrochem. Soc. 155 (2008) A775.

169) Z. Wu, S. Ji, J. Zheng, Z. Hu, S. Xiao, Y. Wei, Z. Zhuo, Y. Lin, W. Yang, K. Xu, K. Amine and F. Pan, Nano Lett. 15 (2015) 5590-5596.

170) G. Alva, C. Kim, T. Yi, J. B. Cook, L. Xu, G. M. Nolis and J. Cabana, J. Phys. Chem. C, 118 (2014) 10596-10605.

171) L. Dahéron, R. Dedryvère, H. Martinez, D. Flahaut, M. Ménétrier, C. Delmas and D. Gonbeau, Chem. Mater. 21 (2009) 5607-5616.

172) A. Eftekhari, J. Power Sources 130 (2004) 260-265.

173) J. T. Son, K. S. Park, H. G. Kim and H. T. Chung, J. Power Sources 126 (2004) 182-185.

174) C. Liu, J. An, R. Guo, Y. Li and L. Liu, J. Alloy. Compd. 563 (2013) 33-38.

175) Y. S. Hu, Y. G. Guo, R. Dominko, M. Gaberscek, J. Jamnik and J. Maier, Adv. Mater., 19 (2007) 1963-1966.

176) Y. Q. Wang, L. Gu, Y. G. Guo, H. Li, X. Q. He, S. Tsukimoto, Y. Ikuhara and L. J.

Wan, J. Am. Chem. Soc. 134 (2012) 7874-7879.

177) D. Becker, M. Börner, A. Friesen, S. Klein, U. Rodehorst, M. Diehl, M. Winter, T. Placke and R. Schmuch, J. Electrochem. Soc. 167 (2020) 060524

178) A. Vadivel Murugan, T. Muraliganth and A. Manthiram, Electrochem. Commun. 10 (2008), 903-906.

179) M. C. Kim, S. H. Kim, V. Aravindan, W. S. Kim, S. Y. Lee and Y. S. Lee, J. Electrochem. Soc. 160 (2013) A1003-A1008.

180) Y.-m. Bai, P. Qiu, Z.-l. Wen and S.-c. Han, Improvement of Electrochemical Performances of LiFePO4 Cathode Materials by Coating of Polythiophene, J. Alloy. Compd., 2010, 508, 1-4.

181) J. Yang, J. Wang, Y. Tang, D. Wang, X. Li, Y. Hu, R. Li, G. Liang, T.-K. Sham and X. Sun, Energy Environ. Sci. 6 (2013) 1521.

182) J. Yang, J. Wang, D. Wang, X. Li, D. Geng, G. Liang, M. Gauthier, R. Li and X. Sun, J. Power Sources 208 (2012) 340-344.

183) J. Yang, J. Wang, X. Li, D. Wang, J. Liu, G. Liang, M. Gauthier, Y. Li, D. Geng, R. Li and X. Sun, J. Mater. Chem. 22 (2012) 7537.

184) J. Yang, J. Wang, Y. Tang, D. Wang, B. Xiao, X. Li, R. Li, G. Liang, T.-K. Sham and X. Sun, J. Mater. Chem. A 1 (2013) 7306.

185) H. K. Noh, H. S. Park, H. Y. Jeong, S. U. Lee and H. K. Song Angew. Chem. Int. Ed., 53 (2014) 5059-5063.

186) J. Wang and X. Sun, Energy Environ. Sci., 5 (2012), 5163.

187) G. G. Amatucci, N. Pereira, T. Zheng and J. M. Tarascon J. Electrochem. Soc., 148 (2001) A171.

188) S. J. Shi, J. P. Tu, Y. J. Mai, Y. Q. Zhang, C. D. Gu and X. L. Wang, Electrochim. Acta, 63 (2012) 112-117.

189) S. Lee, Y. Cho, H. K. Song, K. T. Lee and J. Cho, Angew. Chem. Int. Ed. 51 (2012) 8748-8752.

190) A. T. Appapillai, A. N. Mansour, J. Cho and Y. Shao-Horn Chem. Mater. 19 (2007) 5748-5757.

191) J. Liu and A. Manthiram, Chem. Mater. 21 (2009) 1695-1707.

192) Y. Huang, J. Chen, J. Ni, H. Zhou and X. Zhang, J. Power Sources, 188 (2009) 538-545.

193) D. Wang, X. Li, Z. Wang, H. Guo, Y. Xu, Y. Fan, J. Ru, Electrochimica Acta 188 (2016) 48–56.

194) J. Janek, M. Martin and K. D. Becker, Phys. Chem. Chem. Phys. 11 (2009) 3010.

195) F. Schipper, M. Dixit, D. Kovacheva, M. Talianker, O. Haik, J. Grinblat, E. M. Erickson, C. Ghanty, D. T. Major, B. Markovsky, D. Aurbach, J. Mater. Chem. A 4 (2016) 16073– 16084.

196) M. Aykol, S. Kirklin and C. Wolverton, Adv. Energy Mater. 4 (2014) 1400690.

197) L. Xu, F. Zhou, B. Liu, H. Zhou, Q. Zhang, J. Kong, Q. Wang, Int. J. Electrochem. 2018 (2018) 1–12.

198) D. Weber, D. Tripkovic, K. Kretschmer, M. Bianchini, T. Brezesinski, Eur. J. Inorg. Chem. (2020) 3117–3130.

199) W. Yan, S. Yang, Y. Huang, Y. Yang, G. Yuan, J. Alloys Compd. 819 (2020) 153048.

200) H. J. Bang, B.-C. Park, J. Prakash, Y.-K. Sun, J. Power Sources 174 (2007) 565–568.

201) S.-W. Cho, K.-S. Ryu, Mater. Chem. Phys. 135 (2012) 533–540.

202) J. Lu, Q. Peng, W. Wang, C. Nan, L. Li, Y. Li, J. Am. Chem. Soc. 135 (2013), 1649–1652.

203) F. Wu, J. Tian, N. Liu, Y. Lu, Y. Su, J. Wang, R. Chen, X. Ma, L. Bao, S. Chen, Energy Storage Mater. 8 (2017) 134–140.

204) W. Li, B. Song, A. Manthiram, Chem. Soc. Rev. 46 (2017) 3006–3059.

205) F. Kong, C. Liang, L. Wang, Y. Zheng, S. Perananthan, R. C. Longo, J. P. Ferraris, M. Kim, K. Cho, Adv. Energy Mater. 9 (2019) 1802586.

206) C. Pouillerie, L. Croguennec, P. Biensan, P. Willmann, C. Delmas, J. Electrochem. Soc. 147 (2000) 2061.

207) J. Zheng, T. Liu, Z. Hu, Y. Wei, X. Song, Y. Ren, W. Wang, M. Rao, Y. Lin, Z. Chen, J. Lu, C. Wang, K. Amine, F. Pan, J. Am. Chem. Soc. 138 (2016) 13326–13334.

208) C. Vogler, B. Löffler, W. Weirather, M. Wohlfahrt-Mehrens, J. Garche, Ionics (2002), 92–99.

209) C.-C. Chang, J. Y. Kim, P. N. Kumta, J. Electrochem. Soc. 147 (2000) 1722.

210) D. Aurbach, O. Srur-Lavi, C. Ghanty, M. Dixit, O. Haik, M. Talianker, Y. Grinblat, N. Leifer, R. Lavi, D. T. Major, G. Goobes, E. Zinigrad, E. M. Erickson, M. Kosa, B. Markovsky, J. Lampert, A. Volkov, J.-Y. Shin, A. Garsuch, J. Electrochem. Soc. 162 (2015), A1014–A1027.

211) Z. Yang, W. Yang, Z. Tang, J. Power Sources 184 (2008) 557–561.

212) P. Mohan, K. A. Kumar, G. P. Kalaignan, V. S. Muralidharan, J. Solid State Electrochem. 16 (2012) 3695–3702.

213) D. Liu, J. Hamel-Paquet, J. Trottier, F. Barray, V. Gariépy, P. Hovington, A. Guerfi, A. Mauger, C. M. Julien, J. B. Goodenough, K. Zaghib, J. Power Sources 217 (2012), 400–406.

214) A. Yu, G. V. S. Rao, B. V. R. Chowdari, Solid State Ionics 135 (2000) 131–135.

215) Y. Nishida, K. Nakane, T. Satoh, J. Power Sources 68 (1997) 561–564.

216) S. Sallard, D. Sheptyakov, C. Villevieille, J. Power Sources 359 **(2017)** 27–36.

217) J. Wu, H. Liu, X. Ye, J. Xia, Y. Lu, C. Lin, X. Yu, J. Alloys Compd. 644 (2015) 223–227.

218) C. Mi, E. Han, L. Sun, L. Zhu, Solid State Ion. 340 (2019) 114976.

219) Z. He, Z. Wang, H. Chen, Z. Huang, X. Li, H. Guo, R. Wang, J. Power Sources 299 (2015) 334–341.

220) X.-Z. Liao, Y.-S. He, Z.-F. Ma, X.-M. Zhang, L. Wang, J. Power Sources 174 (2007) 720–725.

221) S.-U. Woo, B.-C. Park, C. S. Yoon, S.-T. Myung, J. Prakash, Y.-K. Sun, J. Electrochem. Soc. 154 (2007) A649.

222) Y.-K. Sun, S. W. Oh, C. S. Yoon, H. J. Bang, J. Prakash, J. Power Sources 161 (2006), 19–26.

223) J. Dai, L. Zhou, X. Han, M. Carter, L. Hu, ACS Appl. Mater. Interfaces 8 (2016) 10820–10825.

224) X. Li, F. Kang, W. Shen, X. Bai, Electrochimica Acta 53 (2007) 1761–1765.

225) F. Kong, C. Liang, R. C. Longo, D.-H. Yeon, Y. Zheng, J.-H. Park, S.-G. Doo, K. Cho, Chem. Mater. 28 (2016) 6942–6952.

226) Z. Chen, Y. Qin, K. Amine, Y.-K. Sun, J. Mater. Chem. 20 (2010), 7606–7612.

227) Y. Liu, Z. Zhang, Y. Fu, Q. Wang, J. Pan, M. Su, V. S. Battaglia, J. Alloys Compd. 685 (2016), 523–532.

228) A. Yano, M. Shikano, A. Ueda, H. Sakaebe, Z. Ogumi, J. Electrochem. Soc. 164 (2017), A6116–A6122.

229) D. Zuo, G. Tian, X. Li, D. Chen, K. Shu, J. Alloys Compd. 706 (2017) 24–40.

230) L. J. Fu, H. Liu, C. Li, Y. P. Wu, E. Rahm, R. Holze, H. Q. Wu, Solid State Sci. 8 (2006), 113–128.

231) I. Belharouak, C. Johnson, K. Amine, Electrochem. Commun. 7 (2005), 983–988.

232) A. Aboulaich, K. Ouzaouit, H. Faqir, A. Kaddami, I. Benzakour, I. Akalay, Mater. Res. Bull. 73 (2016) 362-368.

233) Q. Zhu, S. Zheng, X. Lu, Y. Wan, Q. Chen, J. Yang, L. Zhang, Z. Lu, J. Alloy. Compd. 654 (2016) 384-391

234) X. Zhang, Y. Xu, H. Zhang, C. Zhao, X. Qian, Electrochim. Acta 145 (2014) 201-208.

235) C.S. Kim, S.H. Kwon, J.W. Yoon, J. Alloy. Compd. 586 (2014) 574-580.

236) W. Sun, M. Xie, X. Shi, L. Zhang, Mater. Res. Bull. 61 (2015) 287-291.

237) T. Shi, Y. Dong, C. Wang, F. Tao, L. Chen, J. Power Sources 273 (2015) 959-965.

238) A. Yano, S. Aoyama, M. Shikano, H. Sakaebe, K. Tatsumi, Z. Ogumi, J. Electrochem. Soc. 162 (2015) A3137-A3144.

239) G.R. Hu, J.C. Cao, Z.D. Peng, Y.B. Cao, K. Du, Electrochim. Acta 149 (2014) 49-55.

240) Q.T. Zhou, L. Qu, T. Gengenbach, I. Larson, P.J. Stewart, D.A. Morton, AAPS PharmSciTech 14 (2013) 38-44.

241) C.D. Kablitz, N.A. Pharm. Dev. Technol. 18 (2013) 39-45.

242) M. Herzog, N. Gauquelin, D. Esken, J. Verbeeck, J. Janek, Energy Technol. 9 (2021) 2100028.

243) C.C. Yang, J.H. Jang, J.R. Jiang, Appl. Energy 162 (2016) 1419-1427.

244) M. Islam, S.C. Ur, M.S. Yoon, Appl. Phys. 15 (2015) 541-546.

245) G. Yushin, Energy Environ. Sci. 8 (2015) 1889-1904.

246) M. Yang, Y. Guo, Q. Wang, J. Xie, J. Nanopart. Res. 16 (2014) 1-9.

247) R. Tian, H. Liu, Y. Jiang, J. Chen, X. Tan, G. Liu, L. Zhang, X. Gu, Y. Guo, H. Wang, L. Sun, W. Chu, ACS Appl. Mater. Interfaces 7 (2015) 11377-11386.

248) S. M. George, Chem. Rev. 110 (2010) 111–131.

249) B. Han, T. Paulauskas, B. Key, C. Peebles, J. S. Park, R. F. Klie, J. T. Vaughey, F. Dogan, ACS Appl. Mater. Interfaces 9 (2017)14769–14778.

250) X. Meng, X.-Q. Yang, X. Sun, Adv. Mater. 24 (2012) 3589–3615.

251) C.-C. Wang, J.-W. Lin, Y.-H. Yu, K.-H. Lai, K.-F. Chiu, C.-C. Kei, ACS Sustain. Chem. Eng. 6 (2018) 16941–16950.

252) S. Kalluri, M. Yoon, M. Jo, H. K. Liu, S. X. Dou, J. Cho, Z. Guo, Adv. Mater. 29 (2017) 1605807.

253) D. N. Goldstein, J. A. McCormick, S. M. George, J. Phys. Chem. C 112 (2008) 19530–19539.

254) Y. Shi, M. Zhang, D. Qian, Y. S. Meng, Electrochimica Acta 203 (2016) 154–161.

255) X.M. Wu, S. Chen, M.Y. Ma, J.B. Liu, Ionics 17 (2011) 35-39.

256) Y. Wang, Y. Wang, E. Hosono, K. Wang, H. Zhou, Angew. Chem. Int. Ed. 120 (2008) 7571-7575.

257) I. Ohno, Mater. Sci. Eng. A 146 (1991) 33-49.

258) R. Jiang, C. Cui, H. Ma, H. Ma, T. Chen, J. Electroanal. Chem. 744 (2015) 69-76.

259) J. Liu, X. Liu, T. Huang, A. Yu, J. Power Sources 229 (2013) 203-209.

260) M. Herzog, D. Esken, and J. Janek, Batteries& Supercaps 4 (2021) 1003–1017

261) Y. Oh, D. Ahn, S. Nam, B. Park, J. Solid State Electr. 14 (2010) 1235-1240.

262) Y. Chen, Y. Zhang, B. Chen, Z. Wang, C. Lu, J. Power Sources 256 (2014) 20-27.

263) J.Z. Kong, C. Ren, G.A. Tai, X. Zhang, A.D. Li, D. Wu, H. Li, F. Zhou, J. Power Sources 266 (2014) 433-439.

264) P. Mohan, G.P. Kalaignan, J. Nanosci. Nanotechnol. 13 (2013) 2765-2770.

265) N.V. Kosova, E.T. Devyatkina, J. Power Sources 174 (2007) 959-964.

266) H. Cao, B. Xia, Y. Zhang, N. Xu, Solid State Ionics 176 (2005) 911-914.

267) D. Takamatsu, S. Mori, Y. Orikasa, T. Nakatsutsumi, Y. Koyama, H. Tanida, H. Arai, Y. Uchimoto, Z. Ogumi, J. Electrochem. Soc. 160 (2013) A3054-A3060.

268) N. Ariel, G. Ceder, D.R. Sadoway, E.A. Fitzgerald, J. Appl. Phys. 98 (2005), 023516-023516-7.

269) Y. Lu, L.Y. Sah, J. Appl. Phys. 76 (1994) 4724-4727.

270) F. Wu, X. Zhang, T. Zhao, L. Li, M. Xie, R. Chen, ACS Appl. Mater. Interfaces 7 (2015) 3773-3781.

271) L.L. Xie, L.Q. You, X.Y. Cao, C.F. Zhang, D.W. Song, L.B. Qu, Electro. Mater. Lett. 8 (2012) 411-415.

272) J. Cho, T.J. Kim, J. Kim, M. Noh, B. Park, J. Electrochem. Soc. 151 (2004) A1899-A1904.

273) J. Cho, H. Kim, B. Park, J. Electrochem. Soc. 151 (2004) A1707-A1711.

274) J. Cho, T.G. Kim, C. Kim, J.G. Lee, Y.W. Kim, B. Park, J. Power Sources 146 (2005) 58-64.

275) K. Yoojung, C. Jaephil, J. Electrochem. Soc. 154 (2007) 85-89.

276) K.S. Ryu, H.L. Sang, B.K. Koo, W.L. Ju, K.M. Kim, J.P., J. Appl. Electrochem. 38 (2008) 1385-1390.

277) Y. Fang, L. Xiao, J. Qian, X. Ai, H. Yang, Y. Cao, Nano Lett. 14 (2014) 3539-3543.

278) B. Xiao, J. Liu, Q. Sun, B. Wang, M.N. Banis, D. Zhao, Z. Wang, R. Li, X. Cui, T.K. Sham, X. Sun, Adv. Sci. 2 (2015) 1500022

279) F. Wu, N. Li, Y. Su, H. Shou, L. Bao, W. Yang, L. Zhang, R. An, S. Chen, Adv. Mater. 25 (2013) 3722e3726.

280) D. Luo, G. Li, C. Fu, J. Zheng, J. Fan, Q. Li, L. Li, Adv. Energy. Mater. 4 (2014) 1220-1225.

281) Y.R. Zhu, T.F. Yi, R.S. Zhu, A.N. Zhou, Ceram. Int. 39 (2013) 3087-3094.

282) S.B. Kim, K.J. Lee, W.J. Choi, W.S. Kim, I.C. Jang, H.H. Lim, Y.S. Lee, J. Solid State Electrochem. 14 (2010) 919-922.

283) K.S. Park, A. Benayad, D.J. Kang, S.G. Doo, J. Am. Chem. Soc. 130 (2008)14930-14931.

284) E.M. Sorensen, S.J. Barry, H.K. Jung, J.M. Rondinelli, J.T. Vaughey, K.R. Poeppelmeier, Chem. Mater. 18 (2006) 482-489.

285) L.N. Cong, X.G. Gao, S.C. Ma, X. Guo, Y.P. Zeng, L.H. Tai, R.S. Wang, H.M. Xie, L.Q. Sun, Electrochim. Acta 115 (2014) 399-406.

286) A. Yamada, S.C. Chung, K. Hinokuma, J. Electrochem. Soc. 148 (2001) A224-A229.

287) R. Muruganantham, M. Sivakumar, R. Subadevi, N.L. Wu, J. Mater. Sci. Mater. Electron. 26 (2015) 2095-2106.

288) D.W. Han, S.J. Lim, Y.I. Kim, S.H. Kang, Y.C. Lee, Y.M. Chem. Mater. 26 (2014) 3644-3650.

289) G. He, A. Manthiram,-Adv. Funct. Mater. 24 (2014) 5277-5283.

290) J.D. Wilcox, M.M. Doeff, M. Marcinek, R. Kostecki, J. Electrochem. Soc. 154 (2007) A389-A395.

291) J. Liu, Q. Wang, B. Reeja-Jayan, A. Manthiram, Electrochem. Commun. 12 (2010) 750-753.

292) Y.Z. Jin, Y.Z. Lv, Y. Xue, J. Wu, X. Zhang, Z.B. Wang, Rsc. Adv. 100 (2014) 57041-57047

293) Z. Yang, W. Yang, D.G. Evans, G. Li, Y. Zhao, Electrochem. Commun. 10 (2008) 1136-1139.

294) R.B. Shivashankaraiah, H. Manjunatha, K.C. Mahesh, J. Solid State Electrochem. 16 (2012) 1279-1290.

295) M. Nishizawa, K. Mukai, S. Kuwabata, C.R. Martin, H. Yoneyama, J. Electrochem. Soc. 144 (1997) 1923-1927.

296) P.B. Messersmith, E.P. Giannelis, J. Polym. Sci. A Polym. Chem. 33 (1995) 1047-1057.

297) K.S. Park, J.T. Son, H.T. Chung, S.J. Kim, C.H. Lee, K.T. Kang, H.G. Kim, Solid State Commun. 129 (2004) 311-314.

6. Appendix

6.1 Supporting Information Publication I

Supporting Information

Optimized atomic layer deposition of homogeneous, conductive Al_2O_3 coatings for high-nickel NCM containing ready-to-use electrodes

R. S. Negi[a], S. P. Culver[b], M. Wiche[a], S. Ahmed[c], K. Volz[c], and M.T. Elm[a,b,d*]

[a]*Center for Materials Research (LaMa), Justus Liebig University Giessen, Heinrich-Buff-Ring 16, 35392 Giessen, Germany*

[b]*Institute of Physical Chemistry, Justus Liebig University Giessen, Heinrich-Buff-Ring 17, 35392 Giessen, Germany*

[c]*Materials Science Centre and Faculty of Physics, Philipps University Marburg, Hans-Meerwein-Strasse 6, 35043 Marburg, Germany*

[d]*Institute of Experimental Physics I, Justus Liebig University Giessen, Heinrich-Buff-Ring 16, 35392 Giessen, Germany*

Corresponding Authors

*Email: matthias.elm@phys.chemie.uni-giessen.de

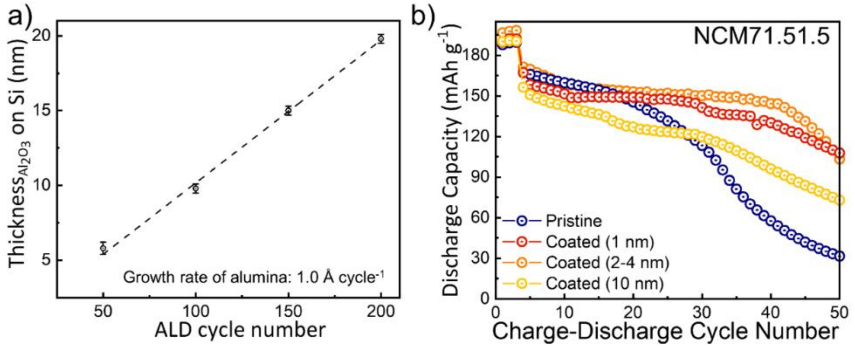

Fig. S1: (a) Thickness of the Al_2O_3 layer as a function of the number of ALD cycles deposited on Si substrates. The thickness was determined using XRR. The determined growth rate is about 1 Å per cycle. (b) Comparison of the long-term cycling stability for pristine and coated samples (NCM71.51.5) with different coating thicknesses.

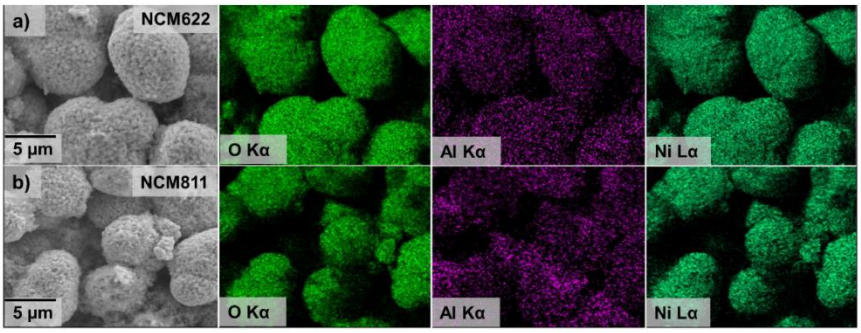

Fig. S2: SEM-EDX mapping of Al_2O_3 coated (a) NCM622, and (b) NCM811

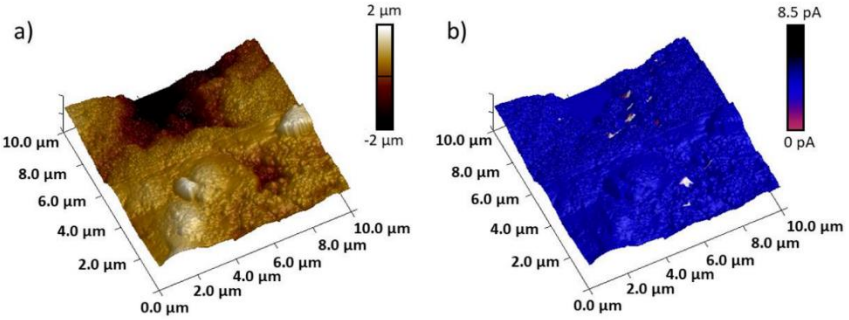

Fig. S3: a) AFM and b) C-AFM measurements of a NCM71.51.5 cathode coated with 20 nm Al_2O_3 revealing the insulating properties of the coating layer.

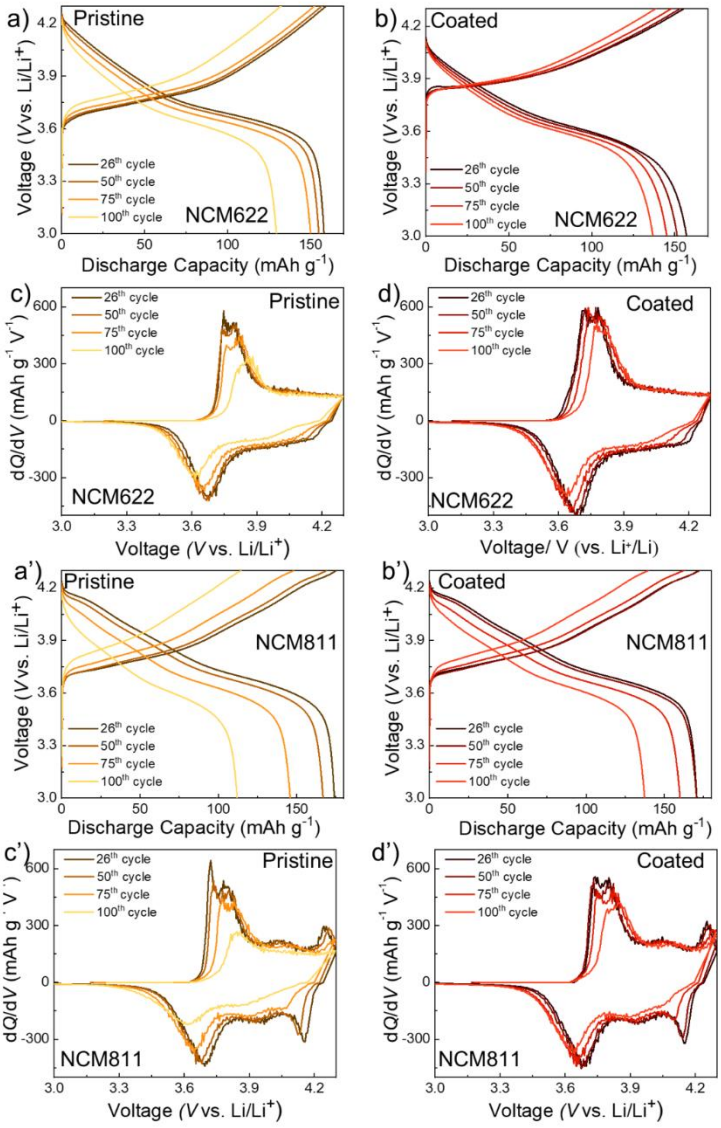

Fig. S4: Galvanostatic charge-discharge curves and corresponding Differential capacity plots of pristine and coated (a,b,c,d) NCM622 and (a',b',c',d') coated NCM811 cycled at 0.5 C after the C-rate test.

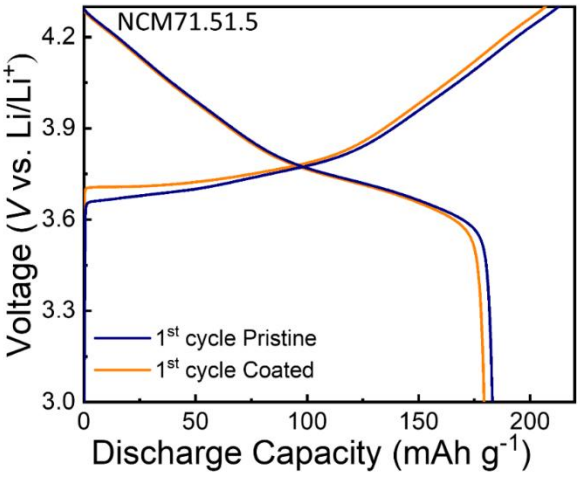

Fig. S5: Comparision of galvanostatic charge-discharge curves for 1st cycles at 0.1C for pristine cathode and coated cathode.

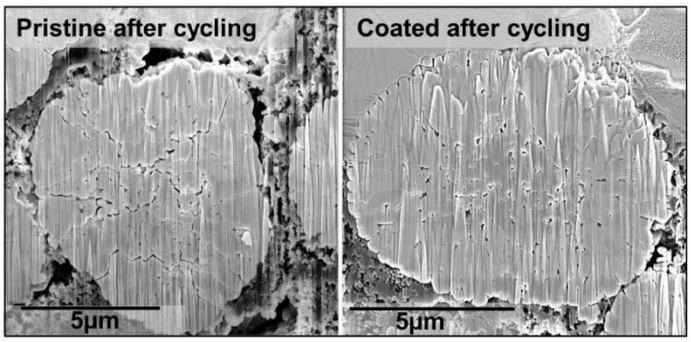

Fig. S6: Cross-sectional SEM micrographs of Pristine and Coated NCM71.51.5 after long-term cycling.

6.2 Supporting Information Publication II

Supporting Information

Enhancing the Electrochemical Performance of $LiNi_{0.70}Co_{0.15}Mn_{0.15}O_2$ Cathodes Using a Practical Solution-Based Al_2O_3 Coating

Rajendra S. Negi[a], Sean P. Culver[b], Andrey Mazilkin[c], Torsten Brezesinski[c], and Matthias T. Elm[a,b,d]*

[a]*Center for Materials Research (LaMa) Justus Liebig University Giessen, Heinrich-Buff-Ring 16, 35392 Giessen, Germany*

[b]*Institute of Physical Chemistry, Justus Liebig University Giessen, Heinrich-Buff-Ring 17, 35392 Giessen, Germany*

[c]*Institute of Nanotechnology, Karlsruhe Institute of Technology (KIT), Hermann-von-Helmholtz Platz 1, 76344 Eggenstein-Leopoldshafen, Germany*

[d]*Institute of Experimental Physics I, Justus Liebig University Giessen, Heinrich-Buff-Ring 16, 35392 Giessen, Germany*

*Email: matthias.elm@phys.chemie.uni-giessen.de

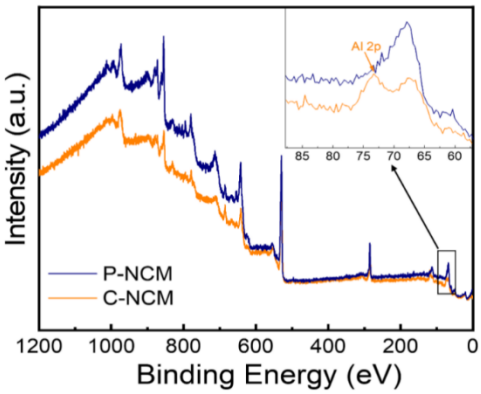

Figure S1. XPS survey spectra of P-NCM and C-NCM.

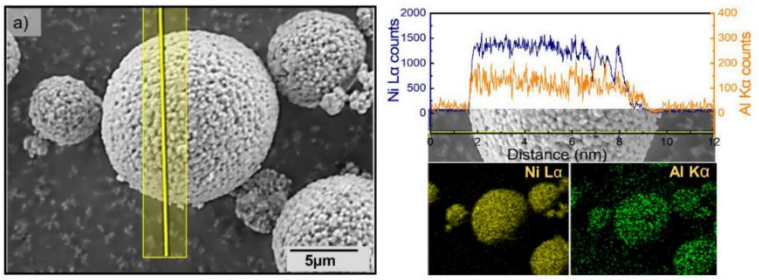

Figure S2. SEM micrograph of (a) C-NCM and the corresponding EDX line scan of Al over the coated NCM particle.

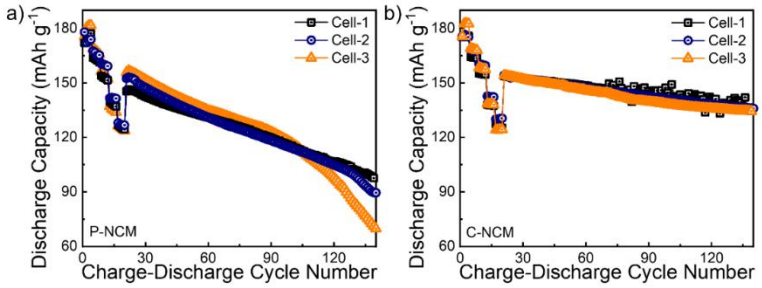

Figure S3. Long-term cycling performance of different cells: (a) P-NCM and (b) C-NCM.

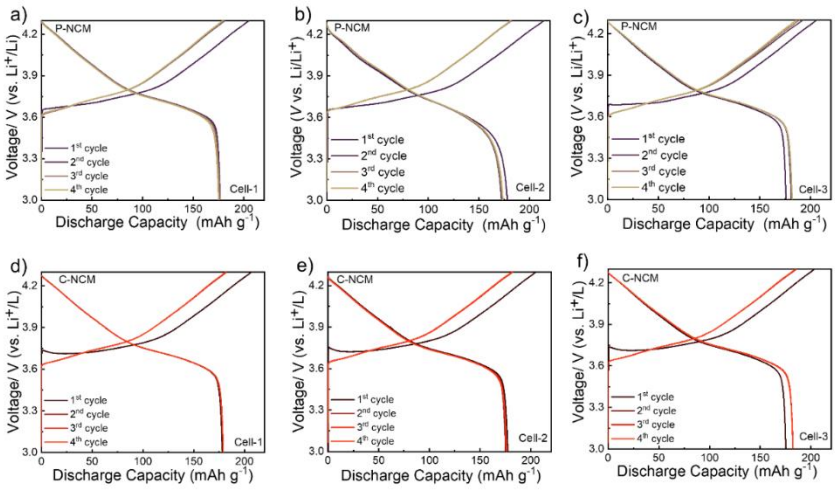

Figure S4. Voltage profiles of the first four cycles for different cells: (a, b, and c) P-NCM and (d, e, and f) C-NCM at 0.1C rate.

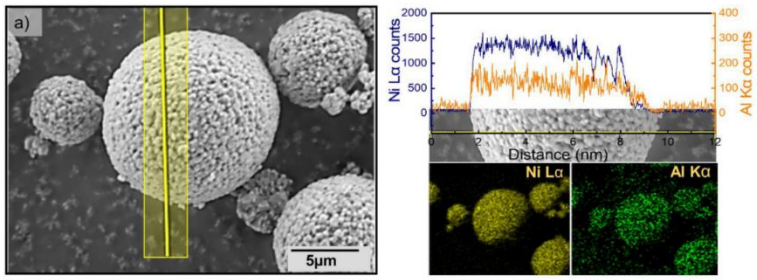

Figure S2. SEM micrograph of (a) C-NCM and the corresponding EDX line scan of Al over the coated NCM particle.

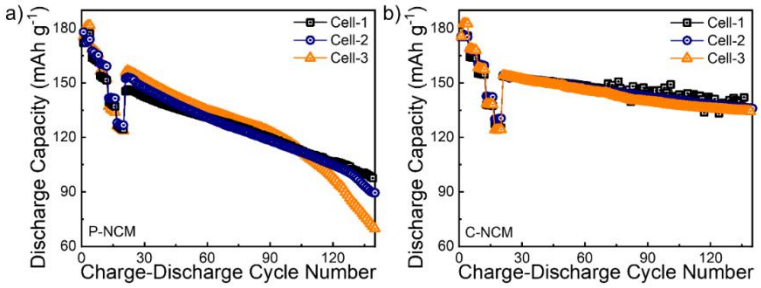

Figure S3. Long-term cycling performance of different cells: (a) P-NCM and (b) C-NCM.

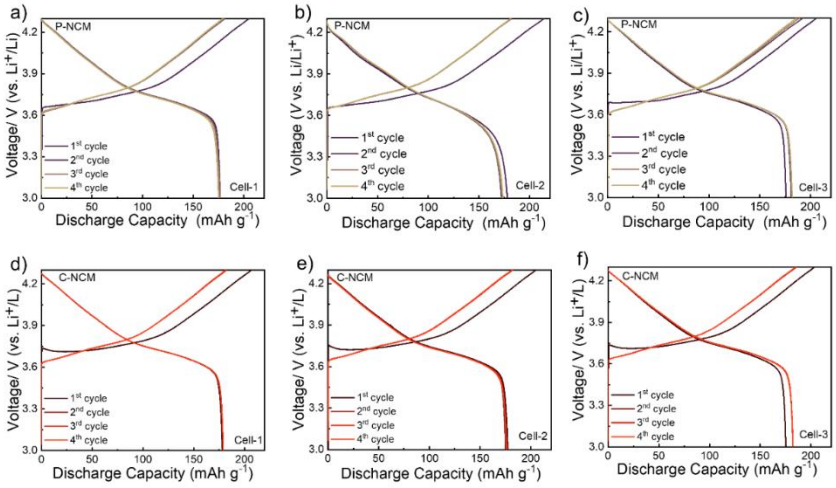

Figure S4. Voltage profiles of the first four cycles for different cells: (a, b, and c) P-NCM and (d, e, and f) C-NCM at 0.1C rate.

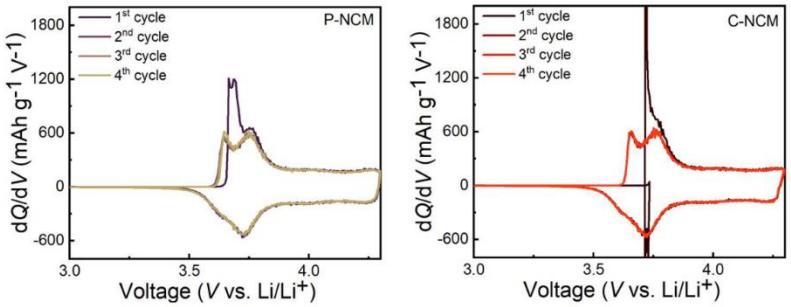

Figure S5. Differential capacity plots of the first four cycles for the P-NCM and C-NCM cells.

6.3 Supporting Information Publication III

Supporting Information

Insights into the positive effect of post-annealing on the electrochemical performance of Al_2O_3 coated Ni-Rich NCM cathode for lithium-ion batteries

Rajendra S. Negi[a], Erdogan Celik[a], Ruijun Pan[a,b], Robert Stäglich[c], Jürgen Senker[c], Matthias T. Elm[a,b,d]*

[a]*Center for Materials Research (ZfM), Justus-Liebig-University Giessen, Heinrich-Buff-Ring 17, D-35392 Giessen, Germany*

[b]*Institute of Physical Chemistry, Justus-Liebig-University Giessen, Heinrich-Buff-Ring 17, D-35392 Giessen, Germany*

[c]*Inorganic Chemistry III and Northern Bavarian NMR Centre, University of Bayreuth, Universitätsstr. 30, D-95440 Bayreuth, Germany*

[d]*Institute of Experimental Physics I, Justus Liebig University Giessen, Heinrich-Buff-Ring 16, 35392 Giessen, Germany*

Corresponding Authors

*Email: matthias.elm@phys.chemie.uni-giessen.de

Table S1: Refined lattice parameters of P-NCM, C-NCM-30 and C-NCM-600.

	a / Å	*c* / Å	V / Å^3	*c* / *a*
P-NCM	2.872	14.190	101.36	4.94
C-NCM-30	2.873	14.192	101.44	4.94
C-NCM-60	2.872	14.219	101.56	4.95

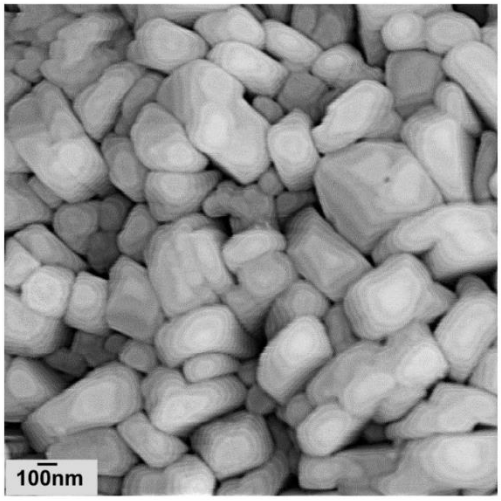

Figure S1 SEM image showing NCM primary particles.

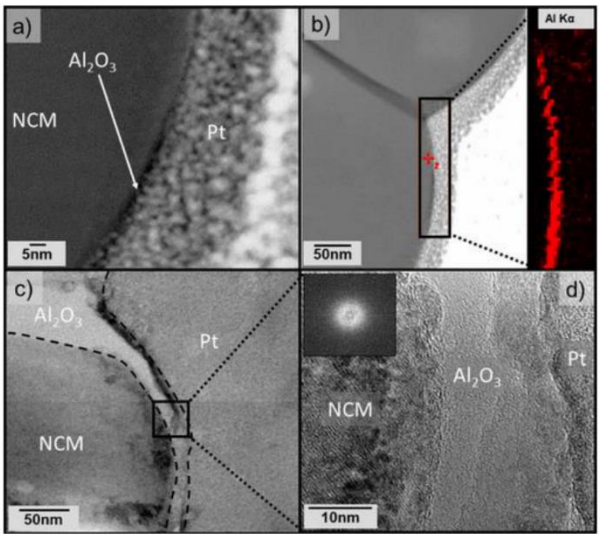

Figure S2: (a, b) STEM-HAADF micrographs and Al map of coated NCM701515. (c, d) Corresponding HRTEM micrographs. The inset in (d) is a FFT pattern of the coating layer. Reprinted with permission from Negi et al., *ACS Appl. Mater. Interfaces* **2020**, *12*, 31392–31400. Copyright 2020 American Chemical Society.

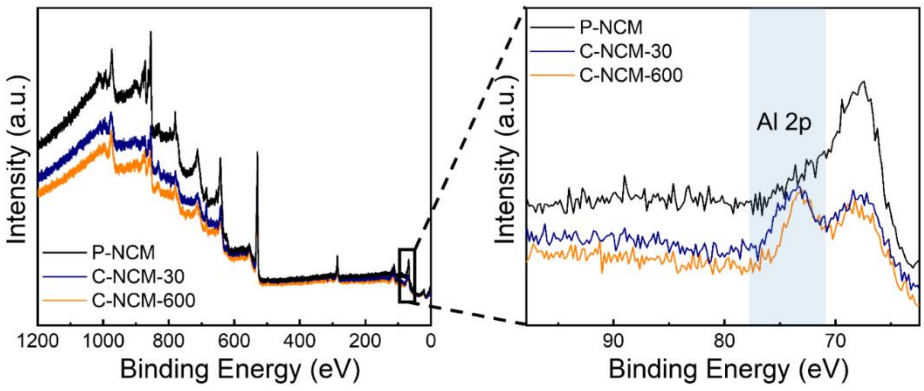

Figure S3: XPS survey spectra and detailed XPS spectra of the characteristic Al 2p peak of all the three samples.

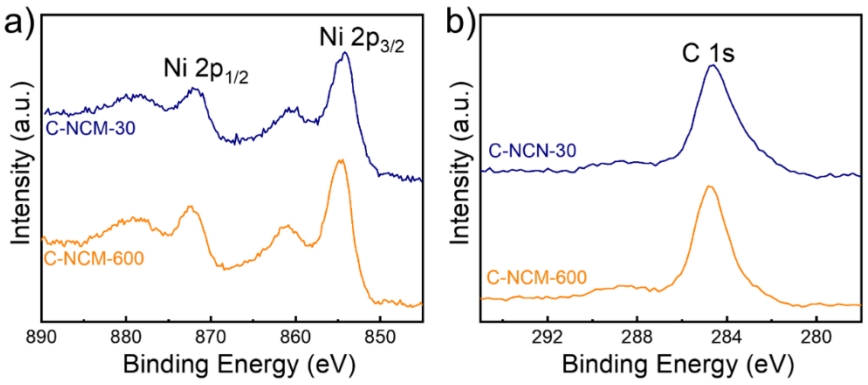

Figure S4: XPS spectra (a) Ni 2p and (b) C 1s peak.

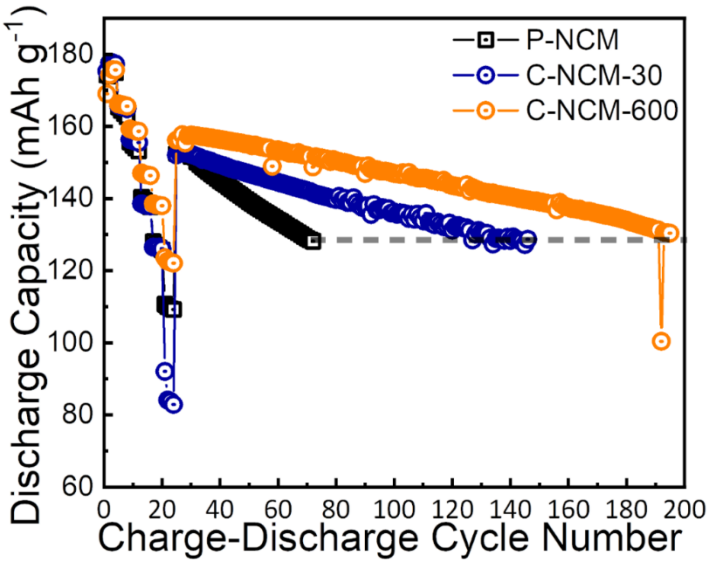

Figure S5: Long-term cycling performance of all the three samples at a C-rate of 0.5 C..

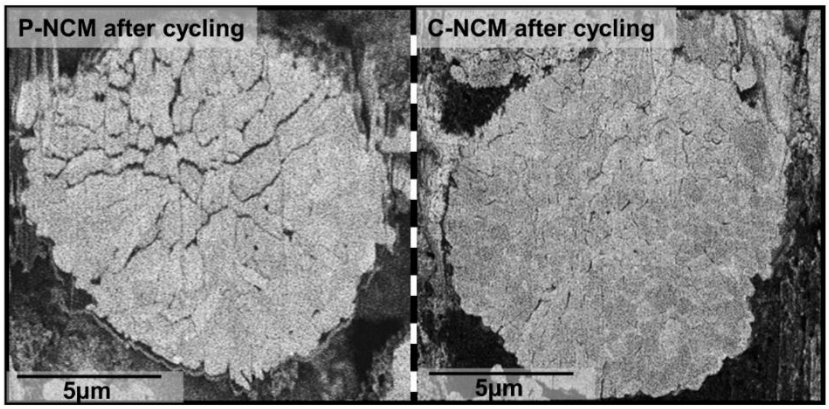

Figure S6: Cross-sectional SEM micrographs for P-NCM and C-NCM after long-term cycling.

6.4 Supporting Information Publication IV

Supplementary Information

Stabilizing the cathode/electrolyte interface using a dry-processed lithium titanate coating for all-solid-state-batteries

Rajendra S. Negi[a], Philip Minnmann[b], Ruijun Pan[b], Shamail Ahmed[c], Marcel J. Herzog[d], Kerstin Volz[c] , Ryo Takata[d], Franz Schmidt[d], Jürgen Janek[a,b] and Matthias T. Elm[a,b,e*]

[a]*Center for Materials Research (LaMa) Justus Liebig University Giessen, Heinrich-Buff-Ring 16, D-35392 Giessen Germany*

[b]*Institute of Physical Chemistry, Justus Liebig University Giessen, Heinrich-Buff-Ring 17, D-35392 Giessen Germany*

[c]*Materials Science Centre and Faculty of Physics, Philipps University Marburg, Hans-Meerwein-Strasse 6, 35043 Marburg, Germany*

[d]*Evonik Operations GmbH, Rodenbacher Chaussee 4, 63457 Hanau, Germany*

[e]*Institute of Experimental Physics I, Justus Liebig University Giessen, Heinrich-Buff-Ring 16, D-35392 Giessen Germany*

Corresponding Authors

*Email: matthias.elm@phys.chemie.uni-giessen.de

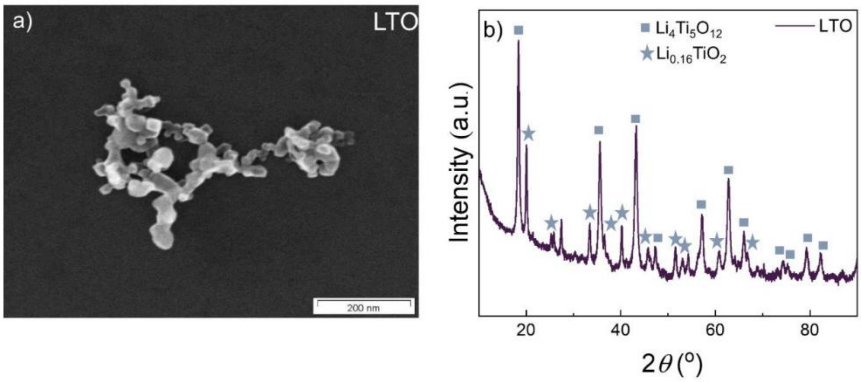

Fig. S1. (a) SEM image of single aggregates of fumed LTO, (b) XRD patterns of the fumed LTO.

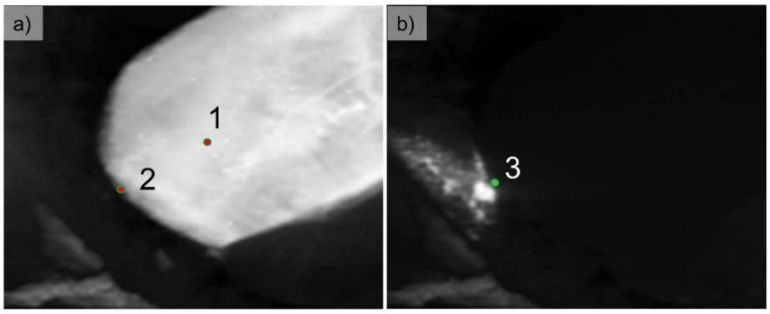

Fig. S2. (a) SPED virtual dark field (VDF) image highlighting a NCM primary particle. SPED-VDF is performed by putting a virtual aperture around the (-1 1 1 6) diffraction spot from diffraction patterns '1' and '2' in Fig. 4. b). (b) SPED-VDF image highlighting one of the LTO particles at the NCM primary particle's surface. This image is obtained by putting a virtual aperture around the (0 0 6) diffraction spot from diffraction pattern '3' in Fig. 4. c).

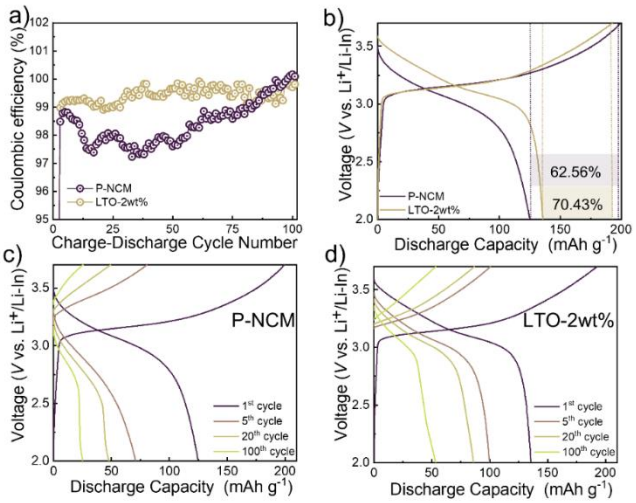

Fig. S3. Comparison of (a) columbic efficiency (CE) plot at 0.25C of P-NCM and LTO-2wt% based cells. (b) First cycle charge-discharge voltage profile of P-NCM and LTO-2wt% cells at 0.1 C. Charge-discharge voltage profile at 0.25 C for long-term cycling of (c) P-NCM and (d) LTO-2wt%.

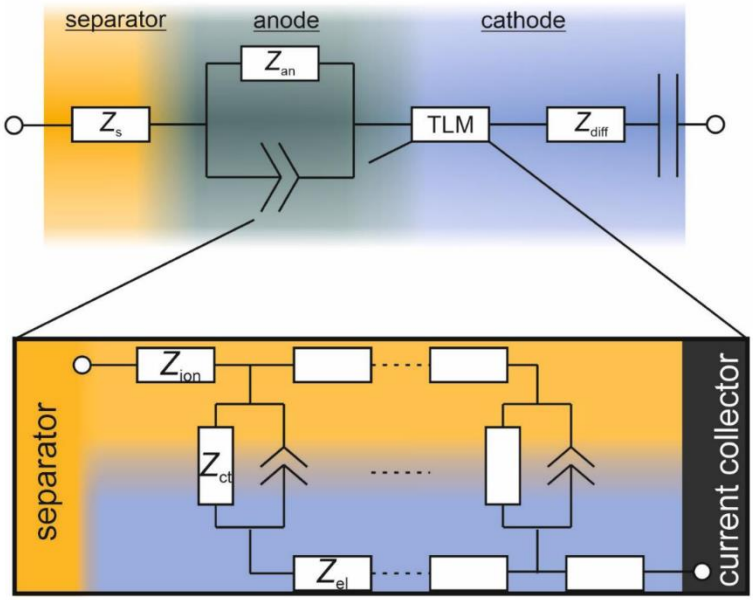

Fig. S4: Equivalent circuit used for the fitting of the impedance spectra. In here, Z_s represents the ohmic resistance of the cell (i.e. resistance from cell component and the electrolyte separator), corresponding to impedance contributions in the high-frequency (HF) region intercept on the real-axis. The impedance contributions in the medium and low frequency range correspond to the charge-transfer resistance (or cathode-electrolyte interface) of the SE-CAM interface (Z_{ct}), the ionic and electronic charge transport within the composite cathode (Z_i, Z_e), the anode-SE interface (Z_{an}) as well as the diffusion inside the CAM particles (Z_{diff}). While Z_{an} was modelled by an R-CPE element, and Z_{diff} by a serial combination of a Warburg impedance element and a capacitor (representing the differential capacitance), Z_i, Z_e and Z_{ct} were modelled by a transmission line model (TLM) with faradaic reactions. Z_e was fixed to zero, since carbon additives were used in the composite cathodes

Table S1: Fitting parameters for the equivalent circuit used to model the impedance response of the ASSB cells at 3.1, 3.4 and 3.7 V vs. $Li^+/In|(InLi)_x$. Listed are the fitting parameters for the first cycle of cells employing pristine (left rows) and coated (right rows) active material.

	Pristine			Coated		
Voltage / V	3.1	3.4	3.7	3.1	3.4	3.7
$R_{separator}$ / Ohm	2.73E+01	2.75E+01	2.85E+01	2.59E+01	2.65E+01	2.70E+01
r_{el} / Ohm m^{-1}	0.00E+00	0.00E+00	0.00E+00	0.00E+00	0.00E+00	0.00E+00
r_{ct} / Ohm m	4.09E-03	7.17E-03	7.13E-02	3.02E-03	3.36E-03	1.69E-02
q_{ct} / F s^{a-1} m	1.15E+00	7.38E-01	4.87E-01	4.19E+00	1.50E+00	1.05E+00
a_{ct}	8.30E-01	8.66E-01	9.15E-01	7.24E-01	8.19E-01	8.95E-01
R_{ion} / Ohm m^{-1}	1.10E+06	1.26E+06	1.20E+06	7.67E+05	1.08E+06	6.38E+05
L / m	5.00E-05	5.00E-05	5.00E-05	5.00E-05	5.00E-05	5.00E-05
R_{anode} / Ohm	1.74E+01	2.69E+01	5.05E+02	2.43E+01	1.88E+01	1.24E+02
Q_{anode} / F s^{a-1}	1.79E-02	2.94E-02	3.12E-03	1.40E-03	2.41E-03	1.17E-03
a_{anode}	3.97E-01	3.48E-01	4.67E-01	5.62E-01	5.70E-01	4.54E-01
Warburg Coeff.	3.22E+00	5.40E+00	3.00E+01	3.86E+00	4.49E+00	1.55E+01

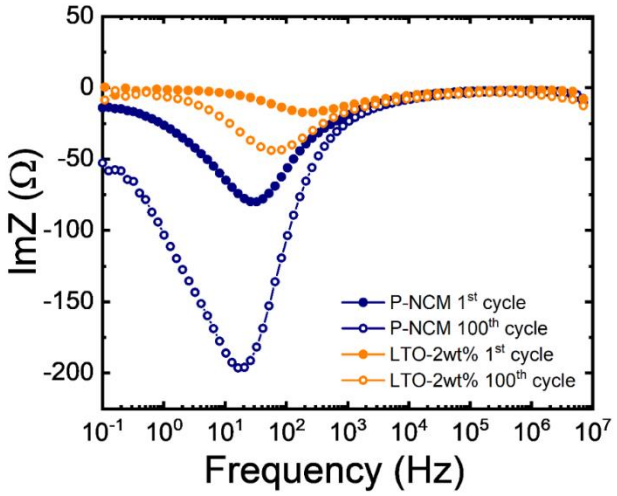

Fig. S5: Comparison of Bode-plots corresponding to P-NCM and LTO-2wt% after the 1st and 100th cycle.

6.5 Supporting Information Publication V

Supporting Information

A dry-processed $Al_2O_3/LiAlO_2$ coating for stabilizing the cathode/electrolyte interface in high-Ni NCM-based all-solid-state batteries

Rajendra S. Negi[a,=], Yuriy Yusim[b,=], Ruijun Pan[a,b,c*], Shamail Ahmed[d], Kerstin Volz[d], Ryo Takata[e], Franz Schmidt[e], Anja Henss[a,b*] and Matthias T. Elm[a,b,f*]

[a]*Center for Materials Research (LaMa), Justus Liebig University Giessen, Heinrich-Buff-Ring 16, 35392 Giessen, Germany*

[b]*Institute of Physical Chemistry, Justus Liebig University Giessen, Heinrich-Buff-Ring 17, 35392 Giessen, Germany*

[c]*Materials Science and Engineering Program and Texas Materials Institute, University of Texas at Austin, Austin, TX, 78712 USA*

[d]*Materials Science Centre and Faculty of Physics, Philipps University Marburg, Hans-Meerwein-Strasse 6, 35043 Marburg, Germany*

[e]*Evonik Operations GmbH, Rodenbacher Chaussee 4, 63457 Hanau, Germany*

[f]*Institute of Experimental Physics I, Justus Liebig University Giessen, Heinrich-Buff-Ring 16, 35392 Giessen, Germany*

=These authors contributed equally to this work

Corresponding Authors

*Email:

Matthias.elm@phys.chemie.uni-giessen.de (M. T. Elm)

Anja.Henss@phys.chemie.uni-giessen.de (A. Henss)

Ruijun.Pan@phys.chemie.uni-geissen.de (R. Pan)

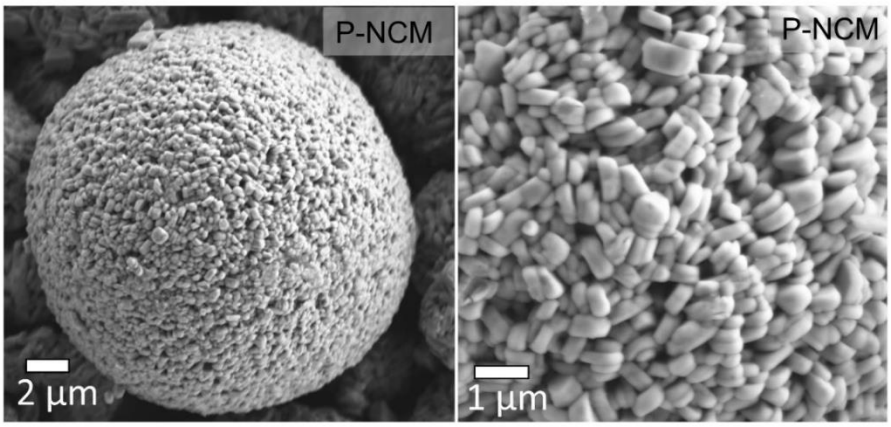

Figure S1: SEM-images of pristine NCM.

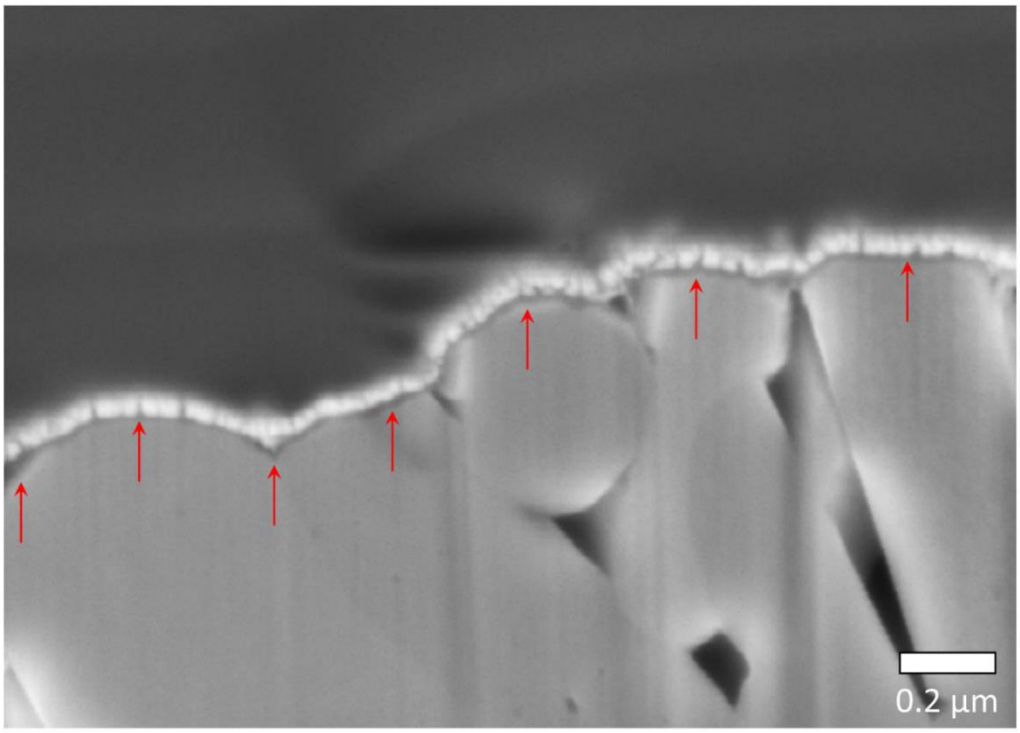

Figure S2: SEM cross-section image of the surface of the secondary particle showing the homogenous covering of the layer for Alu-NCM600.

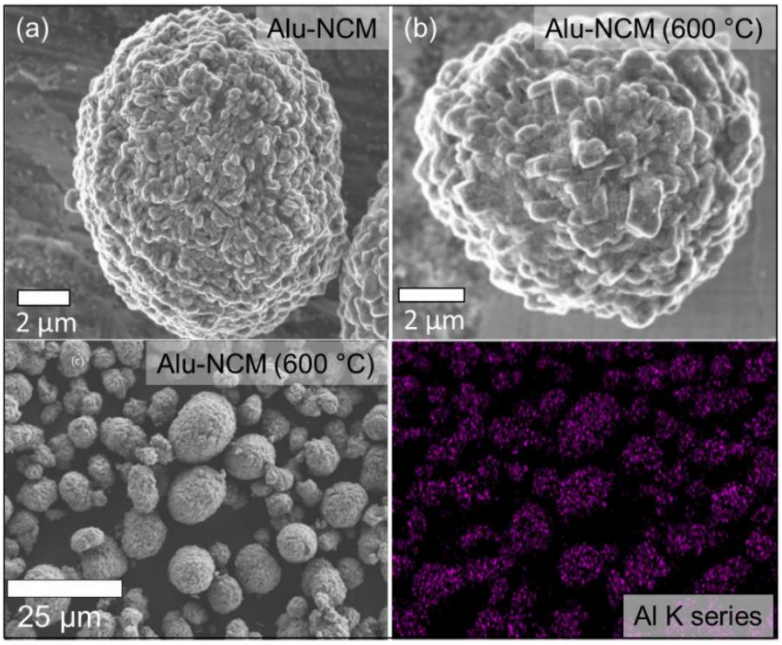

Figure S3: SEM images of the secondary particles of (a) Alu-NCM, (b) Alu-NCM600 and (c) SEM-EDX mapping of Alu-NCM600.

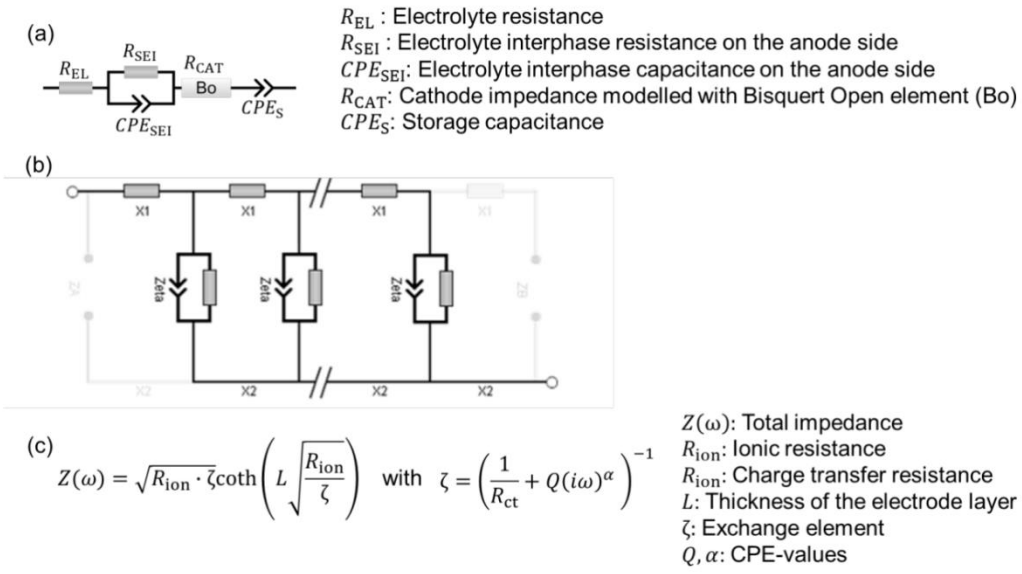

Figure S4: Impedance model used for fitting the full cell impedance spectra: (a) Equivalent circuit model including (b) Bisquert open element, which is based on (c) the Bisquert open-element equation (obtained from Relaxis, RHD instruments).

Impedance spectroscopy on full cells was performed. The resulting data were fitted to an equivalent circuit consisting of a single resistor R_{EL} representing the SSE layer in series to a parallel arrangement of a single resistor R_{SEI} and CPE_{SEI} representing the In/InLi|SSE interface. The time constant as well as feasible resistance values of 10-20 Ω for In/InLi|SSE interface was adopted from P. Minnmann et al.[1] Furthermore, a Bisquert open element[2] shown in Figure S3b was added in series in order to model the porous structure of the composite cathode. The fitting parameters obtained are listed in Table S1.

Table S1: Fitting parameter of impedance spectra after 1st and 100th cycle for P-NCM and Alu-NCM600 full cells.

	Parameter name	P-NCM 1st cycle	P-NCM 100th cycle	Alu-NCM600 1st cycle	Alu-NCM600 100th cycle
Electrolyte	R_{EL} / Ω	31.1	25.4	32.7	40.4
Anode side	R_{SEI} / Ω	10.0	40.0	20.0	41.6
	Q / F/s$^{1-\alpha}$	0.01	0.01	0.02	0.004
	α	1.00	0.92	0.62	0.78
Cathode side	R_{ion} / Ω	75.8	65.0	71.6	67.6
	R_{ct} / Ω	223.4	610.8	118.3	373.9
	L	1	1	1	1
	Q / F/s$^{1-\alpha}$	$8.30 \cdot 10^{-5}$	$6.51 \cdot 10^{-5}$	$1.35 \cdot 10^{-4}$	$4.74 \cdot 10^{-5}$
	α	0.77	0.72	0.72	0.75

References

[1] P. Minnmann, L. Quillman, S. Burkhardt, F. H. Richter, J. Janek, *J. Electrochem Soc.* **2021**, *168*, 040537.

[2] J. Bisquert, *Phys. Chem. Chem. Phys.* **2000**, *2*, 4185.

6.6 List of Abbreviations

AC: Alternating current

ALD: atomic layer deposition

ASSB: all-solid-state battery

BET: Brunauer–Emmett–Teller

CAM: cathode active material

CE: Columbic efficiency

CEI: cathode electrolyte interface

CT: charge transfer

CV: Cyclic voltammetry

CVD: chemical vapour deposition

DEC: Diethyl carbonate

DFT: density functional theory

DMC: Dimethyl carbonate

EDS: Energy dispersive spectroscopy

EELS: electron energy loss spectroscopy

EIS: electrochemical impedance spectroscopy

EMC: Ethylmethyl carbonate

EV: electric vehicle

HAADF: High-angle annular dark-field imaging

HF: hydrogen fluoride

ICE: Initial columbic efficiency

LFP: Lithium iron phosphate

LIB: lithium-ion battery

LLO: Lithium-rich layered oxides

LMO: Lithium manganese oxide

LNMO: Lithium nickel manganese oxide

MLD: Molecular layer deposition

NCA: lithium nickel cobalt aluminium oxide

NMC: lithium nickel manganese cobalt oxide

NMP: N-Methyl-2-pyrrolidone

PC: Propylenecarbonate

PE: Polyethylene

PEDOT: poly(3,4-ethylenedioxy)thiophene

PPy: polypyrrole

PTh: polythiophene

PVD: physical vapour deposition

SEI: solid electrolyte interphase

SEM: scanning electron microscopy

STEM: Scanning transmission electron microscopy

TEM: transmission electron microscopy

TGA: Thermogravimetric analysis

TM: Transition metal

TMA: Trimethyl aluminium

XPS: X-ray photoelectron spectroscopy

XRD: X ray diffraction

6.7 List of Publications and Articles to be Submitted

R. S. Negi, S. P. Culver, A. Mazilkin, T. Brezesinski, M. T. Elm, Enhancing the Electrochemical Performance of $LiNi_{0.70}Co_{0.15}Mn_{0.15}O_2$ Cathodes Using a Practical Solution-Based Al_2O_3 Coating. *ACS Applied Materials & Interfaces* **2020**, 12 (28), 31392-31400

R. S. Negi, S. P. Culver, M. Wiche, S. Ahmed, K. Volz, M. T. Elm, Optimized atomic layer deposition of homogeneous, conductive Al_2O_3 coatings for high-nickel NCM containing ready-to-use. *Physical Chemistry Chemical Physics* **2021**, 23 (11), 6725-6737

R. S. Negi, E. Celik, R. Pan, R. Stäglich, J. Senker, M. T. Elm, Insights into the positive effect of post-annealing on the electrochemical performance of Al_2O_3 coated Ni-Rich NCM cathode for lithium-ion batteries, *ACS Applied Energy Materials* 2021, 12 (28), 31392-31400

R. S. Negi, P. Minnmann, R. Pan, S. Ahmad, M. Herzog, K. Volz, R. Takata, F. Schmidt, J. Janek, M. T. Elm, Stabilizing the cathode/electolyte interface with dry-processed lithium titanate coating for all-solid-state-batteries, *Chemistry of Materials* **2021**, 33 (17), 6713-6723

R. S. Negi, Y. Yusim, R. Pan, S. Ahmad, K. Volz, R. Takata, F. Schmidt, A. Henss, M. T. Elm, A dry-processed $Al_2O_3/LiAlO_2$ coating for stabilizing the cathode/electrolyte

interface in high-Ni NCM-based all-solid-state batteries, accepted *Adv. Mater. Interface* **2021**

R. S. Negi, M. T. Elm, Reproducible long-term cycling stability data on the electrochemical performance of Al_2O_3 coated Ni-Rich NCM cathode for lithium-ion batteries, submitted to *Scientific Data* **2021**

E. Celik, R. S. Negi, M. Bastianello, D. Boll, A. Mazilkin, T. Brezesinski and MT Elm, Tailoring the protonic conductivity of porous yttria-stabilized zirconia thin films by surface modification, *Phys. Chem. Chem. Phys.* **2020**, 22, 11519-11528

S. Randau, F. Walther, A. Neumann, Y. Schneider, R. S. Negi, B. Mogwitz, J. Sann, K. Becker-Steinberger, T. Danner, S. Hein, A.Latz, F. H. Richter, J. Janek, "On the Additive Microstructure in Composite Cathodes and Alumina-Coated Carbon Microwires for Improved All-Solid-State Batteries" *Chemistry of Materials* **2021**, 33 (4), 1380-1393

6.8 List of Patents

D. Esken, M. Herzog, M. Elm, R. Negi, F. Schmidt, R. Takata, Transition metal oxide particles encapsulated in nanostructured lithium titanate or lithium aluminate, and the use thereof in lithium ion batteries, Patent EP20206870

6.9 List of Conference Contributions

DPGR19: DPG Spring Conference of the Condensed Matter Section (SKM), Regensburg, Germany, 31.03. - 05.04.2019, oral presentation: Influence of Al_2O_3 coating on NCM cathodes for Lithium ion batteries.

SSI2019: 22nd International Conference on Solid State Ionics (SSI-22), Pyeong chang-Gun Gangwon-Do, Korea, 16.06-21.06.2019, poster presentation: Influence of ultrathin Al_2O_3 coating on electrochemical performance of Ni-rich NCM cathode for Lithium ion battery.